Universität Rostock

Traditio et Innovatio

Modeling of the Time-Dependent Material Response of Human Articular Cartilage and Substitute Materials

Publikationsbasierte Dissertation

zur Erlangung des akademischen Grades
Doktor-Ingenieur (Dr.-Ing.)
an der Fakultät für Maschinenbau und Schiffstechnik
der Universität Rostock

vorgelegt von
Dipl.-Ing. Alina Weizel
geb. am 28.01.1990 in Omsk
Rostock, 2023

https://doi.org/10.18453/rosdok_id00004607

1. Gutachter:
Prof. Dr.-Ing. Hermann Seitz,
Lehrstuhl für Mikrofluidik, Fakultät für Maschinenbau und Schiffstechnik, Universität Rostock

2. Gutachter:
Prof. Dr.-Ing. Silvia Budday,
Lehrstuhl für Kontinuumsmechanik, Department Maschinenbau, Friedrich-Alexander-Universität Erlangen

3. Gutachter:
Prof. Dr. med. habil. Dipl.-Ing. Rainer Bader,
Forschungslabor für Biomechanik und Implantattechnologie, Orthopädische Klinik und Poliklinik, Universitätsmedizin Rostock

Jahr der Einreichung: 2023
Jahr der Verteidigung: 2024

Table of contents

1 Introduction and Background

1.1 Clinical Aspects and Therapy

With over 300 million cases globally in 2017, osteoarthritis is the prevailing degenerative joint disease, and it is on the rise in most nations. This trend is anticipated to persist due to the increasing life expectancy and aging of the global population [1–5]. Patients with osteoarthritis regularly suffer from severe pain and experience a reduction in quality of life due to physical disabilities [3] [5–7]. The development of osteoarthritis is promoted by traumatic joint injuries and non-physiological mechanical stresses [8]. During the development of osteoarthritis, there are changes in the articular cartilage, ligaments, capsule, and synovial membrane [3] [5–7]. The progression of osteoarthritis is characterized by disorientation and degradation of collagen fibrils, especially in the superficial cartilage zone. Furthermore, osteoarthritis leads to a decrease in collagen and proteoglycans, resulting in an increase in fluid inside the tissue [9]. These structural changes cause an increase in permeability and, at the same time, a reduction in static and dynamic stiffness [10]. Macroscopically, osteoarthritis reduces loading capacity, resulting in higher strains under constant loading [9]. This is favored by decreased elastic properties and increased viscoelastic properties [11] [10].

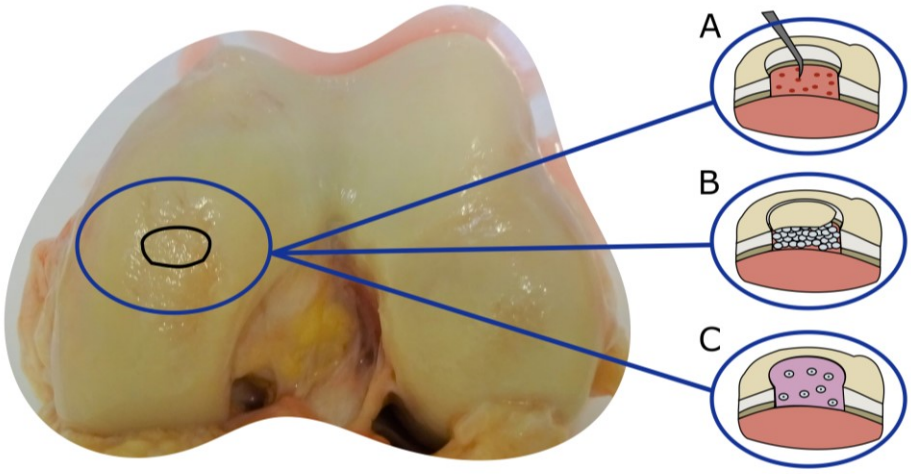

Figure 1: Schematic overview of regeneration techniques of articular cartilage such as A: micro-fracturing; B: autologous chondrocyte implantation (ACI); and C: matrix-assisted autologous chondrocyte implantation (MACI).

Current therapeutic approaches to repair damaged cartilage comprise pharmacological and non-pharmacological therapies and surgical techniques such as arthroscopy and arthroplasty [12].

Figure 1 shows therapeutic techniques to regenerate damaged articular cartilage. Microfracturing represents a conservative surgical therapeutic approach to repairing damaged articular cartilage, but it results in spontaneous healing and fibrous tissue formation. During micro-fracturing, the subchondral bone is penetrated; thus, mesenchymal stem cells can migrate through channels from the marrow to the defect. More advanced transplantation strategies include autologous chondrocyte implantation (ACI) or matrix-associated chondrocyte implantation (MACI) [13]. During ACI, the defect is filled with autologous chondrocytes and covered with a membrane consisting of periost or collagen. In contrast to

ACI, in MACI, the hydrogel matrix embeds chondrocytes in vitro before implantation. However, even these approaches do not develop mechanically identical hyaline cartilage but only a fibrous tissue with reduced mechanical properties. This is due to the low regeneration potential of cartilage resulting from avascularity and low cell turnover [6]. Other disadvantages are, for example, the additional damage to healthy cartilage caused by such interventions and also the need for secondary surgery [14] [15]. Total joint replacement is the last surgical alternative, but it has a limited life span and can usually be performed only once [3]. By focusing research efforts on tissue engineering with its three main blocks illustrated in Figure 2 - scaffold material or biomaterial, biofactors, and chondrogenic cells - attempts are being made to overcome the drawbacks of the therapeutic approaches mentioned before (see Figure 1) [16] [14] [17]. Tissue engineering is an interdisciplinary field that aims to develop substitute materials for scaffolds that can replicate the properties of cartilage and thus attempt to restore its function.

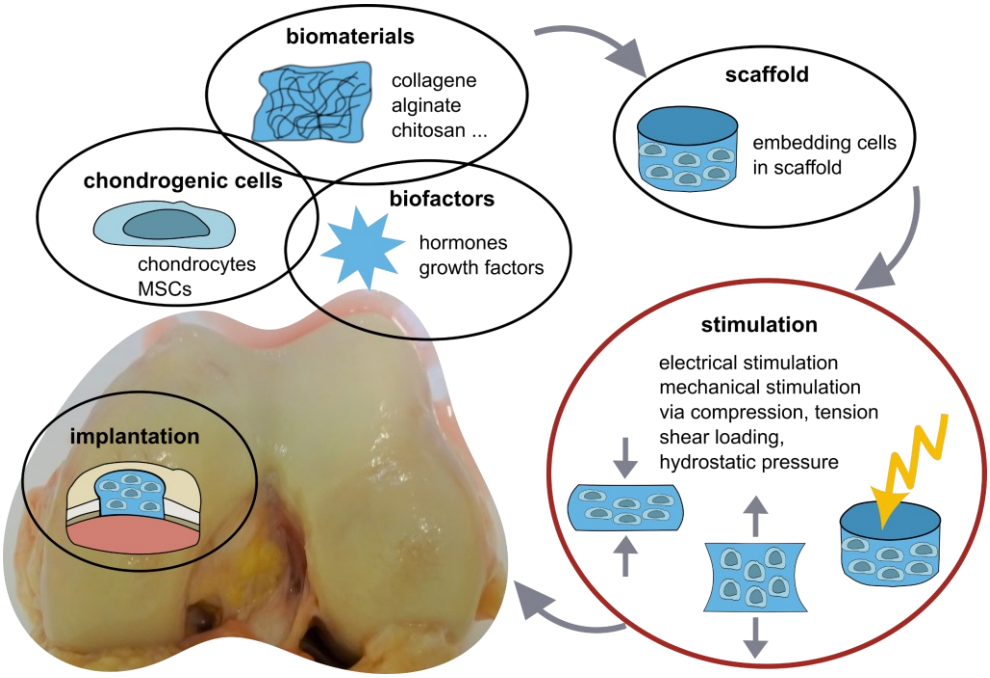

Figure 2: Foundation of tissue engineering using the three fundamental components of biomaterials, biofactors, and chondrogenic cells in the formation of scaffolds using stimulation of the scaffold before implantation.

In general, tissue engineering involves placing cells in a scaffold designed to function as an extracellular matrix. The artificial extracellular matrix should be biocompatible, biodegradable, and able to pass nutrients, biofactors, and molecules to support cell proliferation and viability. Materials already investigated consist of collagen but also alginates, cellulose, and chitosan, to name a few [17]. New approaches include osteochondral scaffolds with two different materials [18].

1.2 Mechanical Characterisation and Cell Mechanical Environment

Cell Stimulation and Cell Responses

An option to overcome the poor mechanical properties of the forming tissue that result from MACI treatment is to use various stimulation mechanisms illustrated in Figure 2 to stimulate the hydrogel implant to form collagen II and glycosaminoglycans (GAGs) and promote chondrogenesis [19] before implantation, thereby making it as similar to cartilage as possible. In this context, the most effective stimulation mechanisms to date are hydrostatic pressure, direct compression, fluid shear [19] [13] [20], and electrical stimulation [21]. The effect of mechanical stimulation of chondrocytes can be attributed to mechanotransduction, which is triggered by mechanoreceptors such as voltage-gated calcium channels, stretch-activated integrins, and the primary cilium in the pericellular matrix [8] [22]. These mechanisms affect cells' differentiation, migration, and survival [19].

In addition to bio-compatibility, adhesion, porosity, and biodegradability, the mechanical environment experienced by the cells also influences the short- and long-term cell response in the tissue. The mechanical environment is simultaneously determined by the material properties of the scaffold and the load applied during stimulation [23] [14] [16] [24]. Simply adjusting the loading parameters with a different scaffold material or with altered mechanical properties would fundamentally change the biomechanical environment and, thus, the cell-material interaction. The elastic and viscoelastic properties of the scaffold affect cell migration, mechanotransduction, differentiation, and proliferation simultaneously [24–32]. For this reason, multiple studies address the impact of individual material properties on chondrocytes or isolate factors that may alter cell responses [24] [33]. Lee et al. demonstrated in their study that faster relaxing alginate hydrogels increase the cartilage extracellular matrix formation [24]. The faster relaxing alginate hydrogels formed pericellular matrices (PCM) – bean-shaped morphologies – that resemble the natural hyaline cartilage [24]. Furthermore, the number of chondrocytes was increased, and the formation of collagen II and GAGs was enhanced.

The cytokine interleukin-1 β (IL-1β) secretion, which initiates cell death, could explain stress relaxation and cell response on the molecular level. In slower relaxing hydrogels, the cell volume expansion of chondrocytes is inhibited, which leads to diminished cell size and induces IL-1β-signalling [24]. In a study by Zahedmanesh et al. [33], chondrogenesis of mesenchymal stem cells was only induced with a combination of compression and interfacial shear loading. Silver et al. published in [34] and [35] that dynamic and cyclic external loading on cartilage promotes aggrecan and collagen II biosynthesis and reduces inflammatory responses. Further, previous studies have shown that pathological alterations in cartilage or degradation of the proteoglycan matrix result in mechanical changes in the tissue [36] [37].

To better understand the cellular environment (as shown in Figure 3) during stimulation or when cells are embedded in a scaffold without stimulation, analyzing the mechanical properties of the scaffold can be helpful. Moreover, this analysis can help obtain parameters for numerical simulations, providing further insights into the stimulation process.

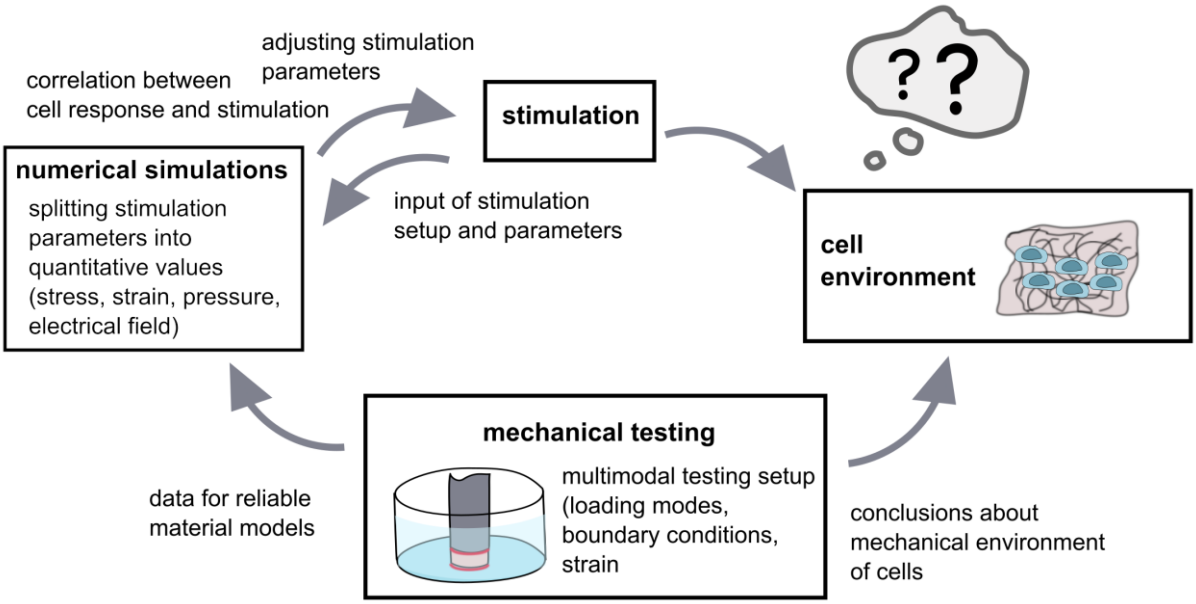

Figure 3: Connection between stimulation, mechanical characterization, and numerical simulations.

Characterization Strategies

Even though strains of 2-6% occur and cartilage thickness decreases during physiological loading of cartilage, such as sitting and standing, or during cyclic loading, such as walking [38], cartilage has not yet been studied under large deformations, different loading modes, and the entire loading history simultaneously [4]. Only a few studies have examined cartilage in both tension and compression [39]. While some studies deal only with tensile tests [40], others have applied indentation and compression tests to the cartilage, as these are the most straightforward to perform, considering the small thickness of human articular cartilage (~2 mm) [41–47]. To determine the viscoelastic behavior of cartilage, mainly stress relaxation experiments with confined or unconfined compressive loadings were carried out [33] [48] [49] [50] [51]. Another approach to determining the time- or strain-rate-dependent behavior is to evaluate the loading curve of compression experiments [52]. Moreover, effects such as the Mullins effect, conditioning, and recovery under cyclic loading conditions have been demonstrated [53–56]. The mechanical behavior of hydrogels reacts to numerous other properties, such as the material's chemical structure, and provides conclusions about the change in polymer concentration [48]. Furthermore, the stiffness of collagen scaffolds depends on the test method and collagen concentration, as well as other parameters like the pH value, temperature, and crosslinking [57]. Crosslinking, for example, increases the stiffness of hydrogels.

In the case of the ADA-GEL scaffolds, a previous study shows that increasing the concentration of microbial transglutaminase (mTG) used for crosslinking can raise the stiffness of the hydrogel [58]. Increasing the mTG crosslinker and GEL concentrations could be a suitable attempt to enhance the stiffness of ADA-GEL to values closer to native cartilage while improving the 3D printability of ADA-GEL through the influence of GEL [59]. As mentioned before and illustrated in Figure 3, insight into the mechanical behavior of cartilage and its substitute materials enables conclusions about cell fate in tissue engineering and the development of in silico computer models for numerical simulations. Natural

cartilage and hydrogels are subjected to mechanical stresses when used as implants, and the resulting stress and strain states can be evaluated and predicted by numerical simulations, contributing to a better understanding of their unique resistance to loading [60] [61]. As with the determination of the mechanical behavior, the mechanical tests for parameter identification for numerical simulations are limited to only one loading mode or to the time-independent behavior [62] [61]. When material parameters are obtained based on data from a single loading condition, they will not adequately represent the behavior with different loading conditions [63]. Therefore, to make reliable predictions, it is essential to test at least the loading modes, strain levels, and time scales encountered in the application of interest.

1.3 Numerical Simulations in Cartilage Regeneration

The importance of numerical simulations in comprehending the mechanisms of stimulation in tissue engineering is highlighted in Figure 3. These simulations can determine the magnitude, orientation, and location of stresses, strains, or electric fields within scaffold materials and allow researchers to correlate different effects on mechanotransduction between the extracellular matrix and chondrocytes under mechanical and electrical loading [33] [64]. Furthermore, these simulations can demonstrate the impact of mechanical properties on osteoarthritis [43].

In finite element simulations, the initial step is to prepare the object through pre-processing. A summary of the involved steps is presented in Figure 4. The geometry can be created using computer-aided design (CAD) software or imported from other sources. Depending on the complexity of the geometry, it may be possible to generate it directly within the finite element (FE) program, such as Ansys® (Ansys, Inc.), COMSOL Multiphysics® (COMSOL AB), ABAQUS FEA (SIMULIA), or FEBio (Finite Elements for Biomechanics). Once the geometry is established, a mesh consisting of finite elements can be generated. This mesh can comprise tetrahedral or quadrahedral elements with varying linear and non-linear trial functions. Possible boundary conditions include displacements and the application of forces, among others. After defining all the boundary conditions, the next step is to select the material model and to decide about isotropy, anisotropy, compressibility, incompressibility, time-dependent or time-independent material behavior or analysis. After the simulation, the results can be evaluated in the so-called post-processing.

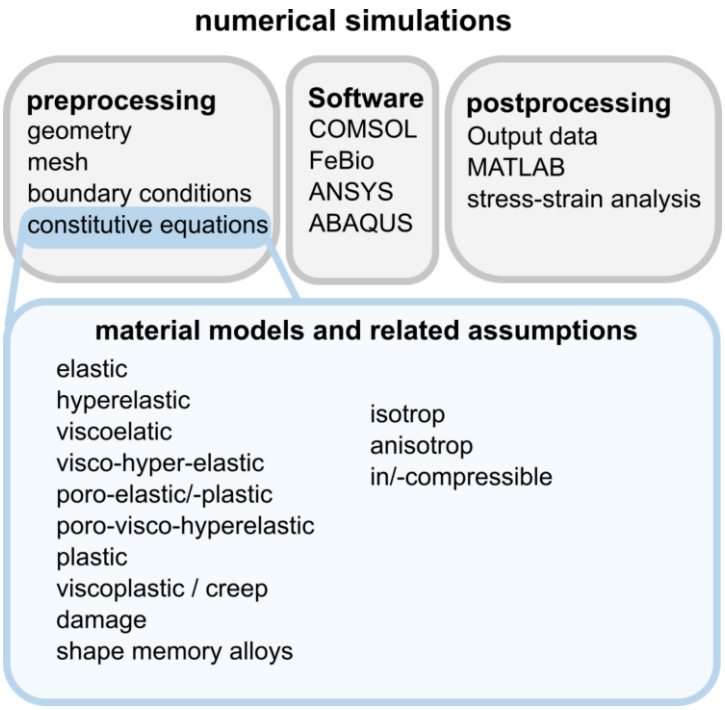

Figure 4: Schematic illustration of the separate stages and elements involved in numerical simulations.

Choosing a suitable material model is crucial in numerical simulations. Various time-independent material models are available for different materials, such as elastomers, hydrogels, and tissues, as well as for different applications. Hyperelastic time-independent material models have been widely used to represent the material behavior of hydrogels [65–69]. For example, Faturechi et al. studied the hyperelastic behavior of Gel/PAA composites using the Yeoh model [66]. At the same time, Distler et al. investigated the mechanical behavior of ADA-GEL hydrogels using the one-term Ogden model [65]. Hyperelastic material models are also used in simulating the entire musculoskeletal system and the interaction of cartilage with the joint [70] [71]. To date, various hyperelastic material models, including Ogden, Mooney-Rivlin, Yeoh, Neo-Hookean, and Arruda-Boyce, have been used for cartilage [43] [72]. A detailed explanation of these hyperelastic material laws can be found in [73]. To consider the time-dependent effects of viscoelasticity or poroelasticity in cartilage, more advanced material models such as viscoelastic, hyper-viscoelastic, or hyper-visco-poroelastic can be used if necessary for the specific application. For instance, Richard et al. [74] used a viscoelastic model to examine the difference in behavior between healthy and osteoarthritic cartilage under tension loading in the micro-range. Additionally, Springhetti et al. [75] modeled the viscoelastic response of cartilage under impact loading. Ahsanizadeh et al. [76] took a similar approach and modeled cartilage's hyperelastic behavior in addition to its viscoelastic behavior. In the research of Kim et al. [77] and Tanska et al. [78], poroelastic models were employed to study cartilage. This study chose a hyper-viscoelastic material behavior with constitutive laws implemented in COMSOL Multiphysics®. The hyperelasticity accounts for the time-independent non-linear material responses even under small deformations, and the viscoelasticity represents the time-dependent effects of cartilage and hydrogels. A detailed explanation of the kinematics and constitutive equations can be found in publications [73] and [79], which serve as a foundation for this thesis.

1.4 Cartilage and Biomaterials for Cartilage Regeneration

Human Hyaline Cartilage

The hyaline cartilage is an avascular tissue with low regeneration potential, which surrounds the joints and primarily provides smooth movement, absorbs shocks by viscous energy dissipation, and transmits elastic energy during movement [80]. Natural hyaline cartilage is 2 to 7 mm thick and consists of an extracellular matrix incorporating chondrocytes. In healthy cartilage, the ECM has a water content of 80%, which decreases to 79% up to the subchondral zone [81] [82]. In addition, the ECM contains hydrophilic and negatively charged proteoglycans, which lead to high water storage, as well as different types of collagen, with collagen type II being the main component of the collagen with 90-95 % [83]. The structure of hyaline cartilage is divided into several zones with different functions and morphology [83] [82]. Figure 5 shows a schematic representation of these zones. The superficial zone represents up to ~10-20 % of the cartilage thickness and consists of flattened chondrocytes and collagen fibers arranged tangentially to the surface (tangential fiber zone). The transition zone absorbs compressive forces and has obliquely arranged collagen fibers. In the radial zone, the collagen fibers and chondrocytes are oriented parallel or perpendicular to the tangential zone, providing the greatest resistance to compressive forces. The tidemark forms the boundary between the deep zone and the calcified cartilage. The calcified cartilage is responsible for the transition and the anchorage between cartilage and bone [83] [84].

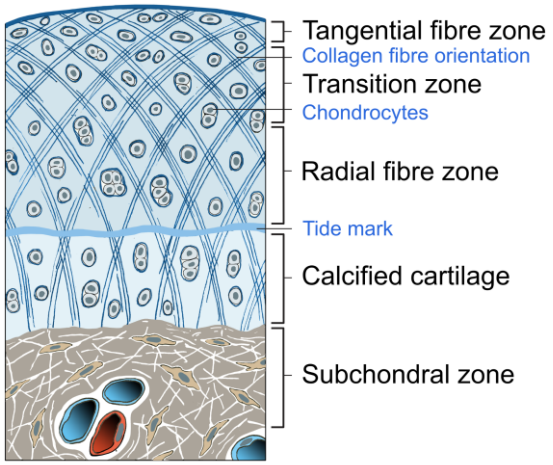

Figure 5: Schematic structure of human articular cartilage. From [85], https://creativecommons.org/licenses/by-nc-nd/4.0/, Copyright © 2020 Elsevier B.V.

Hydrogels as Substitute Materials for Cartilage Repair

Commonly used materials in tissue engineering are hydrogels, which consist of a three-dimensional (3D) polymer network of hydrophilic macromolecules, allowing them to hold a large amount of water up to a thousand times their dry weight [86] [87]. These unique properties ensure that hydrogels are particularly good at replicating biological tissue, such as cartilage. The chemical backbone of hydrogels can be based on various substances, such as collagen, natural polysaccharides like alginates or chitosan, or synthetic polymers like polyethylene glycols (PEG) [13]. Once a hydrogel scaffold has been established, it can be enriched with cells pre or post-implantation [14] [16]. To achieve similar properties

to natural cartilage and make hydrogels attractive to cartilage cells, scaffolds' mechanical properties and chemical composition are undergoing optimization in research studies.

ADA-GEL Hydrogels

Sodium alginate is an anionic natural polysaccharide that can be extracted from brown seaweeds. It has good biocompatibility, low toxicity, and low fabrication costs. It is mainly used in pharmaceutical, biomedical, and tissue engineering fields for wound healing, wound dressing, drug delivery, and cell culture [88] [89]. Due to the divalent cations, sodium alginate can be crosslinked using Ca, Na, Ba, and Sr [89–91]. The crosslinked hydrogel structure resembles that of the extracellular matrices of tissue [89]. However, alginate-based hydrogels lack cell adhesion motifs and sufficient degradability [92] [93]. Chemical modification through oxidation or blending with other materials increases the degradation rate and modulates the cell adhesion potential. Alginate di-aldehyde (ADA) can be synthesized by controlled oxidation of alginate and has tunable degradability. One possible blend is gelatin (GEL), which forms a hydrogel by mixing with ADA due to reversible covalent imine bonds via Schiff base formation (see Figure 6). The hydrogel can be further crosslinked by adding Ca^{2+} and mTG, resulting in ionic crosslinking by divalent cations between the guluronic acid blocks of the ADA chain [94] and enzymatic crosslinking by covalent isopeptide bonds between glutamine and lysine groups of the gelatin [58]. The ADA-GEL hydrogel system features ionic (Ca2+) crosslinking, covalent (enzymatic, ε(γ-glutamyl)lysine) isopeptide binding (facilitated by microbial transglutaminase), and reversible-covalent (Schiff base) crosslinking [58]. Recent studies have demonstrated that ADA-GEL hydrogels are applicable in various areas of tissue engineering, such as bone, blood vessels, and cartilage tissue engineering [95–102].

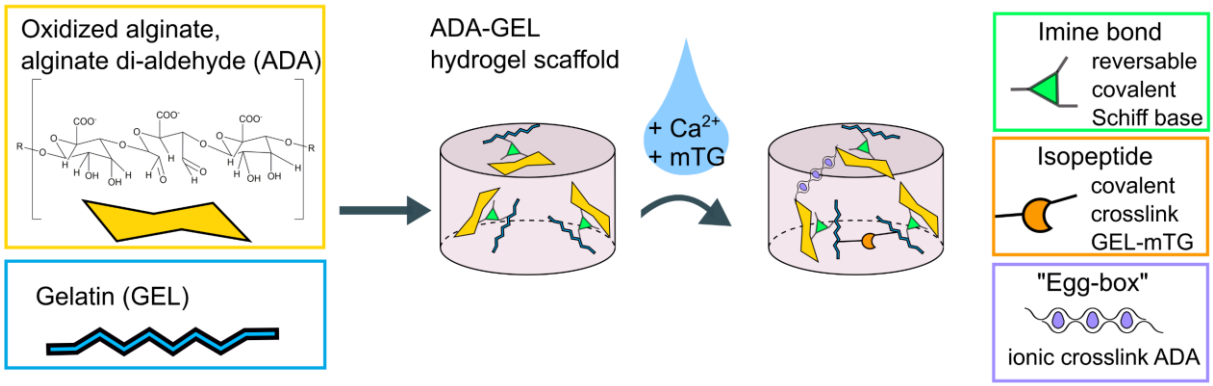

Figure 6: Simplified schematic of the mechanisms for ionic and enzymatic crosslinking of ADA-GEL hydrogels, adopted from [58]. Combining gelatin (GEL) and oxidized alginate (ADA) creates a hydrogel by forming reversible covalent imine bonds via Schiff base formation. The addition of a crosslinking solution containing Ca2+ and mTG ionically crosslinks the guluronic acid blocks of the ADA chain via divalent cations [94]. In contrast, enzymatic crosslinking by mTG leads to covalent isopeptide bonds between the glutamine and lysine groups of the gelatin [58]. From [79], https://creativecommons.org/licenses/by/4.0/, Copyright © 2023 Elsevier B.V.

ChondroFiller^{liquid} Hydrogel

An already established and commercially available substitute material for hyaline cartilage is ChondroFiller^{liquid}, which is based on collagen type I (provided by Meidirx Biomaterials GmbH, Esslingen

Germany)—the collagen type I is produced by acid extraction from rat tail tendons. In the clinical application, ChondroFiller^{liquid} is injected directly into the defect of cartilage (Outerbridge grade III-IV) and forms a pressure-resisting matrix to refill the defect into which the cells can migrate. The hierarchical collagen type I is illustrated in Figure 7 and consists of a triple helix molecular structure built up from peptide chains of proteins such as glycine, proline, and hydroxyproline [103] [104]. The triple helix is stabilized by hydrogen bonds created by the freely moving water between the inter-fibrillar spaces [104].

During fibrillogenesis, fibrils consisting of triple helix molecules assemble into fibrous macrostructures. In the process, the collagen fibers can be randomly aligned or form oriented structures [22]. Aggregation into fibrillar hydrogels is dependent on multiple variables such as gelation temperature, pH value, extraction mechanism (acid extraction or pepsin extraction), and collagen concentration [22] [105] [106]. The ChondroFiller^{liquid} hydrogel fabricated, as described in chapter 3.1, consists of a mixture of fibrillar and non-fibrillar phases, which could be mainly due to the two-syringe mixing mechanism during hydrogel casting and cross-linking.

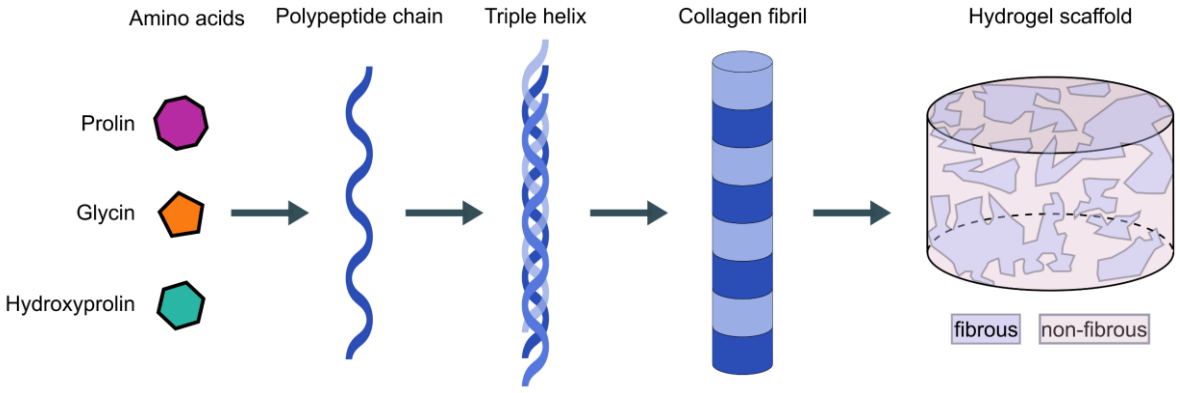

Figure 7: Schematic of the hierarchical collagen type I microstructure of a ChondroFiller^{liquid} hydrogel scaffold. From [79], https://creativecommons.org/licenses/by/4.0/, Copyright © 2023 Elsevier B.V.

2 Motivation

The purpose of this work was to better understand the complex time-independent and time-dependent mechanical behavior of human cartilage and two selected substitutes through the use of mechanical characterization in order to derive suitable parameters for reliable finite element simulations. The FEA has become a valuable tool for research, as it can complement mechanical investigations and provide predictive insights into a particular topic of interest. Numerical simulations can predict complex loading scenarios that occur during mechanical stimulation. These simulations can divide the deformation state into measurable quantities, which provide conclusions about the responses of cells and the mechanotransduction process. To identify the appropriate stimulation parameters that enable cells to create cartilage-like tissue, it is crucial to have a thorough understanding of mechanotransduction in cells. The accuracy of the FEA results depends on the assumed material law and the corresponding material parameters, which are identified through mechanical tests. Three publications were worked out to address these questions, with each publication building upon the previous one.

Publication I

The first publication aimed to characterize the complex mechanical behavior of cartilage and two surrogate hydrogels under multiple loading modes and large deformations and to link the mechanical behavior to the underlying microstructure using multiphoton Second Harmonic Generation (SHG) microscopy. In tissue engineering, the mechanical characterization of human cartilage and its substitutes is becoming increasingly important in evaluating their performance. Although many studies have explored the mechanical behavior of cartilage and hydrogels, it is not yet fully understood how the function, microstructure, and physiology of cartilage are related to its mechanical behavior and which mechanical parameters have a significant impact on the cells in cartilage or the success of implant materials.

Publication II

The second publication focused on the time-independent material behavior of cartilage, ChondroFiller^{liquid}, and ADA-GEL. The aim was to investigate the suitability of commonly used hyperelastic material models, such as Ogden, Mooney-Rivlin, Yeoh, Neo-Hookean, and Arruda-Boyce, to represent the nonlinear material behavior in compression and tension. Assuming the conditions for which the hyperelastic parameters were determined are consistent with the specific application; hyperelastic models can be a reasonable approximation.

Publication III

The third publication explored the time-dependent behavior of cartilage and hydrogels and applied time-dependent modeling approaches with the FEA. Hyperelastic and viscoelastic material models represent monophasic material behavior [75] [107]. Although hyperelastic material models can represent non-linearities [73], they cannot model the conditioning and hysteresis. Hyper-viscoelastic material laws were integrated to combine non-linearities and time-dependent material behavior. The parameter identification method is crucial for the quality of the obtained material parameters and must be chosen

based on the test conditions. An analytically defined function is commonly utilized to fit the test data and assume a homogeneous deformation state. However, this is difficult to achieve, especially for soft materials like hydrogels or for materials such as cartilage whose geometry is constrained by natural physiology. An inverse parameter identification that includes the real boundary conditions could provide more reliable material parameters.

3 Materials and Methods

3.1 Scaffold Fabrication

The specimens presented in Figure 8 illustrate one exemplary sample of human articular cartilage, ADA-GEL, and ChondroFiller^{liquid}, which were mechanically tested in the publication *I*. The samples were obtained by punching 8 mm diameter and 2094 ± 320 µm high samples from the condyle of a 62-year-old donor who passed away due to liver and kidney failures. The samples were stored in a phosphate-buffered saline solution at four °C until testing.

The scaffolds based on collagen I are made of ChondroFiller^{liquid} provided by Meidrix Biomedicals GmbH (Esslingen, Germany). The ChondroFiller^{liquid} system consists of a two-chamber system containing 10g/ml of collagen type I concentrate in the larger chamber and a gel neutralization solution in the smaller chamber. The content of the two chambers is poured into a silicone mold, which has a diameter of 8mm and a height of 4 mm. The scaffolds are then allowed to gel at four °C for 24 hours. The final concentration of the collagen is 8 mg/ml.

The ADA-GEL scaffolds consist of ADA (7.5 % (w/v)), which was dissolved in 5 ml phosphate-buffered saline solution and stirred with 5 ml GEL (7.5 % (w/v)) for 10 min at room temperature until homogeneity was reached.

This hydrogel precursor is also placed in a silicone mold with an 8 mm diameter and 4 mm height, where it is subsequently crosslinked with 0.1 M $CaCl_2$ and 2.5 % (w/v) microbial transglutaminase (mTG, Ajinomoto Co., Inc, ACTIVA® WM, 85 -135 U/g, Japan) for 24 hours [58].

3.2 Mechanical Testing

A multi-modal mechanical analysis was conducted to qualitatively characterize the samples using the testing protocol outlined in Table 1. A combined testing protocol was developed to obtain material data for numerical simulation parameter identification (Table 2). This protocol involved cyclic loading at two strains (10 % and 20 % nominal strain) and three cycles each of ADA-GEL and ChondroFiller^{liquid}, followed by stress relaxation tests in compression and tension at 15 % nominal strain. To account for the relatively high stiffness of cartilage, the maximum strains were reduced from 10 %, 15 %, and 20 % to 1 %, 2.5 %, and 5 %, respectively.

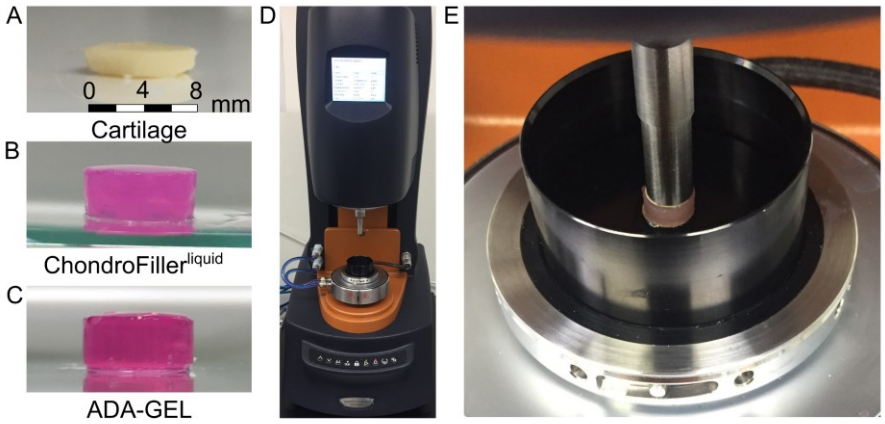

Figure 8: Experimental setup. a) Cartilage specimen b) ChondroFiller^{liquid} specimen c) ADA-GEL specimen d)) Rheometer with upper sample holder and lower cup e) Specimen mounted to the testing setup, glued on its top and bottom surfaces. From [85], https://creativecommons.org/licenses/by-nc-nd/4.0/, Copyright © 2020 Elsevier B.V.

For time-dependent or strain rate-dependent materials such as cartilage and hydrogels, it is essential to pay particular attention to the strain rate at which testing is performed, as the material behavior of cartilage is divided into two strain rate ranges: a quasi-static material behavior dominated by the fluid flow and the interaction between the solid matrix components, leading to a nonlinear stress-strain curve, and a material behavior independent of the fluid flow and no increase of stiffness above a strain rate of 0.05 1/s [42] [43]. The cartilage and the hydrogels were tested at strain rates of ~0.24 1/s and ~0.13 1/s, respectively, i.e., in the range where no change in stiffness is expected.

The mechanical characterization was carried out using a Discovery HR-3 Rheometer from TA Instruments (New Castle, Delaware, USA) at the Friedrich-Alexander University in Erlangen, as depicted in

Figure 13 d and e. To conduct the test, the specimens were affixed to the upper sample holder using cyanoacrylate adhesive and then lowered to attach them to the lower sample holder using cyanoacrylate adhesive. The tests were performed in a hydrated environment at 37 °C.

Additionally, Second Harmonic Generation (SHG) imaging was employed to visualize the microstructure of the cartilage and hydrogels.

Table 1: Testing procedures for the qualitative characterization of the material behavior (n = 1).

Procedures	Loading mode	Loading profile	nominal strain	Strain rate in1/s	cycles	material
I Cyclic compression	Compression	sinusoidal triangle	0.15	0.13	ten	ChondroFiller^{liquid} ADA-GEL Cartilage
II Cyclic tension	Tension	sinusoidal	0.025	0.13	ten	ChondroFiller^{liquid} ADA-GEL Cartilage
III Cyclic compression -tension	compression and tension	sinusoidal	0.15	0.13	ten	ChondroFiller^{liquid} ADA-GEL
IV Stepwise increasing max. strain	compression and tension Compression	sinusoidal triangle	0.15; 0.20; 0.25 0.10; 0.20	0.13	three each cycle	ChondroFiller^{liquid} ADA-GEL Cartilage
V Recovery	Compression	sinusoidal triangle	0.15	0.13	three	ChondroFiller^{liquid} ADA-GEL Cartilage
VI Stress relaxation	compression and tension Compression	sinusoidal	0.05; 0.10; 0.15	highest possible loading speed (6000 µm/s)	one	ChondroFiller^{liquid} ADA-GEL Cartilage

Table 2: Combined testing protocol for material parameter identification (ChondroFiller^{liquid}: n = 9, ADA-GEL: n = 8, Cartilage: n = 3).

Protocol for combined testing	ChondroFiller^{liquid} and ADA-GEL				Cartilage			
	nominal strain	cycles	holding time in s	velocity in µm/s	nominal strain	cycles	holding time in s	velocity in µm/s
cyclic compression and tension	0.1	3	-	500	0.01	3	-	500
cyclic compression and tension	0.2	3	-	500	0.025	3	-	500
stress relaxation in compression	0.15	-	150	6000	0.05	-	1000	6000
stress relaxation in tension	0.15	-	150	6000			-	

3.3 Parameter Identification

3.3.1 Time-Independent Hyperelastic Parameter Identification

Based on the experimental data from publication *I*, the time-independent material behavior was examined by identifying hyperelastic material parameters for the conditioned and unconditioned material response (see Figure 9). Furthermore, the pros and cons of direct vs. inverse parameter identification were evaluated, and the behavior of material models if only one loading mode is used for calibration was investigated.

A segment of the previously generated experimental data, shown in Figure 9, was taken to determine the hyperelastic material parameters. The unconditioned material response is represented by the first cycle of the compression-tension loading, and the conditioned response is represented by the average between loading and unloading during the third loading cycle, as illustrated in Figure 9.

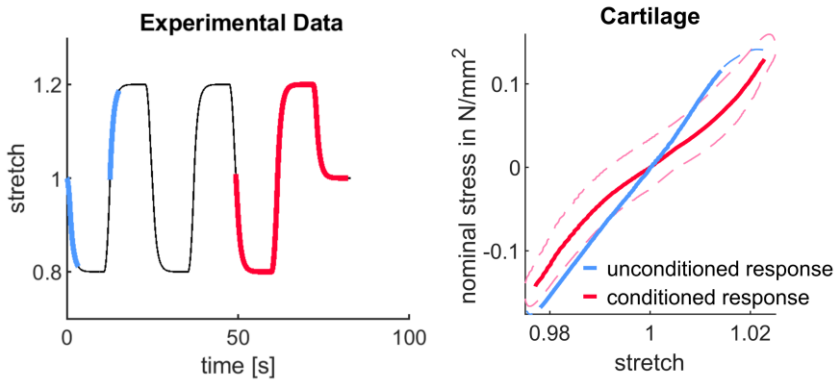

Figure 9: left) The graph shows the relationship between stretch and time for cyclic loading in compression and tension, with minimum and maximum stretches of 0.8 and 1.2. During the first cycle, the compression and tension loading curves (in blue) were used to determine the unconditioned set of parameters. The entire third cycle in compression and tension (in red) served as the basis for determining the conditioned material parameters.
right) Experimental data of human cartilage (left, $n = 3$) utilized for parameter identification. The unconditioned response, as represented by the loading curve during the first cycle, is shown in blue. The conditioned response, as represented by the average between loading and unloading (dashed red line) during the third loading cycle, is displayed in red. Adapted from [73], https://creativecommons.org/licenses/by-nc-nd/4.0/, Copyright © 2022 Elsevier B.V.

For the investigation, common material models in the literature that was also available in COMSOL Multiphysics® v. 5.6. were used and compared for their suitability to represent the nonlinear time-independent behavior of cartilage, ADA-GEL, and ChondroFiller^{liquid}.

The material models to be investigated were the Ogden 1 term model, the Ogden 2 term model, the neo-Hookean model, the Yeoh model, the Mooney-Rivlin 2 terms model, the Mooney-Rivlin 5 terms model, and the Arruda-Boyce model. Isotropy and incompressibility were assumed. The detailed theory of the material laws was presented in publications *II* and *III*.

The hyperelastic models can be expressed in terms of stretches or invariants. The Ogden model is expressed in terms of the principal stretches λ_1, λ_2, and λ_3, has the strain energy function

$$\Psi_{\text{Ogden}} = \sum_{p=1}^{N} \frac{\mu_p}{\alpha_p} \left(\lambda_1^{\alpha_p} + \lambda_2^{\alpha_p} + \lambda_3^{\alpha_p} - 3 \right) \tag{1}$$

where μ_p are the shear moduli and α_p are the non-linearity parameters.

The Mooney-Rivlin model, also known as the polynomial model, is expressed in terms of the invariants. In the case of incompressibility, the third invariant $I_3(C)$ is omitted, and the strain energy function $\Psi(I_1, I_2)$ depends only on $I_1(C)$ and $I_2(C)$. The general formulation for the strain energy function, according to Rivlin, is defined as [108]

$$\Psi_{\text{Mooney-Rivlin}} = \sum_{i,j=0}^{N} C_{i,j} \left(I_1 - 3 \right)^i \left(I_2 - 3 \right)^j \ . \tag{2}$$

The neo-Hookean material model is the most straightforward hyperelastic material model, and it can be derived as a specific case of both the Ogden model (equation (5)) and the Mooney-Rivlin model (equation (10)). When dealing with incompressible materials, the strain energy function

$$\Psi_{\text{neo-Hookean}} = \frac{1}{2} \mu \left(I_1 - 3 \right) \tag{3}$$

only includes the first invariant I_1 and the shear modulus [108].

The Yeoh model is a modified version of the polynomial model with a three-term expansion, including higher-order terms for $I_1(C)$ to better represent nonlinear material behavior. The Yeoh model is described by the strain energy function [109]

$$\Psi_{\text{Yeoh}} = c_1 \left(I_1 - 3 \right) + c_2 \left(I_1 - 3 \right)^2 + c_3 \left(I_1 - 3 \right)^3 \tag{4}$$

where c_1, c_2, and c_3 are material constants.

The Arruda Boycce model is based on an eight-chain network with only two parameters, namely the initial modulus and limiting chain extensibility with

$$\Psi_{\text{Arruda}} = \mu \sum_{i=1}^{N} c_i \left(I_1^i - 3^i \right). \tag{5}$$

Assuming homogeneous deformation, a direct approach to parameter identification was compared with an inverse parameter identification where the realistic boundary conditions of the experiment were simulated using a two-dimensional and axisymmetric finite element model in COMSOL Multiphysics® v. 5.6 consisting of a triangular mesh (see Figure 10).

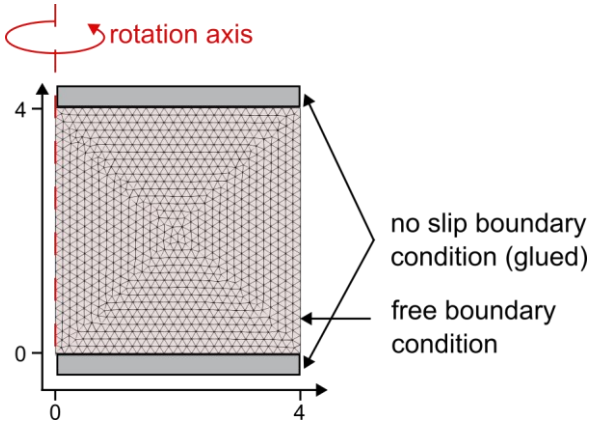

Figure 10: Illustration of a triangulated meshed two-dimensional axisymmetric finite element model with applied boundary conditions. From [73], https://creativecommons.org/licenses/by-nc-nd/4.0/, Copyright © 2022 Elsevier B.V.

A schematic of the direct and inverse parameter identification is shown in Figure 11. In the direct parameter identification, the analytically determined reaction forces F_{mod} for hyperelastic material models were incorporated in MATLAB, and the non-linear least square solver (lsqnonlin) with the trust-region algorithm was utilized to select an upper and lower bound for the parameters. The parameters were determined by minimizing the difference between the measured reaction forces F_{exp} and the forces F_{mod} calculated with the analytic equations.

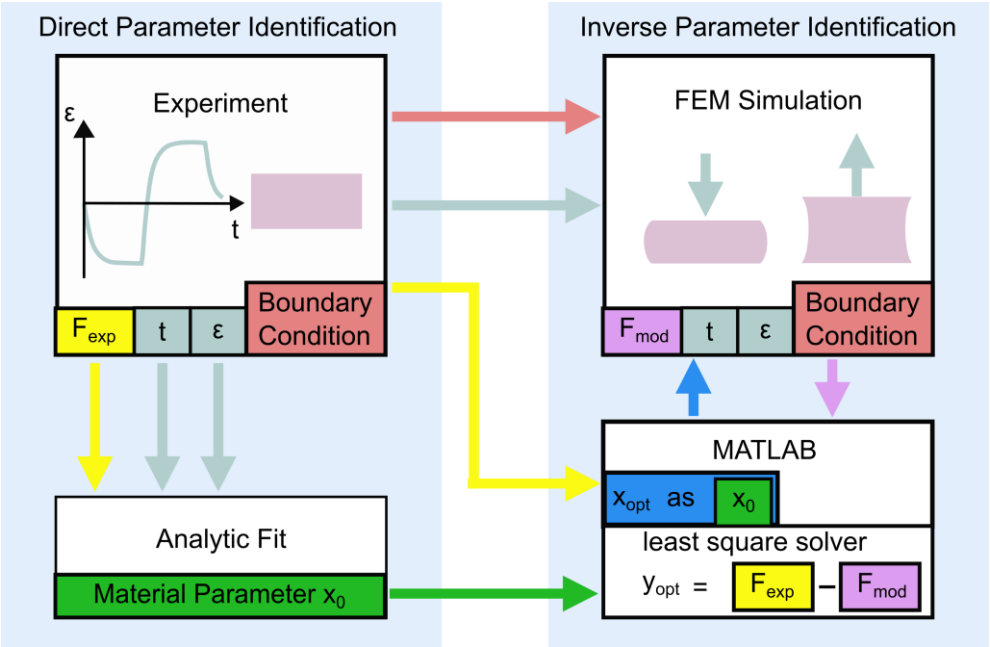

Figure 11: Schematic representation of inverse and direct parameter identification. From [73], https://creativecommons.org/licenses/by-nc-nd/4.0/, Copyright © 2022 Elsevier B.V.

In the inverse parameter identification, the determined parameters from the direct parameter identification were used as starting points and minimized the difference between the reaction forces calculated with a finite element model (illustrated in Figure 11), F_{sim} which captures the exact

experimental sequence with its displacements and boundary conditions and the experimental reaction forces F_{exp}. The reaction force F_{sim} was passed to the least square solver lsqnonlin in MATLAB to minimize the objective function $F(x)$, given by

$$\min_{x} \left\| \mathrm{F(x)} \right\|_2^2 = \sum_{i=1}^{N} F^2(x) = \sum_{i=1}^{N} \left(F_{\mathrm{exp}} - F_{\mathrm{sim}} \right)_i^2 \tag{6}$$

to identify the material parameters x_{opt}.

3.3.2 Time-Dependent Hyper-Viscoelastic Parameter Identification

For the inverse parameter identification of the hyper-viscoelastic material model presented in detail in publication *III,* the entire loading history, including all cycle loading and stress relaxation, was considered.

Two parameter sets were determined separately to depict the unconditioned and conditioned material response of human cartilage, ADA GEL, and ChondroFiller$^{\mathrm{liquid}}$. This was achieved using the first and third loading cycles of cyclic loading, respectively. Following the same approach as for the hyperelastic material parameter identification, the material parameters x_{opt} were identified by utilizing the least square solver in MATLAB (see Figure 12).

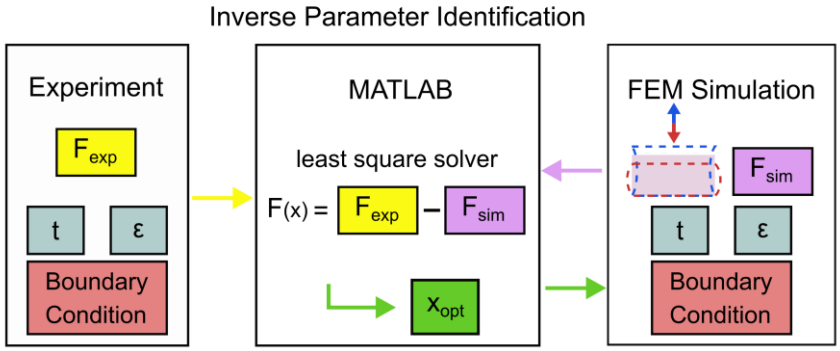

Figure 12: Diagram illustrating the process of inverse parameter identification. From [79], https://creativecommons.org/licenses/by/4.0/, Copyright © 2023 Elsevier B.V.

4 Results and Discussion

The following chapter contains an abstract of the results and a discussion of three publications underlying the publication-based dissertation. A summary and assessment of the objectives of each study is provided. A full description of the work performed, observations, reasoning, and conclusions can be found in the publications *I*, *II,* and *III*.

4.1 Mechanical Behavior and Microstructure

Recoverability

The qualitative analysis of the recoverability revealed a full recovery of cartilage and ADA-GEL within a period of one hour after cyclic compressive loading with 15 % nominal strain, as shown in Figure 13. Therefore, the conditioning behavior and hysteresis were attributed to reversible visco- and poroelastic effects. In contrast, ChondroFiller^{liquid} recovered only 70 % after one hour and showed in the second harmonic imaging a crack formation (see Figure 15).

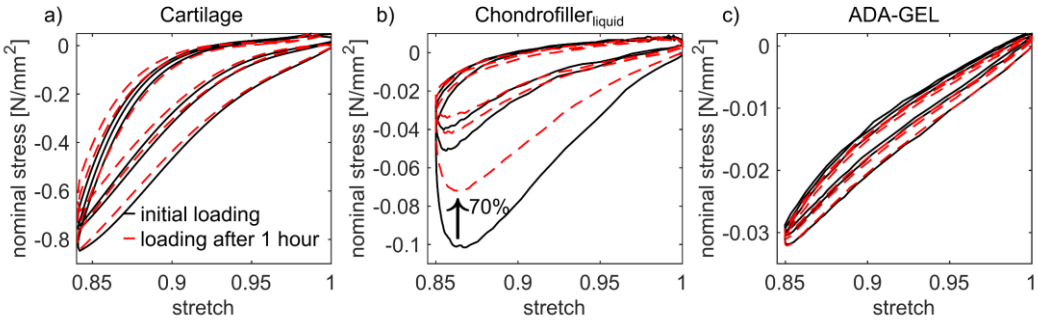

Figure 13: Representative nominal stress versus stretch behavior of a) human cartilage, b) ChondroFiller^{liquid}, and c) ADA-GEL for two unconfined compression tests with three cycles each and 15 % nominal strain, separated by a 60 min recovery period. From [85], https://creativecommons.org/licenses/by-nc-nd/4.0/, Copyright © 2020 Elsevier B.V.

Conditioning

All materials had a pronounced viscoelastic conditioning behavior with each cycle and also with introducing a new strain level. An example of a stress-stretch curve for cyclic compression loading is shown in Figure 14. The hysteresis area of the stress-stretch curve represented the dissipated energy during each loading cycle and decreased notably between the first and second loading cycle and after the third cycle marginally for all materials.

Nonlinearity

Previous results in the literature report that stiffening occurs in a fibrillar network under tensile loading due to mobilization of fibers [62] [110]. Consistent with the literature, stiffening under increasing strain is also observed in ChondroFiller^{liquid} and cartilage, which both have fibrous components. In the case of ADA-GEL, which, in contrast to cartilage and ChondroFiller^{liquid}, does not contain fibrous components,

the strain stiffening is less pronounced (see Figure 14). According to the literature, pure gelatin exhibits an almost linear stress-strain behavior and no significant differences in tensile and compressive loading [111] [112] [24]. For ADA-GEL, it can be assumed that the linear deformation contribution of gelatin superimposes the nonlinear contribution of alginate since concentration-dependent nonlinearity has already been observed in ALG-GEL hydrogels [111]. Furthermore, the enzymatic crosslinking by microbial transglutaminase enhances the network formation of the GEL phase [113], which further explains the more prominent linear compressive-tensile behavior compared to cartilage and ChondroFiller^{liquid}. By specifically changing the concentration and cross-linking, the behavior of ADA-GEL could be adjusted to more closely mimic the mechanical behavior of cartilage and ChondroFiller^{liquid}.

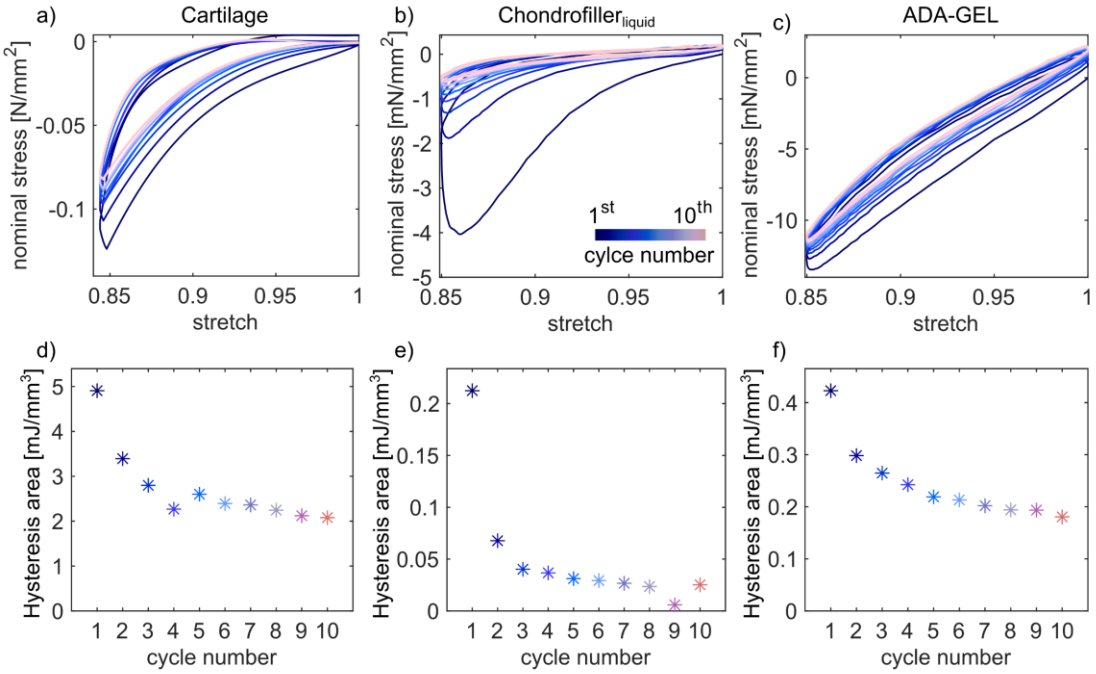

Figure 14: a-c) Representative conditioning behavior in unconfined cyclic compression for cartilage, ChondroFiller^{liquid}, and ADA-GEL with a nominal strain of 0.15, corresponding to a stretch of 0.85; d-f) Hysteresis area as a function of the loading cycle number for cartilage, ChondroFiller^{liquid}, and ADA-GEL. The hysteresis area of the stress-stretch curve represents the dissipated energy during each loading cycle. From [85], https://creativecommons.org/licenses/by-nc-nd/4.0/, Copyright © 2020 Elsevier B.V.

Viscoelastic Behavior

All materials showed viscoelastic behavior in stress relaxation tests. During stress relaxation experiments, ChondroFiller^{liquid} showed the fastest stress relaxation, followed by ADA-GEL, while cartilage exhibited the slowest stress relaxation. The viscosity in hydrogels and in cartilage is due to two different effects: first, to energy dissipation in the collagen-protein matrix, and second, to fluid movement relative to the solid matrix. In this regard, previous studies have shown that in cartilage, both the fibrillar collagen components and the protein matrix individually showed viscoelastic behavior [37] [114] [36]. As previously illustrated in Chapter 1, stress relaxation and mechanical behavior, in general, is an important indicator for assessing the suitability of a hydrogel scaffold for cell embedding in cartilage

engineering. Lee et al. [24] showed that fast relaxing hydrogels promote the formation of cartilage matrix. As a result, modification of the hydrogels to a faster stress relaxation could stimulate ECM formation [24]. As already indicated in Chapter 1, the change in viscoelastic behavior is also connected with functional effects, such as in osteoarthritis or the proteoglycan content in the ECM [24] [36]. Although the ADA-GEL hydrogel system studied here exhibits slower stress relaxation behavior than ChondroFiller^{liquid}, it is possible to adjust not only the degradation and 3D printability (compare chapter 1.4) but also to tune to faster stress relaxation by changing the type of crosslinking and the polymer concentration or by adding cells or molecular spacers [115] [112] [111] [24]. ADA-GEL has a variety of chemical crosslinks (see Figure 6), such as ionic (Ca2+), covalent (enzymatic), and reversible-covalent (Schiff's base) [113]. For instance, a reduction in covalent cross-links or replacement with ionic crosslinks can induce faster stress relaxation [115]. An investigation with alginate-gelatine hydrogels showed that a decrease in hydrogel concentration also resulted in faster stress relaxation [111]. The stress relaxation of ADA-GEL can also be accelerated by embedding high cell numbers (> 6 Mio.ml^{-1}) [112].

Microstructure

All materials had a tension-compression asymmetry (see Figure 16) in which cartilage showed greater stresses under tensile loading than under compressive loading. In contrast, ADA-GEL and ChondroFiller^{liquid} showed an opposite trend with higher stresses in compression. Based on the findings in the SHG imaging, it was concluded that ChondroFillerliquid and cartilage both have fibrous structures, and ADA-GEL is exclusively non-fibrous, as shown in Figure 15. In literature, it is reported that fibrillar materials exhibit lower stresses in compression than in tension, as shown in cartilage. The opposite behavior of the compression-tension asymmetry in ChondroFiller^{liquid} could be attributed to the underlying biphasic microstructure, which exhibits a layered arrangement of 40 % fibrillar and 60 % non-fibrillar phases with a preferred fiber orientation of ~ -45° to the hydrogel surface (Figure 15). Since with a volume fraction of 60%, the non-fibrillar fraction predominated in ChondroFiller^{liquid}, it can be assumed that the compression-tension asymmetry is dominated by the behavior of the non-fibrillar component. This aligns well with previously published data for non-fibrillar materials in the literature [111].

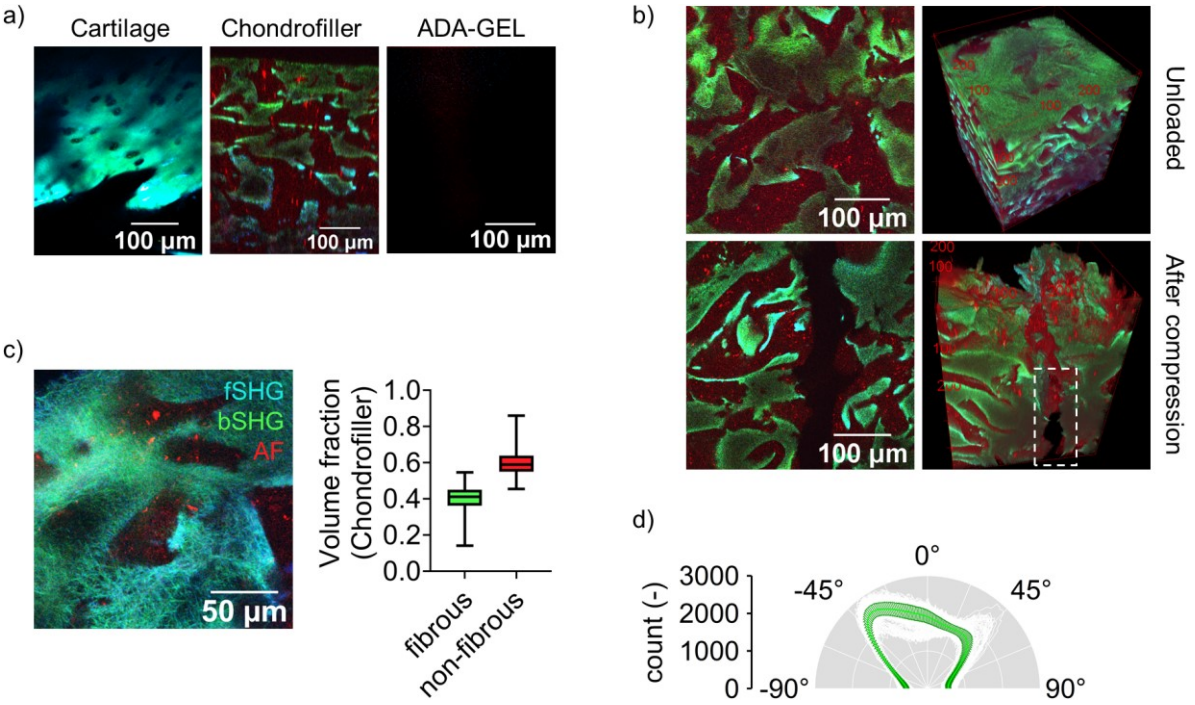

Figure 15: Multiphoton microscopy images of cartilage, ChondroFiller^{liquid}, and ADA-GEL. a) Images captured using two-photon microscopy showing autofluorescence in red and Second Harmonic Generation in green and teal of hyaline cartilage (in-plane), ChondroFiller^{liquid} (cross-sectional), and ADA-GEL (in-plane, 450 µm depth). ADA-GEL was largely transparent without any fibrous structures. b) Close-up images of ChondroFiller^{liquid} in its unloaded state and after loading show a crack formation (white dashed line). c) Detail two-photon images of ChondroFiller^{liquid} with visible fibrous structure (bSHG, fSHG). Box plots showing the quantification (n = 3) of fibrous (bSHG and fSHG) and non-fibrous ChondroFiller^{liquid} hydrogel volume fractions, with the mean (horizontal line) and whiskers representing minimum and maximum values. d) Angles of fiber orientations, mean ± SD, data traces for each slice evaluated (white, 745 slices, n = 3 stacks) analyzed using ImageJ. From [85], https://creativecommons.org/licenses/by-nc-nd/4.0/, Copyright © 2020 Elsevier B.V.

4.2 Data for Parameter Identification

To generate a comprehensive data set for reliable material parameters for numerical simulations based on the qualitative analysis, a combined testing protocol was developed (see Table 2) to capture the main characteristics identified in the qualitative assessment. On this basis, the combined tests included two different loading modes and different loading conditions, such as cyclic tests with three cycles in compression and tension, with different strain levels, as well as stress relaxation tests (see Figure 16). In detail, this means that the combined tests start with three cycles of tension-compression loading at two different strains in order to map the tension-compression asymmetry, the conditioning behavior, and the gradual reduction of the hysteresis area with an increasing number of cycles. In addition, the two strains can be used to capture the nonlinearity at higher strains. The stress relaxation tests identify the time-dependent behavior of the materials.

When designing tests to identify material parameters, it is essential to consider both the mechanical properties (e.g., nonlinearity or viscoelasticity) and the loading conditions that will be applied during the simulations (e.g., loading rates, maximum strains, etc.) [116–118] [63] [61]. It should be noted that at least the loading types and strain levels that occur during the simulations are reflected in the test [63].

Particularly for hydrogels used in surgical implants, large strains (>10 %) can be obtained even at relatively low pressures [15] [119] [120]. Furthermore, it is not sufficient to take only the loading curve when viscoelasticity occurs. It is of particular importance to consider the unloading curve and conduct stress relaxation experiments. The combination of stress relaxation and cyclic experiments allows us to take into account the conditioning effects and the nonlinearities and thus significantly improve the viscoelastic parameterization, e.g., the relaxation times.

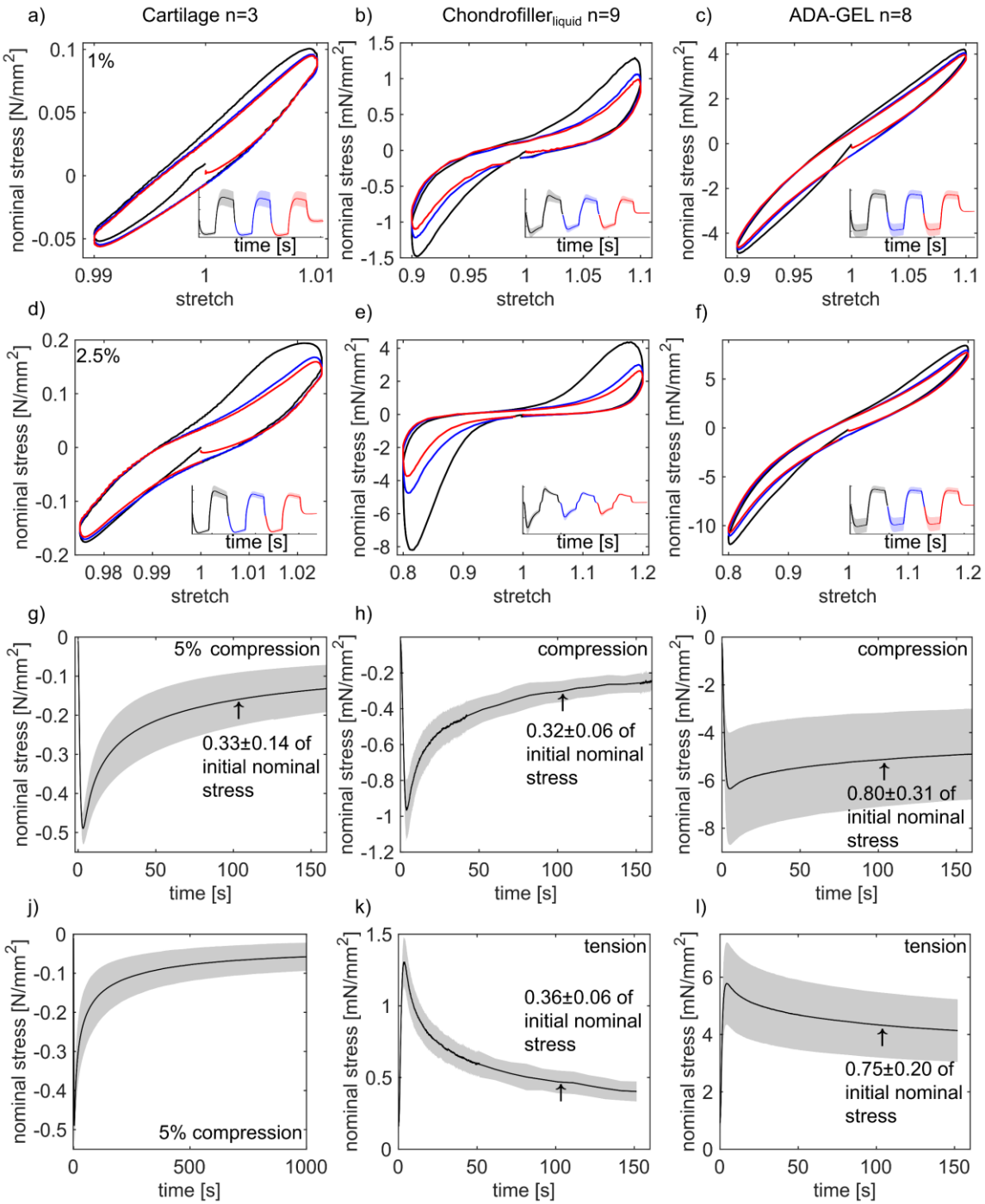

Figure 16: The mechanical response, including its average value and the corresponding standard deviation (represented by shaded areas), for the testing protocol outlined in Table 2.: a) to c) cyclic compression-tension tests with a maximum nominal strain of 0.01 for human cartilage and 0.1 for ChondroFiller^{liquid} and ADA-GEL, and three cycles each. d) to f) cyclic compression-tension tests with a maximum nominal strain of 0.025 for human cartilage and 0.2 for ChondroFiller^{liquid} and ADA-GEL, with three cycles for each. g) to i) stress relaxation tests in compression with a maximum nominal strain of 0.05 for human cartilage and 0.15 for ChondroFiller^{liquid} and ADA-GEL, with a holding time of 150 seconds. j) stress relaxation tests of human cartilage with a holding time of 1,000 seconds. k) to l) stress relaxation tests in tension with a maximum nominal strain of 0.15 for ChondroFill ChondroFiller^{liquid} and ADA-GEL, with a holding time of 150 seconds. From [85], https://creativecommons.org/licenses/by-nc-nd/4.0/, Copyright © 2020 Elsevier B.V.

4.3 Numerical Modelling

Based on the experimental data from the experiments of publication *I*, time-independent hyperelastic material parameters were identified, and different methodologies were evaluated in publication *II*. In the second step, the time-dependent parameters for the conditioned and unconditioned material response were identified (see publication *III*).

4.3.1 Time-Independent Hyperelastic Parameter Identification

For the time-independent parameter identification, the conditioned and unconditioned material response of the individual materials was considered. The corresponding data with standard deviation for the conditioned parameter set is illustrated in Figure 17.

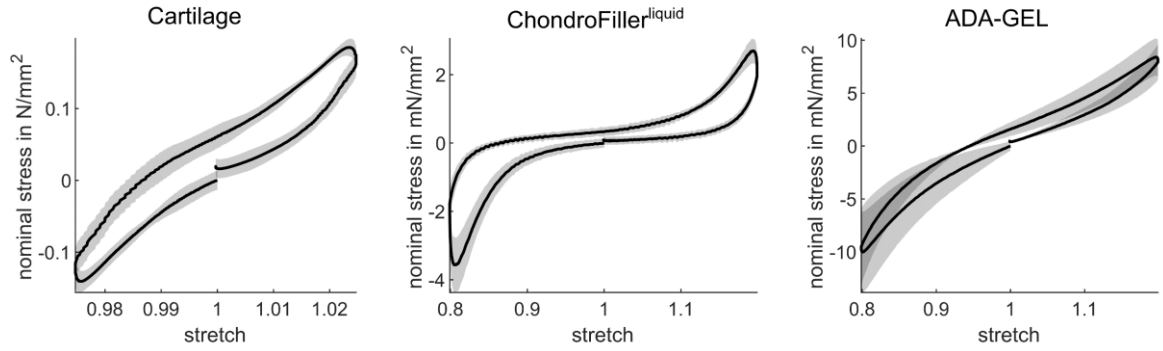

Figure 17: Experimental data from human cartilage, ChondroFiller^{liquid}, and ADA-GEL, including the standard deviation, used for determining parameters. From [73], https://creativecommons.org/licenses/by-nc-nd/4.0/, Copyright © 2022 Elsevier B.V.

In a systematic study, summarized in Figure 18, the effect of considering only compression, only tension data, or both data simultaneously for parameter identification is shown. The results are significantly improved when all loading modes are considered, and in addition, previous studies show that the sensitivity towards the settings of the fitting procedure can be reduced by considering multiple experimental loading conditions simultaneously [121] [122]. Therefore, the sensitivity to the loading modes used for calibration is highly dependent on the particular material model, i.e., how many tests are required to establish reliable model parameters for a particular material. The required number of tests depends on the number of invariants when the model is formulated in terms of invariants [123]. This agrees well with the findings in publication *II* since the neo-Hookean, the Arruda-Boyce, and the Yeoh models revealed a low sensitivity towards the loading modes used for calibration. In contrast, the Mooney-Rivlin models and the Ogden models cannot predict the response of a loading mode that was not used for calibration.

Furthermore, it should be noticed that all materials showed a tension-compression asymmetry, as previously discussed in Chapter 4.1, and this can only be captured if multiple loading modes are considered simultaneously in the parameter identification.

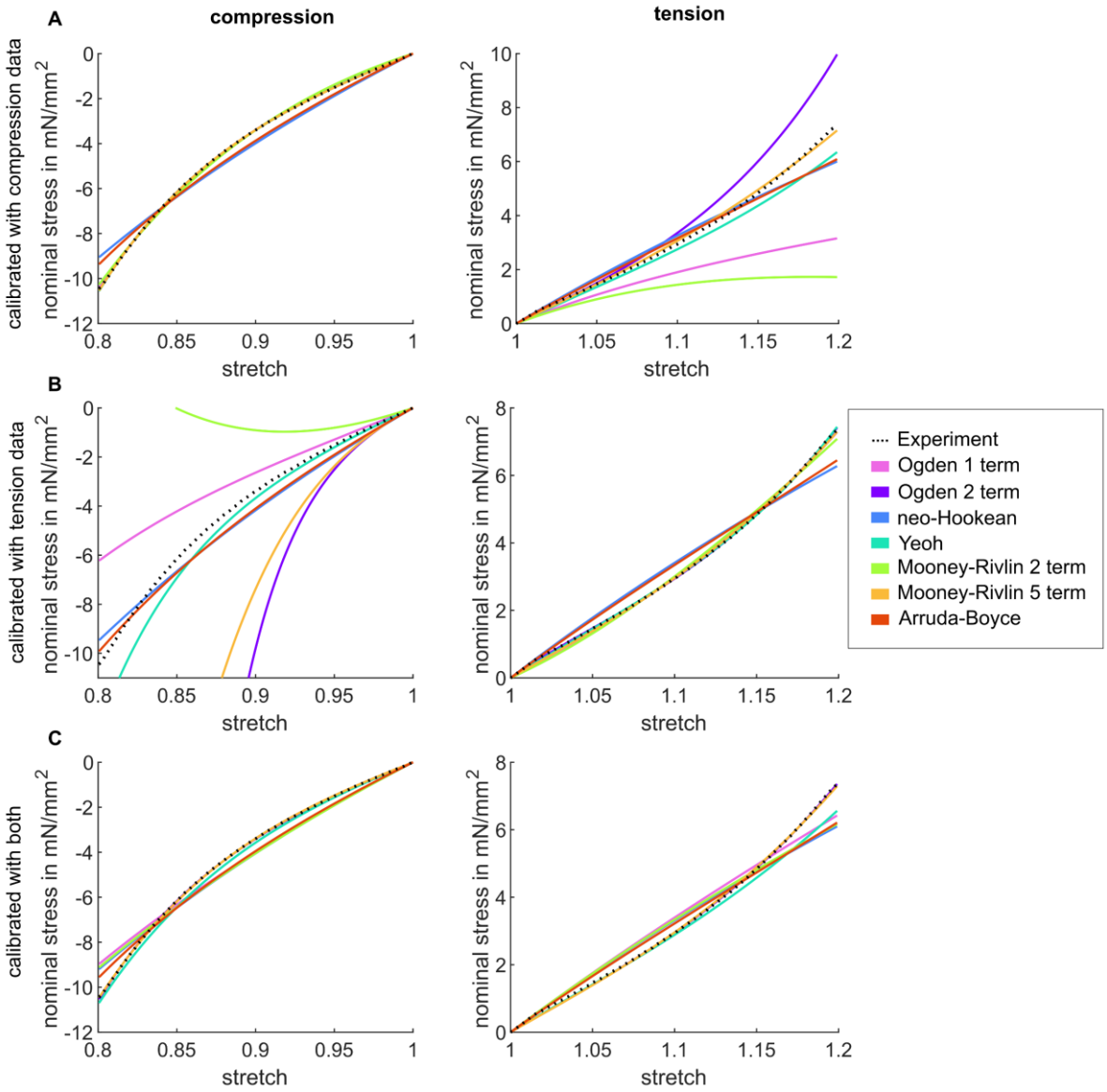

Figure 18: Direct material model calibration based on compression and tension data, exemplary carried out for ADA-GEL. A) Calibration with compression data only. B) Calibration with tension data only. C) Calibration using tension and compression data simultaneously. From [73], https://creativecommons.org/licenses/by-nc-nd/4.0/, Copyright © 2022 Elsevier B.V.

For each of the three materials, the inverse parameters for all mentioned isotropic hyperelastic material models were determined. Figure 21, Figure 20, and Figure 19 show the capability of different isotropic hyperelastic material models to represent the unconditioned and conditioned material response of ADA-GEL, cartilage, and ChondroFiller^{liquid}.

Cartilage

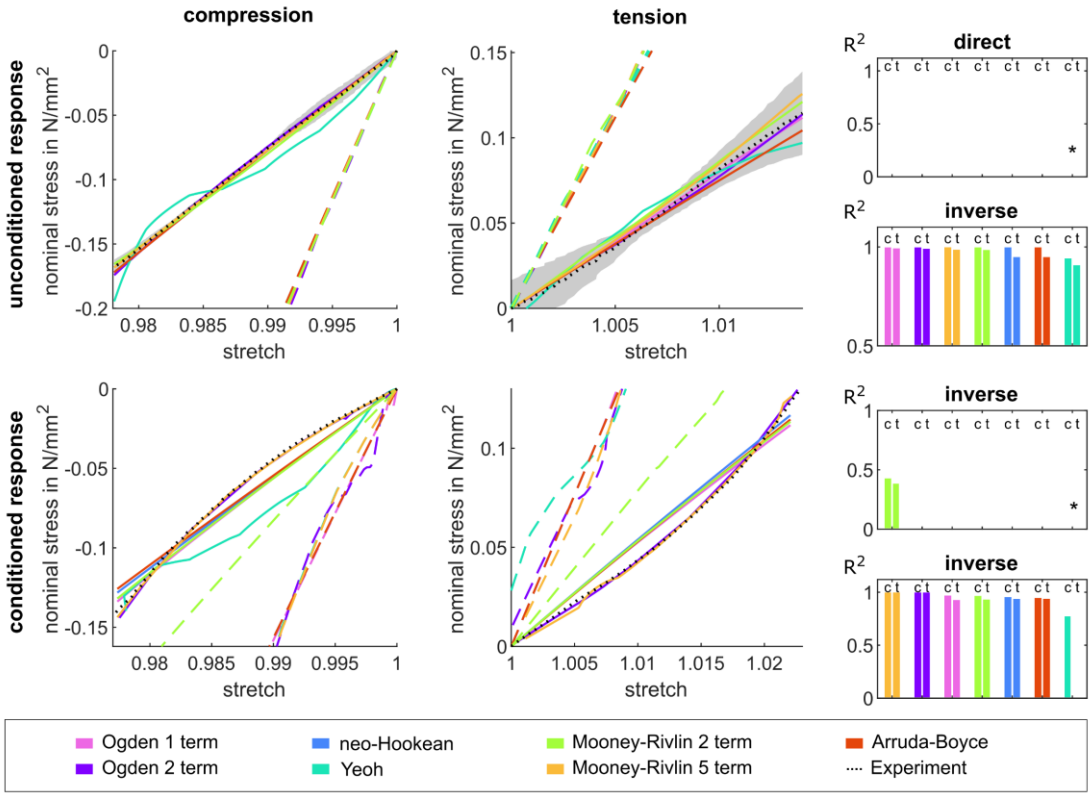

Figure 19: Evaluation of material models using directly identified parameters (dashed lines) and inversely identified parameters (solid lines) for the unconditioned and conditioned material response in compression (left) and tension (center) of cartilage. The experimental data is depicted as dotted lines. The R^2 values for each material model, arranged from best to worst, are displayed on the right. *The R^2 values in compression and tension are 0 for all models except for the Mooney-Rivlin 2-term model in the unconditioned response. From [73], https://creativecommons.org/licenses/by-nc-nd/4.0/, Copyright © 2022 Elsevier B.V.

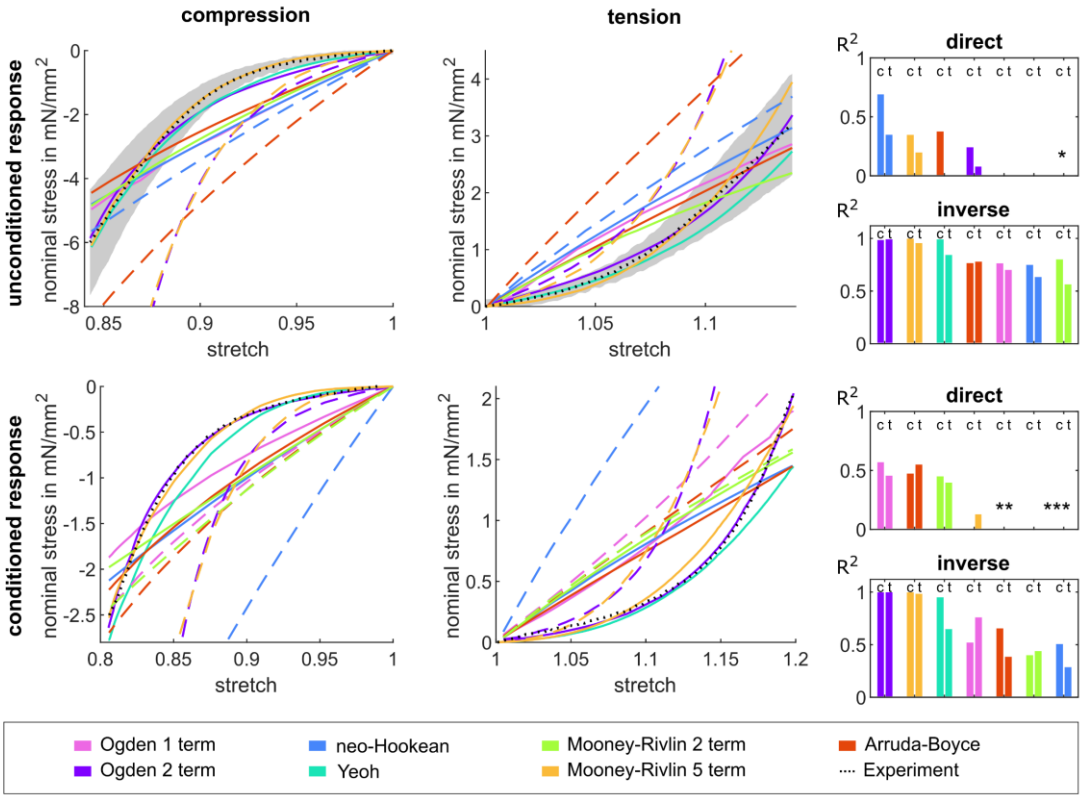

Figure 20: Evaluation of material models using directly identified parameters (dashed lines) and inversely identified parameters (solid lines) for the unconditioned and conditioned material response in compression (left) and tension (center) of ChondroFiller^{liquid}. The experimental data is depicted as dotted lines. The R^2 values for each material model, arranged from the best to the worst outcome, are displayed on the right. * The simulation did not converge for the Ogden 1-term, Yeoh, and Mooney-Rivlin 2-term models and parameters obtained through direct parameter identification. ** The simulation did not converge for the Yeoh model, and parameters were obtained through direct parameter identification. *** The R^2 values in compression and tension are 0 for the Ogden 2-term and neo-Hookean models. From [73], https://creativecommons.org/licenses/by-nc-nd/4.0/, Copyright © 2022 Elsevier B.V.

ADA-GEL

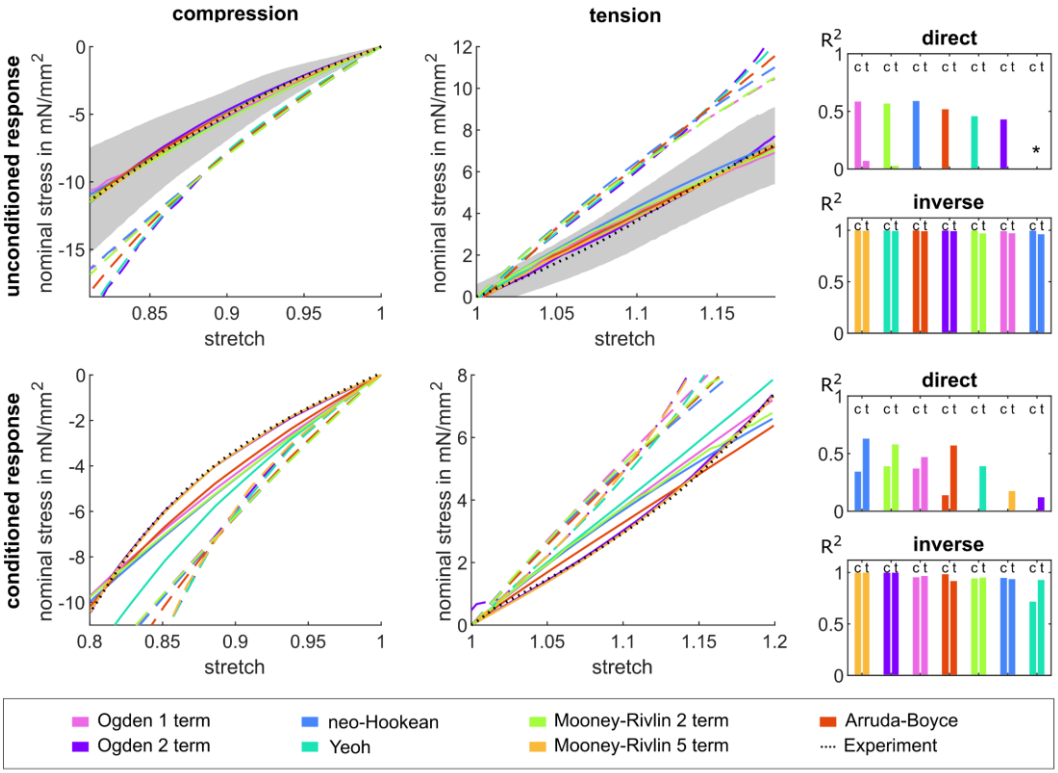

Figure 21: Performance of material models with directly (dashed lines) and inversely (solid lines) identified parameters for the unconditioned and conditioned material response in compression (left) and tension (center) of ADA-GEL. The experimental data is shown as a dotted line. The corresponding R^2 values for each material model, ordered from best to worst, are presented on the right. *Simulation did not converge for the Mooney-Rivlin 5-term model and direct parameter identification. From [73], https://creativecommons.org/licenses/by-nc-nd/4.0/, Copyright © 2022 Elsevier B.V.

The result of the investigation was that the Ogden 1 term and Ogden 2 term models best represent the unconditioned and conditioned material response of cartilage, respectively. For ADA-GEL, the Mooney-Rivlin 5-term model is the most appropriate for an unconditioned and conditioned material response. For ChondroFiller^{liquid}, both the conditioned and unconditioned responses are well represented by the Ogden 2-term and Mooney-Rivlin 5-term models.
To evaluate how the parameters of the direct parameter identification perform in the simulation, the experiment with the parameters of the direct parameter identification was simulated and compared with the experimental dataset. The directly identified material parameters overestimated the stresses in both compression and tension not only for ADA-GEL but also for ChondroFiller^{liquid} and especially for cartilage. This is due to the different boundary conditions, which turn out to be a non-negligible effect. The increased error for cartilage could be due to the low height of the cartilage samples. The low height of the cartilage samples resulted in even more inhomogeneous deformations than with ADA-GEL or ChondroFiller^{liquid}. The reaction force in the axial direction is higher for a specimen fixed at the top and bottom than for a specimen under unconfined conditions. Hence, the parameters determined with direct parameter identification result in an overestimation of the stresses. Therefore, it can be concluded that direct parameter identification is not sufficient to determine the parameters for a FE model. However, it should be noted that the conditions of the test determine whether a direct parameter identification should be used or not. The prerequisite for direct parameter identification is a homogeneous deformation as it is given, for example, in a tensile test with a correspondingly long specimen length or a biaxial tensile test, as described in [40] [124].

From the experiments, two sets of parameters reflecting two different situations were obtained. The unconditioned parameter sets represent a fast and hyperelastic material response without fluid leakage upon deformation of the hydrogel or cartilage. At the application level for cartilage in the human body, the unconditioned behavior is characterized by activities such as running and jumping where impact loading occurs. It is known from the literature that the elastic modulus of cartilage is not significantly changed above a strain rate of 0.05 1/s [42]. Hence, this study focuses on investigating the cartilage behavior under a strain rate of 0.2423 1/s.

The conditioned parameter set is obtained in the third cycle of loading, and the results of publication I show that the hysteresis and conditioning remain nearly constant after the third cycle. Since the hysteresis of viscoelastic materials disappears at slow static loading, the average stress-strain curve was obtained from loading and unloading during the third cycle. In the conditioned material response, it is assumed that the dominant interaction of the matrix molecules leads to a non-linear stress-strain relationship. From the application point of view, this kind of behavior occurs during sustained loads such as standing and sitting or during repetitive cyclic loads such as walking. In these cases, the thickness of the cartilage decreases, and strains of 2-6 % can occur [38]. The conditioned shear modulus was lower for all materials compared to the unconditioned shear modulus. In this regard, compared to the literature, the shear modulus determined ranged from 443.5194 kPa to 868.5304 kPa, which agrees well with the literature with values of 200 and 2500 kPa [125].

4.3.2 Time-Dependent Hyper-Viscoelastic Parameter Identification

Performance of Hyper-Viscoelastic Material Models

Multiple loading modes were used simultaneously to determine hyper-viscoelastic parameters to capture the conditioned and unconditioned response of human articular cartilage, ADA-GEL, and ChondroFillerliquid. These included tension and compression, cyclic loading, and stress relaxation under three strain levels of 10 %, 15 %, and 20 % nominal strain for the two hydrogels and 1 %, 2.5 %, and 5 % nominal strain for cartilage. The results for cartilage, ADA-GEL, and ChondroFillerliquid of the parameter identification are presented in Figure 24, Figure 22, and Figure 23, as well as Table 3, Table 4, and Table 5.

As illustrated in Figure 23, hyper-viscoelastic laws can accurately describe the material behavior of ChondroFiller^{liquid} up to a deformation of 10 %. At strains above 10 %, irreversible deformation occurs and requires the use of more advanced material laws. Furthermore, hyper-viscoelastic material models in COMSOL Multiphysics® v. 5.6 represent conditioning and stress relaxation well. Nevertheless, the first cycle stiffness and hysteresis in the experiment are predicted to be lower in the simulation. Hyperelastic material behavior is characterized by asymmetric behavior in tension and compression as well as pronounced non-linearity. For ChondroFiller^{liquid} and for cartilage, the 2-term model of Ogden and for ADA-GEL, the 5-term model of Mooney-Rivlin was chosen, which, according to publication II, best modeled the equilibrium response.

Cartilage

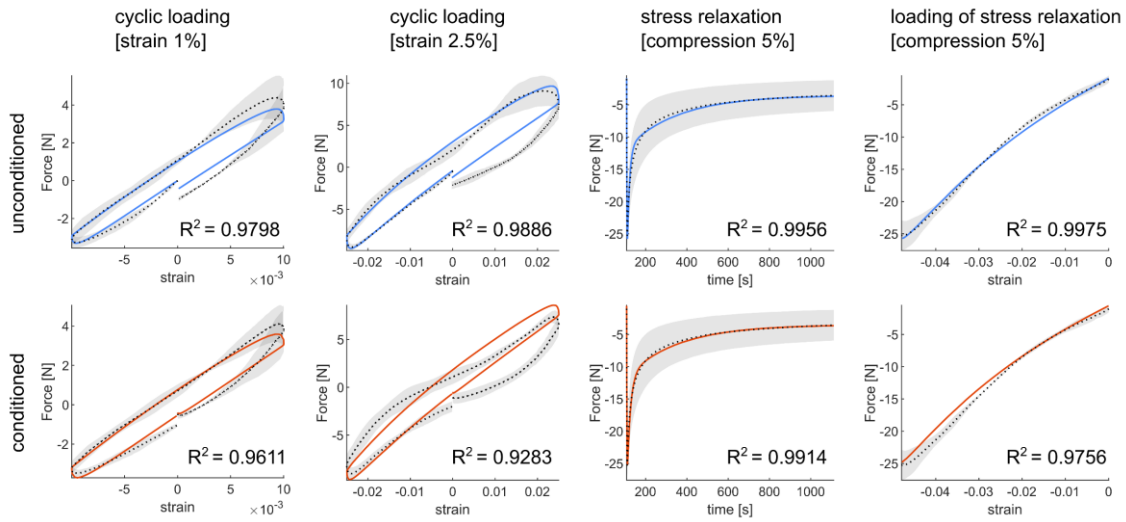

Figure 22: Evaluation of the hyper-viscoelastic model, which is based on the Ogden 2 term hyperelastic model with two viscoelastic elements, to capture the average experimental data of cartilage (represented by the black dashed line with standard deviations shown in shaded grey) for the unconditioned (represented by the blue line at the top) and conditioned (represented by the red line at the bottom) material responses with R^2 as the coefficients of determination. From [79], https://creativecommons.org/licenses/by/4.0/, Copyright © 2023 Elsevier B.V.

Table 3: Hyper-viscoelastic parameters and equilibrium shear modulus μ_∞ for the conditioned and unconditioned material response of cartilage with corresponding coefficients of determination R^2. From [79], https://creativecommons.org/licenses/by/4.0/, Copyright © 2023 Elsevier B.V.

cartilage	hyperelastic parameters					viscoelastic parameters				
	μ_1 in kPa	α_1 in kPa	μ_2 in kPa	α_2 in kPa	μ_∞ in kPa	β_1	τ_1 in s	β_2	τ_2 in s	R^2
unconditioned	15.2937	2.9410	-9.3880	-15.6655	96.0226	5.2909	10.5890	2.3071	250.4918	0.9824
conditioned	14.7483	2.4451	-9.9874	-15.3257	94.5621	4.8260	15.6480	2.2891	249.6252	0.9824

ChondroFiller ^{liquid}

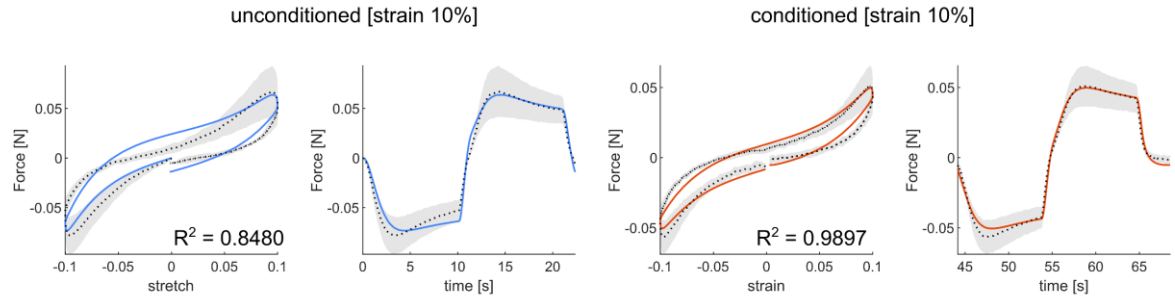

Figure 23: Evaluation of the hyper-viscoelastic model, which is based on the Ogden 2 term hyperelastic model with two viscoelastic elements, to capture the average experimental data of ChondroFiller^{liquid} (represented by the black dashed line with standard deviations shown in shaded grey) for the unconditioned (represented by the blue line at the top) and conditioned (represented by the red line at the bottom) material responses with R^2 as the coefficients of determination. From [79], https://creativecommons.org/licenses/by/4.0/, Copyright © 2023 Elsevier B.V.

Table 4: Hyper-viscoelastic parameters and equilibrium shear modulus μ_∞ for the conditioned and unconditioned material response of ChondroFiller^{liquid} with corresponding coefficients of determination R^2. From [79], https://creativecommons.org/licenses/by/4.0/, Copyright © 2023 Elsevier B.V.

ChondroFiller^{liquid}	hyperelastic parameters					viscoelastic parameters				
	μ_1 in kPa	α_1 in kPa	μ_2 in kPa	α_2 in kPa	μ_∞ in kPa	β_1	τ_1 in s	β_2	τ_2 in s	R^2
unconditioned	0.0187	22.4476	-0.0247	-18.4281	0.4375	0.9890	3.8227	1.2514	100.5009	0.8480
conditioned	0.0197	22.5983	-0.0200	-16.2780	0.3854	0.6916	6.1978	0.9274	101.1096	0.9107

ADA-GEL

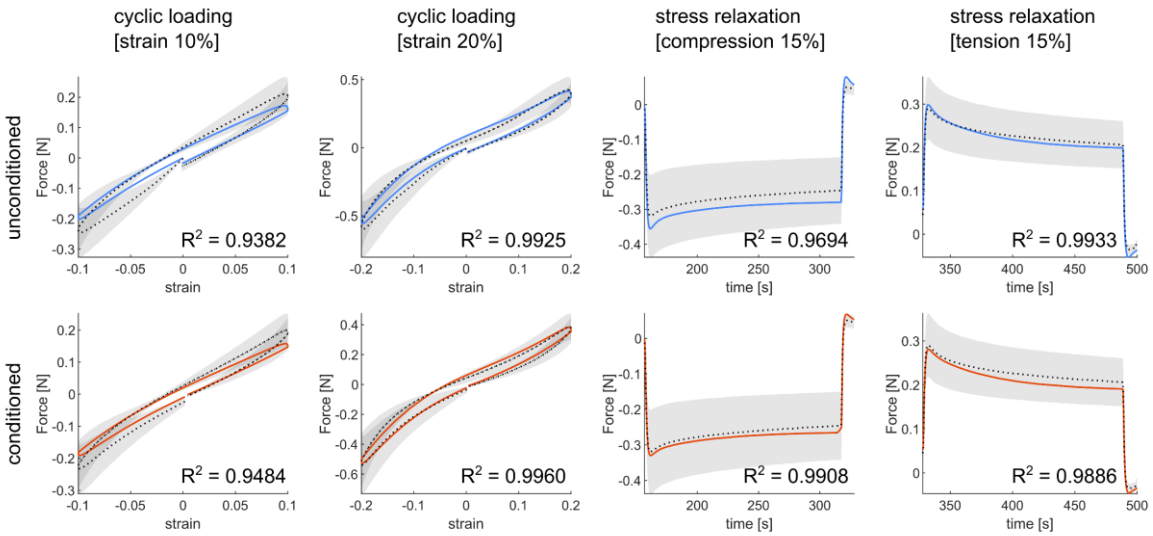

Figure 24: Simultaneous identified hyper-viscoelastic parameters in four loading modes of ADA-GEL with two viscoelastic branches and the Mooney-Rivlin 5-term hyperelastic model. The averaged experimental data (black dashed line) with standard deviations (shaded grey), coefficients of determination R^2 for the corresponding fitted section, and calibrated constitutive models for the unconditioned (blue line) and conditioned (red line) material response. From [79], https://creativecommons.org/licenses/by/4.0/, Copyright © 2023 Elsevier B.V.

Table 5: Hyper-viscoelastic parameters and equilibrium shear modulus μ_∞ for the conditioned and unconditioned material response of ADA-GEL with corresponding coefficients of determination R^2. From [79], https://creativecommons.org/licenses/by/4.0/, Copyright © 2023 Elsevier B.V.

ADA-GEL	hyperelastic parameters						viscoelastic parameters				
	c_{10} in kPa	c_{01} in kPa	c_{11} in kPa	c_{02} in kPa	c_{20} in kPa	μ_∞ in kPa	β_1	τ_1 in s	β_2	τ_2 in s	R^2
unconditioned	2.1264	0.5153	-1.6718	-1.2485	5.6873	5.2834	0.1977	4.7482	0.2097	51.6052	0.9886
conditioned	2.1226	0.3942	-1.6573	-1.1933	5.5141	5.0335	0.1318	4.6654	0.2186	51.2747	0.9861

To capture the viscoelastic effects such as the hysteresis, conditioning, and stress relaxation, the material parameters β_i, which represent the viscoelastic stress components for the non-equilibrium reactions with corresponding time constants τ_i, are additionally determined. Here, two viscoelastic elements are needed to capture the viscoelastic material response of all materials.

The equilibrium shear modulus μ_∞ and the first viscoelastic loss factor β_1 decrease for the conditioned material response compared to the unconditioned material response for all materials, indicating a similar trend (see Table 3, Table 4, and Table 5). When only the conditioned (third) loading cycle is used for parameter identification, the contribution of the unconditioned (first) short-time viscoelastic element to the total loading decreases.

It should be noted that for ChondroFiller^{liquid}, only data of the reversible loading was used. Hence, determining the second time constant and the loss factor is less reliable.

The viscoelasticity is different in all three materials. Cartilage exhibits the greatest viscoelastic dissipation with β_i greater than 1 (see Table 3) and thus the greatest stress relaxation, followed by ChondroFiller^{liquid} and then ADA-GEL. The elastic energy in the material behavior dominates the most in ADA-GEL and is less pronounced in ChondroFiller^{liquid}. Regarding the short-term response of the materials, ChondroFiller^{liquid} and ADA-GEL relax comparatively equally fast, whereas cartilage shows a 2-3 times higher first-time constant τ_1. Furthermore, cartilage takes the most time to reach equilibrium and has the highest time constant τ_2.

ChondroFiller^{liquid} thus resembles cartilage in its viscoelastic material behavior, whereas the elastic material behavior of ADA-GEL is more similar to cartilage.

The influence on embedded cells in a material and the significance of a differentiated consideration of how fast or how much a material relaxes is represented in [126] and [24]: With higher amount of stress relaxation in ADA-GEL hydrogels, cell proliferation, and migration can be increased, according to Hazur et al [126]. Lee et al. [24] showed that the stress relaxation time of ionic cross-linked alginate can be shortened by the addition of polyethylene glycol (PEG) spacers and demonstrated a positive effect on the formation of the chondrocyte matrix and chondrocyte phenotype.

The identified unconditioned and conditioned hyper-viscoelastic parameter set can be used in different application scenarios. It can be purposed to use the unconditioned parameter set rather for initial, dynamic, or in vitro loading. In contrast, the conditioned parameter set is suitable to represent sustained walking, standing, sitting, or in vitro long-term mechanical stimulations in devices such as those presented by Meinert et al. [20]. For cartilage, standing, sitting, or repetitive loading resulting from walking leads to a reduction of cartilage height and strains from 2 % to 6 %, which lies in the tested strain range [38].

Viscoelasticity

The varying viscoelasticity of the studied materials can be explained by structural and compositional reasons. Thus, the chemical bonds can determine the mechanical behavior of the hydrogels, for example [127–129]. Hydrogels with covalent bonds mainly show elastic material behavior, as was observed in ADA-GEL, whereas hydrophobic interactions preferably show visco-(poro)elastic or viscoplastic material behavior [87]. The viscoelastic material behavior is composed of isochoric structural shape changes and small motions of water molecules [87]. In addition, poroelastic effects can also occur due to the long-distance movement of water molecules, in which the volume of the hydrogel is not preserved [87], as water can freely leave the hydrogel network during deformation. For this reason, it is significant to consider the mechanical deformation mechanisms and chemical cross-links underlying the different materials when evaluating the mechanical responses and the corresponding material parameters identified in this work.

The time-dependent behavior of cartilage and hydrogels can be linked to different time scales and physical phenomena. In cartilage, the interaction of proteins such as GAGs and collagen leads to a viscoelastic material response, whereas fluid motion within the extracellular matrix can be explained by poroelastic laws. ChondroFiller^{liquid} features a non-fibrous and a fibrous polymer network surrounded by fluid. The interactions of the polymer network can induce a viscoelastic effect, while the fluid movement in the polymer network results in a poroelastic behavior. ADA-GEL consists of a non-fibrous polymer network, which can also induce viscoelastic behavior, and the fluid within the network can lead to poroelastic effects.

The human articular cartilage is subjected to several types of loading modes simultaneously under physiological conditions. Frictional shear forces occur during locomotion due to the sliding of the joints, resulting in tensile forces in the cartilage tissue [35]. Simultaneously, compressive forces are induced by weight-bearing, which the cartilage can withstand with the help of the swelling pressure produced by the high negative charge of the sulfated glycosaminoglycan chains [35].

The sliding of the adjacent collagen fibrils dissipates energy [80]. Therefore, the viscoelastic behavior of cartilage has a damping function [80]. In contrast, the elastic behavior of the cartilage is related to the energy stored by stretching the collagen molecules in the cross-linked fibrils [80], and its physiological function is storage and redirection of energy to the adjacent bone during locomotion [35].

As explained in Chapter 1.4, the ADA-GEL hydrogel system has a relatively complex chemical structure consisting of ionic (Ca2+) crosslinks, covalent (enzymatic, ε(γ-glutamyl)lysine) isopeptide bonds (facilitated by microbial transglutaminase), and reversible-covalent (Schiff base) crosslinks [58]. Therefore, the mechanisms underlying the time-dependent behavior of ADA-GEL are probably based on superimposed visco- and poroelastic effects. Zhao et al. studied how individual chemical crosslinks in an alginate hydrogel result in different mechanical behaviors [115]. Alginate hydrogels with covalent cross-links revealed characteristic poroelastic material behavior [115]. Meanwhile, in ionically cross-linked alginate, stress relaxation is caused by superimposed viscoelastic and poroelastic effects, depending on the characteristic length [58]. It is expected that the presence of covalent bonds in ADA-

GEL hydrogels will suppress viscoplastic effects, making it likely that viscoplastic deformation will be negligible [87] [115].

The structure of collagen I-based ChondroFiller^{liquid} was presented in chapter 1.4. It is assumed that hydrogen bonds, which are weak compared to primary covalent bonds, dominate the mechanical deformation behavior of collagen type I hydrogels [106]. The results of the mechanical investigations and parameter identification indicate that ChondroFiller^{liquid} exhibits a complex, superimposed elastic, viscoelastic behavior with possible additional poroelastic effects and upon a nominal strain of ~10%, either viscoplastic or damaging effects occur [130]. Silver et al. previously proposed that in self-assembling collagen type I hydrogels, elasticity tends to be caused by direct deformation of the triple helix, and viscosity results from the sliding of adjacent fibrils and fibril bundles [131] [106]. As already mentioned, hydrogels with weak bonds (hydrogen bonds in collagen or ionic crosslinking bonds in ADA-GEL), compared to hydrogels with covalent bonds, show a tendency toward viscoelastic or even viscoplastic behavior [130] [132]. In contrast, the covalent cross-links yield an elastic material response [24] [130]. Furthermore, in parallel to viscoelasticity, viscoplasticity is also associated with mechanical confinement and, therefore, influences cell proliferation, spreading, and migration [132] [130]. Advanced viscoplastic models such as the Bergström-Boyce model, the Arruda-Boyce viscoplastic model, or the three-net model [123] are able to reproduce the complex material behavior of polymers best.
For all three investigated materials, an exact distinction between the individual mechanisms during deformation is not possible with the experimental method presented here. Nevertheless, a possible poroelastic contribution can be hypothesized, implicitly captured by the hyper-viscoelastic model, predicting lower stresses during the first loading cycle than in the subsequent second and third cycles, consistent with the experimental observations for all three materials. It is hypothesized that in the experiment, lower stresses during the second and third loading cycles, which have also been seen in cyclic shear tests of human brain tissue [133], are a result of the leakage of pore fluid during the initial loading.

5 Limitations

A limitation of this study is the neglect of the anisotropy of cartilage, which should have been investigated in the experiments. Additionally, the use of cartilage from only one donor may not reflect individual differences, and samples from multiple donors, both sexes and different age groups should be studied.
Sex hormones play an essential role in the biomechanics of articular cartilage. Therefore, samples from both sexes, as well as from young patients (pre-menopausal) and older patients (post-menopausal), should be studied. Although the samples were taken from macroscopically healthy regions, it can be assumed that the cartilage was degeneratively altered since the donor suffered from osteoarthritis. However, the specimens were not subjected to histological examination to determine the degree of degeneration.

Although compressive and tensile deformations were considered, no data was available from shear tests. Native cartilage experiences shear stress and strain, even with predominantly compressive loading, such as standing [134].
ChondroFiller^{liquid} performed well for reversible hyper-viscoelastic material laws up to 10% nominal strain. For higher strains, however, irreversible deformations were observed, and a crack was detected in the frameworks during the microstructural analysis, which could have slightly influenced the determined material parameters, as damage effects were not considered.

6 Summary and Outlook

Degenerative cartilage diseases such as osteoarthritis lead to constant cartilage degradation, causing patients to suffer and limiting their mobility. Even innovative therapeutic approaches such as MACI cannot completely restore the natural mechanics of cartilage. Therefore, there is a high potential for improvement in the development of suitable methods and materials for cartilage replacement. This potential enables novel research fields such as tissue engineering and stimulation approaches, in which much effort has recently been put into the development and research of new biomaterials and fundamental correlations between cell proliferation, migration and differentiation, and stimulation parameters. With their unique properties and high variability, hydrogels are particularly suitable as cartilage substitutes. The mechanical properties of hydrogels have a significant effect on the physiological mechanotransduction processes of chondrocytes and, therefore, require further characterization.
In this work, complex multimodal mechanical characterization of human articular cartilage and two hydrogels (oxidized alginate-gelatin: ADA-GEL and the commercially available collagen I-based ChondroFiller^{liquid}) serving as surrogates were performed. All materials exhibit nonlinearity and tension-compression asymmetry. Hyaline cartilage developed higher stresses in tension than in compression, in contrast to ADA-GEL and ChondroFiller^{liquid}, which show the opposite behavior. This material behavior can be attributed to the microstructure. Using second harmonic imaging, the microstructure of the materials was investigated, and it was shown that ADA-GEL consists of exclusively non-fibrous, cartilage of predominantly fibrous structure, and ChondroFiller^{liquid} is bi-phasic with fibrous and non-fibrous components. According to the literature, fibrillar components lead to increased stresses in the tensile direction. The proportion of fibrillar structures in ChondroFiller^{liquid} is only 40%, and thus its material behavior, in this case, the tensile-compression asymmetry, is predominated by the non-fibrillar component. In terms of recovery behavior, cartilage, and ADA-GEL were able to fully regenerate within one hour after a load of 15% strain, in contrast to ChondroFiller^{liquid}, where the residual deformation remained at 30%. The results illustrate that the materials exhibit different material responses in terms of compressive-tension asymmetry, nonlinearity, recovery, conditioning, and stress relaxation behavior, which are related to their microstructure. In addition to a qualitative characterization, a test protocol was developed that allows the identification of material parameters for numerical simulations. This parameter set includes cyclic loading and stress relaxation in tension and compression under multiple strain levels.

Numerical simulations are a powerful tool in the field of tissue engineering for cartilage repair to understand which mechanical properties influence the behavior of chondrocytes and contribute to the success or failure of replacement materials as implants. Special attention should also be paid to the determination of the material parameters since only carefully selected approaches result in reliable numerical predictions about the response of the material.

In the first step, the time-independent behavior of all materials was investigated by identifying hyperelastic material parameters for numerical simulations in COMSOL Multiphysics® v. 5.6. Thereby, several hyperelastic isotropic material models like the neo-Hookean, Ogden, Mooney-Rivlin, Yeoh and Arruda-Boyce material models were taken into account and provide separate parameter sets for the unconditioned and the conditioned material response, respectively. Two different approaches to parameter identification were compared: a direct approach assuming an ideal homogeneous deformation of the whole specimen and the inverse parameter identification where the experiment is simulated using a finite element model with realistic boundary conditions. It was also proven that only the simultaneous consideration of tension and compression data and the use of the inverse approach leads to reliable parameters. It was shown that the Ogden model with 1-term best represents the conditioned and the Ogden model with 2-terms the unconditioned material response of cartilage. The Mooney-Rivlin model with 5-terms and the Ogden model with 2-terms are particularly well suited for the material behavior of ADA-GEL and ChondroFiller^{liquid}, respectively.

After studying the time-independent behavior, the focus was shifted to the time-dependent hyper-viscoelastic material behavior in the next step. Also, for the time-dependent material response, parameter sets for the unconditioned and conditioned material response were provided separately, and how viscoelastic effects are related to the microstructure of the materials was discussed. It was demonstrated that stress relaxation is faster in the hydrogels ADA-GEL and ChondroFiller^{liquid} than in cartilage. Furthermore, cartilage exhibits the largest viscoelastic stress contribution. At the same time, ADA-GEL has the largest elastic stress contribution in comparison. The elastic material response predominates in both ADA-GEL and ChondroFiller^{liquid} in contrast to cartilage. As already noted in the qualitative characterization, ChondroFiller^{liquid} also deforms irreversibly. The hyper-viscoelastic material model was able to reproduce the material behavior well up to a deformation of 10% nominal strain. In conclusion, ADA-GEL is closer to cartilage in its elastic properties, while ChondroFiller^{liquid} is more similar to cartilage in its viscous properties. In addition to the hyperelastic and hyper-viscoelastic material parameters, the equilibrium shear modulus was determined for each material, which can be utilized for poroelastic considerations, for instance.

The provided data sets are usable in different situations and application areas. For example, dynamic processes can be simulated using the unconditioned data set, and repetitive physiological loads and in vitro stimulations can be simulated using the conditioned parameter sets.

The effects caused by fluid movement are implicitly included. To further investigate the influence of fluid movement on the material behavior and on the cells, suitable experiments could be developed to decouple the viscoelasticity from the poroelasticity. In addition to the experimental methods, the simulation models and the parameter identification could be expanded to include poroelasticity. Furthermore, the experimental methods could be further extended to include the influence of anisotropy.

Cell experiments should be performed to investigate the influence of the mechanical characteristics of the two hydrogels, ChondroFillerliquid and ADA-GEL. These results will be helpful to simulate mechanical stimulations and, at the same time, explore the effect on cells in cell experiments and quantified through the material characterization and parameter identification presented here by modifying the elastic and/or viscoelastic material behavior of the hydrogels. The study will support the design of suitable materials with different mechanical properties to mimic cartilage as closely as possible in the future and to provide parameters and insights into the time-dependent and time-independent material behavior of human articular cartilage and two substitute materials. In addition, the results will contribute to the selection of appropriate material models and parameters for whole joint simulations.

7 List of Figures

8 Tables Directory

9 Abbreviations

3D	three-dimensional
ACI	autologous chondrocyte implantation
ADA	alginate di-aldehyde
Ba	barium
Ca	calcium
$CaCl_2$	calcium chloride
CAD	Computer-Aided Design
ECM	extracellular matrix
FE	finite element
FEM	finite element method
GAGs	glycosaminoglycans
GEL	gelatin
MACI	matrix-associated chondrocyte implantation
MSCs	mesenchymal stem cells
mTG	microbial transglutaminase
Na	sodium
OA	osteoarthritis
PCM	pericellular matrices
PEG	polyethylene glycol
SHG	Second Harmonic Generation
Sr	strontium

10 References

[1] S. Safiri, A.-A. Kolahi, E. Smith, C. Hill, D. Bettampadi, M.A. Mansournia, D. Hoy, A. Ashrafi-Asgarabad, M. Sepidarkish, A. Almasi-Hashiani, G. Collins, J. Kaufman, M. Qorbani, M. Moradi-Lakeh, A.D. Woolf, F. Guillemin, L. March, M. Cross, Global, regional and national burden of osteoarthritis 1990-2017: a systematic analysis of the Global Burden of Disease Study 2017, Annals of the Rheumatic Diseases 79 (2020) 819–828. https://doi.org/10.1136/annrheumdis-2019-216515.

[2] Y. Zhang, J.M. Jordan, Epidemiology of osteoarthritis, Clin. Geriatr. Med. 26 (2010) 355–369. https://doi.org/10.1016/j.cger.2010.03.001.

[3] Johanne Martel-Pelletier, Andrew J. Barr, Flavia M. Cicuttini, Philip G. Conaghan, Cyrus Cooper, Mary B. Goldring, Steven R. Goldring, Graeme Jones, Andrew J. Teichtahl, Jean-Pierre Pelletier, Osteoarthritis, Nat Rev Dis Primers 2 (2016) 1–18. https://doi.org/10.1038/nrdp.2016.72.

[4] M. Seidenstuecker, J. Watrinet, A. Bernstein, N.P. Suedkamp, S.H. Latorre, A. Maks, H.O. Mayr, Viscoelasticity and histology of the human cartilage in healthy and degenerated conditions of the knee, J. Orthop. Surg. Res. 14 (2019) 256. https://doi.org/10.1186/s13018-019-1308-5.

[5] David J. Hunter, Felix Eckstein, Exercise and osteoarthritis, Journal of Anatomy 214 (2009) 197–207. https://doi.org/10.1111/j.1469-7580.2008.01013.x.

[6] M.B. Goldring, Articular Cartilage Degradation in Osteoarthritis, HSS J. 8 (2012) 7–9. https://doi.org/10.1007/s11420-011-9250-z.

[7] R.F. Loeser, S.R. Goldring, C.R. Scanzello, M.B. Goldring, Osteoarthritis: A Disease of the Joint as an Organ, Arthritis Rheum. 64 (2012) 1697–1707. https://doi.org/10.1002/art.34453.

[8] Z. Zhao, Y. Li, M. Wang, S. Zhao, Z. Zhao, J. Fang, Mechanotransduction pathways in the regulation of cartilage chondrocyte homoeostasis, J. Cell. Mol. Med. 24 (2020) 5408–5419. https://doi.org/10.1111/jcmm.15204.

[9] S. Saarakkala, P. Julkunen, P. Kiviranta, J. Mäkitalo, J.S. Jurvelin, R.K. Korhonen, Depth-wise progression of osteoarthritis in human articular cartilage: investigation of composition, structure and biomechanics, Osteoarthr. Cartil. 18 (2010) 73–81. https://doi.org/10.1016/j.joca.2009.08.003.

[10] M. Ebrahimi, S. Ojanen, A. Mohammadi, M.A. Finnilä, A. Joukainen, H. Kröger, S. Saarakkala, R.K. Korhonen, P. Tanska, Elastic, Viscoelastic and Fibril-Reinforced Poroelastic Material Properties of Healthy and Osteoarthritic Human Tibial Cartilage, Ann Biomed Eng 47 (2019) 953–966. https://doi.org/10.1007/s10439-019-02213-4.

[11] R.U. Kleemann, D. Krocker, A. Cedraro, J. Tuischer, G.N. Duda, Altered cartilage mechanics and histology in knee osteoarthritis: relation to clinical assessment (ICRS Grade), 2005.

[12] Z. Ge, Y. Hu, B.C. Heng, Z. Yang, H. Ouyang, E.H. Lee, T. Cao, Osteoarthritis and therapy, Arthritis Rheum. 55 (2006) 493–500. https://doi.org/10.1002/art.21994.

[13]T. Stampoultzis, P. Karami, D.P. Pioletti, Thoughts on cartilage tissue engineering: A 21st century perspective, Current Research in Translational Medicine 69 (2021) 103299. https://doi.org/10.1016/j.retram.2021.103299.

[14]E.B. Hunziker, K. Lippuner, M. Keel, N. Shintani, An educational review of cartilage repair: precepts & practice – myths & misconceptions – progress & prospects, Osteoarthr. Cartil. 23 (2015) 334–350. https://doi.org/10.1016/j.joca.2014.12.011.

[15]Matthias Jacobi, Vincent Villa, Robert A Magnussen, Philippe Neyret, MACI - a new era?, BMC Sports Sci Med Rehabil 3 (2011) 1–7. https://doi.org/10.1186/1758-2555-3-10.

[16]C. Vinatier, J. Guicheux, Cartilage tissue engineering: From biomaterials and stem cells to osteoarthritis treatments, Annals of Physical and Rehabilitation Medicine 59 (2016) 139–144. https://doi.org/10.1016/j.rehab.2016.03.002.

[17]C. Vinatier, J. Guicheux, Cartilage tissue engineering: From biomaterials and stem cells to osteoarthritis treatments, Annals of Physical and Rehabilitation Medicine 59 (2016) 139–144. https://doi.org/10.1016/j.rehab.2016.03.002.

[18]G. Filardo, E. Kon, F. Perdisa, B. Di Matteo, A. Di Martino, F. Iacono, S. Zaffagnini, F. Balboni, V. Vaccari, M. Marcacci, Osteochondral scaffold reconstruction for complex knee lesions: a comparative evaluation, 2013.

[19]D. Martínez-Moreno, G. Jiménez, P. Gálvez-Martín, G. Rus, J.A. Marchal, Cartilage biomechanics: A key factor for osteoarthritis regenerative medicine, Biochim. Biophys. Acta Mol. Basis Dis. 1865 (2019) 1067–1075. https://doi.org/10.1016/j.bbadis.2019.03.011.

[20]C. Meinert, K. Schrobback, D.W. Hutmacher, T.J. Klein, A novel bioreactor system for biaxial mechanical loading enhances the properties of tissue-engineered human cartilage, Sci Rep 7 (2017) 16997. https://doi.org/10.1038/s41598-017-16523-x.

[21]C.T. Brighton, W. Wang, C.C. Clark, The effect of electrical fields on gene and protein expression in human osteoarthritic cartilage explants, J. Bone Joint Surg. Am. 90 (2008) 833–848. https://doi.org/10.2106/JBJS.F.01437.

[22]S.O. Sarrigiannidis, J.M. Rey, O. Dobre, C. González-García, M.J. Dalby, M. Salmeron-Sanchez, A tough act to follow: collagen hydrogel modifications to improve mechanical and growth factor loading capabilities, Materials Today Bio 10 (2021) 100098. https://doi.org/10.1016/j.mtbio.2021.100098.

[23]O.M. Babalola, L.J. Bonassar, Parametric finite element analysis of physical stimuli resulting from mechanical stimulation of tissue engineered cartilage, J Biomech Eng 131 (2009) 61014. https://doi.org/10.1115/1.3128672.

[24]H.-P. Lee, L. Gu, D.J. Mooney, M.E. Levenston, O. Chaudhuri, Mechanical confinement regulates cartilage matrix formation by chondrocytes, Nat. Mater. 16 (2017) 1243–1251. https://doi.org/10.1038/nmat4993.

[25]A.R. Cameron, J.E. Frith, J.J. Cooper-White, The Influence of Substrate Creep on Mesenchymal Stem Cell Behaviour and Phenotype, Biomaterials 32 (2011). https://doi.org/10.1016/j.biomaterials.2011.04.003.

[26]O. Chaudhuri, L. Gu, M. Darnell, D. Klumpers, S.A. Bencherif, J.C. Weaver, N. Huebsch, D.J. Mooney, Substrate stress relaxation regulates cell spreading, Nat. Commun. 6 (2015) 6364. https://doi.org/10.1038/ncomms7365.

[27]O. Chaudhuri, L. Gu, D. Klumpers, M. Darnell, S.A. Bencherif, J.C. Weaver, N. Huebsch, H.-P. Lee, E. Lippens, G.N. Duda, D.J. Mooney, Hydrogels with tunable stress relaxation regulate stem cell fate and activity, Nat. Mater. 15 (2016) 326–334. https://doi.org/10.1038/nmat4489.

[28]K. Dey, S. Agnelli, L. Sartore, Dynamic freedom: substrate stress relaxation stimulates cell responses, Biomater. Sci. 7 (2019) 836–842. https://doi.org/10.1039/c8bm01305e.

[29]D.D. McKinnon, D.W. Domaille, J.N. Cha, K.S. Anseth, Biophysically defined and cytocompatible covalently adaptable networks as viscoelastic 3D cell culture systems, Adv. Mater. Weinheim. 26 (2014) 865–872. https://doi.org/10.1002/adma.201303680.

[30]B.P. Kanungo, L.J. Gibson, Density-property relationships in collagen-glycosaminoglycan scaffolds, Acta Biomater. 6 (2010) 344–353. https://doi.org/10.1016/j.actbio.2009.09.012.

[31]M.L. Oyen, Mechanical characterisation of hydrogel materials, International Materials Reviews 59 (2014) 44–59. https://doi.org/10.1179/1743280413Y.0000000022.

[32]P.M. Freeman, R.N. Natarajan, J.H. Kimura, T.P. Andriacchi, Chondrocyte cells respond mechanically to compressive loads, J. Orthop. Res. 12 (1994). https://doi.org/10.1002/jor.1100120303.

[33]H. Zahedmanesh, M. Stoddart, P. Lezuo, C. Forkmann, M.A. Wimmmer, M. Alini, H. van Oosterwyck, Deciphering mechanical regulation of chondrogenesis in fibrin-polyurethane composite scaffolds enriched with human mesenchymal stem cells: a dual computational and experimental approach, Tissue Eng. Part A 20 (2014) 1197–1212. https://doi.org/10.1089/ten.TEA.2013.0145.

[34]F.H. Silver, G. Bradica, A. Tria, Do changes in the mechanical properties of articular cartilage promote catabolic destruction of cartilage and osteoarthritis?, Matrix Biology 23 (2004) 467–476. https://doi.org/10.1016/j.matbio.2004.08.003.

[35]F.H. Silver, G. Bradica, Mechanobiology of cartilage: how do internal and external stresses affect mechanochemical transduction and elastic energy storage?, Biomech Model Mechanobiol 1 (2002) 219–238. https://doi.org/10.1007/s10237-002-0017-9.

[36]M.B. Schmidt, V.C. Mow, L.E. Chun, D.R. Eyre, Effects of proteoglycan extraction on the tensile behavior of articular cartilage, J. Orthop. Res. 8 (1990) 353–363. https://doi.org/10.1002/jor.1100080307.

[37]W.M. Lai, V.C. Mow, W. Zhu, Constitutive modeling of articular cartilage and biomacromolecular solutions, J. Biomech. Eng. 115 (1993) 474–480. https://doi.org/10.1115/1.2895527.

[38]B. Liu, N.K. Lad, A.T. Collins, P.K. Ganapathy, G.M. Utturkar, A.L. McNulty, C.E. Spritzer, C.T. Moorman, E.G. Sutter, W.E. Garrett, L.E. DeFrate, In Vivo Tibial Cartilage Strains in Regions of Cartilage-to-Cartilage Contact and Cartilage-to-Meniscus Contact in Response to Walking, Am. J. Sports Med. 45 (2017) 2817–2823. https://doi.org/10.1177/0363546517712506.

[39]K.S. Halonen, M.E. Mononen, J.S. Jurvelin, J. Töyräs, J. Salo, R.K. Korhonen, Deformation of articular cartilage during static loading of a knee joint--experimental and finite element analysis, J. Biomech. 47 (2014) 2467–2474. https://doi.org/10.1016/j.jbiomech.2014.04.013.

[40]M. Charlebois, M.D. McKee, M.D. Buschmann, Nonlinear tensile properties of bovine articular cartilage and their variation with age and depth, J Biomech Eng 126 (2004) 129–137. https://doi.org/10.1115/1.1688771.

[41]J.M. Deneweth, S.G. McLean, E.M. Arruda, Evaluation of hyperelastic models for the non-linear and non-uniform high strain-rate mechanics of tibial cartilage, J. Biomech. 46 (2013) 1604–1610. https://doi.org/10.1016/j.jbiomech.2013.04.014.

[42]A. Oloyede, R. Flachsmann, N.D. Broom, The dramatic influence of loading velocity on the compressive response of articular cartilage, Connective Tissue Research 27 (1992) 211–224. https://doi.org/10.3109/03008209209006997.

[43]C.P. Brown, T.C. Nguyen, H.R. Moody, R.W. Crawford, A. Oloyede, Assessment of common hyperelastic constitutive equations for describing normal and osteoarthritic articular cartilage, Proc. Inst. Mech. Eng. H 223 (2009) 643–652. https://doi.org/10.1243/09544119JEIM546.

[44]H. Lee, W.D. Campbell, K.M. Theis, M.E. Canning, H.Y. Ennis, R.L. Jackson, R.R. Hanson, Comparison Between the Hyperelastic Behavior of Fresh and Frozen Equine Articular Cartilage in Various Joints, J. Biomech. Eng. 142 (2020). https://doi.org/10.1115/1.4044031.

[45]W.C. Bae, C.W. Lewis, M.E. Levenston, R.L. Sah, Indentation testing of human articular cartilage: effects of probe tip geometry and indentation depth on intra-tissue strain, J. Biomech. 39 (2006) 1039–1047. https://doi.org/10.1016/j.jbiomech.2005.02.018.

[46]E. Langelier, M.D. Buschmann, Increasing strain and strain rate strengthen transient stiffness but weaken the response to subsequent compression for articular cartilage in unconfined compression, J. Biomech. 36 (2003) 853–859. https://doi.org/10.1016/s0021-9290(03)00006-x.

[47]F. Boschetti, G. Pennati, F. Gervaso, G.M. Peretti, G. Dubini, Biomechanical properties of human articular cartilage under compressive loads, Biorheology 41 (2004) 159–166.

[48]D. Caccavo, S. Cascone, S. Poto, G. Lamberti, A.A. Barba, Mechanics and transport phenomena in agarose-based hydrogels studied by compression-relaxation tests, Carbohydr. Polym. 167 (2017) 136–144. https://doi.org/10.1016/j.carbpol.2017.03.027.

[49]P.A. Smyth, I. Green, R.L. Jackson, R.R. Hanson, Biomimetic Model of Articular Cartilage Based on *In Vitro* Experiments, JBBBE 21 (2014) 75–91. https://doi.org/10.4028/www.scientific.net/JBBBE.21.75.

[50]Q.-M. Wang, A.C. Mohan, M.L. Oyen, X.-H. Zhao, Separating viscoelasticity and poroelasticity of gels with different length and time scales, Acta Mech Sin 30 (2014) 20–27. https://doi.org/10.1007/s10409-014-0015-z.

[51]N. Hosoda1, N. Sakai2, Y. Sawae2 and T. Murakami2, Finite Element Analysis of Articular Cartilage Model Considering the Configuration and Biphasic Property of the Tissue.

[52]A.E. Forte, F. D'Amico, M.N. Charalambides, D. Dini, J.G. Williams, Modelling and experimental characterisation of the rate dependent fracture properties of gelatine gels, Food Hydrocolloids 46 (2015) 180–190. https://doi.org/10.1016/j.foodhyd.2014.12.028.

[53]A. Ghorbanoghli, K. Narooei, A new hyper-viscoelastic model for investigating rate dependent mechanical behavior of dual cross link self-healing hydrogel, International Journal of Mechanical Sciences 159 (2019) 278–286. https://doi.org/10.1016/j.ijmecsci.2019.06.019.

[54]R. Long, K. Mayumi, C. Creton, T. Narita, C.-Y. Hui, Time Dependent Behavior of a Dual Cross-Link Self-Healing Gel: Theory and Experiments, Macromolecules 47 (2014) 7243–7250. https://doi.org/10.1021/ma501290h.

[55]B. Hoyer, A. Bernhardt, A. Lode, S. Heinemann, J. Sewing, M. Klinger, H. Notbohm, M. Gelinsky, Jellyfish collagen scaffolds for cartilage tissue engineering, Acta Biomater. 10 (2014) 883–892. https://doi.org/10.1016/j.actbio.2013.10.022.

[56]Q. Wang, Z. Gao, A constitutive model of nanocomposite hydrogels with nanoparticle crosslinkers, Journal of the Mechanics and Physics of Solids 94 (2016) 127–147. https://doi.org/10.1016/j.jmps.2016.04.011.

[57]D. Harjanto, J.S. Maffei, M.H. Zaman, Quantitative analysis of the effect of cancer invasiveness and collagen concentration on 3D matrix remodeling, PLoS ONE 6 (2011) e24891. https://doi.org/10.1371/journal.pone.0024891.

[58]T. Distler, K. McDonald, S. Heid, E. Karakaya, R. Detsch, A.R. Boccaccini, Ionically and Enzymatically Dual Cross-Linked Oxidized Alginate Gelatin Hydrogels with Tunable Stiffness and Degradation Behavior for Tissue Engineering, ACS biomater. sci. eng. 6 (2020) 3899–3914. https://doi.org/10.1021/acsbiomaterials.0c00677.

[59]T. Kreller, T. Distler, S. Heid, S. Gerth, R. Detsch, A.R. Boccaccini, Physico-chemical modification of gelatine for the improvement of 3D printability of oxidized alginate-gelatine hydrogels towards cartilage tissue engineering, Materials & Design 208 (2021) 109877. https://doi.org/10.1016/j.matdes.2021.109877.

[60]M. Freutel, H. Schmidt, L. Dürselen, A. Ignatius, F. Galbusera, Finite element modeling of soft tissues: Material models, tissue interaction and challenges, Clinical Biomechanics 29 (2014) 363–372. https://doi.org/10.1016/j.clinbiomech.2014.01.006.

[61]R. Shirazi, A. Shirazi-Adl, M. Hurtig, Role of cartilage collagen fibrils networks in knee joint biomechanics under compression, J. Biomech. 41 (2008) 3340–3348. https://doi.org/10.1016/j.jbiomech.2008.09.033.

[62]B. Agoram, V.H. Barocas, Coupled macroscopic and microscopic scale modeling of fibrillar tissues and tissue equivalents, J. Biomech. Eng. 123 (2001) 362–369. https://doi.org/10.1115/1.1385843.

[63]S. Evans, How Can We Measure the Mechanical Properties of Soft Tissues?, in: S. Avril, S. Evans (Eds.), Material Parameter Identification and Inverse Problems in Soft Tissue Biomechanics, Springer International Publishing, Cham, 2017, pp. 67–83.

[64]C.T. Brighton, W. Wang, C.C. Clark, The effect of electrical fields on gene and protein expression in human osteoarthritic cartilage explants, J. Bone Joint Surg. Am. 90 (2008) 833–848. https://doi.org/10.2106/JBJS.F.01437.

[65]T. Distler, L. Kretzschmar, D. Schneidereit, S. Girardo, R. Goswami, O. Friedrich, R. Detsch, J. Guck, A.R. Boccaccini, S. Budday, Mechanical properties of cell- and microgel bead-laden oxidized alginate-gelatin hydrogels, Biomater. Sci. 9 (2021) 3051–3068. https://doi.org/10.1039/d0bm02117b.

[66]R. Faturechi, A. Karimi, A. Hashemi, H. Yousefi, M. Navidbakhsh, Influence of Poly(acrylic acid) on the Mechanical Properties of Composite Hydrogels, Adv. Polym. Technol. 34 (2015) n/a-n/a. https://doi.org/10.1002/adv.21487.

[67]K. Upadhyay, G. Subhash, D. Spearot, Hyperelastic constitutive modeling of hydrogels based on primary deformation modes and validation under 3D stress states, International Journal of Engineering Science 154 (2020) 103314. https://doi.org/10.1016/j.ijengsci.2020.103314.

[68]H. Martin, O. Sahmel, T. Eickner, N. Grabow, C. Kreiner, R. Guthoff, Determination of the hyperelastic material behavior of hydrogel specimens for expandable lens implants, Current Directions in Biomedical Engineering 5 (2019) 351. https://doi.org/10.1515/cdbme-2019-0088.

[69]A. Sasson, S. Patchornik, R. Eliasy, D. Robinson, R. Haj-Ali, Hyperelastic mechanical behavior of chitosan hydrogels for nucleus pulposus replacement-experimental testing and constitutive modeling, J. Mech. Behav. Biomed. Mater. 8 (2012) 143–153. https://doi.org/10.1016/j.jmbbm.2011.12.008.

[70]M. Freutel, H. Schmidt, L. Dürselen, A. Ignatius, F. Galbusera, Finite element modeling of soft tissues: material models, tissue interaction and challenges, Clin. Biomech. (Bristol, Avon) 29 (2014) 363–372. https://doi.org/10.1016/j.clinbiomech.2014.01.006.

[71]K.D. Butz, D.D. Chan, E.A. Nauman, C.P. Neu, Stress distributions and material properties determined in articular cartilage from MRI-based finite strains, J. Biomech. 44 (2011) 2667–2672. https://doi.org/10.1016/j.jbiomech.2011.08.005.

[72]T. Reuter, I. Ponomarev, Biomechanical parameter determination of scaffold-free cartilage constructs (SFCCs) with the hyperelastic material models Yeoh, Ogden and Demiray, Current Directions in Biomedical Engineering 1 (2015) 442–445. https://doi.org/10.1515/cdbme-2015-0106.

[73]A. Weizel, T. Distler, R. Detsch, A.R. Boccaccini, L. Bräuer, F. Paulsen, H. Seitz, S. Budday, Hyperelastic parameter identification of human articular cartilage and substitute materials, J. Mech. Behav. Biomed. Mater. (2022) 105292. https://doi.org/10.1016/j.jmbbm.2022.105292.

[74]F. Richard, M. Villars, S. Thibaud, Viscoelastic modeling and quantitative experimental characterization of normal and osteoarthritic human articular cartilage using indentation, J. Mech. Behav. Biomed. Mater. 24 (2013) 41–52. https://doi.org/10.1016/j.jmbbm.2013.04.012.

[75]R. Springhetti, N.S. Selyutina, Viscoelastic modeling of articular cartilage under impact loading, Meccanica 53 (2018) 519–530. https://doi.org/10.1007/s11012-017-0717-y.

[76]S. Ahsanizadeh, L. Li, Visco-hyperelastic constitutive modeling of soft tissues based on short and long-term internal variables, Biomed. Eng. Online 14 (2015) 29. https://doi.org/10.1186/s12938-015-0023-7.

[77]E. Kim, F. Guilak, M.A. Haider, The dynamic mechanical environment of the chondrocyte: a biphasic finite element model of cell-matrix interactions under cyclic compressive loading, J Biomech Eng 130 (2008) 61009. https://doi.org/10.1115/1.2978991.

[78]P. Tanska, M.S. Venäläinen, A. Erdemir, R.K. Korhonen, A multiscale framework for evaluating three-dimensional cell mechanics in fibril-reinforced poroelastic tissues with anatomical cell distribution - Analysis of chondrocyte deformation behavior in mechanically loaded articular cartilage, J. Biomech. 101 (2020) 109648. https://doi.org/10.1016/j.jbiomech.2020.109648.

[79]A. Weizel, T. Distler, R. Detsch, A.R. Boccaccini, H. Seitz, S. Budday, Time-dependent hyper-viscoelastic parameter identification of human articular cartilage and substitute materials, J. Mech. Behav. Biomed. Mater. 138 (2023) 105618. https://doi.org/10.1016/j.jmbbm.2022.105618.

[80]F.H. Silver, G. Bradica, A. Tria, Elastic energy storage in human articular cartilage: estimation of the elastic modulus for type II collagen and changes associated with osteoarthritis, 2002.

[81]C. van Mow, M.H. Holmes, W. Michael Lai, Fluid transport and mechanical properties of articular cartilage: A review, J. Biomech. 17 (1984) 377–394. https://doi.org/10.1016/0021-9290(84)90031-9.

[82]A.J. Sophia Fox, A. Bedi, S.A. Rodeo, The basic science of articular cartilage: structure, composition, and function, Sports Health 1 (2009) 461–468. https://doi.org/10.1177/1941738109350438.

[83]J. Eschweiler, N. Horn, B. Rath, M. Betsch, A. Baroncini, M. Tingart, F. Migliorini, The Biomechanics of Cartilage-An Overview, Life (Basel) 11 (2021). https://doi.org/10.3390/life11040302.

[84]F. Paulsen, J. Waschke (Eds.), Sobotta Atlas of anatomy, 16th ed., Elsevier, München, 2018.

[85]A. Weizel, T. Distler, D. Schneidereit, O. Friedrich, L. Bräuer, F. Paulsen, R. Detsch, A.R. Boccaccini, S. Budday, H. Seitz, Complex mechanical behavior of human articular cartilage and hydrogels for cartilage repair, Acta Biomater. 118 (2020) 113–128. https://doi.org/10.1016/j.actbio.2020.10.025.

[86]T. Billiet, M. Vandenhaute, J. Schelfhout, S. van Vlierberghe, P. Dubruel, A review of trends and limitations in hydrogel-rapid prototyping for tissue engineering, Biomaterials 33 (2012) 6020–6041. https://doi.org/10.1016/j.biomaterials.2012.04.050.

[87]D. Caccavo, S. Cascone, G. Lamberti, A.A. Barba, Hydrogels: experimental characterization and mathematical modelling of their mechanical and diffusive behaviour, Chem. Soc. Rev. 47 (2018) 2357–2373. https://doi.org/10.1039/c7cs00638a.

[88]A.D. Augst, H.J. Kong, D.J. Mooney, Alginate hydrogels as biomaterials, Macromol. Biosci. 6 (2006) 623–633. https://doi.org/10.1002/mabi.200600069.

[89]D.R. Sahoo, T. Biswal, Alginate and its application to tissue engineering, SN Appl. Sci. 3 (2021) 1–19. https://doi.org/10.1007/s42452-020-04096-w.

[90]I. Braccini, S. Pérez, Molecular basis of C(2+)-induced gelation in alginates and pectins: the egg-box model revisited, Biomacromolecules 2 (2001) 1089–1096. https://doi.org/10.1021/bm010008g.

[91]Y.A. Mørch, I. Donati, B.L. Strand, G. Skjåk-Braek, Effect of Ca2+, Ba2+, and Sr2+ on alginate microbeads, Biomacromolecules 7 (2006) 1471–1480. https://doi.org/10.1021/bm060010d.

[92]K.H. Bouhadir, K.Y. Lee, E. Alsberg, K.L. Damm, K.W. Anderson, D.J. Mooney, Degradation of partially oxidized alginate and its potential application for tissue engineering, Biotechnol. Prog. 17 (2001) 945–950. https://doi.org/10.1021/bp010070p.

[93]J. Venkatesan, B. Lowe, S. Anil, P. Manivasagan, A.A.A. Kheraif, K.-H. Kang, S.-K. Kim, Seaweed polysaccharides and their potential biomedical applications, Starch - Stärke 67 (2015) 381–390. https://doi.org/10.1002/star.201400127.

[94]Y.A. Mørch, I. Donati, B.L. Strand, G. Skjåk-Braek, Effect of Ca2+, Ba2+, and Sr2+ on alginate microbeads, Biomacromolecules 7 (2006) 1471–1480. https://doi.org/10.1021/bm060010d.

[95]F. Ruther, T. Distler, A.R. Boccaccini, R. Detsch, Biofabrication of vessel-like structures with alginate di-aldehyde-gelatin (ADA-GEL) bioink, J. Mater. Sci. Mater. Med. 30 (2018) 8. https://doi.org/10.1007/s10856-018-6205-7.

[96]T. Distler, F. Ruther, A.R. Boccaccini, R. Detsch, Development of 3D Biofabricated Cell Laden Hydrogel Vessels and a Low-Cost Desktop Printed Perfusion Chamber for In Vitro Vessel Maturation, Macromol. Biosci. 19 (2019) e1900245. https://doi.org/10.1002/mabi.201900245.

[97]H. Park, K.Y. Lee, Cartilage regeneration using biodegradable oxidized alginate/hyaluronate hydrogels, J. Biomed. Mater. Res. A 102 (2014) 4519–4525. https://doi.org/10.1002/jbm.a.35126.

[98]S. Schwarz, S. Kuth, T. Distler, E. Al., 3D printing and characterization of human nasoseptal chondrocytes laden dual crosslinked oxidized alginate-gelatin hydrogels for cartilage repair approaches, Mater. Sci. Eng. C Mater. Biol. Appl. 2020 (2020).

[99]S. Reakasame, A.R. Boccaccini, Oxidized Alginate-Based Hydrogels for Tissue Engineering Applications: A Review, Biomacromolecules 19 (2018) 3–21. https://doi.org/10.1021/acs.biomac.7b01331.

[100]T. Zehnder, B. Sarker, A.R. Boccaccini, R. Detsch, Evaluation of an alginate-gelatine crosslinked hydrogel for bioplotting, Biofabrication 7 (2015) 25001. https://doi.org/10.1088/1758-5090/7/2/025001.

[101]B. Wright, P.A. de Bank, K.A. Luetchford, F.R. Acosta, C.J. Connon, Oxidized alginate hydrogels as niche environments for corneal epithelial cells, J. Biomed. Mater. Res. A 102 (2014) 3393–3400. https://doi.org/10.1002/jbm.a.35011.

[102]B. Sarker, W. Li, K. Zheng, R. Detsch, A.R. Boccaccini, Designing Porous Bone Tissue Engineering Scaffolds with Enhanced Mechanical Properties from Composite Hydrogels Composed of Modified Alginate, Gelatin, and Bioactive Glass, ACS biomater. sci. eng. 2 (2016) 2240–2254. https://doi.org/10.1021/acsbiomaterials.6b00470.

[103]A.P.G. Castro, J. Yao, T. Battisti, D. Lacroix, Poroelastic Modeling of Highly Hydrated Collagen Hydrogels: Experimental Results vs. Numerical Simulation With Custom and Commercial Finite Element Solvers, Front. Bioeng. Biotechnol. 6 (2018) 142. https://doi.org/10.3389/fbioe.2018.00142.

[104]L. Salvatore, N. Gallo, M.L. Natali, A. Terzi, A. Sannino, M. Madaghiele, Mimicking the Hierarchical Organization of Natural Collagen: Toward the Development of Ideal Scaffolding Material for Tissue Regeneration, Front. Bioeng. Biotechnol. 9 (2021) 644595. https://doi.org/10.3389/fbioe.2021.644595.

[105]E.E. Antoine, P.P. Vlachos, M.N. Rylander, Review of collagen I hydrogels for bioengineered tissue microenvironments: characterization of mechanics, structure, and transport, Tissue Eng. Part B Rev. 20 (2014) 683–696. https://doi.org/10.1089/ten.TEB.2014.0086.

[106]Peter Fratzl, Collagen: Structure and Mechanics.

[107]F. Richard, M. Villars, S. Thibaud, Viscoelastic modeling and quantitative experimental characterization of normal and osteoarthritic human articular cartilage using indentation, J. Mech. Behav. Biomed. Mater. 24 (2013) 41–52. https://doi.org/10.1016/j.jmbbm.2013.04.012.

[108]M.C. Boyce, E.M. Arruda, Constitutive Models of Rubber Elasticity: A Review, Rubber Chemistry and Technology 73 (2000) 504–523. https://doi.org/10.5254/1.3547602.

[109]O.H. Yeoh, Some Forms of the Strain Energy Function for Rubber, Rubber Chemistry and Technology 66 (1993) 754–771. https://doi.org/10.5254/1.3538343.

[110]S. Münster, L.M. Jawerth, B.A. Leslie, J.I. Weitz, B. Fabry, D.A. Weitz, Strain history dependence of the nonlinear stress response of fibrin and collagen networks, PNAS 110 (2013) 12197–12202. https://doi.org/10.1073/pnas.1222787110.

[111]T. Distler, E. Schaller, P. Steinmann, A.R. Boccaccini, S. Budday, Alginate-based hydrogels show the same complex mechanical behavior as brain tissue, Mech. Behav. Biomed. Mater. 2020 (accepted 2020).

[112]L. Kretschmar, T. Distler, D. Girardo, Salvatore, Schneidereit, O. Friedrich, J. Guck, A. Boccaccini, S. Budday, On the Influence of Cell and Polyacrylamide Microgel Bead Density in Oxidized Alginate Gelatin Bioink on Hydrogel Mechanics 2020 (2020).

[113]T. Distler, K. McDonald, S. Heid, R. Detsch, A.R. Boccaccini, Ionically and Enzymatically dual-crosslinked Oxidized Alginate Gelatine Hydrogels with Tuneable Stiffness and Degradation Behaviour for Tissue Engineering, ACS Biomaterials Science and Engineering submitted.

[114]D.M. Pierce, W. Trobin, S. Trattnig, H. Bischof, G.A. Holzapfel, A phenomenological approach toward patient-specific computational modeling of articular cartilage including collagen fiber tracking, J. Biomech. Eng. 131 (2009) 91006. https://doi.org/10.1115/1.3148471.

[115]X. Zhao, N. Huebsch, D.J. Mooney, Z. Suo, Stress-relaxation behavior in gels with ionic and covalent crosslinks, Journal of Applied Physics 107 (2010) 63509. https://doi.org/10.1063/1.3343265.

[116]S. Avril, Hyperelasticity of Soft Tissues and Related Inverse Problems, in: S. Avril, S. Evans (Eds.), Material Parameter Identification and Inverse Problems in Soft Tissue Biomechanics, Springer International Publishing, Cham, 2017, pp. 37–66.

[117]C. Oomens, Mechanical Behaviour of Skin: The Struggle for the Right Testing Method, in: S. Avril, S. Evans (Eds.), Material Parameter Identification and Inverse Problems in Soft Tissue Biomechanics, Springer International Publishing, Cham, 2017, pp. 119–132.

[118]G.R. Meloni, M.B. Fisher, B.D. Stoeckl, G.R. Dodge, R.L. Mauck, Biphasic Finite Element Modeling Reconciles Mechanical Properties of Tissue-Engineered Cartilage Constructs Across Testing Platforms, Tissue Eng. Part A 23 (2017) 663–674. https://doi.org/10.1089/ten.tea.2016.0191.

[119]W. Bartlett, S. P. Krishnan, J. A. Skinner, R. W. J. Carrington, T. W. R. Briggs, G. Bentley, Collagen-covered versus matrix-induced autologous chondrocyte implantation for osteochondral defects of the knee: a comparison of tourniquet times, Eur J Orthop Surg Traumatol 16 (2006) 315–317. https://doi.org/10.1007/s00590-006-0096-x.

[120]S.P. Abelow, P. Guillen, T. Ramos, Arthroscopic Technique for Matrix-Induced Autologous Chondrocyte Implantation for the Treatment of Large Chondral Defects in the Knee and Ankle,

Operative Techniques in Orthopaedics 16 (2006) 257–261. https://doi.org/10.1053/j.oto.2006.08.006.

[121]S. Budday, T.C. Ovaert, G.A. Holzapfel, P. Steinmann, E. Kuhl, Fifty Shades of Brain: A Review on the Mechanical Testing and Modeling of Brain Tissue, Arch Computat Methods Eng 53 (2019) 2284. https://doi.org/10.1007/s11831-019-09352-w.

[122]S. Budday, G. Sommer, G.A. HOLZAPFEL, P. Steinmann, E. Kuhl, Viscoelastic parameter identification of human brain tissue, J. Mech. Behav. Biomed. Mater. 74 (2017) 463–476. https://doi.org/10.1016/j.jmbbm.2017.07.014.

[123]J. Bergström, Mechanics of solid polymers: Theory and computational modeling, Elsevier, Amsterdam [u.a.], 2015.

[124]L.R.G. Treloar, Stress-strain data for vulcanised rubber under various types of deformation, Trans. Faraday Soc. 40 (1944) 59. https://doi.org/10.1039/TF9444000059.

[125]C. van Mow, A. Ratcliffe, A. Robin Poole, Cartilage and diarthrodial joints as paradigms for hierarchical materials and structures, 1992.

[126]J. Hazur, N. Endrizzi, D.W. Schubert, A.R. Boccaccini, B. Fabry, Stress relaxation amplitude of hydrogels determines migration, proliferation, and morphology of cells in 3-D culture, Biomater. Sci. 10 (2021) 270–280. https://doi.org/10.1039/D1BM01089A.

[127]F. Charbonier, D. Indana, O. Chaudhuri, Tuning Viscoelasticity in Alginate Hydrogels for 3D Cell Culture Studies, Curr. Protoc. 1 (2021) e124. https://doi.org/10.1002/cpz1.124.

[128]Y.S. Zhang, A. Khademhosseini, Advances in engineering hydrogels, Science 356 (2017). https://doi.org/10.1126/science.aaf3627.

[129]A. Vedadghavami, F. Minooei, M.H. Mohammadi, S. Khetani, A. Rezaei Kolahchi, S. Mashayekhan, A. Sanati-Nezhad, Manufacturing of hydrogel biomaterials with controlled mechanical properties for tissue engineering applications, Acta Biomater. 62 (2017) 42–63. https://doi.org/10.1016/j.actbio.2017.07.028.

[130]S. Nam, J. Lee, D.G. Brownfield, O. Chaudhuri, Viscoplasticity Enables Mechanical Remodeling of Matrix by Cells, Biophys. J. 111 (2016) 2296–2308. https://doi.org/10.1016/j.bpj.2016.10.002.

[131]F.H. Silver, A. Ebrahimi, P.B. Snowhill, Viscoelastic properties of self-assembled type I collagen fibers: molecular basis of elastic and viscous behaviors, Connective Tissue Research 43 (2002) 569–580.

[132]O. Chaudhuri, J. Cooper-White, P.A. Janmey, D.J. Mooney, V.B. Shenoy, Effects of extracellular matrix viscoelasticity on cellular behaviour, Nature 584 (2020) 535–546. https://doi.org/10.1038/s41586-020-2612-2.

[133]S. Budday, G. Sommer, J. Haybaeck, P. Steinmann, G. Holzapfel, E. Kuhl, Rheological characterization of human brain tissue, undefined (2017).

[134]D.D. Chan, L. Cai, K.D. Butz, S.B. Trippel, E.A. Nauman, C.P. Neu, In vivo articular cartilage deformation: noninvasive quantification of intratissue strain during joint contact in the human knee, Sci. Rep. 6 (2016). https://doi.org/10.1038/srep19220.

Publications and Own Contributions

Publication I: A.Weizel; T.Distler; D.Schneidereit; O.Friedrich; L.Bräuer; F.Paulsend; R.Detsch; A.R.Boccaccini; S.Budday; H.Seitz. Complex mechanical behavior of human articular cartilage and hydrogels for cartilage repair. Acta Biomaterialia, Volume 118, 2020, Pages 113-128, ISSN 1742-7061, https://doi.org/10.1016/j.actbio.2020.10.025

Impact Factor (2020): 8.947

- Conceptualization, design, and implementation of mechanical experiments
- Production of ChondroFiller^{liquid} and cartilage scaffolds
- Data analysis and visualization
- Data interpretation
- Writing and publishing.

Publication II: A.Weizel; T.Distler; R.Detsch; A.R.Boccaccini; L.Bräuer; F.Paulsend; H.Seitz; S.Budday. Hyperelastic parameter identification of human articular cartilage and substitute materials. Journal of the Mechanical Behavior of Biomedical Materials, 2022, https://doi.org/10.1016/j.jmbbm.2022.105292.

Impact Factor (2022-2023): 4.042

- Data analysis and preparation
- Numerical simulations
- Direct and inverse parameter identification
- Data analysis and visualization
- Data interpretation
- Writing and publishing

Publication III: A. Weizel, T. Distler, R. Detsch, A.R. Boccaccini, H. Seitz, S. Budday, Time-dependent hyper-viscoelastic parameter identification of human articular cartilage and substitute materials, J. Mech. Behav. Biomed. Mater. 138 (2023) 105618. https://doi.org/10.1016/j.jmbbm.2022.105618.

Impact Factor (2022-2023): 4.042

- Data analysis and preparation
- Numerical simulations
- Direct and inverse parameter identification
- Data analysis and visualization
- Data interpretation
- Writing and publishing

Acta Biomaterialia 118 (2020) 113–128

Contents lists available at ScienceDirect

Acta Biomaterialia

journal homepage: www.elsevier.com/locate/actbio

Complex mechanical behavior of human articular cartilage and hydrogels for cartilage repair

A. Weizel[a], T. Distler[b], D. Schneidereit[c], O. Friedrich[c], L. Bräuer[d], F. Paulsen[d,e], R. Detsch[b], A.R. Boccaccini[b], S. Budday[f,*], H. Seitz[a,g,*]

[a] Chair of Microfluidics, Faculty of Mechanical Engineering and Marine Technology, University of Rostock, Rostock, Germany
[b] Institute of Biomaterials, Department of Materials Science and Engineering, Friedrich-Alexander-University Erlangen-Nürnberg, 91058 Erlangen, Germany
[c] Institute of Medical Biotechnology, Department of Chemical and Biological Engineering, Friedrich-Alexander-University Erlangen-Nürnberg, 91056 Erlangen, Germany
[d] Institute of Functional and Clinical Anatomy, Friedrich-Alexander-University Erlangen-Nürnberg Erlangen, Germany
[e] Sechenov University, Department of Operative Surgery and Topographic Anatomy, Moscow, Russia
[f] Institute of Applied Mechanics, Department of Mechanical Engineering, Friedrich-Alexander-University Erlangen-Nürnberg Erlangen, Germany
[g] Department Life, Light & Matter, University of Rostock, 18059 Rostock, Germany

ARTICLE INFO

Article history:
Received 15 July 2020
Revised 12 October 2020
Accepted 13 October 2020
Available online 17 October 2020

Keywords:
Mechanical testing
Human articular cartilage
Hydrogels
Tissue engineering
Microstructure

ABSTRACT

The mechanical behavior of cartilage tissue plays a crucial role in physiological mechanotransduction processes of chondrocytes and pathological changes like osteoarthritis. Therefore, intensive research activities focus on the identification of implant substitute materials that mechanically mimic the cartilage extracellular matrix. This, however, requires a thorough understanding of the complex mechanical behavior of both native cartilage and potential substitute materials to treat cartilage lesions. Here, we perform complex multi-modal mechanical analyses of human articular cartilage and two surrogate materials, commercially available ChondroFiller$_{liquid}$, and oxidized alginate-gelatin (ADA-GEL) hydrogels. We show that all materials exhibit nonlinearity and compression-tension asymmetry. However, while hyaline cartilage yields higher stresses in tension than in compression, ChondroFiller^{liquid} and ADA-GEL exhibit the opposite trend. These characteristics can be attributed to the materials' underlying microstructure: Both cartilage and ChondroFiller^{liquid} contain fibrillar components, but the latter constitutes a bi-phasic structure, where the 60% nonfibrillar hydrogel proportion dominates the mechanical response. Of all materials, ChondroFiller^{liquid} shows the most pronounced viscous effects. The present study provides important insights into the microstructure-property relationship of cartilage substitute materials, with vital implications for mechanically-driven material design in cartilage engineering. In addition, we provide a data set to create mechanical simulation models in the future.

Statement of significance

Understanding the complex mechanical behavior of cartilage tissue and implant substitute materials - beyond a single modulus in a linear elastic regime - is key for tissue engineering applications and cartilage repair, where complex loading conditions and large deformations occur. We therefore present a multi-modal mechanical assessment of human articular cartilage and two potential substitute materials, ChondroFiller^{liquid} and ADA-GEL hydrogels, with close consideration of the underlying microstructure. The results will have important implications for mechanically-driven material design in cartilage tissue engineering, and for any biomaterial with a known microstructure. The provided dataset lays the ground for more reliable numerical simulations in the future to eventually reduce the necessity of tedious experimental studies.

* Corresponding authors
E-mail addresses: silvia.budday@fau.de (S. Budday), hermann.seitz@uni-rostock.de (H. Seitz).

https://doi.org/10.1016/j.actbio.2020.10.025

1. Introduction

Osteoarthritis (OA) is the most common degenerative disease of articular joints with increasing frequency due to an aging population [1–4]. OA is characterized by alterations in the articular cartilage, ligaments, capsule, and synovial membrane. Patients with OA regularly suffer from severe pain and experience physical disability alongside a reduction in the quality of life [2,4–6]. The primary function of articular cartilage is to enable a lubricated articular movement and the protection against cyclic compressive loadings during movement [6]. Hyaline cartilage is 2 up to 7 mm thick and is composed of an ECM built by chondrocytes. The ECM mainly consists of water, proteoglycans, and different collagen types with collagen II making up the majority of 90-95% of the ECM. Hyaline cartilage is divided into several zones, wherein each zone has its specific morphology and function, as illustrated in Fig. 1a. The thin superficial zone (SZ, 10-20% of total thickness) comprises numerous flat chondrocytes and protects the deeper layers. The collagen fibers are orientated tangentially to the surface (tangential fibre zone). The SZ goes continuously into the middle zone (transition zone, 40-60% of total thickness). Here the collagen fibers align themselves along the arches of arcades (isotropically orientated collagen fibers). The primary function of the middle zone is the absorption of compressive forces. In the deep zone (radial fiber zone, 30% of the total thickness), the chondrocytes and collagen fibers are aligned in parallel and perpendicular to the SZ. This zone offers the highest resistance to compressive forces [7]. The border to the calcified cartilage layer beneath is termed the tide mark. The calcified cartilage layer represents a transition and anchoring between cartilage and bone [5,7,8].

Once damaged, articular cartilage has only a very low regeneration potential due to low cell turnover and a lack of vascularization [5]. Conservative surgical therapeutic approaches to repair damaged articular cartilage via abrasion chondroplasty and micro fracturing can trigger spontaneous healing and the formation of fibrous tissue. Other techniques based on transplantation strategies, such as mosaicplasty and autologous-chondrocyte implantation (ACI), or matrix-associated chondrocyte implantation (MACI), do not yield better results. Besides, there are disadvantages, such as a secondary intervention and damage to healthy cartilage by such treatments [9,10]. The last resort for surgical therapy of OA is the total joint replacement. However, such a highly invasive technique has a finite lifespan and can usually only be performed once [2]. To overcome these disadvantages, current research efforts mostly focus on tissue engineering approaches. Tissue engineering comprises three main building blocks: the scaffold material or biomaterial, biofactors, and chondrogenic cells [9,11]. The present work focuses on the scaffold material, which should mimic the natural extracellular matrix (ECM).

Frequently used materials in tissue engineering are hydrogels, which are three-dimensional (3D) polymeric networks that can absorb a large amount of water up to thousands of times of their dry weight [12]. Due to their unique properties, they can well resemble the properties of biological tissues, and specifically those of cartilage. The hydrogel polymer matrix can be based on a wide variety of polymeric components, such as collagen-based, natural polysaccharide-based such as alginates or chitosan, or synthetic polymer-based such as polyethyleneglycols (PEG), to name just a few. The biomaterial matrix is then seeded or infiltrated by cells pre- or post-implantation [9,11].

In the current study, we focus on the commercially available collagen I-based hydrogel ChondroFiller^{liquid} (Meidirx Biomaterials GmbH, Esslingen Germany), an oxidized alginate-gelatine-based hydrogel (ADA-GEL) [13,14], and hyaline human cartilage. We specifically chose those materials as ChondroFiller^{liquid} is frequently used in clinical practice for cartilage repair and the ADA-GEL hydrogel system is a promising material with enough versatility and chemical functionalization capability to tackle the challenges associated with long-term cell culture in tissue engineering applications [15].

The collagen type I in ChondroFiller^{liquid} is obtained by acid extraction from rat tail tendons. In clinical practice, ChondroFiller^{liquid}

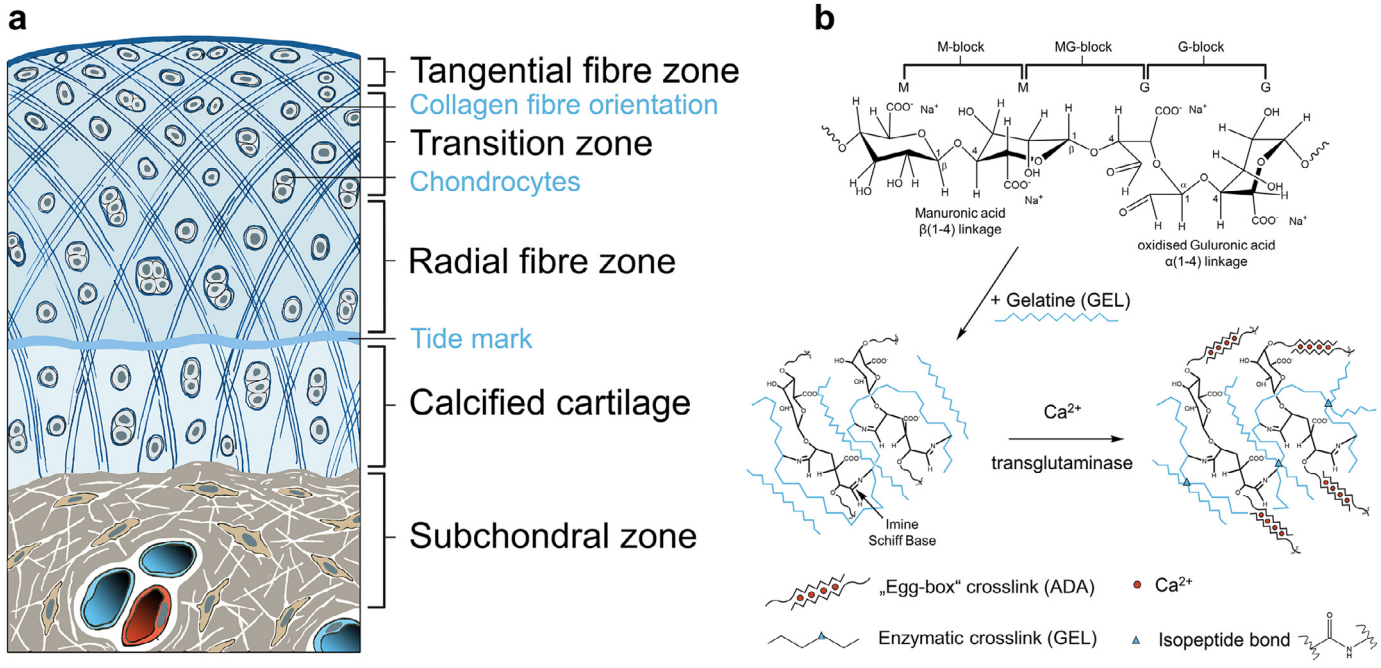

Fig. 1. a) Schematic structure of hyaline cartilage with chondrocyte distribution and zone division; b) Chemical structure of partially oxidised sodium alginate, alginate-dialdehyde (ADA), and gelatine (GEL) hydrogel, forming an imine bond between amino groups of lysine and aldehyde groups of the ADA backbone (Schiff Base). Ca^{2+} and microbial transglutaminase facilitate additional ionic and enzymatic crosslinking of the polysaccharide chain (red) and the gelatine network (teal), respectively. A detailed schematic has been reported in previous studies [16].

is directly injected into the cartilage defect (Outerbridge grade III-IV) and forms a pressure-resistant gel to fill the defect. It provides the cells with a matrix into which they can migrate.

Alginate-based hydrogels are prominently used for tissue engineering [17]. The main advantage of this system is the ease of ionic crosslinking via divalent cations, such as Ca^{2+}, Ba^{2+}, and Sr^{2+} [18,19], as well as its biocompatibility [17]. However, pristine-alginate-based hydrogels lack sufficient degradability and cell adhesion motifs [20,21]. Oxidized alginate (ADA)-based hydrogels offer tuneability degradability as well as the potential for crosslinking with proteins via Schiff's base formation (Fig. 1b) [20,22]. Thus, this material system offers both, ionic crosslinking via cationic interaction as well as reversible covalent crosslinking via Schiff's base formation in the hydrogel [14]. Previous studies showed that ADA-GEL hydrogels allow applicability in various tissue engineering approaches, such as bone, blood vessel, and cartilage tissue engineering [15,23–29]. For instance, enzymatically crosslinked ADA-GEL showed promising cell-material interaction with primary human nasoseptal chondrocytes confirming that it allows for Col II and glycosaminoglycans expression of the cells [29]. It was possible to tailor the degradation behavior of ADA-GEL by enzymatic crosslinking using microbial transglutaminase to fabricate hydrogel matrices stable for up to 30 days of cell culture [16]. This renders them suitable for long-term cell culture required for cartilage tissue engineering applications. In addition, the use of temperature-treated ADA-GEL of high gelatin content allowed for improved 3D-printability in comparison to previous ADA-GEL compositions [30]. As a result, 3D-printable high gelatin content ADA-GEL with enzymatic crosslinking may be a suitable future matrix for cartilage regeneration applications. However, the detailed mechanical response of the hydrogel in comparison to native cartilage tissue still needs to be addressed.

Factors such as the material's biocompatibility, adhesion motifs, porosity, and biodegradability influence the short- and long-term cell response in the engineered tissue [31–33]. Bioactive molecules such as proteins, growth factors, cytokines, or hormones, just to name a few, can modulate cellular behavior due to biomolecular interactions and cellular recognition [34–36,87]. Besides biomolecular cues, physical cues such as substrate stiffness can alter cell response and development through mechanosensing [37–39]. As a result, the mechanical properties of scaffolds resulting in biomechanical cues through cell-material interactions can dictate cell behavior and are, therefore, vital for successful biomaterial design and tissue engineering [9,11,40]. Importantly, both elastic and viscoelastic properties influence the mechanotransduction, differentiation, migration, and proliferation of cells [40–49]. Lee et al. [40] have shown that mechanical stress relaxation, hence stress dissipation in the hydrogel caused by chondrocyte ECM expression, is an important mechanotransducton factor to increase ECM expression of chondrocytes in fast relaxing hydrogels. In addition, previous studies have shown that pathological changes in cartilage or degradation of the proteoglycan matrix result in mechanical changes of the tissue [50,51]. As a result, the mechanical characterization of both native and engineering materials is becoming increasingly important in the field of tissue engineering. It is essential to compare the mechanics of cartilage and the ingrown implant as a performance criterion [52].

Understanding the complex mechanical behavior of scaffold materials is not only important for cell fate in tissue engineering but also enables to develop *in silico* computer models for numerical simulations. With the help of such simulations, magnitude, orientation and location of stresses and strains within the scaffold materials can be predicted, and conclusions can be drawn about the mechanoactive transduction of chondrocytes. Computational predictions allow us to separate or extract different effects on the mechanotransduction between ECM and chondrocytes under mechanical and electrical loading, such as strain levels, strain direction, or electrical fields [49,53]. Both natural cartilage and hydrogels are exposed to mechanical loadings when used as implants. The corresponding stress and strain states can be assessed and predicted through numerical simulations, which help to better understand their unique resistance against loading [54,55].

A still unsolved question is how the function, microstructure and physiology of cartilage is related to its mechanical behavior. The question arises which mechanical parameters affect cells in cartilage or are critical for the success of implant materials. Numerous studies have investigated different mechanical parameters of hydrogels and cartilage. The most frequently used tests to assess the time-dependent viscoelastic behavior are stress relaxation experiments in confined or unconfined compression [49,56–59]. Similarly, the loading segment during compression tests has been used to investigate the time-dependent or rate-dependent behavior [60]. In addition, cyclic loading conditions have shown effects such as the Mullins effect, conditioning, and recovery [61–64]. Interestingly, the measured properties are sensitive to a change in the polymer concentration and thus reveal information about the chemical structure of the material [56]. Although human cartilage experiences relatively high strains (up to 10% principal strain) *in vivo* when loaded in compression direction with only half of the body weight [65], most previous studies have not considered large deformations, different loading modes, and the entire loading history [3]. Often the mechanical tests for parameter identification for numerical simulations only represent one loading mode or are limited to the time-independent behavior [55,66]. If material parameters are determined based on data from a single loading mode, however, they do not well represent the behavior under different loading conditions [67]. To allow for reliable predictions, it is, therefore, key to test at least the loading modes, loading levels, and time scales that will occur during the application of interest.

In the present work, we investigate the mechanical behavior of human hyaline articular cartilage, ChondroFiller^{liquid}, and ADA-GEL under large deformations and multiple loading modes. We study the conditioning behavior through cyclic compression and tension tests, supplemented by stress relaxation experiments. To link the macroscopic mechanical response to the materials' underlying microstructure, we examine collagen-based ChondroFiller^{liquid} hydrogels by using multiphoton Second Harmonic Generation (SHG) microscopy. We aim to generate a data set that is not only valuable for applications in tissue engineering but will also serve as a basis to calibrate numerical models in the future that can predict stress and strain states in native and artificial cartilage.

1. Materials and Methods

1.1. Materials

1.1.1. Cartilage specimens

We obtained one left knee from a human cadaver. The body donor was a 62 year old woman who died of liver and kidney failure. We pre-punched cylindrical cartilage samples from the condyle and extracted them with a scalpel, as illustrated in Fig. 2. The specimens had a diameter of approximately 8 mm and a height of approximately 2 mm, as illustrated in Fig. 3a. The height of the specimens was restricted by the natural cartilage thickness. Due to the higher stiffness of native cartilage compared to the hydrogels, fewer boundary effects can be expected. The native cartilage was kept refrigerated at 4°C and hydrated by phosphate buffered saline solution to minimize tissue degradation.

1.1.2. ChondroFiller^{liquid}

ChondroFiller^{liquid} is a two-chamber syringe system and was provided by the Meidrix Biomedicals GmbH (Esslingen, Germany).

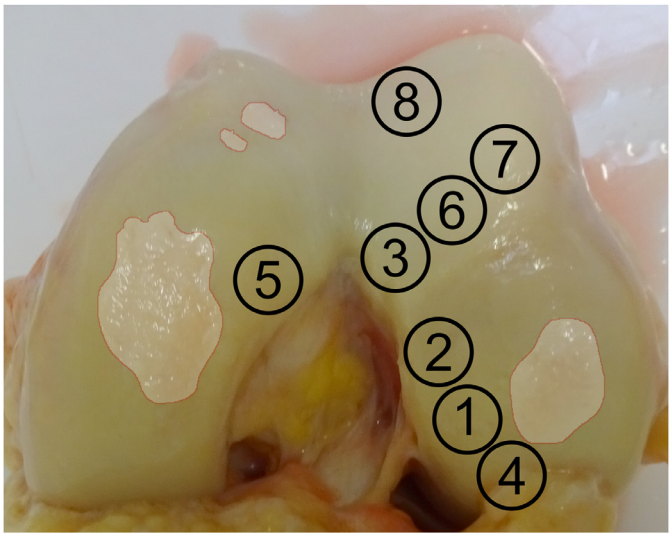

Specimen	Test
1	Recovery
2	Cyclic compression
3	Cyclic tension
4	Step-wise increasing maximum strain
5	Stress relaxation
6, 7, 8	Combined tests

	Age	Gender	cause of death
Donor Information	62	woman	liver and kidney failure

Fig. 2. Left knee cartilage with specimen location and number: Overview of conducted tests on specimens. Herds of osteoarthritis are schematically marked.

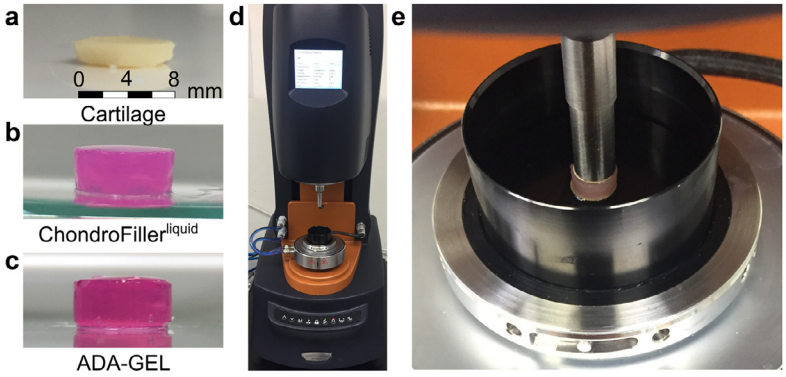

Fig. 3. Experimental setup. a) Cartilage specimen. b) ChondroFiller^{liquid} specimen. c) ADA-GEL specimen. d) Rheometer with upper sample holder and immersion cup. e) Specimen mounted to the testing setup, glued on its top and bottom surfaces.

The larger chamber contains 10 mg/ml collagen type I and the smaller chamber gel neutralization solution. The gel neutralization solution consists of water, HEPES buffer (Gibco HEPES, 4-(2-hydroxyethyl)-1-piperazineethanesulfonic acid, Thermofisher Scientific, Germany), NaCl and NaOH. We applied the content of the syringe in cylindrical shaped silicone molds with a diameter of 8 mm and a height of 4 mm. The hydrogel specimen height of 4 mm (see Fig. 3b) was chosen to reduce edge effects. Figure S1 shows one syringe with ChondroFiller^{liquid} and the silicon mold. The collagen gelates when its pH value of 3.8 is adjusted by mixing it with the gel neutralization buffer. The final scaffold has a concentration of 8 mg/ml collagen. On the top of the open scaffold, we put glass coverslips to ensure an even surface geometry. We kept the mold with the scaffolds refrigerated for 24 h at 4°C to trigger gelation. We tested all samples within the next 12 hours.

1.1.3. Oxidized alginate-gelatine (ADA-GEL) hydrogels

Material synthesis. Alginate di-aldehyde (ADA) was synthesized by controlled oxidation of sodium alginate (average molecular weight (Mw) ~250 kg mol^{-1} [68], ~46% guluronic acid, ~54% mannuronic acid [68], VIVAPHARM PH176, by JRS PHARMA GmbH & Co. KG, Germany) as described earlier [14]. All reaction steps were performed in the absence of light. In brief, 10 g of alginate were dispersed in a mixture of ethanol (50 ml) and water (50 ml, MilliQ ultra-pure, Merck, Germany) containing 9.375 mmol $NaIO_4$. Next, the reaction was stirred for 6 hours at 22°C (room temperature, RT). To quench the reaction, 10 ml of ethylene glycol (VWR chemicals international, USA) were added, followed by additional stirring for 30 minutes. The reaction product was allowed to sediment for 5 minutes, followed by decanting of the ethanol. The oxidized alginate was transferred to dialysis tubes (MWCO: 6500 kDA, Repligen, USA) and dialyzed for 7 days against 17 L of ultra-pure water. The product was frozen for at least 24 hours and lyophilized using a freeze dryer (Alpha 1-2LD plus, Martin Christ, Germany)

Hydrogel formation. For ADA-GEL hydrogel specimen preparation, ADA (7.5% (w/v)) in phosphate buffered saline solution, 5 ml) and 5 ml GEL (7.5% (w/v), in H_2O MilliQ, 5 ml) (Typ A, Bloom 300, Sigma Aldrich, Germany) were homogenously mixed for 10 minutes at RT. GEL was pre-treated by dissolving the gelatin in H_2O at 80°C for 3 hours under continuous stirring as described elsewhere [16,30]. The ADA-GEL hydrogel precursor (200 µl) was moulded in custom-made cylindrical polydimethylsiloxan (PDMS, Sylgard 184, VWR chemicals international, USA) molds (diameter, d =8 mm) to yield hydrogel cylinders of height = 4 mm, d = 8 mm Fig. 3. The samples were crosslinked in 0.1 M $CaCl_2$ containing 2.5% (w/v) microbial transglutaminase (mTG, Ajinomoto Co.,Inc, ACTIVA® WM, 85 – 135 U/g, Japan) for 24 hours to ensure homogenous crosslinking throughout the hydrogels.

1.2. Experimental setup

To perform the mechanical characterization, we used a Discovery HR-3 Rheometer from TA instruments (New Castle, Delaware, USA), as shown in Fig. 3d. First, we glued a circular piece of sand-

Table 1
Testing procedures for the qualitative characterization of the material behavior (n=1).

Procedures	Loading mode	Loading profile	nominal strain	Strain rate [1/s]	cycles	material
I Cyclic compression	Compression	sinusoidal	0.15	0.13	ten	ChondroFiller^{liquid}
						ADA-GEL
		triangle				Cartilage
II Cyclic tension	Tension	sinusoidal	0.15	0.13	ten	ChondroFiller^{liquid} & ADA-GEL
			0.025			Cartilage
III Cyclic compression -tension	compression and tension	sinusoidal	0.15	0.13	ten	ChondroFiller^{liquid} & ADA-GEL
IV Stepwise increasing max. strain	compression and tension	sinusoidal	0.15; 0.20; 0.25	0.13	three each strain	ChondroFiller^{liquid}& ADA-GEL
	Compression	triangle	0.10; 0.20			Cartilage
V Recovery	Compression	sinusoidal	0.15	0.13	three	
						ChondroFiller^{liquid} & ADA-GEL
		triangle				Cartilage
VI Stress relaxation	compression and tension	sinusoidal	0.05; 0.10; 0.15	highest possible loading speed (6,000 µm/s)	one	
						ChondroFiller^{liquid} & ADA-GEL
	Compression					Cartilage

paper onto the upper specimen holder and the heating plate with a thin layer of cyanoacrylate to increase the contact surface. After that, we placed the immersion cup on the Peltier element, to ensure a constant 37°C environment during testing. We glued each specimen with cyanoacrylate adhesive to the upper specimen holder, and applied adhesive to the lower surface of the specimen. Then, we lowered the upper specimen holder until we detected an axial force of 0.01 N showing that contact between the specimen and the heating plate was established, as illustrated in Fig. 3e. To prevent the specimen from dehydration, we filled the cup with cell culture medium (DMEM) until the specimen was fully immersed in fluid. For data evaluation, we used the software MATLAB (version R2019b, The MathWorks, Inc., Natick, Massachusetts, USA).

1.2.1. Testing procedures

Firstly, we performed a series of testing procedures to thoroughly assess the mechanical characteristics of the different materials. In total, we conducted six testing protocols under different loading modes, compression and tension, and different loading conditions, cyclic loading and stress relaxation experiments, to assess the nonlinear, conditioning, and hysteretic behavior in an unconfined testing setup. All testing procedures I-VI for the qualitative characterization were performed on a single representative specimen from each of the three materials and are summarized in Table 1.

The first testing protocols (I-III) consisted of ten loading cycles in compression and tension, separately and combined. For the ChondroFiller^{liquid} and ADA-GEL specimens, we applied a maximum strain of 15%, corresponding to stretches of $\lambda = 0.85$in compression and $\lambda = 1.15$in tension. Due to the higher stiffness of human cartilage, we had to limit the maximum strain in tension to 2.5%, as the glued specimens would have detached at higher strains. To even better understand the conditioning behavior of the different materials, we additionally performed cyclic experiments at stepwise increasing maximum strains (procedure IV).

To answer the important question whether conditioning is irreversible resulting from damage or permanent remodeling, such as the Mullins effect, or whether it is the result of the material viscoelasticity, and thus reversible, we performed two cyclic compression tests up to 15% strain separated by a 60 minutes recovery period (procedure V). During the recovery period, the sample remained glued in the testing setup and was surrounded by cell medium (DMEM). In addition, we investigated potentially nonlinear time-dependent effects through a series of stress relaxation tests at different maximum strains. Here, we chose a maximum loading speed of 6,000 µm/s to imitate an instantaneous loading. The specimen was loaded at four different strains in compression first, and afterwards in tension with a holding period of 100 s (procedure VI).

We note that we had to use different loading profiles for the hydrogels (ChondroFiller^{liquid} and ADA-GEL) and the native cartilage, respectively, as indicated in Table 1. While a sinusoidal loading profile allowed us to continuously record data during testing, the velocity in positive z-direction was fixed to 500 µm/s. Thus, for the much stiffer native cartilage, we reached the maximum force limit of the rheometer. Therefore, we instead used a triangular loading profile to enable the accurate adjustment of the velocity in both tension and compression. Due to the limited sampling rate of recorded stresses at high speeds, the data was not completely recorded during the directional change from compression to tension and vice versa. Therefore, in these instances, the curves were fitted to polynomial functions to extrapolate missing data points.

In addition to these protocols, which aimed to qualitatively characterize the materials, we performed a combined testing protocol, as summarized in Table 2, to generate a data set for quantitative material parameter identification. For ChondroFiller^{liquid} (n=9) and ADA-GEL (n=8), we started with cyclic compression-tension loadings with a maximum nominal strain of 0.1 for three cycles, and another three cycles with a maximum nominal strain of 0.2. This was followed by a relaxation test in compression and in tension with a maximum nominal strain of 0.15 each. For cartilage (n=3), we had to reduce the nominal strain in all tests since the specimens detached during tensile loading, and the maximum force of the rheometer was reached at 500 µm/s.

1.2.2. Multiphoton Microscopy Imaging

For the analysis of the hydrogel microstructure of collagenous (ChondroFiller^{liquid}) and gelatin (ADA-GEL)-based hydrogels, Second Harmonic Generation imaging (SHG) was conducted using a multiphoton microscope (TriMScope II, LaVision BioTec, Bielefeld, Germany). Fibrillar collagen was analyzed using nonlinear frequency doubling caused by collagen fibrils via multiphoton SHG [69]. A modelocked ps-pulsed Ti:Sa laser (Chameleon vision II, Coherent, Santa Clara, USA) at 810 nm wavelength was used to excite SHG signals. A single bandpass filter (405/20 nm, Chroma Technology group, Acal BFi Germany GmbH, Germany) in combination

Table 2
Combined testing protocol for material parameter identification (ChondroFiller^{liquid}: n=9, ADA-GEL: n=8, Cartilage: n=3).

Protocol for combined test	ChondroFiller^{liquid} and ADA-GEL				Cartilage			
	nominal strain	cycles	holding time [s]	velocity [µm/s]	nominal strain	cycles	holding time [s]	velocity [µm/s]
cyclic compression and tension	0.1	3	-	500	0.01	3	-	500
cyclic compression and tension	0.2	3	-	500	0.025	3	-	500
stress relaxation in compression	0.15	-	150	6000	0.05	-	1000	6000
stress relaxation in tension	0.15	-	150	6000			-	

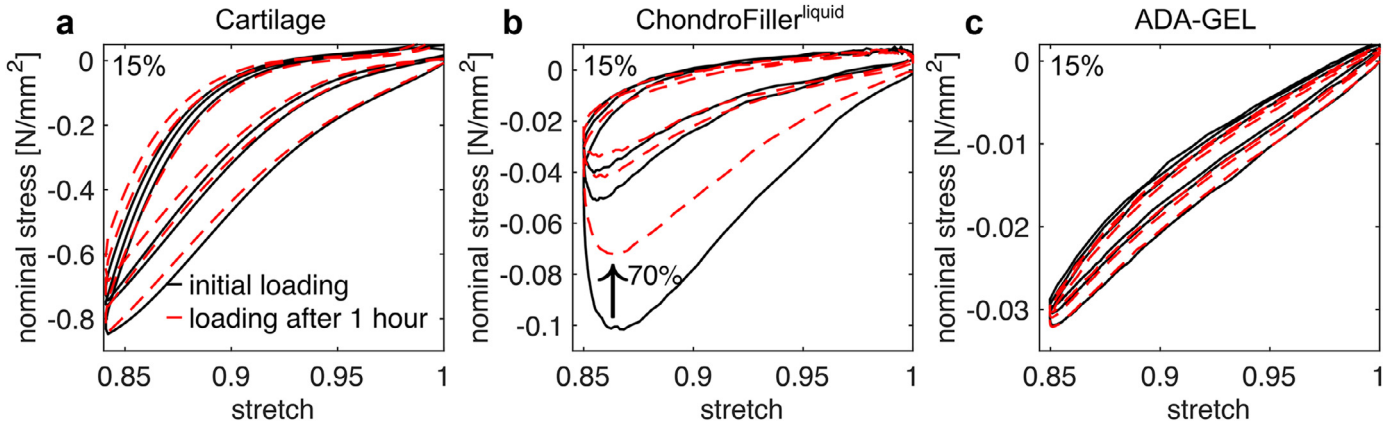

Fig. 4. a-c) Representative conditioning behavior in unconfined cyclic compression for human cartilage, ChondroFiller^{liquid} and ADA-GEL with a nominal strain of 0.15, corresponding to a stretch of 0.85; d-f) Hysteresis area as a function of the loading cycle number for cartilage, ChondroFiller^{liquid} and ADA-GEL. The hysteresis area of the stress-stretch curve represents the dissipated energy during each loading cycle.

with non-descanned ultrasensitive photomultiplier tubes (PMT, H 7422-40 LV 5 M, Hamamatsu Photonics, Japan) was used to detect the SHG signal in transmission and backscatter orientation [70]. To visualize non-fibrillar hydrogel components, sample two-photon (2P) excited autofluorescence (AF) was recorded using a 525/50 nm single bandpass filter (Chroma Technology group) and a non-descanned PMT in a backscattered configuration. The voxel size of acquired stacks was 0.8 × 0.8 × 2 µm with a field of view of 400 × 400 µm and a stack depth of 500 µm. Orientation analysis and quantification of fibrous hydrogel content were performed from z-stacks (n = 3) with 745 slices using a custom written ImageJ macro (Image J software, imageJ.nih.gov) [71]. Hydrogel specimens of ChondroFiller^{liquid} in an unloaded state after compressive loading were analysed using SHG. For comparison, ADA-GEL hydrogels were analysed, featuring gelatin as a denatured form of collagen as a hydrogel component.

2. Results

2.1. Recovery test

Fig. 4a-c show the stress-stretch response of cartilage, ChondroFiller^{liquid} and ADA-GEL during two sets of three loading cycles in unconfined compression up to 15% strain, corresponding to a stretch of 0.85, separated by a 60 min recovery period (testing procedure V). For cartilage and ADA-GEL, the results indicate that after 60 minutes, the specimens were fully recovered and showed a similar mechanical behavior during the initial loading. ChondroFiller^{liquid}, in contrast, displayed maximum stresses of only approximately 70% of the initial maximum stress after the one hour recovery period. This observation motivated us to perform an additional recovery test (for ChondroFiller^{liquid} only) with a recovery period of only 20 minutes instead of 60 minutes, which, interestingly, showed a maximum force of 50% of the initial loading response.

2.2. Conditioning behavior

2.2.1. Cyclic compression

Fig. 5a to c show the representative mechanical response of cartilage, ChondroFiller^{liquid} and ADA-GEL during cyclic unconfined compression tests. Cartilage and ChondroFiller^{liquid} displayed a pronounced nonlinearity in the stress-stretch relation and strain-stiffening, while ADA-GEL shows only slight nonlinearity. All materials showed a decrease in the hysteresis area after the first, second and third loading cycle. This effect was most pronounced for ChondroFiller^{liquid}, as shown in Fig. 5e. Furthermore, we observe a decrease in the maximum stresses between the first, second and third loading cycle, whereas only minor conditioning takes place for all subsequent cycles. While we observed an almost constant offset force at 0% strain for cartilage and ChondroFiller^{liquid}, for ADA-GEL the offset increased with each cycle. Therefore, we can mostly attribute the continuing conditioning of ADA-GEL after the third cycle to an increasing offset force.

2.2.2. Cyclic tension

Fig. 6 depicts the conditioning behavior of cartilage, ChondroFiller^{liquid} and ADA-GEL under cyclic unconfined tension loading. The qualitative mechanical behavior of ChondroFiller^{liquid} and ADA-GEL in tension is comparable to the material response in compression. We note that for the cartilage specimen, we had to reduce the load to a nominal strain of only 0.025, as described in Section 2.2.1. The risk that the sample detached from the specimen holder can also be seen in Fig. 6a, where we observe a drop in the stresses during the third cycle of loading. In direct comparison to the compression of cartilage at higher strains, the tissue shows a rather linear nominal stress-stretch behavior similar to ADA-GEL in both tension and compression. Still, cartilage shows more pronounced conditioning effects and a larger hysteresis. Similar to our observations under compression, the hysteresis area decreases during the first three loading cycles but stays almost constant after that for all materials (see Fig. 6d-f).

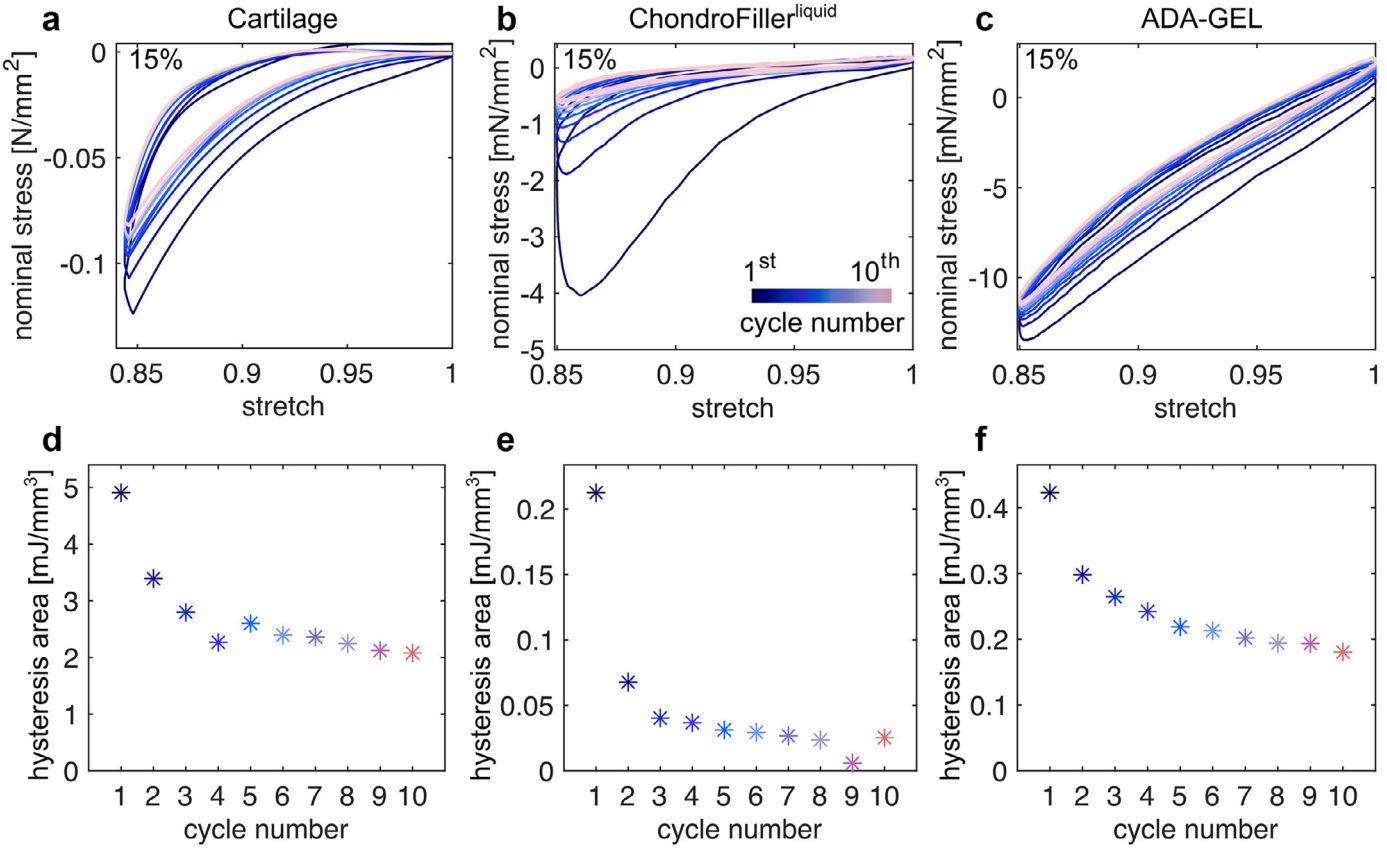

Fig. 5. Representative nominal stress versus stretch behavior of a) human cartilage, b) ChondroFiller^{liquid}, and c) ADA-GEL for two unconfined compression tests with three cycles each, separated by a 60 min recovery period.

2.2.3. Cyclic compression-tension

Fig. 7 shows cyclic compression-tension tests in an unconfined testing setup with a maximum nominal strain of 0.15. Both ChondroFiller^{liquid} and ADA-GEL exhibit a compression-tension asymmetry with higher stresses in compression than in tension. While ChondroFiller^{liquid} shows a highly nonlinear behavior, ADA-GEL only shows minor nonlinearity, as already observed in the individual cyclic compression and tension loadings. We also observe similar conditioning effects as for the individual experiments in Figs. 5 and 6. Especially for ChondroFiller^{liquid}, the hysteresis area decreases with increasing loading cycles.

2.2.4. Stepwise increasing maximum strain

Fig. 8a to c shows the nominal stress versus stretch behavior of cartilage, ChondroFiller^{liquid} and ADA-GEL for cyclic compression-tension loadings with stepwise increasing maximum strain. We loaded the specimens with three cycles per strain level. Again, it was not possible to subject the cartilage sample to high tensile strains, so that we limited the loading to compression only. Pronounced conditioning occurred after each loading cycle and for each new strain level. Futhermore, the strain-stiffening is shifted to higher strains when a higher strain level is applied.

2.3. Stress relaxation behavior

Fig. 9a to f display the normalized stress relaxation behavior of cartilage (a,d), ChondroFiller^{liquid} (b,e) and ADA-GEL (c,f) for different strain levels. In compression, cartilage, ChondroFiller^{liquid} and ADA-GEL show no difference in the relaxed stress levels after 100 s of holding time. In tension, ADA-GEL relaxes faster when loaded to only 0.05 nominal strain compared to 0.10, 0.15 and 0.2 nominal strain. ChondroFiller^{liquid} showed the fastest stress relaxation, where 0.12±0.03 of the initial nominal stress was reached after 100 s, followed by cartilage with 0.35±0.04 and ADA-GEL 0.81±0.03 of the initial nominal stress. After an extended holding time of 1,000 s, cartilage further relaxed to a value of 0.11±0.01 of the initial nominal stress, as illustrated in Fig. 9d.

In tension, ChondroFiller^{liquid} showed a slower relaxation behavior with 0.45±0.03 of the initial nominal stress compared to 0.12±0.03 in compression. For ADA-GEL, we observed a similar behavior as in compression, despite the deviation at 0.05 nominal strain, with a value of 0.81 of the initial nominal stress reached after 100 s.

2.4. Combined Tests

Fig. 10 displays the average results with standard deviations from the combined testing protocol summarized in Table 2. Similar to the observations in Section 3.2.3, ChondroFiller^{liquid} and ADA-GEL show a compression-tension asymmetry with higher stresses in compression than in tension. In contrast, human cartilage exhibits higher stresses in tension than in compression for both 0.01 and 0.025 maximum nominal strains. Unlike the response under compression only, the stresses do not drop between the first and second cycle under compressive loading. This could be attributed to the offset force that arises from tensile loading. This high offset for cartilage in tension was also observed in Section 3.2.2. The hysteresis area highly depends on the strain level and decreases with consecutive loading cycles (see Fig. 11). Interestingly, for higher compressive strains of 0.2, even the response of ADA-GEL becomes nonlinear, as illustrated in Fig. 10f.

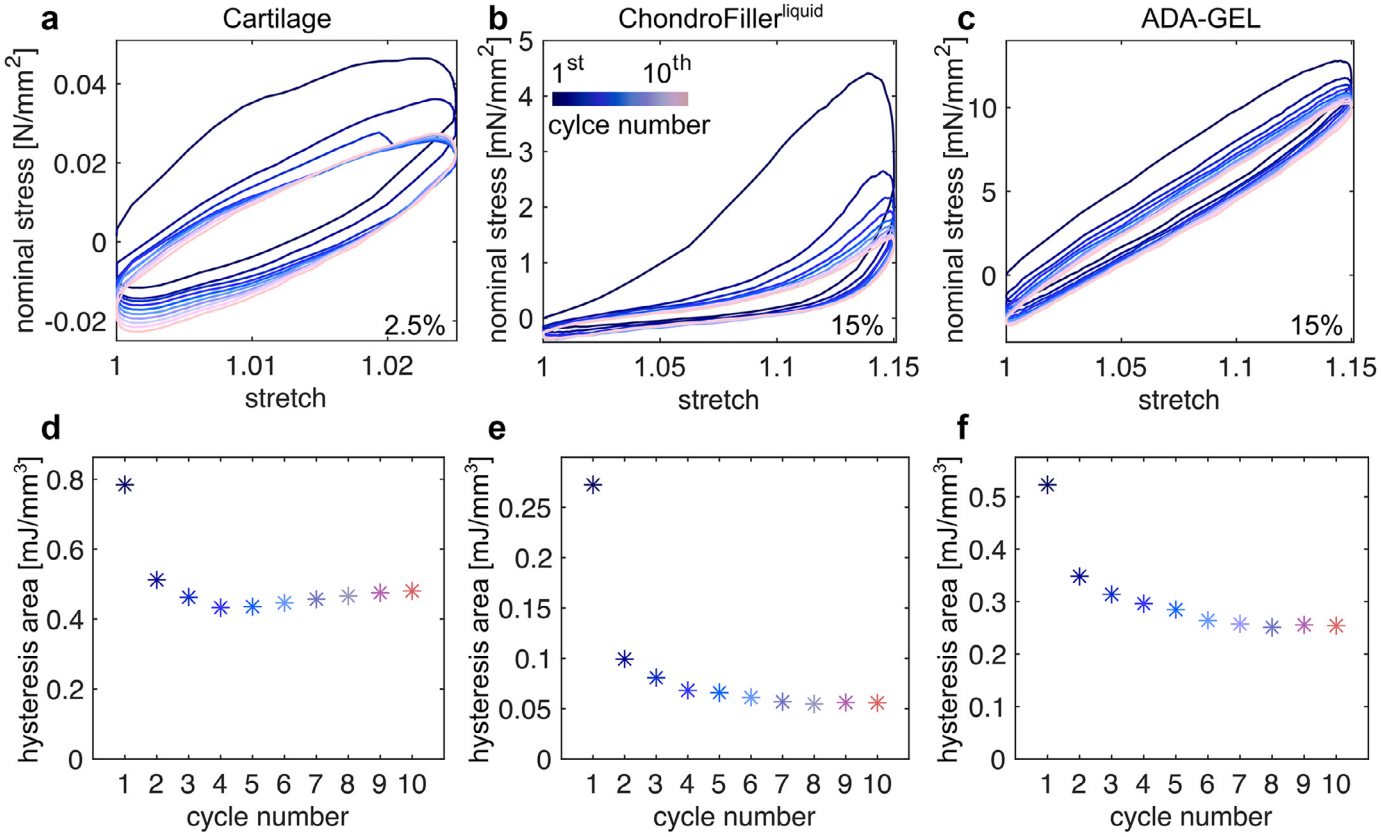

Fig. 6. a-c) Representative conditioning behavior in unconfined cyclic tension for human cartilage, ChondroFiller^{liquid}, ADA-GEL with a nominal strain of 0.15, corresponding to a stretch of 1.15, for Chondrfiller^{liquid} and ADA-GEL, and a strain of 0.025, corresponding to a stretch of 1.025 for cartilage; e-f) Hysteresis area as a function of the loading cycle number for cartilage, ChondroFiller^{liquid} and ADA-GEL. The hysteresis area of the stress-stretch curve represents the dissipated energy during each loading cycle.

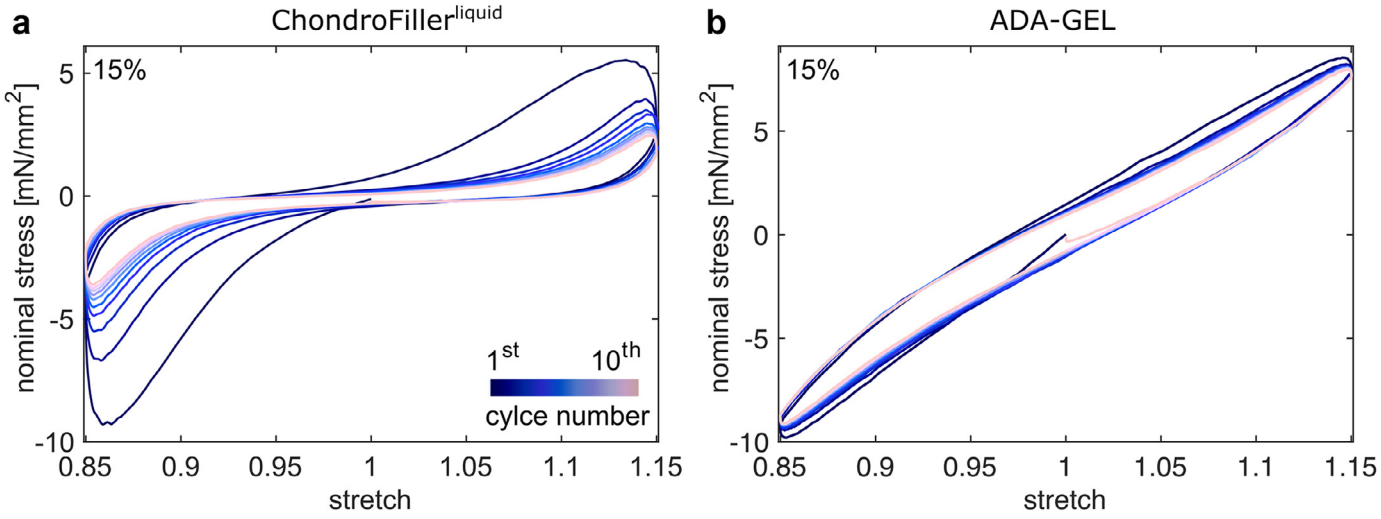

Fig. 7. Representative cyclic compression-tension response during ten loading cycles with maximum nominal strain of 0.15 for ChondroFiller^{liquid} and ADA-GEL.

In addition, the stress relaxation experiments with a holding time of 150s in Fig. 10g-i generally agree with the previously observed trends. For human cartilage and ChondroFiller^{liquid} almost 70% of the initial stress has relaxed after 150s, while ADA-GEL only shows a 20% decrease in stresses within the same amount of time. The exemplary responses of cartilage and ADA-GEL in Section 3.3 lie within the standard deviation of the stress relaxation tests performed during the combined testing protocol. For ChondroFiller^{liquid}, however, the relaxation is slightly faster in compression and slower in tension than reported in Section 3.3 Table 3. summarizes the characteristic time constants corresponding to the realaxtion curves in Fig. 10g-i and k-l. We determine the time constants by adopting a multi-term Prony series $\sigma(t) = \sigma_\infty + [\sigma_i - \sigma_\infty] \sum_{i=1}^{n} \exp(-t/\tau_i)$, with $n$characteristic time constants τ_i. We found the best approximation for a two-term Prony series. The short and long time scales of all the three materials differ by about one order of magnitude. Both time constants of human cartilage in compression, $\tau_1 = 16.76$ sand $\tau_2 = 210.47$ s, are approxi-

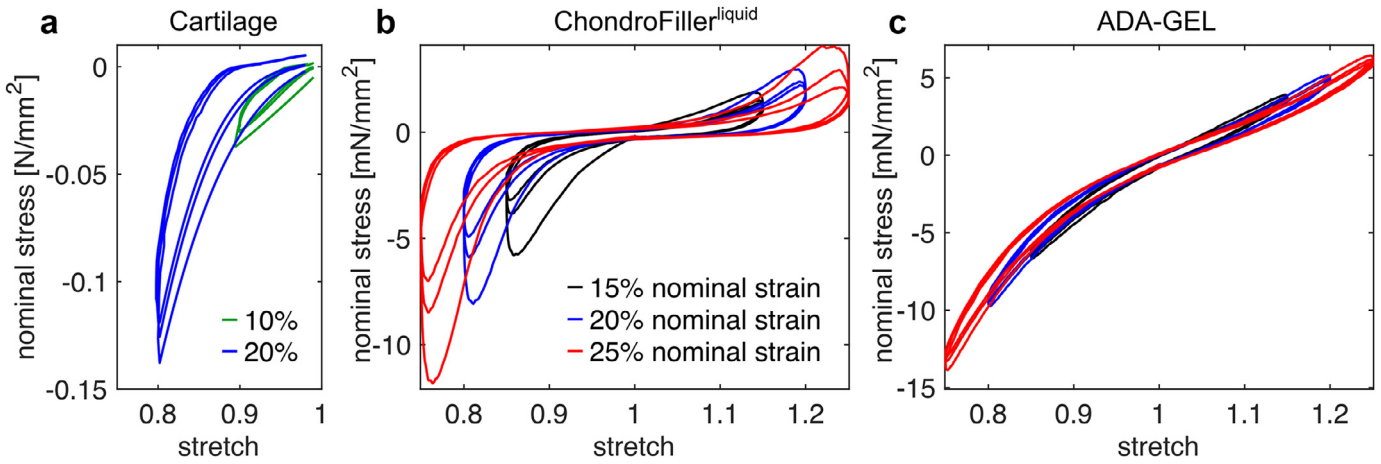

Fig. 8. Representative nominal stress versus stretch behavior of a) human cartilage, b) ChondroFiller^{liquid} and c) ADA-GEL under cyclic unconfined compression-tension loading with stepwise increasing maximum nominal strain and three cycles per strain level.

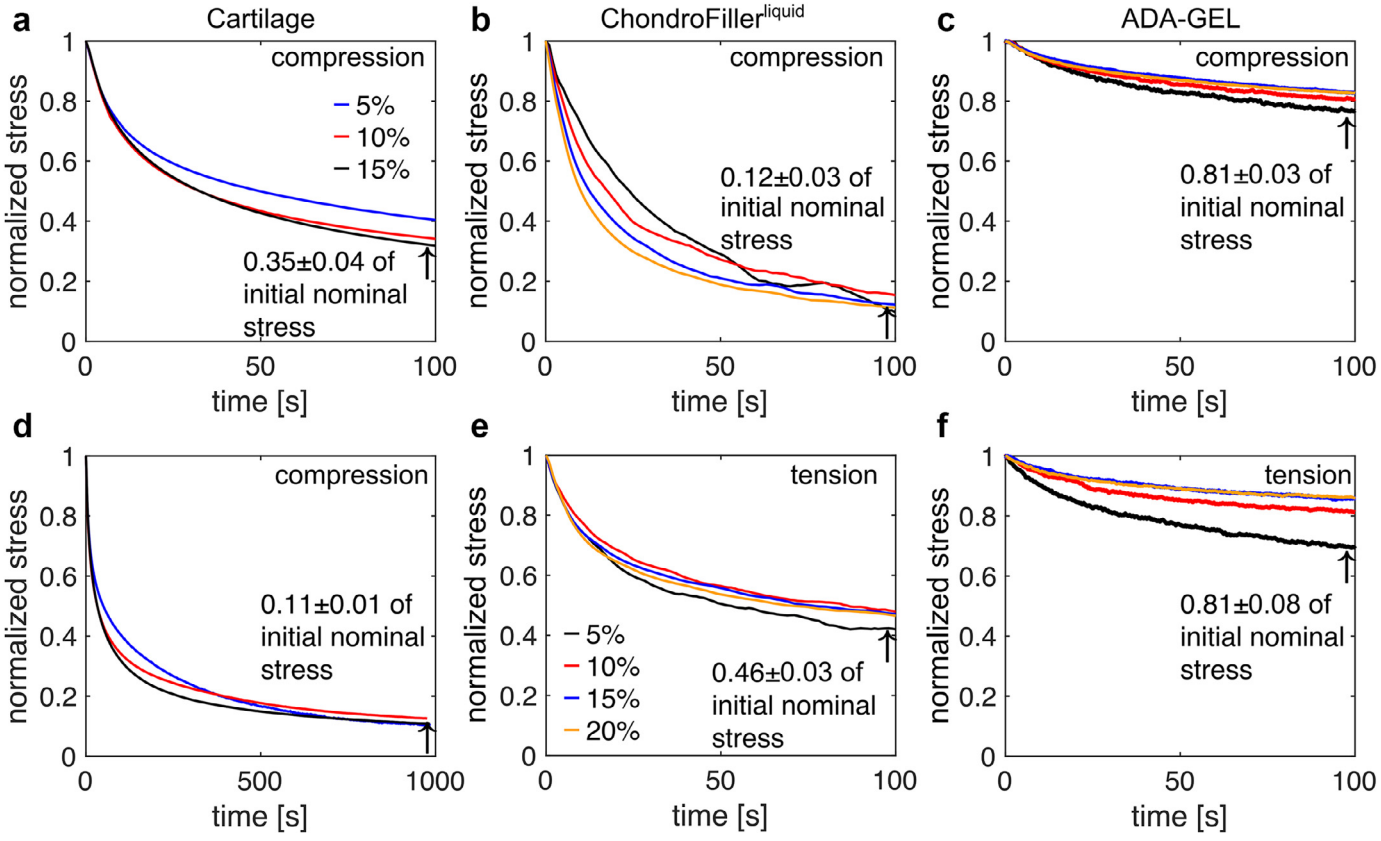

Fig. 9. Normalized stress relaxation behavior of human cartilage, ChondroFiller^{liquid} and ADA-GEL and corresponding values of the relative nominal stress remaining after the holding time with respect to the initial stress (mean ±STD). a) to c) Normalized stress relaxation curves in compression for different strain levels with a holding time of 100s. d) Normalized stress relaxation behavior of human cartilage in compression with a holding time of 1,000 s. e) and f) Normalized stress relaxation behavior of ChondroFiller^{liquid} and ADA-GEL in tension for different strain levels and a holding time of 100 s.

mately twice as high as those of ADA-GEL with $\tau_1 = 8.82$ *s*and $\tau_2 = 97.85$ *s*. The time constants of ChondroFiller^{liquid}, $\tau_1 = 6.89$ *s*and $\tau_2 = 64.34$ *s*, are lowest, indicating that this material relaxes fastest. The time constants for tensile loadings are slightly lower but in the same range as those for compressive loading.

In a direct comparison, natural human cartilage exhibits the stiffest response, followed by ADA-GEL, while ChondroFiller^{liquid} shows the softest mechanical response. For all loading conditions, the standard deviation is highest for ADA-GEL specimens and lowest for ChondroFiller^{liquid}. This can be attributed to the fact that we observed a slight stiffening of the ADA-GEL specimens during the day of testing.

2.5. Imaging

Fig. 12 depicts 2P microscopy images of hyaline cartilage tissue, ChondroFiller^{liquid}, and ADA-GEL. It was possible to visualize the microstructure of the ChondroFiller^{liquid} hydrogels, while ADA-GEL hydrogels were transparent for the light excitation (810 nm / 405 nm) with neither auto fluorescence (AF, red) nor Second Harmonic Generation (SHG) signal (Fig. 12a). A dense hydrogel struc-

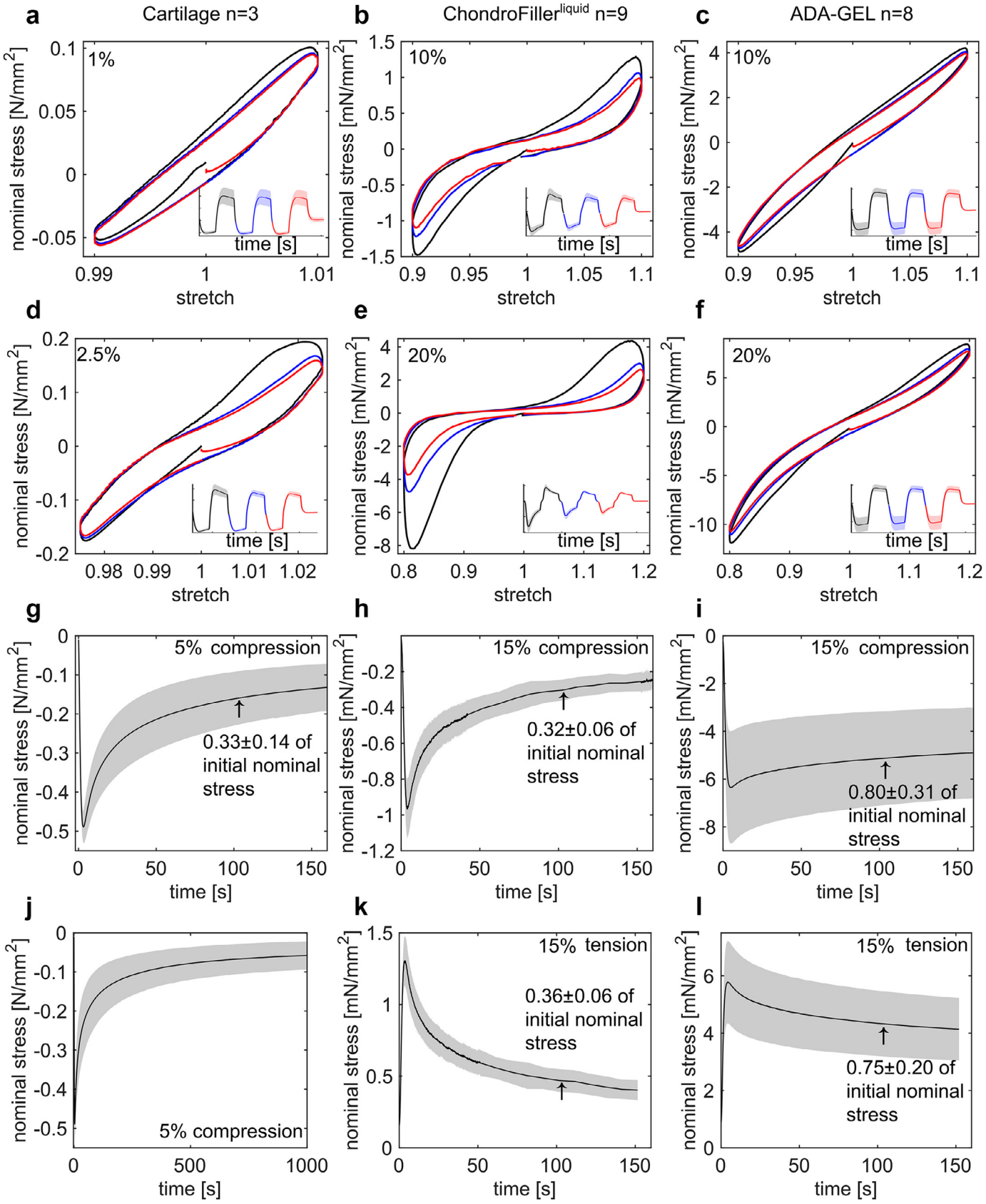

Fig. 10. Average mechanical response with corresponding shaded standard deviations (SD) for combined testing protocol in Table 2. a) to c) Cyclic compression-tension with a maximum nominal strain of 0.01 for human cartilage and 0.1 for ChondroFiller^{liquid} and ADA-GEL, three cycles each. d) to f) Cyclic compression–tension with a maximum nominal strain of 0.025 for cartilage and 0.2 for ChondroFiller^{liquid} and ADA-GEL, three cycles each. g) to i) Stress relaxation in compression with a maximum nominal strain of 0.05 for human cartilage and 0.15 for ChondroFiller^{liquid} and ADA-GEL with a holding time of 150 s. j) Stress relaxation of human cartilage with a 1,000 s holding time. k) to l) Stress relaxation in tension with a maximum nominal strain of 0.15 for ChondroFiller^{liquid} and ADA-GEL with a holding time of 150 s.

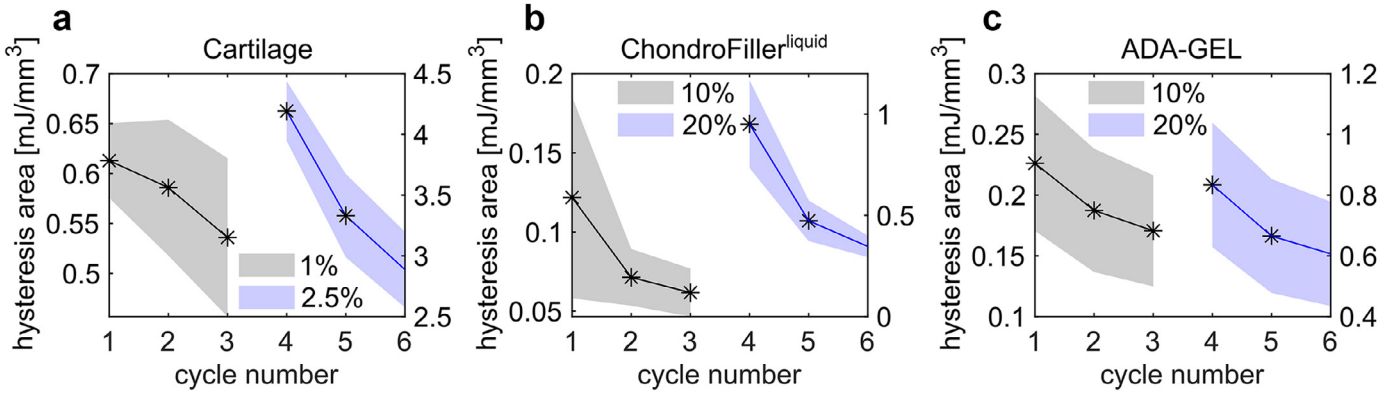

Fig. 11. Hysteresis area for cyclic experiments of the combined testing protocol in Table 2 for human cartilage, ChondroFiller^{liquid} and ADA-GEL for two different strain levels. The hysteresis area represents the dissipated energy during each loading cycle.

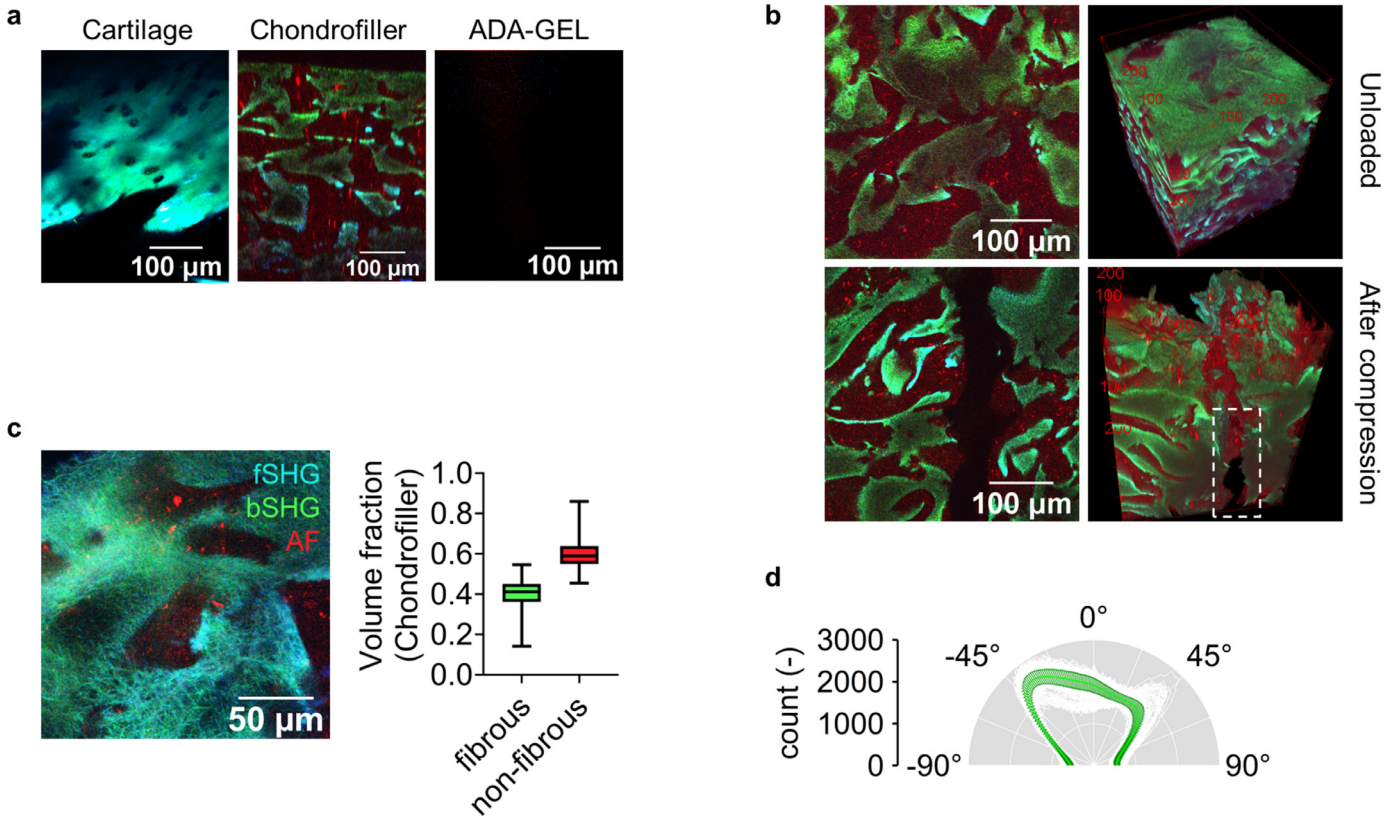

Fig. 12. Multiphoton microscopy images of cartilage, ChondroFiller^{liquid}, and ADA-GEL. a) 2P microscopy images with autofluorescence (red) and Second Harmonic Generation (backward bSHG, green; forward fSHG, teal) of natural hyaline cartilage (in plane), ChondroFiller^{liquid} (cross-sectional), and ADA-GEL (in plane, 450 µm depth). ADA-GEL appeared mostly transparent without the presence of any fibrous structure. b) Detail images of ChondroFiller^{liquid} in unloaded state and after compressive loading. A crack formation is visible in the material (white dashed line). c) Detail 2P images of ChondroFiller^{liquid} with fibrous strucuture visible (bSHG, fSHG). Quantification (n = 3) of fibrous (bSHG and fSHG) and non-fibrous ChondroFiller^{liquid} hydrogel volume-fractions. Data are shown as box plots with mean (horizontal line) and whiskers for minimum and maximum values. d) Angles of fiber orientations, mean ± SD, data traces for each evaluated slice in white (745 slices, n = 3 stacks) analyzed using ImageJ.

ture with embedded chondrons was observed for native cartilage tissue (Fig.12a). Only a limited penetration depth into the cartilage sample was observed, due to little light transparency of the tissue. ChondroFiller^{liquid} showed a bi-phasic hydrogel structure (Fig. 12a-c) with regions of fibrous hydrogel (teal, green) corresponding to forward and backward Second Harmonics (fSHG, bSHG), respectively, as well as non-fibrous hydrogel regions (AF). The surface of the ChondroFiller^{liquid} hydrogels consisted of a dense, fibrous network (Fig. 12b). We observed a crack formation in one of the analyzed ChondroFiller^{liquid} samples (n = 3) after loading (Fig. 12b), dashed white box). The fibrous hydrogel content of ChondroFiller^{liquid} was ~ 40% (c), with small and large fibrous hydrogel components in the hydrogel (Fig. 12c), image bottom-left), which confirmed the partially fibrous, collagen-based hydrogel composition. A preferential orientation of ~ -45° to the hydrogel surface of the microfibers inside the hydrogel was observed (Fig. 12d).

3. Discussion

The regeneration of damaged cartilage tissue remains a major challenge in clinical practice. The present work provides new insights into the complex mechanical behavior of human articular

Table 3
Characteristic time constants for stress relaxation experiments in compression (Fig. 12g-i) and tension (Figure 13k and l) of human cartilage, ChondroFiller^{liquid} and ADA-GEL.

		Cartilage	ChondroFiller^{liquid}	ADA-GEL
Compression	τ_1	16.76 s	6.89 s	8.82 s
	τ_2	210.47 s	64.34 s	97.85 s
Tension	τ_1	-	5.96 s	8.52 s
	τ_2	-	49.22 s	74.77 s

cartilage and two substitute materials, ChondroFiller^{liquid} and ADA-GEL, under compression and tension loadings. Both hydrogel systems are used for regenerative medicine and tissue engineering approaches. Our systematic study combined several testing procedures, revealing important mechanical characteristics such as nonlinearity, recovery, conditioning behavior, and stress relaxation of the different materials, by closely taking into account the underlying material microstructure. In addition to a systematic study revealing characteristic qualitative mechanical features of the different materials, we have performed a series of experiments involving different loading modes to generate a comprehensive data set to identify material parameters for mechanical numerical simulations in the future.

3.1. The nonlinear stress-strain response traces to the underlying microstructure

The present study has shown that human articular cartilage, ChondroFiller^{liquid} and ADA-GEL, exhibit a nonlinear and compression-tension asymmetric mechanical response. While cartilage tissue yields higher stresses under tensile than under compressive loading, ChondroFiller^{liquid} and ADA-GEL show the opposite trend. This disparity is an intriguing observation since both ChondroFiller^{liquid} and cartilage contain fibrillar structures (Figure 12). It has been shown that fibrillar materials exhibit higher stresses in tension than in compression due to the distinct contribution of the fibers [66,72]. The reversed compression-tension asymmetry for ChondroFiller^{liquid} may be attributed to its underlying biphasic microstructure, featuring a layer-like assembly of fibrous and non-fibrous phases with a preferential fiber orientation of ~ −45° to the hydrogel surface (Figure 12). Considering the volume fraction of 60% non-fibrillar hydrogel components to 40% fibrillar components, we assume that the compression-tension asymmetry is dominated by the behavior of the non-fibrous hydrogel. This notion is supported by the observation that ADA-GEL hydrogels, which show no fibrillar regions in the 2P microscopy images, indeed exhibit higher stresses in compression than in tension. This also agrees well with previously reported data for non-fibrillar materials in the literature [73].

ChondroFiller^{liquid} and cartilage both show pronounced strain-stiffening for increasing strains. This is consistent with previous results in the literature [66,72], demonstrating that strain stiffening occurs when fibers in a fibrillar network are immobilized under tensile loading [72]. In contrast, strain stiffening for ADA-GEL specimens is much less pronounced (Fig. 10f). As reported in literature, pure gelatin exhibits mostly a linear response with no significant difference between compression and tension [40,73]. In the ADA-GEL blend, the linear contribution of GEL superimposes the nonlinear mechanical contribution of the alginate. A similar effect of concentration-dependent nonlinearity has been observed for the ALG-GEL hydrogel system [73]. As a result, increasing the GEL concentration to achieve enhanced three-dimensional (3D) printability [30] for cartilage tissue engineering applications, will not only alter the cell adhesion [16] and processing properties [30] of the hydrogel, but will also affect its mechanical response. In addition, the enzymatic crosslinking by microbial transglutaminase used in the present work facilitates network formation of the GEL phase [16], which further explains the almost linear compression-tension behavior observed (Fig. 8c, Fig. 10). We note that it may be possible to tune the response of ADA-GEL to more closely resemble the response of ChondroFiller^{liquid} or cartilage by adapting concentrations and crosslinking.

Taken together, our results highlight that it is crucial to understand the underlying microstructure of hydrogels developed as proxy-materials for cartilage substitution to estimate and predict their final complex mechanical behavior. In addition, we have shown that the mechanical response strongly depends on strain rate, strain magnitude, and loading mode, which highlights the necessity of complex assessment going beyond a single modulus quantifying the tissue stiffness in a linear elastic deformation regime.

3.2. The viscoelastic behavior differs for the different materials

All materials showed viscoelastic effects during cyclic compression-tension and stress relaxation experiments. The hysteresis area during cyclic loading decreased notably between the first and second loading cycle, and marginally between all subsequent cycles. This effect was more pronounced for ChondroFiller^{liquid} than for ADA-GEL and cartilage. ChondroFiller^{liquid} also showed the fastest relaxation during stress relaxation tests, while human cartilage showed the slowest stress relaxation with time constants that were approximately twice as high as for the hydrogels. While cartilage and ChondroFiller^{liquid} specimens relaxed to approximately 30% of the initial stress within 150s, ADA-GEL only relaxed to approximately 80% of the initial stress within the same amount of time. We may, therefore, conclude that ChondroFiller^{liquid} and cartilage are more viscous than ADA-GEL.

The viscoelastic effects in native cartilage and hydrogels can be attributed to two different mechanisms: firstly, energy dissipation in the collagen-protein matrix, and secondly, fluid movement relative to the solid matrix. Interestingly, previous studies have shown that in cartilage, both the fibrillar collagen components and the protein matrix, individually exhibit viscoelastic behavior [50,51,74]. Structural changes that affect the viscoelastic behavior of the material are also associated with functional modifications. For instance, changes in the stress relaxation behavior of cartilage have been shown to closely relate to osteoarthritis [40]. Similarly, a reduction in viscous dissipation has been observed for decreasing proteoglycan content in the ECM of cartilage due to the mechanical, electrical, and chemical interaction between collagen fibers and proteoglycans [50].

In tissue engineering, the formation and composition of the extracellular matrix (ECM) is an essential factor for the function of cartilage. The corresponding stress relaxation behavior is an important indicator to assess the suitability of a hydrogel scaffold to embed cells for cartilage engineering. Lee et al. [40], have demonstrated that faster stress relaxation of alginate hydrogels enhances cartilage matrix formation [40]. To overcome this, tuning the hydrogel towards faster stress relaxation could be a promising approach to stimulate ECM formation [40]. The relatively fast relaxing alginate hydrogels showed the formation of canonical pericellular matrices (PCM), which exhibit bean-shaped morphologies that well resemble the natural hyaline cartilage [40]. Furthermore, the number of chondrocytes was increased, and chondrocytes seemed to build more collagen and sGAG in faster relaxing hydrogels [40]. Schwarz et al. [29] showed the expression of collagen II and aggrecan as relevant markers for hyaline cartilage formation in nasoseptal chondrocytes embedded in microbial transglutaminase crosslinked ADA-GEL [29]. In the present work, we have presented

a detailed mechanical analysis of the ADA-GEL hydrogel. The stress relaxation (approx. 80% of initial stress after 150 s) was lower than for hyaline cartilage and ChondroFiller^{liquid} (approx. 30% of initial stress after 150 s), and also than for alginate-PEG based hydrogels reported earlier [40]. We assume that the formation of ECM can still be triggered by degradation of the ADA-GEL system [29], reducing stiffness and ultimately accelerating stress relaxation with incubation time [16]. The change of viscoelasticity, nonlinearity, and stress relaxation of the hydrogels with incubation times > 14 days will be subject of future studies to assess the influence of hydrogel degradation on hydrogel mechanics.

In addition to degradation, it is possible to tune the viscoelasticity and stress relaxation behavior through the adaption of the type of crosslinking, inclusion of cells and molecular spacers, or the polymer concentration [40,73,75]. It has been shown that ADA-GEL hydrogels with embedded high cell numbers (> 6 mio.ml^{-1}) show significantly faster stress relaxation in comparison to pristine ADA-GEL. Hence, while featuring the least stress relaxation in the present mechanical analysis, ADA-GEL hydrogels could be tuned to a stress relaxation behavior that better matches human cartilage by embedding cells, e.g. chondrocytes, or by further modifications of the alginate by, e.g. spacer molecules to alter the ionic crosslinking of the polysaccharide [40]. Zhao et al. [75] reported that the stress relaxation of ionically crosslinked alginate gels was faster in comparison to covalently crosslinked alginates [75]. The hydrogel system used in the present study consisted of ionic (Ca^{2+}), covalent (enzymatic, $\varepsilon(\gamma$-glutamyl)lysine) isopeptide bond faciliated by microbial transglutaminase) [16], and reversible-covalent (Schiff's base) crosslinking [16], with a high degree of complexity. Reducing the amount of covalent crosslinks by lowering the enzymatic or GEL-based crosslinking in the hydrogel could enhance stress relaxation (Fig. 9). In addition, a decrease in hydrogel concentrations can lead to increased stress relaxation as previously shown for alginate-gelatine gels [73]. In future studies, we will assess the effect of pH and ionic crosslinker concentration on hydrogel swelling and mechanical properties combined with NMR investigations to gain further knowledge about the individual contributions of ionic, covalent, and reversible-covalent crosslinking on the overall hydrogel mechanical properties of the presented ADA-GEL system.

The complex assessment of the viscoelastic behavior of hydrogels and hyaline cartilage in the present work could serve as a basis to re-engineer hydrogel matrices to better meet the properties of native cartilage tissue in the future.

3.3. ChondroFiller^{liquid} is more susceptible to mechanical damage than ADA-GEL and human cartilage

Through repeated cyclic experiments, we have investigated whether the characteristic conditioning behavior of the materials is related to reversible viscoelastic effects or whether irreversible damage occurs. Such recovery tests have only rarely been carried out in the literature but provide valuable insights [76], for instance for the field of tissue engineering to stake out areas of application. Cartilage and ADA-GEL both fully recover within a period of one hour (Fig. 4). Therefore, the conditioning behavior, hysteresis, and offset-force may be attributed to visco- and poroelastic effects [77]. Similar recovery properties of cartilage have previously been reported in the literature [57]. In contrast, ChondroFiller^{liquid} only reaches 70% of its initial stiffness after the same amount of time. This indicates that besides reversible viscoelastic effects, irreversible structural changes occur during loading. This notion is supported by crack formation, which we observed in some of the ChondroFiller^{liquid} samples after compression testing, suggesting that even at low loading of 15% strain fracture and damage within the samples can occur. It has to be noted, however, that we only detected rupture in one ChondroFiller^{liquid} specimen. Yet, the results indicate that partial hydrogel damage may lead to the observed reduction in stresses, even after a recovery period of one hour. We suppose that localized stress peaks evolve at the interface between the non-fibrous and fibrous hydrogel phase of ChondroFiller^{liquid} (Figure 14) which induce the fracture. In addition, inhomogeneous diffusion properties may contribute to the difference in the recovery behavior in comparison to uniform ADA-GEL and cartilage specimens.

3.4. Towards testing procedures and parameters for reliable numerical simulations

With the goal of generating a comprehensive data set to identify material parameters for reliable mechanical numerical simulations, we have performed a testing protocol combining two different loading modes, compression and tension, as well as different loading conditions, such as cyclic and stress-relaxation experiments. The proposed combined testing procedure starts with three cycles of compression-tension loadings at two different strain levels to capture the compression-tension asymmetry, the conditioning behavior, and a successive reduction in the hysteresis area with increasing loading cycle. Furthermore, through the incorporation of two strain levels, it will be possible to identify parameters that capture the increasing nonlinearity for higher strains [78]. The subsequent stress relaxation tests quantify the time-dependent behavior of the material. Importantly, mechanical data used for material parameter identification should include at least the loading modes and strain levels that occur during the corresponding simulations [67].

When selecting an appropriate testing protocol for material parameter identification procedures, it is, therefore, important to consider both, the mechanical characteristics (e.g., nonlinearity or viscoelasticity) and the loading conditions that will be applied during simulations (e.g., loading rates, maximum strains, etc) [55,67,79–81]. Especially for hydrogels, handled in surgical implantations, large strains (>10%) may occur even at relatively low pressure [10,82,83]. Due to viscoelastic effects, it is not sufficient to record the initial loading curve but it is key to include unloading and to perform stress relaxation experiments. Through the combination of cyclic and stress relaxation experiments, we can significantly improve the viscoelastic parameterization, e.g. relaxation times, as conditioning effects and nonlinearity are taken into account. Due to the observed compression-tension-asymmetry, both loading modes need to be included for the identification of material parameters to allow for reliable mechanical numerical predictions.

The presented assessment featuring multi-modal (tension, compression) analyses at different strains (5% - 25%) combined with relaxation tests provides valuable information for the calibration of material models in a follow-up study of the present work. When appropriately parameterized [78], computer simulations can be a powerful tool for understanding fundamental processes in mechanotransduction of chondrocytes by extracting magnitude, locations and orientations of stresses and strains [49]. In addition, numerical simulations could help to estimate the internal stresses and strains in native cartilage under physiological loadings and thus could improve the use of implant materials [49,65].

3.5. Limitations

One limitation of our study is the lack of shear data. Native cartilage most certainly experiences shear stresses and strains, even under mostly compressive loading such as standing [65]. In addition, we did not investigate anisotropic effects due to fibrillar components [84,85] and the permeability of the materials, which are important properties to establish more complex (poro-elastic)

material models for numerical simulations. Furthermore, we had to reduce the maximum strains applied to cartilage under tensile loadings and during the combined protocol to adapt to its higher stiffness compared to the hydrogels. To overcome these limitations in the future, it would be possible to adapt the loading velocity. Also, to provide more reliable data for human articular cartilage, data from significantly more donors should be gathered in the future to increase the total number of samples tested and to account for inter-individual variations. Such patient-specific properties have for instance been included in computational models through the incorporation of quantitative magnetic resonance imaging data [84]. In addition, the great time effort of preparing and testing the hydrogel samples limited the amount of specimens analyzed in the present study.

It will be of great importance to examine not only joint cartilage of the human knee, but also from regions with very thick or thin cartilage to take into account the mechanical environment. In addition, sex hormones play an essential role in the biomechanics of articular cartilage so that both sexes and earlier (premenopausal) and later points in time must be taken into account. For the present investigations, articular cartilage from a single body donor was used. She suffered from osteoarthritis (Fig. 2). The cartilage punches used originated from areas with macroscopically healthy cartilage. Nevertheless, we cannot exclude the possibility that degenerative changes already prevailed in the samples we took and thus influenced our results. In this case, it would be desirable to analyse cartilage stumps that do not yet show any signs of osteoarthritis macroscopically. The large standard deviation in the data of ADA-GEL may be attributed to the stiffening of the material throughout the day of testing due to prolonged storage required for measuring multiple successive samples, which will have some effect on the results. Potentially, a modification in the storage could overcome this problem. Interestingly, we experienced no difference in the stress relaxation behavior for different maximum strains. As strain-dependent viscoelasticity was observed in the literature, at least for human articular cartilage, however, this issue should be further investigated in the future [86]. To allow for additional structure-property relationship analysis and a better interpretation of the mechanical characteristics observed, we will perform further morphological and microstructural assessments of the samples such as histological, antibody, or scanning electron microscopy in future studies.

4. Conclusion

In the present study, we have characterized the mechanical behavior of human cartilage, ChondroFiller^{liquid}, and ADA-GEL under multiple loading modes, as well as cyclic loading, and stress relaxation experiments. The results indicate that the materials exhibit different characteristics regarding compression-tension asymmetry, nonlinearity, recoverability, conditioning, and stress relaxation behavior, which are in accordance with differences in the materials' microstructure. By using Second Harmonic Generation imaging, we have shown that ChondroFiller^{liquid} consists of a bi-phasic microstructure, with fibrous and non-fibrous components in contrast to cartilage which is mostly fibrillar, and ADA-GEL, which only contains non-fibrillar structures. These insights imply important microstructural attributes for the interpretation of the complex mechanical behavior investigated in this study. Our results may provide a guideline for the design of novel biomaterials for cartilage tissue engineering based on collagen I (fibrous) or alginate (non-fibrous) components. We have revealed how the choice of fibrous and non-fibrous components might affect the final detailed material characteristics. The provided data set may, therefore, have important implications for mechanical-stimulation-assisted cartilage tissue engineering based on different deformation modes. The performed tests identify parameters that could be modified specifically during material development in the tissue engineering process. Furthermore, we have generated a multi-modal data set valuable to identify viscoelastic parameters for numerical simulations of these materials in the future.

Author contributions

SB, HS and AW conceptualized the study. AW performed the main experimentation, analyzed and visualized the mechanical data. HS, ARB and RD acquired funding. SB supervised the mechanical testing and analyses. FP and LB provided human cartilage specimens and substantially contributed to the interpretation of the data. TD, RD, and ARB conceptualized hydrogel design and fabrication. TD provided oxidized alginate gelatin specimens. TD, DS, and OF conceptualized and performed hydrogel imaging, TD and DS analyzed and visualized the imaging data. AW wrote the original draft. SB, TD, and DS contributed to manuscript writing and formatting. SB mentored the writing process. All authors have reviewed and approved the final manuscript.

Data availability

The raw/processed data required to reproduce these findings cannot be shared at this time due to technical or time limitations.

Declaration of Competing Interest

The authors declare that they have no known competing financial interests or personal relationships that could have appeared to influence the work reported in this paper.

Acknowledgements

The authors cordially thank Jörg Pekarsky for creating Fig. 1a. In addition, the funding by the Deutsche Forschungsgemeinschaft (DFG, German Research Foundation) through the Collaborative Research Centre 1270/1 - 299150580 ELAINE - Electrically Active Implants to ARB and HS, the grant BU 3728/1-1 to SB, the grant PA738/15-1 to FP, and the grant 326998133 – TRR 225 (subproject B08 to OF) is gratefully acknowledged. We also acknowledge the kind support by the Emerging Fields Initiative (EFI) by the FAU to FP, ARB, and SB.

Supplementary materials

Supplementary material associated with this article can be found, in the online version, at doi:10.1016/j.actbio.2020.10.025.

References

[1] Y. Zhang, J.M. Jordan, Epidemiology of osteoarthritis, Clin. Geriatr. Med. 26 (2010) 355–369, doi:10.1016/j.cger.2010.03.001.
[2] J. Martel-Pelletier, A.J. Barr, F.M. Cicuttini, P.G. Conaghan, C. Cooper, M.B. Goldring, S.R. Goldring, G. Jones, A.J. Teichtahl, J.-P. Pelletier, Osteoarthritis, Nat. Rev. Dis. Primers 2 (2016) 16072, doi:10.1038/nrdp.2016.72.
[3] M. Seidenstuecker, J. Watrinet, A. Bernstein, N.P. Suedkamp, S.H. Latorre, A. Maks, H.O. Mayr, Viscoelasticity and histology of the human cartilage in healthy and degenerated conditions of the knee, J, Orthop. Surg. Res. 14 (2019) 256, doi:10.1186/s13018-019-1308-5.
[4] David J. Hunter, Felix Eckstein, Exercise and osteoarthritis, Journal of Anatomy 214 (2009) 197–207, doi:10.1111/j.1469-7580.2008.01013.x.
[5] M.B. Goldring, Articular Cartilage Degradation in Osteoarthritis, HSS J 8 (2012) 7–9, doi:10.1007/s11420-011-9250-z.
[6] R.F. Loeser, S.R. Goldring, C.R. Scanzello, M.B. Goldring, Osteoarthritis: A Disease of the Joint as an Organ, Arthritis Rheum 64 (2012) 1697–1707, doi:10.1002/art.34453.
[7] A.J. Sophia Fox, A. Bedi, S.A. Rodeo, The basic science of articular cartilage: structure, composition, and function, Sports Health 1 (2009) 461–468, doi:10.1177/1941738109350438.

[8] F. Paulsen, J. Waschke, Sobotta Atlas of anatomy, Eds.16th ed., Elsevier, München, 2018.
[9] E.B. Hunziker, K. Lippuner, M.J.B. Keel, N. Shintani, An educational review of cartilage repair: precepts & practice – myths & misconceptions – progress & prospects, Osteoarthr. Cartil. 23 (2015) 334–350, doi:10.1016/j.joca.2014.12.011.
[10] Matthias Jacobi, Vincent Villa, Robert A Magnussen, Philippe Neyret, MACI - a new era? BMC Sports Sci Med Rehabil 3 (2011) 1–7, doi:10.1186/1758-2555-3-10.
[11] C. Vinatier, J. Guicheux, Cartilage tissue engineering: From biomaterials and stem cells to osteoarthritis treatments, Annals of Physical and Rehabilitation Medicine 59 (2016) 139–144, doi:10.1016/j.rehab.2016.03.002.
[12] T. Billiet, M. Vandenhaute, J. Schelfhout, S. van Vlierberghe, P. Dubruel, A review of trends and limitations in hydrogel-rapid prototyping for tissue engineering, Biomaterials 33 (2012) 6020–6041, doi:10.1016/j.biomaterials.2012.04.050.
[13] R. Detsch, B. Sarker, T. Zehnder, G. Frank, A.R. Boccaccini, Advanced alginate-based hydrogels, Materials Today 18 (2015) 590–591, doi:10.1016/j.mattod.2015.10.013.
[14] B. Sarker, D.G. Papageorgiou, R. Silva, T. Zehnder, F. Gul-E-Noor, M. Bertmer, J. Kaschta, K. Chrissafis, R. Detsch, A.R. Boccaccini, Fabrication of alginate–gelatin crosslinked hydrogel microcapsules and evaluation of the microstructure and physico-chemical properties, J. Mater. Chem. B 2 (2014) 1470, doi:10.1039/c3tb21509a.
[15] S. Reakasame, A.R. Boccaccini, Oxidized Alginate-Based Hydrogels for Tissue Engineering Applications: A Review, Biomacromolecules 19 (2018) 3–21, doi:10.1021/acs.biomac.7b01331.
[16] T. Distler, K. McDonald, S. Heid, R. Detsch, A.R. Boccaccini, Ionically and Enzymatically dual-crosslinked Oxidized Alginate Gelatine Hydrogels with Tuneable Stiffness and Degradation Behaviour for Tissue Engineering, ACS Biomaterials Science and Engineering submitted.
[17] A.D. Augst, H.J. Kong, D.J. Mooney, Alginate hydrogels as biomaterials, Macromol. Biosci. 6 (2006) 623–633, doi:10.1002/mabi.200600069.
[18] I. Braccini, S. Pérez, Molecular basis of C(2+)-induced gelation in alginates and pectins: the egg-box model revisited, Biomacromolecules 2 (2001) 1089–1096, doi:10.1021/bm010008g.
[19] Y.A. Mørch, I. Donati, B.L. Strand, G. Skjåk-Braek, Effect of Ca2+, Ba2+, and Sr2+ on alginate microbeads, Biomacromolecules 7 (2006) 1471–1480, doi:10.1021/bm060010d.
[20] K.H. Bouhadir, K.Y. Lee, E. Alsberg, K.L. Damm, K.W. Anderson, D.J. Mooney, Degradation of partially oxidized alginate and its potential application for tissue engineering, Biotechnol. Prog 17 (2001) 945–950, doi:10.1021/bp010070p.
[21] J. Venkatesan, B. Lowe, S. Anil, P. Manivasagan, A.A.A. Kheraif, K.-H. Kang, S.-K. Kim, Seaweed polysaccharides and their potential biomedical applications, Starch - Stärke 67 (2015) 381–390, doi:10.1002/star.201400127.
[22] B. Sarker, J. Rompf, R. Silva, N. Lang, R. Detsch, J. Kaschta, B. Fabry, A.R. Boccaccini, Alginate-based hydrogels with improved adhesive properties for cell encapsulation, Int. J. Biol. Macromol. 78 (2015) 72–78, doi:10.1016/j.ijbiomac.2015.03.061.
[23] T. Zehnder, B. Sarker, A.R. Boccaccini, R. Detsch, Evaluation of an alginate-gelatine crosslinked hydrogel for bioplotting, Biofabrication 7 (2015) 25001, doi:10.1088/1758-5090/7/2/025001.
[24] B. Wright, P.A. de Bank, K.A. Luetchford, F.R. Acosta, C.J. Connon, Oxidized alginate hydrogels as niche environments for corneal epithelial cells, J. Biomed. Mater. Res. A 102 (2014) 3393–3400, doi:10.1002/jbm.a.35011.
[25] B. Sarker, W. Li, K. Zheng, R. Detsch, A.R. Boccaccini, Designing Porous Bone Tissue Engineering Scaffolds with Enhanced Mechanical Properties from Composite Hydrogels Composed of Modified Alginate, Gelatin, and Bioactive Glass, ACS biomater. sci. eng. 2 (2016) 2240–2254, doi:10.1021/acsbiomaterials.6b00470.
[26] F. Ruther, T. Distler, A.R. Boccaccini, R. Detsch, Biofabrication of vessel-like structures with alginate di-aldehyde-gelatin (ADA-GEL) bioink, J. Mater. Sci. Mater. Med. 30 (2018) 8, doi:10.1007/s10856-018-6205-7.
[27] T. Distler, F. Ruther, A.R. Boccaccini, R. Detsch, Development of 3D Biofabricated Cell Laden Hydrogel Vessels and a Low-Cost Desktop Printed Perfusion Chamber for In Vitro Vessel Maturation, Macromol. Biosci. 19 (2019) e1900245, doi:10.1002/mabi.201900245.
[28] H. Park, K.Y. Lee, Cartilage regeneration using biodegradable oxidized alginate/hyaluronate hydrogels, J. Biomed. Mater. Res. A 102 (2014) 4519–4525, doi:10.1002/jbm.a.35126.
[29] S. Schwarz, S. Kuth, T. Distler, E. Al, 3D printing and characterization of human nasoseptal chondrocytes laden dual crosslinked oxidized alginate-gelatin hydrogels for cartilage repair approaches, Mater. Sci. Eng. C Mater. Biol. Appl (2020) 2020.
[30] T. Kreller, T. Distler, S. Heid, S. Gerth, R. Detsch, A.R. Boccaccini, Physico-chemical modification of gelatine as a valuable tool for the improvement of 3D printability of oxidized alginate-gelatine hydrogels towards cartilage tissue engineering submitted.
[31] N. Annabi, J.W. Nichol, X. Zhong, C. Ji, S. Koshy, A. Khademhosseini, F. Dehghani, Controlling the porosity and microarchitecture of hydrogels for tissue engineering, Tissue Eng. Part B Rev. 16 (2010) 371–383, doi:10.1089/ten.teb.2009.0639.
[32] C.M. Madl, B.L. LeSavage, R.E. Dewi, C.B. Dinh, R.S. Stowers, M. Khariton, K.J. Lampe, D. Nguyen, O. Chaudhuri, A. Enejder, S.C. Heilshorn, Maintenance of neural progenitor cell stemness in 3D hydrogels requires matrix remodelling, Nat. Mater. 16 (2017) 1233–1242, doi:10.1038/nmat5020.
[33] K. Hozumi, M. Nomizu, Cell Adhesion Activity of Peptides Conjugated to Polysaccharides, Curr. Protoc. Cell Biol. 80 (2018) e53, doi:10.1002/cpcb.53.
[34] M.J.R. Yunta, H. Prez-Snchez (Ed.), Bioinformatics, InTech, 2012.
[35] A. Atala, J.J. Yoo, S.J. Lee (Eds.), In situ tissue regeneration: Host cell recruitment and biomaterial design, Academic Press is an imprint of Elsevier, London, United Kingdom, 2016.
[36] M.S.F. Kurtis Kasper, A.G. Mikos, in: Tissue Engineering Scaffolds, Biomaterials Science, Elsevier, 2013, pp. 1138–1159.
[37] M. Urbanczyk, S.L. Layland, K. Schenke-Layland, The role of extracellular matrix in biomechanics and its impact on bioengineering of cells and 3D tissues, Matrix Biol 85-86 (2020) 1–14, doi:10.1016/j.matbio.2019.11.005.
[38] P.A. Janmey, R.T. Miller, Mechanisms of mechanical signaling in development and disease, J. Cell Sci 124 (2011) 9–18, doi:10.1242/jcs.071001.
[39] K. Franze, P.A. Janmey, J. Guck, Mechanics in neuronal development and repair, Annu. Rev. Biomed. Eng. 15 (2013) 227–251, doi:10.1146/annurev-bioeng-071811-150045.
[40] H.-P. Lee, L. Gu, D.J. Mooney, M.E. Levenston, O. Chaudhuri, Mechanical confinement regulates cartilage matrix formation by chondrocytes, Nat. Mater. 16 (2017) 1243–1251, doi:10.1038/nmat4993.
[41] A.R. Cameron, J.E. Frith, J.J. Cooper-White, The Influence of Substrate Creep on Mesenchymal Stem Cell Behaviour and Phenotype, Biomaterials (2011) 32, doi:10.1016/j.biomaterials.2011.04.003.
[42] O. Chaudhuri, L. Gu, M. Darnell, D. Klumpers, S.A. Bencherif, J.C. Weaver, N. Huebsch, D.J. Mooney, Substrate stress relaxation regulates cell spreading, Nat. Commun. 6 (2015) 6364, doi:10.1038/ncomms7365.
[43] O. Chaudhuri, L. Gu, D. Klumpers, M. Darnell, S.A. Bencherif, J.C. Weaver, N. Huebsch, H.-P. Lee, E. Lippens, G.N. Duda, D.J. Mooney, Hydrogels with tunable stress relaxation regulate stem cell fate and activity, Nat. Mater. 15 (2016) 326–334, doi:10.1038/nmat4489.
[44] K. Dey, S. Agnelli, L. Sartore, Dynamic freedom: substrate stress relaxation stimulates cell responses, Biomater. Sci. 7 (2019) 836–842, doi:10.1039/c8bm01305e.
[45] D.D. McKinnon, D.W. Domaille, J.N. Cha, K.S. Anseth, Biophysically defined and cytocompatible covalently adaptable networks as viscoelastic 3D cell culture systems, Adv. Mater. Weinheim. 26 (2014) 865–872, doi:10.1002/adma.201303680.
[46] B.P. Kanungo, L.J. Gibson, Density-property relationships in collagen-glycosaminoglycan scaffolds, Acta Biomater 6 (2010) 344–353, doi:10.1016/j.actbio.2009.09.012.
[47] M.L. Oyen, Mechanical characterisation of hydrogel materials, International Materials Reviews 59 (2014) 44–59, doi:10.1179/1743280413Y.0000000022.
[48] P.M. Freeman, R.N. Natarajan, J.H. Kimura, T.P. Andriacchi, Chondrocyte cells respond mechanically to compressive loads, J. Orthop. Res (1994) 12, doi:10.1002/jor.1100120303.
[49] H. Zahedmanesh, M. Stoddart, P. Lezuo, C. Forkmann, M.A. Wimmmer, M. Alini, H. van Oosterwyck, Deciphering mechanical regulation of chondrogenesis in fibrin-polyurethane composite scaffolds enriched with human mesenchymal stem cells: a dual computational and experimental approach, Tissue Eng. Part A 20 (2014) 1197–1212, doi:10.1089/ten.TEA.2013.0145.
[50] M.B. Schmidt, V.C. Mow, L.E. Chun, D.R. Eyre, Effects of proteoglycan extraction on the tensile behavior of articular cartilage, J. Orthop. Res. 8 (1990) 353–363, doi:10.1002/jor.1100080307.
[51] W.M. Lai, V.C. Mow, W. Zhu, Constitutive modeling of articular cartilage and biomacromolecular solutions, J, Biomech. Eng. 115 (1993) 474–480, doi:10.1115/1.2895527.
[52] G. Marchiori, M. Berni, M. Boi, G. Filardo, Cartilage mechanical tests: Evolution of current standards for cartilage repair and tissue engineering. A literature review, Clin. Biomech, (Bristol, Avon) 68 (2019) 58–72, doi:10.1016/j.clinbiomech.2019.05.019.
[53] C.T. Brighton, W. Wang, C.C. Clark, The effect of electrical fields on gene and protein expression in human osteoarthritic cartilage explants, J. Bone Joint Surg. Am. 90 (2008) 833–848, doi:10.2106/JBJS.F.01437.
[54] M. Freutel, H. Schmidt, L. Dürselen, A. Ignatius, F. Galbusera, Finite element modeling of soft tissues: Material models, tissue interaction and challenges, Clinical Biomechanics 29 (2014) 363–372, doi:10.1016/j.clinbiomech.2014.01.006.
[55] R. Shirazi, A. Shirazi-Adl, M. Hurtig, Role of cartilage collagen fibrils networks in knee joint biomechanics under compression, J. Biomech 41 (2008) 3340–3348, doi:10.1016/j.jbiomech.2008.09.033.
[56] D. Caccavo, S. Cascone, S. Poto, G. Lamberti, A.A. Barba, Mechanics and transport phenomena in agarose-based hydrogels studied by compression-relaxation tests, Carbohydr. Polym. 167 (2017) 136–144, doi:10.1016/j.carbpol.2017.03.027.
[57] P.A. Smyth, I. Green, R.L. Jackson, R.R. Hanson, Biomimetic Model of Articular Cartilage Based on *In Vitro* Experiments, JBBBE 21 (2014) 75–91, doi:10.4028/www.scientific.net/JBBBE.21.75.
[58] Q.-M. Wang, A.C. Mohan, M.L. Oyen, X.-H. Zhao, Separating viscoelasticity and poroelasticity of gels with different length and time scales, Acta Mech Sin 30 (2014) 20–27, doi:10.1007/s10409-014-0015-z.
[59] N. Hosoda1, N. Sakai2, Y. Sawae2 and T. Murakami2, Finite Element Analysis of Articular Cartilage Model Considering the Configuration and Biphasic Property of the Tissue.
[60] A.E. Forte, F. D'Amico, M.N. Charalambides, D. Dini, J.G. Williams, Modelling and experimental characterisation of the rate dependent fracture properties of gelatine gels, Food Hydrocolloids 46 (2015) 180–190, doi:10.1016/j.foodhyd.2014.12.028.

[61] A. Ghorbanoghli, K. Narooei, A new hyper-viscoelastic model for investigating rate dependent mechanical behavior of dual cross link self-healing hydrogel, International Journal of Mechanical Sciences 159 (2019) 278–286, doi:10.1016/j.ijmecsci.2019.06.019.
[62] R. Long, K. Mayumi, C. Creton, T. Narita, C.-Y. Hui, Time Dependent Behavior of a Dual Cross-Link Self-Healing Gel: Theory and Experiments, Macromolecules 47 (2014) 7243–7250, doi:10.1021/ma501290h.
[63] B. Hoyer, A. Bernhardt, A. Lode, S. Heinemann, J. Sewing, M. Klinger, H. Notbohm, M. Gelinsky, Jellyfish collagen scaffolds for cartilage tissue engineering, Acta Biomater 10 (2014) 883–892, doi:10.1016/j.actbio.2013.10.022.
[64] Q. Wang, Z. Gao, A constitutive model of nanocomposite hydrogels with nanoparticle crosslinkers, Journal of the Mechanics and Physics of Solids 94 (2016) 127–147, doi:10.1016/j.jmps.2016.04.011.
[65] D.D. Chan, L. Cai, K.D. Butz, S.B. Trippel, E.A. Nauman, C.P. Neu, In vivo articular cartilage deformation: noninvasive quantification of intratissue strain during joint contact in the human knee, Sci. Rep. (2016) 6, doi:10.1038/srep19220.
[66] B. Agoram, V.H. Barocas, Coupled macroscopic and microscopic scale modeling of fibrillar tissues and tissue equivalents, J. Biomech. Eng. 123 (2001) 362–369, doi:10.1115/1.1385843.
[67] S. Evans, How Can We Measure the Mechanical Properties of Soft Tissues?, in: S. Avril, S. Evans (Eds.) Material Parameter Identification and Inverse Problems in Soft Tissue Biomechanics, Eds., Springer International Publishing, Cham, 2017, pp. 67–83.
[68] J. Hazur, R. Detsch, E. Karakaya, J. Kaschta, J. Teßmar, D. Schneidereit, O. Friedrich, D.W. Schubert, A.R. Boccaccini, Improving alginate printability for biofabrication: establishment of a universal and homogeneous pre-crosslinking technique, Biofabrication 12 (2020) 45004, doi:10.1088/1758-5090/ab98e5.
[69] M. Strupler, A.-M. Pena, M. Hernest, P.-L. Tharaux, J.-L. Martin, E. Beaurepaire, M.-C. Schanne-Klein, Second harmonic imaging and scoring of collagen in fibrotic tissues, Opt. Express, OE 15 (2007) 4054–4065, doi:10.1364/OE.15.004054.
[70] R.M. Williams, W.R. Zipfel, W.W. Webb, Interpreting second-harmonic generation images of collagen I fibrils, Biophys. J. 88 (2005) 1377–1386, doi:10.1529/biophysj.104.047308.
[71] Z. Püspöki, M. Storath, D. Sage, M. Unser, Transforms and Operators for Directional Bioimage Analysis: A Survey, Adv. Anat. Embryol. Cell Biol. 219 (2016) 69–93, doi:10.1007/978-3-319-28549-8_3.
[72] S. Münster, L.M. Jawerth, B.A. Leslie, J.I. Weitz, B. Fabry, D.A. Weitz, Strain history dependence of the nonlinear stress response of fibrin and collagen networks, PNAS 110 (2013) 12197–12202, doi:10.1073/pnas.1222787110.
[73] T. Distler, E. Schaller, P. Steinmann, A.R. Boccaccini, S. Budday, Alginate-based hydrogels show the same complex mechanical behavior as brain tissue, Mech. Behav. Biomed. Mater. (2020) accepted 2020.
[74] D.M. Pierce, W. Trobin, S. Trattnig, H. Bischof, G.A. Holzapfel, A phenomenological approach toward patient-specific computational modeling of articular cartilage including collagen fiber tracking, J. Biomech. Eng. 131 (2009) 91006, doi:10.1115/1.3148471.
[75] X. Zhao, N. Huebsch, D.J. Mooney, Z. Suo, Stress-relaxation behavior in gels with ionic and covalent crosslinks, Journal of Applied Physics 107 (2010) 63509, doi:10.1063/1.3343265.
[76] S. Budday, G. Sommer, C. Birkl, C. Langkammer, J. Haybaeck, J. Kohnert, M. Bauer, F. Paulsen, P. Steinmann, E. Kuhl, G.A. HOLZAPFEL, Mechanical characterization of human brain tissue, Acta Biomater 48 (2017) 319–340, doi:10.1016/j.actbio.2016.10.036.
[77] Ester Comellas, Silvia Budday, Jean-Paul Pelteret, Gerhard A. Holzapfel, Paul Steinmann, Modeling the porous and viscous responses of human brain tissue behavior submitted.
[78] S. Kaessmair, T. Distler, E. Schaller, A.R. Boccaccini, P. Steinmann, S. Budday, Proc. Appl. Math. Mech., ., Identification of mechanical models and parameters for alginate-based hydrogels as proxy materials for brain tissue, in: Proceedings in applied mathematics and mechanics, 2020.
[79] S. Avril, Hyperelasticity of Soft Tissues and Related Inverse Problems, in: S. Avril, S. Evans (Eds.), Material Parameter Identification and Inverse Problems in Soft Tissue Biomechanics, Eds., Springer International Publishing, Cham, 2017, pp. 37–66.
[80] C. Oomens, Mechanical Behaviour of Skin: The Struggle for the Right Testing Method, in: S. Avril, S. Evans (Eds.), Material Parameter Identification and Inverse Problems in Soft Tissue Biomechanics, Eds., Springer International Publishing, Cham, 2017, pp. 119–132.
[81] G.R. Meloni, M.B. Fisher, B.D. Stoeckl, G.R. Dodge, R.L. Mauck, Biphasic Finite Element Modeling Reconciles Mechanical Properties of Tissue-Engineered Cartilage Constructs Across Testing Platforms, Tissue Eng. Part A 23 (2017) 663–674, doi:10.1089/ten.tea.2016.0191.
[82] W. Bartlett, S.P. Krishnan, J.A. Skinner, R.W.J. Carrington, T.W.R. Briggs, G. Bentley, Collagen-covered versus matrix-induced autologous chondrocyte implantation for osteochondral defects of the knee: a comparison of tourniquet times, Eur J Orthop Surg Traumatol 16 (2006) 315–317, doi:10.1007/s00590-006-0096-x.
[83] S.P. Abelow, P. Guillen, T. Ramos, Arthroscopic Technique for Matrix-Induced Autologous Chondrocyte Implantation for the Treatment of Large Chondral Defects in the Knee and Ankle, Operative Techniques in Orthopaedics 16 (2006) 257–261, doi:10.1053/j.oto.2006.08.006.
[84] K. Linka, A. Schäfer, M. Hillgärtner, M. Itskov, M. Knobe, C. Kuhl, L. Hitpass, D. Truhn, J. Thuering, S. Nebelung, Towards Patient-Specific Computational Modelling of Articular Cartilage on the Basis of Advanced Multiparametric MRI Techniques, Sci. Rep. 9 (2019) 7172, doi:10.1038/s41598-019-43389-y.
[85] B. Sarker, R. Singh, T. Zehnder, T. Forgber, C. Alexiou, I. Cicha, R. Detsch, A.R. Boccaccini, Macromolecular interactions in alginate–gelatin hydrogels regulate the behavior of human fibroblasts, Journal of Bioactive and Compatible Polymers 32 (2017) 309–324, doi:10.1177/0883911516668667.
[86] R.K. June, S. Ly, D.P. Fyhrie, Cartilage stress-relaxation proceeds slower at higher compressive strains, Arch. Biochem. Biophys. 483 (2009) 75–80, doi:10.1016/j.abb.2008.11.029.
[87] F.K. Kasper, A.G. Mikos, Biomaterials and gene therapy, in: N. Peppas, M.V. Sefton (Eds.), Molecular and Cellular Foundations of Biomaterials (pp. 131–163), Academic Press, 2004.

journal of the mechanical behavior of biomedical materials 133 (2022) 105292

Contents lists available at ScienceDirect

Journal of the Mechanical Behavior of Biomedical Materials

journal homepage: www.elsevier.com/locate/jmbbm

Hyperelastic parameter identification of human articular cartilage and substitute materials

A. Weizel [a,**], T. Distler [b], R. Detsch [b], A.R. Boccaccini [b], L. Bräuer [c], F. Paulsen [c], H. Seitz [a,d], S. Budday [e,*]

[a] Chair of Microfluidics, Faculty of Mechanical Engineering and Marine Technology, University of Rostock, 18059 Rostock, Germany
[b] Institute of Biomaterials, Department of Materials Science and Engineering, Friedrich-Alexander-University Erlangen-Nürnberg, 91058 Erlangen, Germany
[c] Institute of Functional and Clinical Anatomy, Friedrich-Alexander-University Erlangen-Nürnberg, 91054 Erlangen, Germany
[d] Department Life, Light & Matter, University of Rostock, 18059 Rostock, Germany
[e] Institute of Applied Mechanics, Department of Mechanical Engineering, Friedrich-Alexander-University Erlangen-Nürnberg, 91058 Erlangen, Germany

ARTICLE INFO

Keywords:
Parameter identification
Finite hyperelasticity
Human articular cartilage
Hydrogels
Tissue engineering

ABSTRACT

Numerical simulations are a valuable tool in the field of tissue engineering for cartilage repair and can help to understand which mechanical properties affect the behavior of chondrocytes and contribute to the success or failure of surrogate materials as implants. However, special attention needs to be paid when identifying corresponding material parameters in order to provide reliable numerical predictions of the material's response. In this study, we identify hyperelastic material parameters for numerical simulations in COMSOL Multiphysics® v. 5.6 for human articular cartilage and two surrogate materials, commercially available ChondroFiller^{liquid}, and oxidized alginate-gelatin (ADA-GEL) hydrogels. We consider several hyperelastic isotropic material models and provide separate parameter sets for the unconditioned and the conditioned material response, respectively, based on previously generated experimental data including both compression and tension experiments. We compare a direct parameter identification approach assuming homogeneous deformation throughout the specimen and an inverse approach, where the experiments are simulated using a finite element model with realistic boundary conditions in COMSOL Multiphysics® v. 5.6. We demonstrate that it is important to consider both compression and tension data simultaneously and to use the inverse approach to obtain reliable parameters. The one-term Ogden model best represents the unconditioned response of cartilage, while the conditioned response of cartilage and ADA-GEL is equally well represented by the two-term Ogden and five-term Mooney-Rivlin models. The five-term Mooney-Rivlin model is also most suitable to model the unconditioned response of ADA-GEL. For ChondroFiller^{liquid}, we suggest using the five-term Mooney-Rivlin or two-term Ogden model for the unconditioned and the two-term Ogden model for the conditioned material response. These results will help to choose appropriate material models and parameters for simulations of whole joints or to advance mechanical-stimulation assisted cartilage tissue engineering in the future.

1. Introduction

The finite element method (FEM) has become an indispensable tool for fundamental research. It can complement experimental mechanical investigations and allows for predictive insights into the respective topic of interest. Valuable correlations can be discovered and investigated further. Regarding the application of cartilage repair, previous works have used the FEM to evaluate correlations between the local stress and strain state and mechanotransduction. (Zahedmanesh et al., 2014) Other examples are simulations revealing the dependence of osteoarthritis on the mechanical properties. (Brown et al., 2009) Mechanical tests are an important prerequisite to identify material parameters for finite element simulations. Hydrogels are promising materials for cartilage replacement and are already used as cartilage substitutes in numerous studies as well as in clinical use. Therefore, their mechanical characterization is as important as that of natural articular cartilage. Our previous work has shown the complex mechanical behavior of cartilage and two substitute materials, ADA-GEL and ChondroFiller^{liquid}. All materials exhibit a

* Corresponding author.
** Corresponding author.
E-mail addresses: alina.weizel@uni-rostock.de (A. Weizel), silvia.budday@fau.de (S. Budday).

https://doi.org/10.1016/j.jmbbm.2022.105292
Received 7 January 2022; Received in revised form 19 May 2022; Accepted 20 May 2022
Available online 2 June 2022

nonlinear stress-strain response in compression and tension, show a pronounced hysteresis during cyclic loading, and significant conditioning effects. (Weizel et al., 2020) ADA showed promising results in cell testing with chondrocytes regarding cell growth and collagen II expression (Schwarz et al., 2020) and ChondroFiller^{liquid} is already used in the clinic as an implant material for defects in articular cartilage. We showed in previous studies that ADA-GEL mimics cartilage better in terms of stiffness, however, native human cartilage is mimicked by ChondroFiller^{liquid} better regarding its fibrous components and viscoelasticity. (Weizel et al., 2020)

Cartilage has been investigated in both tension and compression in only a few studies. (Halonen et al., 2014) Some studies are exclusively concerned with tensile tests (Charlebois et al., 2004), while others have subjected cartilage to indentation and compressive tests as those are easiest to implement due to the small thickness of human articular cartilage (~2 mm). (Deneweth et al., 2013) (Oloyede et al., 1992) (Brown et al., 2009) (Lee et al., 2020) (Bae et al., 2006) (Langelier and Buschmann, 2003) (Boschetti et al., 2004)

Although cartilage and hydrogels exhibit a hyper-visco-poroelastic behavior (Garc í a and Cort é s, 2006), we will focus on the hyperelastic characterization in this work, which is a valuable first step to understand the material response. Hyperelastic material models have the advantage to be less computationally expensive than viscoelastic and poroelastic models and are therefore still commonly used. Examples are simulations of the interaction of cartilage with the whole joint or even the whole musculoskeletal system. (Butz et al., 2011) In case the conditions in which the hyperelastic parameters were determined match the specific application, hyperelastic models can be a reasonable approximation to save computation time. Constitutive models previously used for cartilage and hydrogels are quite diverse and include the Ogden, Mooney-Rivlin, Yeoh, neo-Hookean and Arruda-Boyce models. (Brown et al., 2009) (Sasson et al., 2012) (Reuter and Ponomarev, 2015) Here, we investigate to which extend these five material models are suitable to represent the multimodal nonlinear material behavior of human cartilage, ChondroFiller^{liquid} and ADA-GEL, and provide parameters for the commercial software COMSOL Multiphysics® v. 5.6.

When focusing on the hyperelastic mechanical response of cartilage, it is important to consider the strain rate for which the corresponding hyperelastic parameters are valid. Brown et al., for instance, studied the influence of the loading velocity on the behavior of cartilage (Brown et al., 2009) and considered two different strain rates: A fast deformation with a rate of 0.1 1/s, where fluid is kept inside the tissue, and a slow deformation with a rate of 0.025 1/s dominated by fluid outflow. Other studies focused on the entire velocity spectrum at which cartilage can be loaded (Oloyede et al., 1992) and found that there is no increase in stiffness above a loading rate of about 0.05 1/s. They also divided the response of cartilage into a quasi-static material behavior dominated by fluid outflow and the interaction of the solid matrix components, resulting in a nonlinear stress-strain curve, and a material behavior independent of fluid outflow above a strain rate of around 0.05 1/s. (Oloyede et al., 1992) Based on these considerations, we tested cartilage and the hydrogels above the threshold strain rates with ~0.24 1/s and ~0.13 1/s, respectively. (Weizel et al., 2020).

In numerous studies, the parameter identification (PI) has been limited to the fit of an analytically determined function (further referred to here as direct PI), which is based on the assumption of a homogeneous deformation throughout the specimens during the corresponding experiments. (Brown et al., 2009) (Sasson et al., 2012) Achieving a truly homogeneous deformation state is challenging, especially for extremely soft material such as hydrogels. To address this problem, during an inverse parameter identification, a FE model with the actual boundary conditions of the experimental test is used to determine parameters. (Dusfour et al., 2020) In an even more complex procedure, a whole joint can be used to inversely identify material parameters. (Freutel et al., 2015)

In this work, we evaluate the suitability of material parameters determined through direct and inverse PI, respectively, for numerical simulations. We identify hyperelastic material parameters for human cartilage, ADA-GEL and ChondroFiller^{liquid}, which best represent the unconditioned and conditioned (drained) material responses, respectively, and can directly be used for finite element simulations in the future. The unconditioned parameter set can be used to predict the response during initial loading after a rest period, while the conditioned parameter set is suitable for repetitive loading, e.g., during walking.

2. Materials and methods

2.1. Experiment

2.1.1. Materials

In this study, we determine material parameters for three different materials, human cartilage (n=3), as well as two hydrogels for cartilage repair, namely ChondroFiller^{liquid} (n=10) and ADA-GEL (n=8). (Weizel et al., 2020) Fig. 1 shows one exemplary sample for each material, which we prepared for our previous mechanical experiments in (Weizel et al., 2020).

We extracted the human cartilage samples from a knee of a 62-year-old donor who died of liver and kidney failure. For this purpose, we punched the samples with a diameter of 8 mm from the condyle of the knee. The thickness of the cartilage determines the height of the samples and was, in our case, approximately 2094 ± 320 μm. The cartilage was kept refrigerated at 4°C and hydrated by phosphate-buffered saline solution until testing.

ChondroFiller^{liquid} is a collagen-based hydrogel supplied by Meidrix Biomedicals GmbH (Esslingen, Germany). It is a dual-chamber syringe system containing 10 mg/l collagen type I in the larger chamber and a neutralisation gel in the smaller chamber. We injected the ChondroFiller^{liquid} into a silicone mold with a diameter of 8 mm and a height of 4 mm in which the samples gelled at 4°C for 24 h. The final samples have a collagen concentration of 8 mg/ml.

ADA-GEL hydrogels are composed of ADA (alginate di-aldehyde, oxidized alginate) and gelatin. ADA (7.5 % (w/v)) dissolved in 5 ml phosphate-buffered saline solution was stirred with 5 ml GEL (7.5 % (w/v)) for 10 min at room temperature (22°C) until homogeneity. We placed the hydrogel precursor in the same silicone mold as ChondroFiller^{liquid} to be crosslinked using 0.1 M $CaCl_2$ and 2.5 % (w/v) microbial transglutaminase (mTG, Ajinomoto Co.,Inc, ACTIVA® WM, 85–135 U/g, Japan) for 24h. (Distler et al., 2020)

2.1.2. Experimental setup and testing protocols

For a detailed description of all experimental procedures and results we refer to our previous publication. (Weizel et al., 2020) Here, we only present a short overview of the setup (see Fig. 2), the testing procedures and the relevant results. For the mechanical characterization, we used the Discovery HR-3 rheometer from TA instruments (New Castle, Delaware, USA). We glued the upper and lower surface of all samples to the sample holder with cyanoacrylate adhesive. The loading in compression and tension direction was applied by moving the upper specimen holder according to our previously defined protocol (see Table 1). During the tests, the samples were kept in a hydrated environment at 37 °C, as illustrated in Fig. 2. After preliminary tests, we had developed a combined testing protocol for the reliable identification of

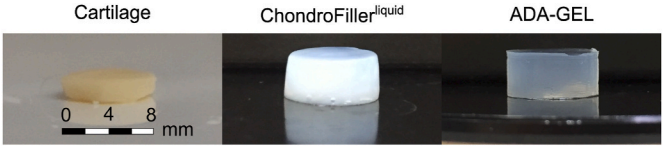

Fig. 1. Cylindrical specimens of the materials of interest: Human hyaline cartilage, ChondroFiller^{liquid} and ADA-GEL.

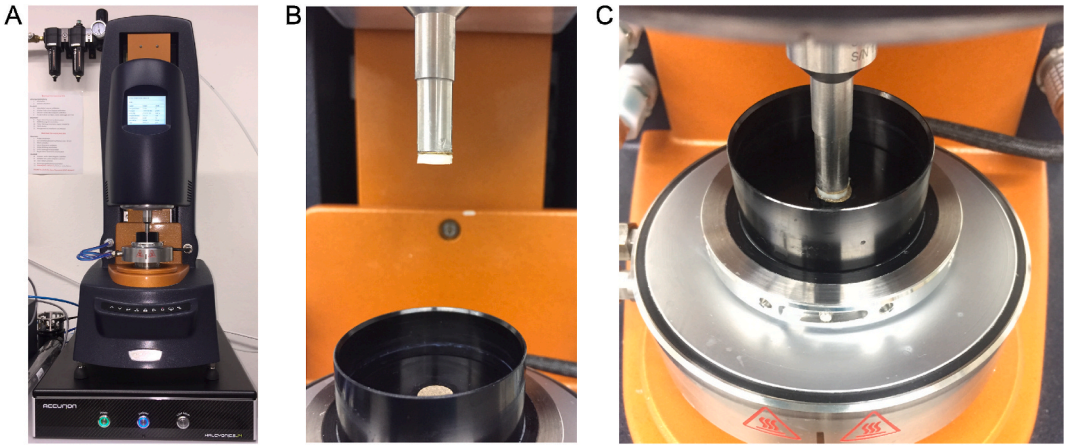

Fig. 2. Overview of experimental setup: A) Discovery HR-3 rheometer B) Cartilage specimen glued to the upper sample holder C) Final position of the cartilage specimen before adding a phosphate-buffered saline solution for hydration.

Table 1
Combined testing protocol for material parameter identification. (Weizel et al., 2020).

	ADA-GEL and ChondroFiller^{liquid}				Cartilage			
	ε_{nom}	cycles	t_{hold} [s]	v [µm/s]	ε_{nom}	cycles	t_{hold} [s]	v [µm/s]
cyclic compression and tension	0.1	3		500	0.01	3		500
cyclic compression and tension	0.2	3		500	0.025	3		500
stress relaxation in compression	0.15		150	6000	0.5		1000	6000
stress relaxation in tension	0.15		150	6000	–			
cyclic compression and tension	ChondroFiller^{liquid}				ADA-GEL		Cartilage	
strain rate in 1/s ± standarddeviation	0.1308 ± 0.0043				0.1265 ± 0.0177		0.2423 ± 0.0348	

material parameters. ChondroFiller^{liquid} und ADA-GEL were first subjected to cyclic loading with two sets of three cycles in compression and tension, respectively, with 10% strain and 20% maximum strains. Those tests were followed by a stress relaxation test at 15% strain, first in compression and then in tension. For cartilage, the maximum strain had to be reduced from 10%, 20% and 15%–1%, 2.5% and 5%, respectively. An overview of the testing protocol is given in Table 1.

2.1.3. Experimental data analysis

The results from the combined testing protocol comprehensively describe the material behavior of ChondroFiller^{liquid}, ADA-GEL and cartilage and are presented in (Weizel et al., 2020). We restricted ourselves here to the identification of hyperelastic material parameters. For this, we distinguished between two parameter sets. The first set of parameters is intended to represent an unconditioned, relatively fast loading. To this end, we evaluated the loading part of the first of three cycles with 20% strain in tension and compression for ChondroFiller^{liquid} and ADA-GEL, as indicated in blue in Fig. 3 and Fig. 4. For cartilage, we choose the first cycle with 2.5% maximum strain accordingly.

The second parameter set describes the conditioned behavior. For this, we used the average between the loading and unloading during the third loading cycle at 20% strain and 2.5% strain for the hydrogels and cartilage, respectively, as indicated in red in Figs. 3 and 4. (Budday et al., 2017a) We note that in our previous study, we found that from the third cycle onward, further conditioning effects were negligible (see Fig. 5 in (Weizel et al., 2020)).

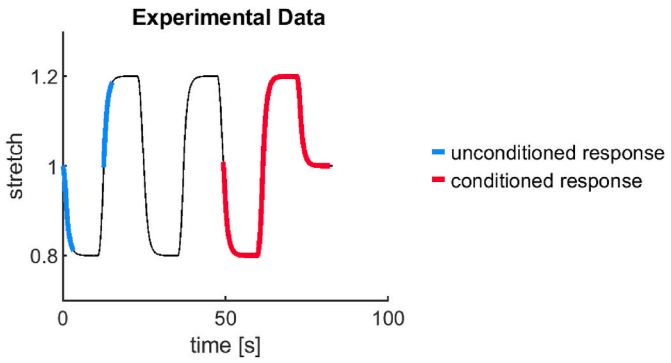

Fig. 3. Stretch-time diagram for cyclic loading in compression and tension with minimum and maximum stretches of 0.8 and 1.2. The loading curves in compression and tension (blue) during the first cycle were used to identify the unconditioned set of parameters. The whole third cycle in compression and tension (red) were used as a basis to identify the conditioned material parameters.

2.2. Modelling

2.2.1. Kinematics of finite deformations

To model the hyperelastic response of cartilage and the two hydrogels, we use the theory of nonlinear continuum mechanics describing the physical phenomena of the system at continuum level without explicitly considering the complex microstructure. The continuum body $B_0 \in \mathbb{R}^3$ consists of continuum points $P \in B_0$ and has a continuous and homogenous distribution of matter in space and time. The dimensions of a continuum body are larger than those of microstructures in the body. We assume that the continuum body is placed in the three-dimensional Euclidean space at time t, as illustrated in Fig. 5. The configuration of a body corresponds to the place which the body occupies in the Euclidean space. The kinematics of finite deformations of the undeformed body B_0 at time $t = 0$ can be described by the deformation map $\boldsymbol{\varphi}$, which maps the position $\boldsymbol{X}$ in the reference or material configuration B_0 to its new position $\boldsymbol{x} = \boldsymbol{\varphi}(\boldsymbol{X}, t)$ in the deformed, current or spatial configuration B_t. Furthermore, we introduce the deformation gradient $\boldsymbol{F}(\boldsymbol{X}, t) = \nabla_{\boldsymbol{X}} \boldsymbol{\varphi}(\boldsymbol{X}, t)$, which maps undeformed line elements to deformed

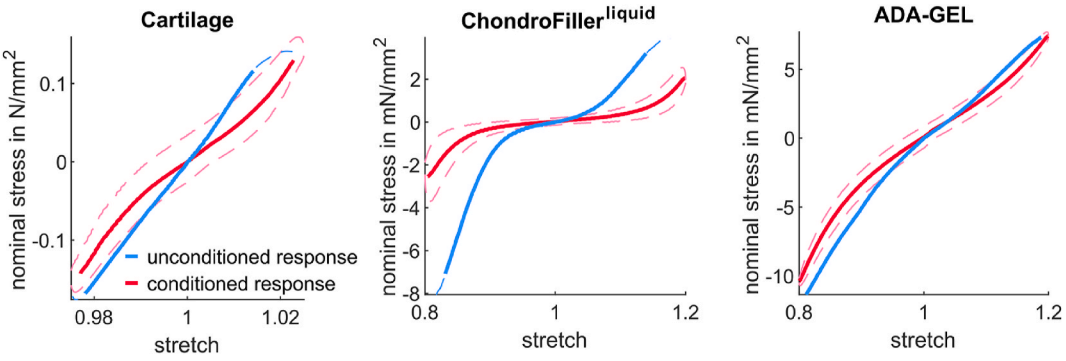

Fig. 4. Experimental data of human cartilage (left, n = 3), ChondroFiller^{liquid} (center, n = 10) and ADA-GEL (right, n = 8) used for parameter identification. The unconditioned response represented by the loading curve during the first cycle is shown in blue. The conditioned response represented by the average between loading and unloading (dashed red line) during the third loading cycle is shown in red.

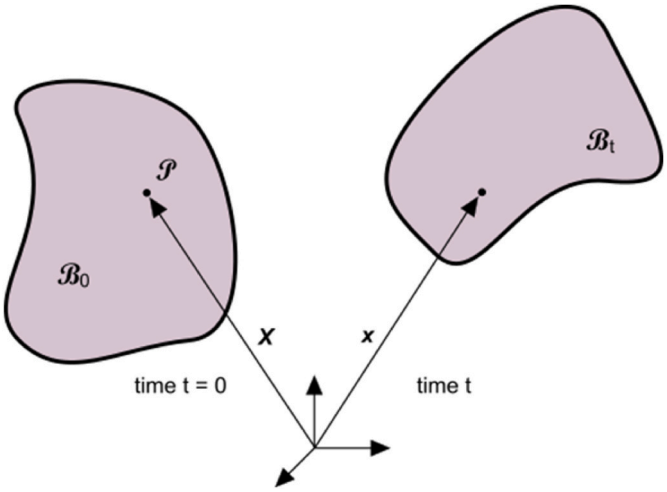

Fig. 5. Configuration and motion of a continuum body.

line elements. (Holzapfel, 2010)

For a uniaxial incompressible and homogeneous deformation in compression and tension, the deformation gradient reads

$$\boldsymbol{F} = \begin{bmatrix} \lambda_1 & & \\ & \lambda_2 & \\ & & \lambda_3 \end{bmatrix} \cdot with \cdot \lambda_1 = \lambda \cdot and \cdot \lambda_{2,3} = 1 \Big/ \sqrt{\lambda}$$

where λ_1, λ_2 and λ_3 are the principal stretches, i.e., the square roots of the eigenvalues of the right Cauchy-Green deformation tensor $\boldsymbol{C}$, and λ is the axial stretch. $\boldsymbol{C}$ is defined as $\boldsymbol{C} = \boldsymbol{F}^{\mathrm{T}} \cdot \boldsymbol{F}$, and its invariants $\boldsymbol{I}_1$ and $\boldsymbol{I}_2$ are

$$I_1(C) = trace\ (C) I_1 = \lambda_1^2 + \lambda_2^2 + \lambda_3^2 \tag{1}$$

$$I_2(C) = \frac{1}{2}\left[trace(C)^2 - trace\ \left(C^2\right)\right] I_2(C) = \lambda_1^2\lambda_2^2 + \lambda_2^2\lambda_3^2 + \lambda_3^2\lambda_1^2. \tag{2}$$

2.2.2. Isotropic hyperelastic material models

The mechanical behavior of materials can be expressed in mathematical models, also known as constitutive equations. Here, we focus on the large-strain, nonlinear time-independent material response, also called finite hyperelastic response, and neglect viscous and porous effects. The latter can be added to the modeling framework in a next step. (Ogden, 1972)

The constitutive law for a hyperelastic material relates the strain energy function Ψ to the deformation gradient $\boldsymbol{F}$, the invariants I_1, I_2 and I_3 or the principal stretches λ_1, λ_2 and λ_3. (Holzapfel, 2010)

A stress measure that is suitable for the analysis of experimental data is the nominal stress, the force divided by the undeformed area of the continuum body, also called Piola stress defined as

$$P = JF^{-1}\,\boldsymbol{\sigma} \cdot or \cdot for\ uniaxial\ comparison\ and\ tension P = \frac{\partial \Psi}{\partial \lambda} \tag{3}$$

where $\boldsymbol{\sigma}$ is the Cauchy stress tensor.

In our studies, we assume incompressible material behavior, such that $J = \det(F) = 1$.

In the FE model the auxiliary pressure p_w is added as a weak condition to enforce incompressibility and is used as a pressure during the stress calculation (COMSOL).

Furthermore, we introduce the generalized shear modulus

$$\mu = \mu\ (I_1, I_2) = 2\left(\frac{\partial \Psi}{\partial I_1} + \frac{\partial \Psi}{\partial I_2}\right) \tag{4}$$

wherein all materials must satisfy $\mu > 0$ (COMSOL).

In the following, we present the hyperelastic material models, which we consider in the present study to describe the behavior of cartilage, ChondroFiller^{liquid} and ADA-GEL.

2.2.2.1. Ogden model. The Ogden model, is a versatile model that has previously been used for rubbers, polymers as well as biological materials. (Budday et al., 2019) (Ogden, 1972) (OGDEN et al., 2004) (Freutel et al., 2014)

The corresponding strain energy function is expressed in terms of the principal stretches λ_1, λ_2, λ_3 with

$$\Psi_{Ogden} = \sum_{p=1}^{N} \frac{\mu_p}{\alpha_p}\left(\lambda_1^{\alpha_p} + \lambda_2^{\alpha_p} + \lambda_3^{\alpha_p} - 3\right) \tag{5}$$

where μ_p are the shear moduli and α_p are the nonlinearity parameters. For our investigations, we considered the Ogden model with one and two terms, for which the Piola stress yields

$$P_{Ogden1t} = \mu_1 \lambda^{\alpha_1 - 1} - \mu_1 \lambda^{-\left(\frac{\alpha_1}{2}+1\right)} \tag{6}$$

and

$$P_{Ogden2t} = \mu_1 \lambda^{\alpha_1 - 1} - \mu_1 \lambda^{-\left(\frac{\alpha_1}{2}+1\right)} + \mu_2 \lambda^{\alpha_2 - 1} - \mu_2 \lambda^{-\left(\frac{\alpha_2}{2}+1\right)} \tag{7}$$

respectively. The initial shear modulus, known from the linear theory, can be calculated as

$$\mu = \frac{1}{2}\sum_{p=1}^{N} \mu_p\, \alpha_p \tag{8}$$

and results in

$$\mu_{Ogden1t} = \frac{1}{2}\,\mu_1\,\alpha_1 \cdot and \mp \cdot \mu_{Ogden2t} = \frac{1}{2}\,(\mu_1\,\alpha_1 + \mu_2\,\alpha_2) \tag{9}$$

The Ogden Model has been shown to be capable of capturing the entire strain range of rubber materials with high accuracy, even with a small number of terms. Furthermore, the material model can describe rapid stiffness increase for larger deformations. Still, it is a phenomenological model, which has no direct relation to physical mechanisms. (Arruda and Boyce, 1993)

2.2.2.2. Mooney-Rivlin model. The second constitutive model we consider is expressed in terms of the invariants. In the case of incompressibility, the third invariant $I_3(C)$ is omitted, and the strain energy function $\Psi(I_1, I_2)$ depends only on $I_1(C)$ and $I_2(C)$. The general formulation for the strain energy function, according to Rivlin, is defined as (Boyce and Arruda, 2000)

$$\Psi_{MR} = \sum_{i,j=0}^{n} C_{i,j}\,(I_1-3)^{\,i}\,(I_2-3)^{\,j} \tag{10}$$

The appropriate number of terms n in equation (10) depends on the shape of the stress-strain curve, e.g., for higher terms such as n≥3, the stress-strain curve shows an inverse S-shape. If we keep only the first two terms, we arrive at the Mooney-Rivlin model with

$$\Psi_{MR\ 2\ term} = C_{10}\,(I_1-3) + C_{01}\,(I_2-3). \tag{11}$$

The corresponding Piola stress can be expressed as

$$P_{MR\ 2\ term} = C_{10}\left(2\lambda - \frac{2}{\lambda^2}\right) - C_{01}\left(\frac{2}{\lambda^3} - 2\right) \tag{12}$$

and the initial shear modulus as

$$\mu_{MR\ 2\ term} = 2\,(C_{10} + C_{01}) \tag{13}$$

where, C_{10} and C_{01} denote the material constants. The Mooney-Rivlin model with two terms exhibits a stress-strain relationship without inflection points. To represent a more complex stress-strain relationship with one inflection point, the Mooney-Rivlin model with five terms can be used. This model is defined as

$$\Psi_{MR\ 5\ term} = C_{10}\,(I_1-3) + C_{01}\,(I_2-3) + C_{20}\,(I_1-3)^{\,2} + C_{02}\,(I_2-3)^{\,2} + C_{11}\,(I_1-3)(I_2-3) \tag{14}$$

with the Piola stress

$$P_{MR5term} = C_{10}\left(2\lambda - \frac{2}{\lambda^2}\right) - C_{01}\left(\frac{2}{\lambda^3} - 2\right) + C_{11}\left(2\lambda - \frac{2}{\lambda^2}\right)\left(2\lambda + \frac{1}{\lambda^2} - 3\right) - 2C_{02}\left(\frac{2}{\lambda^3} - 2\right)\left(2\lambda + \frac{1}{\lambda^2} - 3\right) + 2C_{20}\left(2\lambda - \frac{2}{\lambda^2}\right)\left(\frac{2}{\lambda} + \lambda^2 - 3\right) - C_{11}\left(\frac{2}{\lambda^3} - 2\right)\left(\frac{2}{\lambda} + \lambda^2 - 3\right) \tag{15}$$

and the initial shear modulus

$$\mu_{MR\ 5\ term} = 2\,(C_{10} + C_{01}) + 2C_{11}(I_1-3) + 2C_{11}(I_2-3) + 4C_{02}(I_2-3) + 4C_{20}(I_1-3) \tag{16}$$

2.2.2.3. Neo-Hookean model. The simplest hyperelastic material model is the neo-Hookean material model. It is a special case of both the Ogden model (see equation (5)) and the Mooney-Rivlin model (see equation (10)). For the incompressible case, the strain energy function is defined only in terms of the first invariant I_1

$$\Psi_{neo-Hookean} = \frac{1}{2}\mu\,(I_1-3) \tag{17}$$

where μ is the shear modulus. (Boyce and Arruda, 2000) The Piola stress for compression and tension loadings yields

$$P_{neo-Hookean} = \mu\,\left(\lambda - \lambda^{-2}\right). \tag{18}$$

The advantages of the neo-Hookean model are, on the one hand, the simplicity of the model. On the other hand, only one parameter is needed in the case of incompressibility. Therefore, the number of different tests required to calibrate the model is small. However, it cannot capture highly nonlinear and complex material responses as the strain energy function only linearly depends on $I_1(C)$. In addition, due to the independence of $I_2(C)$, the model may underestimate stresses in the biaxial loading case. (Bergström, 2015)

2.2.2.4. Yeoh model. In the Yeoh model, higher-order terms are introduced for $I_1(C)$ in order to better represent a nonlinear material behavior. The Yeoh model is described by the strain energy function (Yeoh, 1993)

$$\Psi_{Yeoh} = c_1(I_1-3) + c_2(I_1-3)^2 + c_3(I_1-3)^3 \tag{19}$$

where c_1, c_2 and c_3 are material constants. The Piola stress yields

$$P_{Yeoh} = \frac{\partial \Psi_{Yeoh}}{\partial \lambda} = c_1\left(2\lambda - \frac{2}{\lambda^2}\right) + 2c_2\left(2\lambda - \frac{2}{\lambda^2}\right)\left(\frac{2}{\lambda} + \lambda^2 - 3\right) + 3c_3\left(2\lambda - \frac{2}{\lambda^2}\right)\left(\frac{2}{\lambda} + \lambda^2 - 3\right)^2 \tag{20}$$

This representation of the strain energy function also leads to the fact that the shear modulus depends on the strain and results in

$$\mu_{Yeoh} = 2c_1 + 4c_2(I_1-3) + 6c_3(I_1-3)^2 \tag{21}$$

For smaller strains, the shear modulus decreases with increasing strain, and for larger strains, the shear modulus increases with increasing strain.

2.2.2.5. Arruda-Boyce model. The Arruda-Boyce model also referred to as the 8-chain model is generally defined as

$$\Psi_{Arruda} = \mu \sum_{i=1}^{n} c_i\left(I_1^i - 3^i\right) \tag{22}$$

where each individual c_i up to n=5 is determined as a function of N, the number of segments. An overview of the coefficients c_i is given in Table 2.

Table 2
Coefficients of the Arruda-Boyce model.

c_1	c_2	c_3	c_4	c_5
$\frac{1}{2}$	$\frac{1}{20N}$	$\frac{11}{1050N^2}$	$\frac{19}{7000N^3}$	$\frac{519}{673750N^4}$

Inserting the coefficients into the model yields the following strain energy function, Piola stress, and shear modulus

$$\Psi_{Arruda} = \mu\left[\frac{1}{2}(I_1-3) + \frac{1}{20N}\left(I_1^2-9\right) + \frac{11}{1050\,N^2}\left(I_1^3-27\right) + \frac{19}{7000N^3}\left(I_1^4-81\right) + \frac{519}{673750N^4}\left(I_1^5-243\right)\right] \tag{23}$$

$$P_{Arruda} = \mu\left[\lambda - \frac{1}{\lambda^2} + \left(\frac{11\left(2\lambda - \frac{2}{\lambda^2}\right)\left(\frac{2}{\lambda} + \lambda^2\right)^2}{350N^2}\right) + \left(\frac{19\left(2\lambda - \frac{2}{\lambda^2}\right)\left(\frac{2}{\lambda} + \lambda^2\right)^3}{1750N^3}\right) + \left(\frac{519\left(2\lambda - \frac{2}{\lambda^2}\right)\left(\frac{2}{\lambda} + \lambda^2\right)^4}{134750N^4}\right) + \left(\frac{\left(2\lambda - \frac{2}{\lambda^2}\right)\left(\frac{2}{\lambda} + \lambda^2\right)}{10N}\right)\right] \quad (24)$$

$$\mu_{Arruda} = 2\mu\left(\frac{I_1}{10\,N} + \frac{11I_1^2}{350N^2} + \frac{19I_1^3}{1750\,N^3} + \frac{519I_1^4}{134750N^4} + \frac{1}{2}\right) \quad (25)$$

It is generally possible to transfer parameters determined from one loading mode to another even for large strains. Thus, only one experiment is needed to determine the material parameters. Furthermore, the model is characterized by the existence of a physical background of the parameters N as the number of segments and μ as the shear modulus. (Arruda and Boyce, 1993)

2.2.3. Stability of hyperelastic material models

We evaluate the stress range in which our fitted material models are stable, i.e., there is no sign change in the slope of the stress versus strain curve, by using Drucker's criterion given as

$$\sum \partial\sigma i \partial\varepsilon i \geq 0i \quad (26)$$

where $\partial\sigma i$ is the stress increment and $\partial\varepsilon i$ is the associated strain increment. (Aldeen et al., 2020) For some material models, choosing appropriate upper and /or lower bounds for material parameters during the parameter fit is sufficient to ensure stability. Here, we prove the stability for a defined stretch range of 0–10. A corresponding graphical illustration (see Figure S 1) and a table (see Table S 1) can be found in the supplementary materials.

Parameter Identification.

We consider two approaches for the determination of the material parameters. The first approach determines the parameters of the respective material models through a so-called direct or analytical parameter identification. The second approach, also known as inverse parameter identification, takes the results of the direct method as initial values and incorporates the underlying finite element model to capture local inhomogeneous deformation states during experiments. In the following, we present and explain both approaches in more detail.

2.2.4. Direct parameter identification

We implement all material models introduced in Section 2.2.2 in MATLAB (MATLAB, 2018), and used the nonlinear least-square solver (lsqnonlin) to determine the model parameters by minimizing the difference between the model predicted and the measurement data, as summarized in Fig. 6. We used the trust-region algorithm as it allowed us to select an upper and lower bound, which were chosen in order to fulfil the stability requirements introduced in Section 2.2.3. We solve the following minimization problem

$$\min_x F(x)_2^2 = \sum_i F^2(x) = \sum_i \left(F^c_{mod} - F^c_{exp};\ F^t_{mod} - F^t_{exp}\right)_i^2 \quad (27)$$

where i represents the individual data points, F_{mod} represents the calculated force and F_{exp} the measured data in compression, denoted as F^c , and in tension, denoted as, F^t. Furthermore, for each curve fit, the variation of the initial point x_0 is used to check whether the result is independent of the starting point.

2.2.5. Inverse parameter identification

Fig. 6 summarizes the scheme of the inverse parameter identification. Here, we also used the nonlinear least-square solver lsqnonlin in MATLAB and inserted the material parameters determined through the direct parameter identification as initial values x_0. In contrast to the direct parameter identification, we do not compare the experimental force F_{exp} with an analytically calculated force F_{mod} from the equations introduced in Section 2.2.2, but we evaluate the reaction force calculated through a finite element (FE) simulation capturing the experimental sequence with associated exact displacements and boundary conditions.

The two dimensional and axisymmetric finite element model with a triangular mesh is shown in Fig. 7. At the boundary, we evaluate the reaction force F_{sim} which serves as a basis for the least-square solver to solve the problem of the form

$$\min_x F(x)_2^2 = \sum_i F^2(x) \cdot = \cdot \sum_i \left(F_{exp} - F_{sim}\right)_i^2 \quad (28)$$

In each iteration step the FE model is solved in COMSOL Multiphysics® v. 5.6 x_{opt} +1 times to adjust the material parameters x_{opt}.

2.3. Statistical analysis of the quality of the curve fits

We use the coefficient of determination to evaluate how well the fitted parameters (stretch vs. force data from the analytical model or

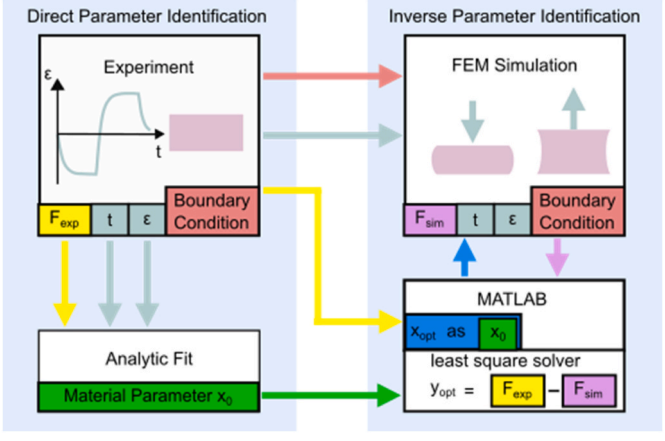

Fig. 6. Schematic illustration of inverse and direct parameter identification.

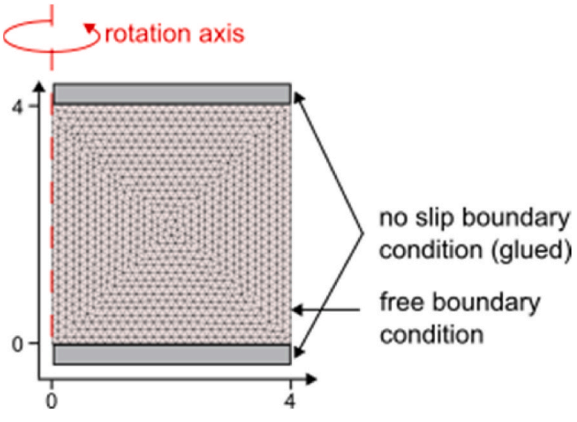

Fig. 7. Two-dimensional axisymmetric finite element model of an exemplary specimen with triangulated mesh and boundary conditions.

simulation) capture the experimental data (stretch vs. force data). The coefficient of determination is defined as

$$R^2 = 1 - \frac{SSR}{SST} \tag{29}$$

where SSR is the **S**um of the **S**quares of the **R**esidual defined as $SSR = \sum_{i=!}^{n} (y_i - \breve{y}_i)^2$ with the measured values y and the fitted function $\breve{y}$. SST represents the **S**um of **S**quares **T**otal with $SST = \sum_{i=!}^{n} (y_i - \bar{y}_i)^2$, where $\bar{y}$ are the mean values of the measured data. The coefficient of determination can take values between 0 and 1: $0 \leq R^2 \leq 1$. If the coefficient of determination takes a value of 1 in the extreme case, the measured data perfectly agrees with the fitted function. Values smaller than 1 indicate a certain deviation of the measured values from the fitted function. The goal is to find parameters for the hyperelastic models so that R^2 is close to 1. We consider the compression and tension directions independently with R_c^2.and R_t^2.

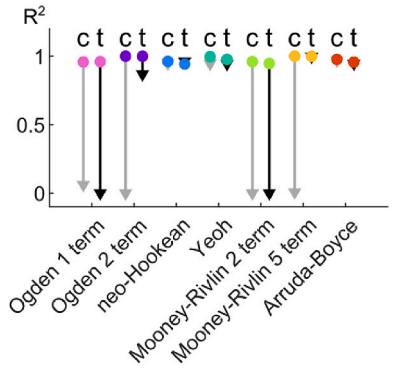

Fig. 9. Sensitivity of the performance of material models towards the loading modes used for calibration, quantified through coefficients of determination R^2: The grey arrows indicate the decrease in the value for compressive loading R_c^2 when the parameters are calibrated based on tension data only. Similarly, the black arrows indicate the decrease in the value for tensile loading R_t^2 when the parameters are calibrated based on compression data only.

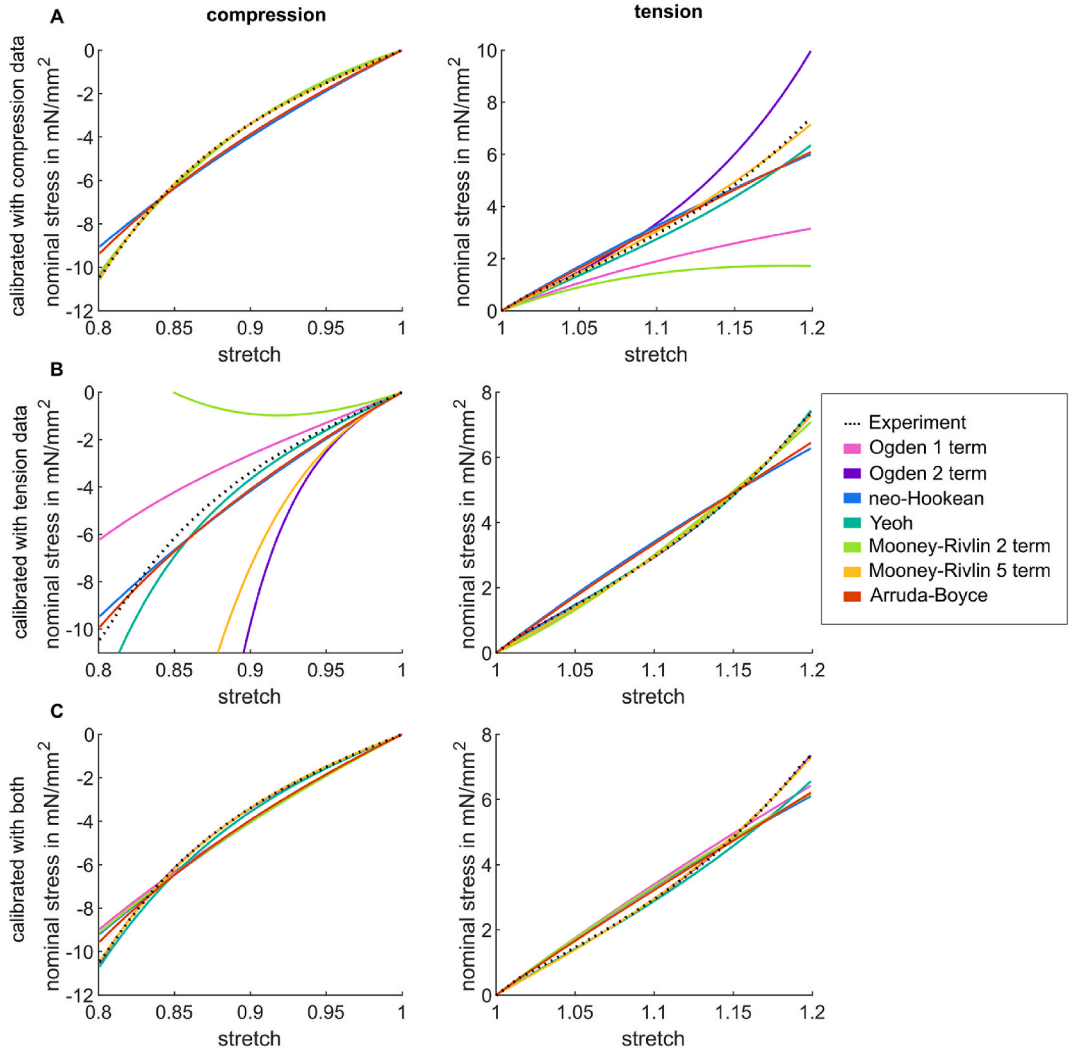

Fig. 8. Direct material model calibration based on compression and tension data, exemplary carried out for ADA-GEL. A) Calibration with compression data only. B) Calibration with tension data only. C) Calibration using tension and compression data simultaneously.

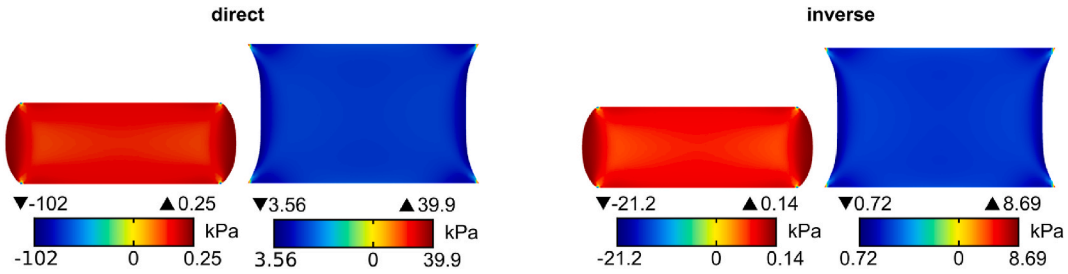

Fig. 10. Nominal stress distribution of a scaffold under compression and tension with parameters from direct and inverse PI for the example of ChondroFiller^{liquid}, the conditioned loading response, and the Ogden 2 term material model. Minimum and maximum nominal stresses in kPa are indicated by black triangles.

3. Results

3.1. The importance of considering tension and compression data simultaneously

Experimentally, we have previously observed an asymmetry between stresses in tension and compression, which was most pronounced for the ADA-GEL hydrogel. (Weizel et al., 2020) Many previous studies, however, have involved tensile loading or compressive loading of the material only for material parameter identification. (Oloyede et al., 1992) (Brown et al., 2009) (Boschetti et al., 2004) (Deneweth et al., 2013) (Lee et al., 2016) (Bae et al., 2006) (Langelier and Buschmann, 2003) (Charlebois et al., 2004) The reason for this is that the specimen geometry can be selected more freely when only compression is applied. In addition, biomaterial specimens are challenging to fix in conventional tensile testing machines.

Fig. 8 a-c demonstrates that the direct calibration of material parameters for several hyperelastic material models using compression tests only results in the false prediction of stresses in tensile direction and vice versa, exemplarily shown for the example of ADA-GEL. The results for human cartilage and ChondroFiller^{liquid} can be found in the supplementary material (Figure S 3 and Figure S 4). When both tensile and compressive loading are considered for calibration, the results are significantly improved for all material models, as shown in Fig. 8 C. Interestingly, the material models show different sensitivity towards parameter identification with only one loading mode. A graphical presentation of the sensitivity to the loading modes is shown in Fig. 9. The neo-Hookean, Arruda-Boyce and Yeoh models, have the lowest sensitivity compared to all other material models. The Mooney-Rivlin model with 5 terms shows exceptionally high deviations in compression when the parameters are determined from tension data only, but not vice versa. The Ogden and Mooney-Rivlin models with 2 terms lead to

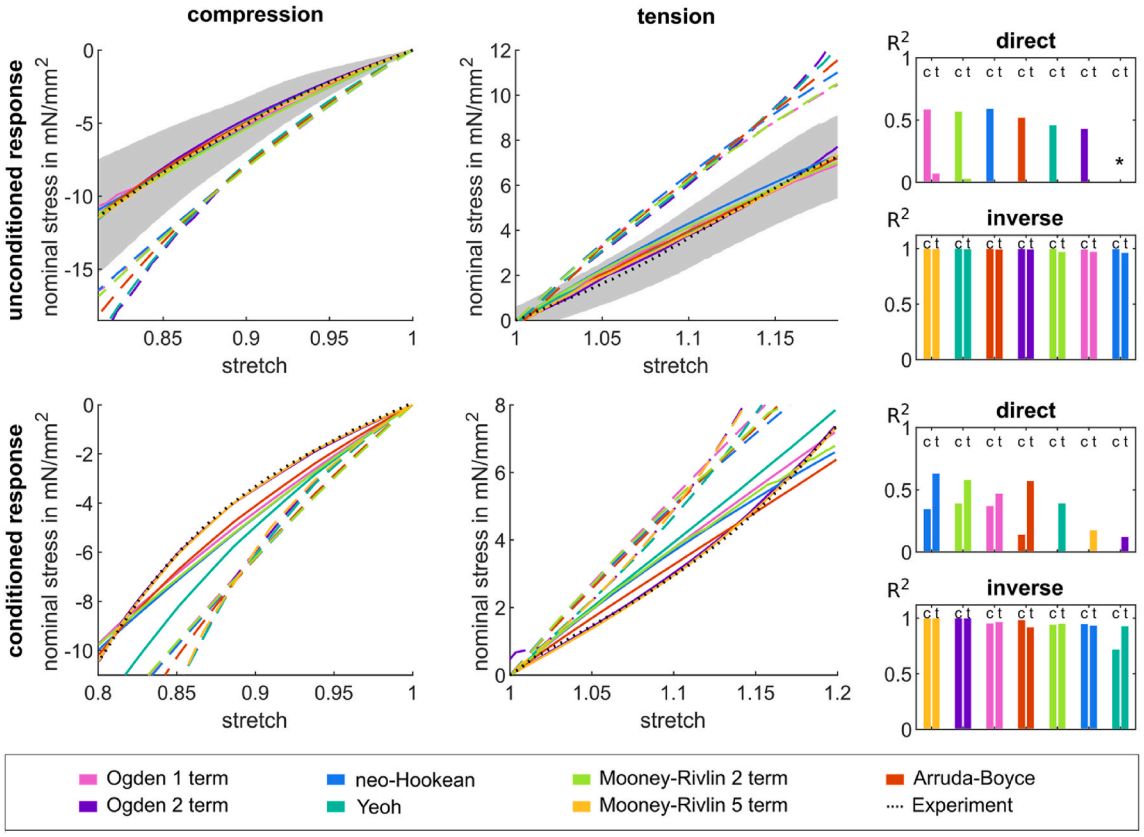

Fig. 11. Performance of material models with directly (dashed lines) and inversely (solid lines) identified parameters for the unconditioned and conditioned material response in compression (left) and tension (center) of ADA-GEL. The experimental data are shown as dotted line with standard deviations in shaded grey for the unconditioned material response. For the standard deviation of the conditioned response, we refer to Figure S 5 in the supplementary material. The corresponding R^2 values for each material model, ordered from best to worst, are presented on the right. *Simulation did not converged for the Mooney-Rivlin 5 term model and direct PI.

significant errors for the loading not considered during parameter identification. This highlights the importance of considering compression and tension data simultaneously when aiming to calibrate hyperelastic material parameters for human cartilage and hydrogels for cartilage repair that are valid for arbitrary loading conditions.

3.2. Material parameter identification

To describe the time-independent material behavior of human cartilage, ADA-GEL and ChondroFiller^{liquid}, we determine two sets of material parameters, representing the unconditioned and conditioned material response, respectively, for different hyperelastic material models. We compare two different approaches to identify the parameters, a direct and an inverse approach.

In the first, direct approach, we minimise the difference between the experimentally measured force and the force calculated using the material model under the assumption of a homogeneous deformation throughout the specimen during testing, which yields an analytical formula, by using a least-square optimization algorithm. In the second, inverse approach, we simulate the experiment with its actual boundary conditions and use the corresponding force from the simulation results to determine the parameters. Both methods are described in detail in Chapter 2.3.

As we eventually aim to provide material parameters suitable for finite element simulations, we will in the following focus on discussing the performance of the individual parameter sets during finite element simulations of the experimental procedure. The individual results of the direct parameter identification (PI) (without simulations) and the corresponding comparison with experimental data can be found in the supplementary material (Figure S 2, Figure S 3 and Figure S 4).

Fig. 11, Fig. 12 and Fig. 13, show the results of the inverse parameter identification as well as the force predictions when using the parameters identified through the direct approach in the finite element (FE) model for ADA-GEL, ChondroFiller^{liquid}, and human cartilage. The model parameters resulting from the inverse fit and the corresponding initial shear moduli calculated according to the formulas introduced in Section 2.2.2 are summarized in Table 3, Table 4 and Table 5, respectively.

All parameter sets identified through the direct approach yield stresses during the FE simulations that are significantly higher than the experimentally recorded stresses. This demonstrates that the assumption of a homogeneous deformation is not valid for such soft materials and the parameters from the direct PI overestimate the material stiffness.

Fig. 10 illustrates the stress distribution in the scaffold for the parameters from the direct PI and from the inverse PI for ChondroFiller^{liquid}. It is clearly visible that the stress is not homogeneously distributed over the entire scaffold, contrary to the assumption in the direct PI. Therefore, the nominal stresses based on the direct PI are higher than those based on the inverse PI.

3.3. ADA-GEL

Fig. 11 illustrates the capability of different isotropic material models to capture the unconditioned and conditioned hyperelastic responses of ADA-GEL. All parameter sets determined through the direct approach, summarized in Table 3, overestimate the stresses, both in compression and in tension. According to the inverse parameter

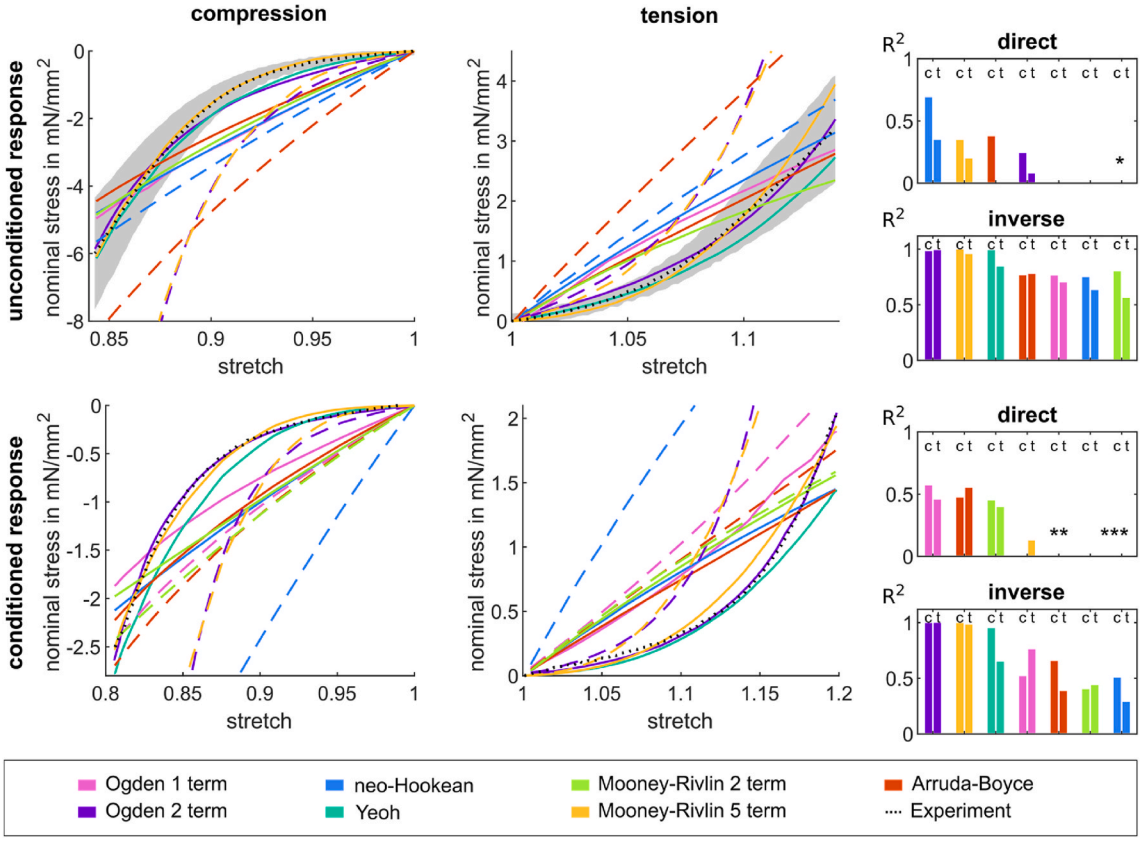

Fig. 12. Performance of material models with directly (dashed lines) and inversely (solid lines) identified parameters for the unconditioned and conditioned material response in compression (left) and tension (center) of ChondroFiller^{liquid}. The experimental data are shown as dotted line with standard deviations in shaded grey for the unconditioned material response. For the standard deviation of the conditioned response, we refer to Figure S 5 in the supplementary material. The corresponding R^2 values for each material model, ordered from the best to the worst result, are presented on the right.* Simulation did not converged for the Ogden 1 term, Yeoh and Mooney-Rivlin 2 term models and parameters from the direct PI. **Simulation did not converge for Yeoh model and parameters from the direct PI. ***R^2 values in compression and tension are 0 for Ogden 2 term and neo-Hookean models.

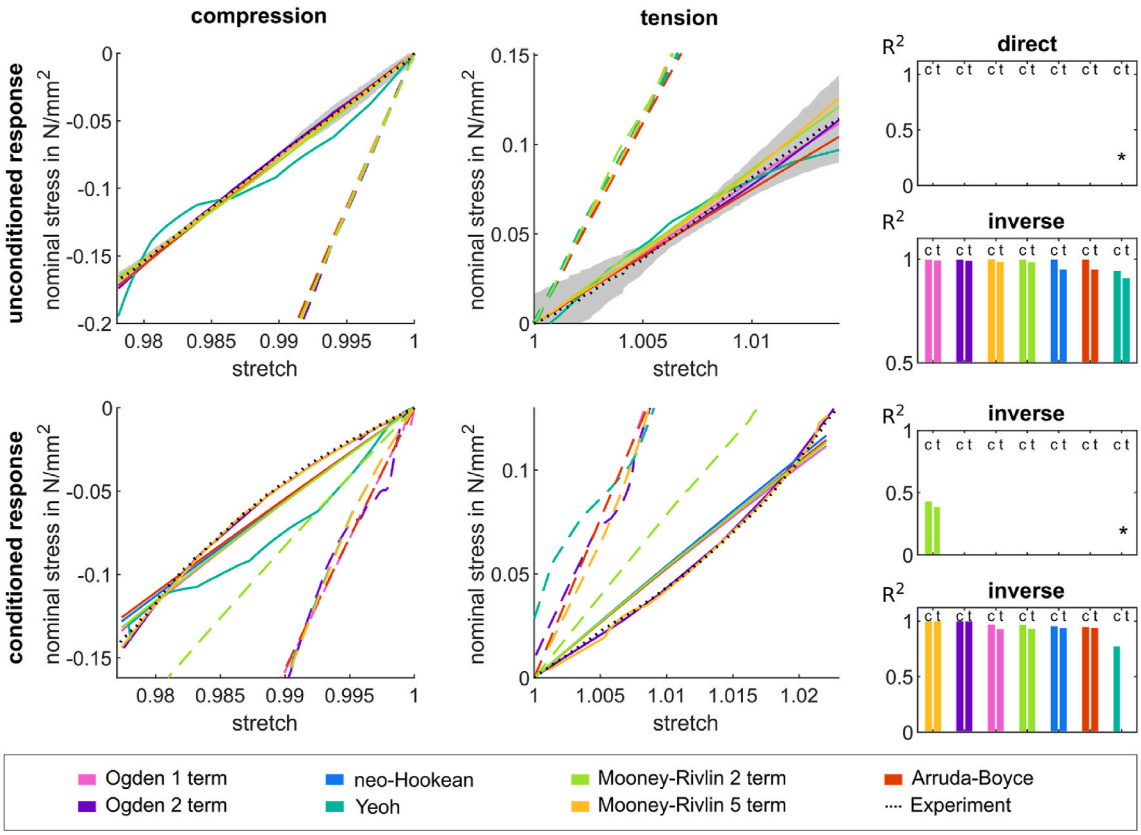

Fig. 13. Performance of material models with directly (dashed lines) and inversely (solid lines) identified parameters for the unconditioned and conditioned material response in compression (left) and tension (center) of cartilage. The experimental data are shown as dotted line with standard deviations in shaded grey for the unconditioned material response. For the standard deviation of the conditioned response, we refer to Figure S 5 in the supplementary material. The corresponding R^2 values for each material model, ordered from best to worst, are presented on the right. *R^2 values in compression and tension are 0 for all models except the Mooney-Rivlin 2 term model in the unconditioned response.

Table 3
Material parameters determined through the inverse PI with coefficients of determination R_c^2 and R_t^2 in compression and tension, respectively, and the corresponding initial shear modulus for ADA-GEL.

Ogden		μ_1 in kPa	α_1				R_c^2	R_t^2	μ_0 in kPa
	unconditioned	13.0151	1.5463				0.9906	0.9709	10.0626
	conditioned	5.0559	3.4024				0.9533	0.9659	8.6011
Ogden 2 term		μ_1 in kPa	α_1	μ_2 in kPa	α_2		R_c^2	R_t^2	μ_0 in kPa
	unconditioned	0.2517	12.4494	−13.5752	−1.0189		0.9965	0.9909	8.4826
	conditioned	1.1242	8.1636	−0.4586	−6.5442		0.9998	0.9990	6.0891
neo-Hookean		μ_0 in kPa					R_c^2	R_t^2	μ_0 in kPa
	unconditioned	10.3417					0.9948	0.9612	10.3417
	conditioned	8.8297					0.9466	0.9352	8.8297
Yeoh		c_1 in kPa	c_2 in kPa	c_3 in kPa			R_c^2	R_t^2	μ_0 in kPa
	unconditioned	4.5003	2.1263	−0.3074			0.9992	0.9931	9.0005
	conditioned	3.6335	1.9097	−0.0900			0.7165	0.9273	7.2669
Mooney-Rivlin 5 term		c_{10} in kPa	c_{01} in kPa	c_{11} in kPa	c_{02} in kPa	c_{20} in kPa	R_c^2	R_t^2	μ_0 in kPa
	unconditioned	3.0197	1.4526	−1.9136	−1.4987	5.6877	0.9998	0.9953	8.9446
	conditioned	4.6307	−1.7085	−2.4405	0.4027	6.4161	0.9999	0.9992	5.8442
Mooney-Rivlin 2 term		c_{10} in kPa	c_{01} in kPa				R_c^2	R_t^2	μ_0 in kPa
	unconditioned	4.1755	0.9212				0.9976	0.9698	10.1935
	conditioned	4.9589	−0.5042				0.9415	0.9501	8.9094
Arruda Boyce		μ in kPa	N				R_c^2	R_t^2	μ_0 in kPa
	unconditioned	3.1576	1.0858				0.9976	0.9904	9.6593
	conditioned	2.3037	1.0115				0.9823	0.9174	7.6689

identification (PI), the Mooney-Rivlin 5 term model best represents the unconditioned stress-stretch behavior, closely followed by the Yeoh, the Arruda-Boyce, and the Ogden 2 term models with coefficients of determination R^2>0.99 and shear moduli of μ_0 = 8.9446 kPa, μ_0 = 9.0005 kPa, μ_0 = 9.6593 kPa, and μ_0 = 8.4826 kPa, respectively. Those four models also yielded the best fits according to the direct PI, although the coefficients of determination were in general slightly lower than during the inverse PI (see supplementary Figure S 2). This is not surprising as the inverse PI is capable of capturing the actual boundary conditions during the experiments. The Mooney-Rivlin 2 term, the Ogden 1 term, and neo-Hookean models fail to capture the nonlinear course of the tensile stress.

Table 4
Material parameters determined through the inverse PI with coefficients of determination R_c^2 and R_t^2 in compression and tension, respectively, and the corresponding initial shear modulus for ChondroFiller^{liquid}.

Ogden		μ_1 in kPa	α_1				R_c^2	R_t^2	μ_0 in kPa
	unconditioned	49.4616	0.2232				0.7635	0.7007	5.5211
	conditioned	0.4133	7.2963				0.5200	0.7591	1.5077
Ogden 2 term		μ_1 in kPa	α_1	μ_2 in kPa	α_2		R_c^2	R_t^2	μ_0 in kPa
	unconditioned	0.1174	19.0428	−0.2166	−11.3264		0.9845	0.9919	2.3443
	conditioned	0.0208	19.9586	−0.0246	−13.2899		0.9974	0.9991	0.3712
neo-Hookean		μ_0 in kPa					R_c^2	R_t^2	μ_0 in kPa
	unconditioned	5.6418					0.7486	0.6327	5.6418
	conditioned	1.9431					0.5057	0.2861	1.9431
Yeoh		c_1 in kPa	c_2 in kPa	c_3 in kPa			R_c^2	R_t^2	μ_0 in kPa
	unconditioned	0.2153	3.2415	0.0000			0.9916	0.8435	0.4307
	conditioned	0.0853	2.7136	−0.7626			0.9499	0.6476	0.1706
Mooney-Rivlin 2 term		c_{10} in kPa	c_{01} in kPa				R_c^2	R_t^2	μ_0 in kPa
	unconditioned	0.1035	2.3082				0.8007	0.5628	4.8235
	conditioned	1.3156	−0.3283				0.4002	0.4386	1.9747
Mooney-Rivlin 5 term		c_{10} in kPa	c_{01} in kPa	c_{11} in kPa	c_{02} in kPa	c_{20} in kPa	R_c^2	R_t^2	μ_0 in kPa
	unconditioned	3.7048	−3.3786	8.6021	−8.3977	14.5039	0.9986	0.9560	0.6525
	conditioned	0.8832	−0.8276	−0.6417	−0.2677	3.8557	0.9972	0.9834	0.1111
Arruda Boyce		μ in kPa	N				R_c^2	R_t^2	μ_0 in kPa
	unconditioned	1.4027	1.0010				0.7655	0.7793	4.7295
	conditioned	0.5150	1.0010				0.6545	0.3849	1.7366

Table 5
Material parameters determined through the inverse PI with coefficients of determination R_c^2 and R_t^2 in compression and tension, respectively, and the corresponding initial shear modulus for cartilage.

Ogden		μ_1 in kPa	α_1				R_c^2	R_t^2	μ_0 in kPa
	unconditioned	117.0267	14.8433				0.9977	0.9925	868.5304
	conditioned	−215.7265	−5.6605				0.9689	0.9264	610.5566
Ogden 2 term		μ_1 in kPa	α_1	μ_2 in kPa	α_2		R_c^2	R_t^2	μ_0 in kPa
	unconditioned	33.8994	30.3516	−501.0743	−1.2646		0.9976	0.9910	831.2754
	conditioned	9.0025	45.0050	−12.9700	−38.7800		0.9985	0.9978	454.0671
neo-Hookean		μ_0					R_c^2	R_t^2	μ_0
	unconditioned	855.0511					0.9979	0.9489	855.0511
	conditioned	615.7566					0.9545	0.9359	615.7566
Yeoh		c_1 in kPa	c_2 in kPa	c_3 in kPa			R_c^2	R_t^2	μ_0 in kPa
	unconditioned	670	−98647	8921729			0.9419	0.9075	1339.8571
	conditioned	249	−1138	947076			0.7714	0.0000	497.2442
Mooney-Rivlin 2 term		c_{10} in kPa	c_{01} in kPa				R_c^2	R_t^2	μ_0 in kPa
	unconditioned	2866	−2400				0.9977	0.9846	933.0797
	conditioned	−86	393				0.9647	0.9303	615.4381
Mooney-Rivlin 5 term		c_{10} in kPa	c_{01} in kPa	c_{11} in kPa	c_{02} in kPa	c_{20} in kPa	R_c^2	R_t^2	μ_0 in kPa
	unconditioned	3759	−3310	−28785	−2175	35468	0.9998	0.9857	898.5780
	conditioned	−281	503	−235429	89299	156045	0.9998	0.9986	443.5194
Arruda Boyce		μ in kPa	N				R_c^2	R_t^2	μ_0 in kPa
	unconditioned	854.9470	126334				0.9979	0.9488	854.9510
	conditioned	431.2515	2.4353				0.9456	0.9371	666.6371

The Mooney-Rivlin 5 term and the Ogden 2 term models best represent the conditioned response of ADA-GEL with coefficients of determination R^2>0.99, and shear moduli of $\mu_0 = 5.8442$ kPa, and $\mu_0 = 6.0891$ kPa. All other models fail to capture the pronounced nonlinearity of the conditioned response. This again agrees well with the order of models according to the direct PI. The shear moduli for the conditioned response are 34.66 % lower for the Mooney-Rivlin 5 term model and 28.22 % lower for the Ogden 2 term model than those for the unconditioned response.

3.4. ChondroFiller^{liquid}

Fig. 12 shows the suitability of different isotropic material models to represent the unconditioned and conditioned hyperelastic response of ChondroFiller^{liquid}. Similar to ADA-GEL, all parameter sets determined through the direct approach (see Table 4) overestimate the stresses in compression and tension. According to the inverse PI, the Ogden 2 term model best represents the unconditioned ($R_c^2 = 0.9845$, $R_t^2 = 0.9919$) and conditioned ($R_c^2 = 0.9974$, $R_t^2 = 0.9991$) stress-stretch behavior, closely followed by the Mooney-Rivlin 5 term model (unconditioned: $R_c^2 = 0.9986$, $R_t^2 = 0.9560$; conditioned: $R_c^2 = 0.9972$, $R_t^2 = 0.9834$). The shear moduli determined with the Ogden 2 term and the Mooney-Rivlin 5 term models for the unconditioned response are $\mu_0 = 2.3443$ kPa, and $\mu_0 = 4.8235$ kPa and for the conditioned response 84.17 % ($\mu_0 = 0.3712$ kPa) and 97.7 % ($\mu_0 = 0.1111$ kPa) lower, respectively.

Those two models also yielded the best fits according to the direct PI. Since the stress-stretch behavior of ChondroFiller^{liquid} is highly nonlinear, the material models with the most terms represent the behavior best, while the Ogden 1 term, Yeoh, Arruda-Boyce, Mooney-Rivlin 2 term, and neo-Hookean models fail to capture response.

3.4.1. Cartilage

Fig. 13 shows the capability of different isotropic material models to capture the unconditioned and conditioned hyperelastic response of cartilage. All parameter sets determined through the direct approach (see Table 5) overestimate the stresses, both in compression and tension, as already seen for ADA-GEL and ChondroFiller^{liquid}. According to the inverse PI, the Ogden 1 term and the Ogden 2 term models best represent

the unconditioned stress-stretch behavior with coefficients of determination $R^2>0.99$ and shear moduli of $\mu_0 = 868.5304$ kPa and $\mu_0 = 831.2754$ kPa, closely followed by the Mooney-Rivlin 5 term and Mooney-Rivlin 2 term models with coefficients of determination $R^2>0.98$ and shear moduli of $\mu_0 = 898.5780$ kPa and $\mu_0 = 933.0797$ kPa, respectively. Those four models also yielded the best fits according to the direct PI. The neo-Hookean, Arruda-Boyce and Yeoh models fail to capture the stress-stretch response.

The Mooney-Rivlin 5 term and the Ogden 2 term models best represent the conditioned response of cartilage with coefficients of determination $R^2>0.99$ and shear moduli of $\mu_0 = 443.5194$ kPa, and $\mu_0 = 454.0671$ kPa (45.38 % lower than unconditioned), respectively. All other models fail to capture the more pronounced nonlinearity of the conditioned response. This again agrees well with the order of models according to the direct PI.

4. Discussion

In our study, we have determined hyperelastic material model parameters for cartilage, ADA-GEL and ChondroFiller^{liquid} based on compression and tension data. We have compared a direct and inverse parameter identification (PI) approach and have evaluated which hyperelastic material models are suitable to describe the conditioned and unconditioned nonlinear material responses. Furthermore, we have assessed how well the material models predict one loading mode when the parameters are identified based on another.

4.1. Using compression and tension data simultaneously for PI

Previous studies calibrating material parameters for cartilage have often only considered either tension or compression data. (Charlebois et al., 2004) (Lee et al., 2020) (Deneweth et al., 2013) (Bae et al., 2006) (Oloyede et al., 1992) (Langelier and Buschmann, 2003) (Brown et al., 2009) (Boschetti et al., 2004) Here, we have investigated how well parameters calibrated from one loading mode are capable of predicting the response under another mode. Our results show that the sensitivity towards the loading mode(s) used for calibration highly depends on the specific material model, i.e., how many tests are needed to determine reliable model parameters for a specific material. According to Bergström (Bergstr ö m, 2015), for models formulated in terms of invariants, the number of tests required depends on the number of invariants. For a model with one, only one test is needed, for a model with two different invariants, at least two tests are required for parameter identification. Thus, for the neo-Hookean, Arruda-Boyce and Yeoh models, only one test should be sufficient, but for the Ogden and Mooney-Rivlin models, two tests are required. This agrees well with our results since the Arruda-Boyce, Yeoh and neo-Hookean models show a low sensitivity towards the loading modes used for calibration. In turn, they are limited in their capabilities of capturing complex material responses. For the Mooney-Rivlin 2 term model, parameters calibrated exclusively with one loading mode cannot predict the response under a different mode. If we increase the number of model terms to 5 parameters calibrated with compression data can also predict the response in tension, but interestingly not vice versa. These observations demonstrate that it is important to consider at least two loading modes to provide reliable material parameters. A previous study has also shown that the Mooney-Rivlin model reasonably well predicts shear loading and triaxial indentation when parameters are determined based on experimental data under tension and compression loadings. (Upadhyay et al., 2020) Similarly, Ogden et al. (OGDEN et al., 2004) demonstrated that only considering multiple loading modes can yield accurate material parameters. Furthermore, it is highlighted that the parameters can have more than one solution, and the result depends on the settings during the fit, such as tolerances and initial values. However, we could previously show that the sensitivity towards the settings of the fitting procedure can be significantly reduced by considering multiple experimental loading conditions simultaneously. (Budday et al., 2019) (Budday et al., 2017b)

Another aspect that needs to be considered is that all materials studied here show an asymmetry between tension and compression stresses, which is not apparent when only one loading mode is considered. Taken together, our investigations and also previous results in the literature (Budday et al., 2017b) emphasize why it is essential not to use only one type of loading to characterize a material, to choose an appropriate material model, and to determine the corresponding material parameters.

4.2. Direct vs inverse parameter identification

In this study, we have compared two different approaches, a direct and an inverse one, to identify the model parameters for hyperelastic material models based on experimental data. The major advantage of the direct parameter identification (PI) is that the model-predicted streses can be calculated analytically and the result is available in a few seconds or minutes, depending on the computing power by using a single software (in our case MATLAB). The disadvantage is that the analytical derivations are based on the assumption of an unconfined and homogenous deformation throughout the specimen during loading. However, when performing both compression and tension experiments, which is essential according to the discussion in Section 4.1, specimens need to be glued to the specimen holder so that the actual deformation field is not homogeneous (see Fig. 10). When using the inverse method, the finite element (FE) model allows us to consider the exact boundary conditions that occurred during the experiment. However, the required time for the parameter identification increases immensely, as the full FE model has to be solved in each optimization iteration.

In order to evaluate the validity of parameters obtained through the direct method, we have used the corresponding parameter sets for detailed FE simulations of the test and compared the result to the experimental curves. Our analyses show that the parameters determined through the direct PI lead to a significant overestimation of stresses in the FE model. This can be attributed to the different boundary conditions, which prove to have an effect that is not negligible. The reaction force in axial direction for a specimen fixed on the top and bottom surfaces is higher than for a specimen under unconfined conditions. Therefore, parameters obtained through the direct PI lead to an overestimation of stresses.

Consequently, a direct PI is not sufficient to determine parameters for an FE model. However, direct PI provides us with good qualitative information and a first estimate on appropriate material models. Material models that are unable to reproduce the nonlinearity in the direct PI will also fail to do so in the inverse PI. Some material models, however, show an even worse result in the inverse than in the direct PI. Thus, a short, direct PI can be performed in advance to evaluate the suitability of individual material models and exclude them for the inverse PI. In addition, a direct PI can help identify suitable initial values for the inverse PI to save computation time.

Interestingly, the deviation between the results for the inversely and directly identified parameters is highest for cartilage. This can most probably be attributed to the even lower sample height of cartilage specimens. With a lower sample height, the effect of the boundary conditions becomes more prominent. Since the physiological anatomy limits the maximum sample height of cartilage, we recommend to use an inverse PI in the future.

Finally, we would like to emphasize that it is highly dependent on the experimental settings whether direct parameter identification is applicable. The experiments have to assure a homogeneous deformation like tensile (with an appropriately long specimen), or biaxial tensile tests reported, for example in (Charlebois et al., 2004) (Treloar, 1944).

4.3. Choice of material models

We have determined two different parameter sets representing the unconditioned and conditioned material behavior, respectively. The conditioned response shows a more pronounced nonlinearity and is slightly softer than the unconditioned response, which also affects the corresponding choice of suitable hyperelastic material models for FE simulations. Accordingly, the Ogden 2 term and the Mooney-Rivlin model with 5 terms achieve the best predictions for the conditioned responses of all materials. This can be attributed to the additional terms and higher-order exponents, which better reproduce the pronounced nonlinearity in the conditioned response. We note, however, that with the additional terms in the Mooney-Rivlin 5-term model one needs to be careful with overparameterization. While the model may well represent any experimental curve, the predictive power outside the tested range could be limited. The Yeoh model is less suitable for cartilage but shows promising results for the two hydrogels. It has previously also yielded good results for bovine cartilage but had been used in a different loading range than the one considered here. (Brown et al., 2009) However, for large deformations and complex strain states, the Yeoh model may be inaccurate because I_2 is neglected. (Yeoh, 1993) As expected, the neo-Hookean, Mooney-Rivlin 2 term, and the Ogden 1 term models fail to represent pronounced nonlinearities. Still, the Ogden 1 term model best represented the unconditioned, less nonlinear stress-stretch response of cartilage.

In summary, we propose to use the Ogden 1 term model for the unconditioned response of cartilage with the parameters presented in Table 5, while Mooney-Rivlin 5 term and the Ogden 2 term models are equally good choices for the conditioned response of cartilage. When computationally modelling the unconditioned response of ADA-GEL, our results suggest that the Moony-Rivlin 5 term model is the best choice with parameters presented in Table 3. The conditioned response is best represented by the Mooney-Rivlin 5 term and Ogden 2 term models. Finally, the unconditioned response of ChondroFiller^{liquid} is best represented by the Ogden 2 term and the Moony-Rivlin 5 term models with the parameters presented in Table 4, while the conditioned response is best represented by the Ogden 2 term model.

4.4. Application of specific material parameters

We obtained two sets of parameters from our experiments describing two different situations. The unconditioned parameter set represents a fast, purely hyperelastic material response, where no fluid is assumed to leak from the cartilage or hydrogel. On the application level, activities characterized by impact loading such as running and jumping are in focus for articular cartilage in the human body. We know from literature that cartilage does not change its elastic modulus significantly above a strain rate of 0.05 1/s. (Oloyede et al., 1992) Consequently, we here focused on the response of cartilage at a strain rate of 0.2423 1/s.

In addition, we have provided a parameter set representing the conditioned material response after the third cycle. Our previous investigations had revealed that the hysteresis and conditioning remain almost constant after the third cycle. (Weizel et al., 2020) Therefore, we have used the average stress-stretch curve from loading and unloading during the third cycle since the hysteresis of a viscoelastic material will disappear at sufficiently slow static loading. This conditioned material response is dominated by the interaction of matrix molecules, leading to a nonlinear stress-stretch relationship. From a physiological point of view, this type of behavior occurs in cartilage, for example, during sustained loadings such as standing and sitting or during repetitive cyclic loading like walking, where the thickness of cartilage decreases and strains ranging from 2% to 6% could be measured. (Liu et al., 2017)

We have observed a lower shear modulus for the conditioned response than for the unconditioned response for all materials. For cartilage, we obtained values ranging from 443.5194 kPa to 868.5304 kPa, which is in excellent agreement with values from the literature suggesting that the shear modulus lies between 200 and 2500 kPa. (van Mow et al., 1992)

For ChondroFiller^{liquid}, which consists mainly of collagen type I with a concentration of 8 mg/ml, we obtained a conditioned and unconditioned shear modulus of 0.3712 kPa and 2.3443 kPa for the Ogden 2 term model. The shear modulus and mechanical properties of collagen scaffolds are highly dependent on the testing procedure on the one hand and on the concentration of collagen on the other hand, among other factors like ph-value, temperature and crosslinking. (Harjanto et al., 2011) For this reason, it is challenging to make direct comparisons with data in the literature. Nevertheless, an estimate for the order of magnitude of the shear modulus can be made based on measured values of the Young's modulus of type I collagen (assuming a Poisson's ratio of $v = 0.5$). According to the literature, a collagen type I scaffold at 4 mg/ml has a shear modulus of 0.550 kPa. With increasing collagen concentration, the shear modulus increases. (Harjanto et al., 2011) Furthermore, a study examining collagen at a concentration of 10 mg/ml and varying degrees of crosslinking yielded shear moduli ranging from 1.163 kPa to 2.41 kPa (Sheu et al., 2001) These studies show that the determined shear modulus of ChondroFiller^{liquid} agrees well with literature data of other collagen type I based scaffolds.

ADA-GEL consists of ADA (alginate di-aldehyde, oxidized alginate) and gelatin and is a non-fibrous material. We obtained conditioned and unconditioned shear moduli ranging from 5.8442 kPa to 8.9446 kPa for the Mooney-Rivlin 5 term model, respectively. Our ADA-GEL hydrogel crosslinked with microbial transglutaminase and with (3.75% (w/v)) ADA and (3.75% (w/v)) gelatin has not been characterized in the literature before. (Weizel et al., 2020) However, in a recent study (Distler et al., 2021), non-crosslinked ADA-GEL with the same composition was mechanically tested, and a shear modulus of 3.788 kPa was determined, which is slightly lower than the shear moduli we have obtained. As expected, crosslinking increases the elastic modulus of the hydrogel, which is in accordance to previous studies. Regarding materials design, we showed in a previous study that increasing mTG concentration used for crosslinking increases hydrogel elastic modulus up to values of > 50 kPa. (Distler et al., 2020) While we showed that increasing gelatin concentration (c_fin = 7.5 %) can enhance 3D-printability of ADA-GEL (Kreller et al., 2021), increasing mTG crosslinker and GEL concentration may be a suitable attempt to enhance the shear modulus of ADA-GEL to values closer to native cartilage as determined in this study.

5. Limitations and future directions

One limitation of our study is that we consider only hyperelasticity. We neglect the time-dependent component and assume a dissipation-free process for the deformation of the materials. In reality, cartilage, ADA-GEL, and ChondroFiller^{liquid} are viscoelastic and biphasic. (Weizel et al., 2020) (Sophia Fox et al., 2009) Still, hyperelastic models are often used for finite element simulations of cartilage. (Brown et al., 2009) (Lee et al., 2020) In the future, the hyperelastic models identified here can be extended to hyper-visco and/or -poroelastic models to additionally capture conditioning, hysteresis, and stress relaxation. In this context, we would like to note that both sets of parameters identified in the current work represent a specific application case and must therefore be used with close consideration of the particular loading case of interest.

Another aspect that was neglected is the anisotropy of cartilage. In the case of ADA-GEL, isotropy can be assumed due to the manufacturing process and our previous investigations of the microstructure. (Weizel et al., 2020) In the case of ChondroFiller^{liquid}, we have previously shown that it contains fibrous and non-fibrous components, where the fibrous part shows a preferred orientation of 45° with respect to the surface. (Weizel et al., 2020) However, we did not investigate the anisotropy in our experiments. Furthermore, we have not considered shear data during the material parameter identification.

Furthermore, we used cartilage from a single donor and do not take

into account subject-specific differences. We took the cartilage specimens from macroscopically healthy areas, but the donor suffered from osteoarthritis and we cannot assure that degenerative changes were already present in our cartilage specimens. (Weizel et al., 2020)

Finally, in the case of ChondroFiller^{liquid}, we found that the deformation is not fully reversible, and a crack in the scaffolds was observed during the microstructure analysis, which might have slightly affected the identified material parameters as we did not consider damage effects.

Another important point to consider is that the parameters determined here are only fully valid for the implementations of the material laws and incompressibility used in COMSOL Multiphysics®. Moreover, the parameters identified only represent the averaged response of the three materials.

6. Conclusion

We have evaluated the suitability of different hyperelastic material models to capture the unconditioned and conditioned responses of human hyaline cartilage and two materials for cartilage regeneration, ADA-GEL and ChondroFiller^{liquid}, and have provided corresponding sets of material parameters that can be used for finite element (FE) simulations in the future. For all materials, the unconditioned material response was expectedly stiffer than the conditioned response.

We have shown that it is essential to perform an inverse parameter identification, where the exact boundary conditions are simulated using the FE method when iteratively optimizing the material parameters. In addition, we have shown that it is important to consider both compression and tension data to provide reliable parameters.

Our results show that the Ogden 1 term and the Ogden 2 term models are best suitable for the unconditioned response of cartilage. In contrast, the Mooney-Rivlin 5 term and Ogden 2 term models best represent the conditioned material response. For ChondroFiller^{liquid}, both the conditioned and unconditioned responses are well captured by the Ogden 2 term and the Mooney-Rivlin 5 term models. For ADA-GEL, both the unconditioned and conditioned responses were best represented by the Mooney-Rivlin 5 term model. For each model, we have provided material parameters that can be immediately used for FE programs such as COMSOL Multiphysics® v. 5.6. The results from this study will be used to guide materials design by providing material parameters which allow for simulation of materials response and to aid materials design to mimic the complex mechanical properties of articular cartilage.

CRediT authorship contribution statement

A. Weizel: Writing – review & editing, Writing – original draft, Investigation, Formal analysis, Data curation, Conceptualization. **T. Distler:** Writing – review & editing, Methodology. **R. Detsch:** Methodology, Funding acquisition. **A.R. Boccaccini:** Methodology, Funding acquisition. **L. Bräuer:** Methodology. **F. Paulsen:** Methodology. **H. Seitz:** Writing – review & editing, Funding acquisition. **S. Budday:** Writing – review & editing, Writing – original draft, Conceptualization.

Declaration of competing interest

The authors declare that they have no known competing financial interests or personal relationships that could have appeared to influence the work reported in this paper.

7 Acknowledgements

The authors cordially thank the support from the German Research Foundation (DFG) through the Collaborative Research Center 1270/1–299150580 ELAINE - Electrically Active Implants to ARB and HS and the grant BU 3728/1-1 to SB is gratefully acknowledged. We also acknowledge the kind support by the Emerging Fields Initiative (EFI) by the FAU to ARB, FP and SB.

Appendix A. Supplementary data

Supplementary data to this article can be found online at https://doi.org/10.1016/j.jmbbm.2022.105292.

References

Aldeen, A.N., Can, Y., Yazici, M., 2020. Modelling Hyperelastic Materials by MATLAB. https://doi.org/10.22399/ijcesen.662707.

Arruda, E.M., Boyce, M.C., 1993. A three-dimensional constitutive model for the large stretch behavior of rubber elastic materials. J. Mech. Phys. Solid. 41, 389–412. https://doi.org/10.1016/0022-5096(93)90013-6.

Bae, W.C., Lewis, C.W., Levenston, M.E., Sah, R.L., 2006. Indentation testing of human articular cartilage: effects of probe tip geometry and indentation depth on intra-tissue strain. J. Biomech. 39, 1039–1047. https://doi.org/10.1016/j.jbiomech.2005.02.018.

Bergström, J., 2015. Mechanics of Solid Polymers: Theory and Computational Modeling. Elsevier, Amsterdam [u.a.

Boschetti, F., Pennati, G., Gervaso, F., Peretti, G.M., Dubini, G., 2004. Biomechanical properties of human articular cartilage under compressive loads. Biorheology 41, 159–166.

Boyce, M.C., Arruda, E.M., 2000. Constitutive models of rubber elasticity: a review. Rubber Chem. Technol. 73, 504–523. https://doi.org/10.5254/1.3547602.

Brown, C.P., Nguyen, T.C., Moody, H.R., Crawford, R.W., Oloyede, A., 2009. Assessment of common hyperelastic constitutive equations for describing normal and osteoarthritic articular cartilage. Proc. Inst. Mech. Eng. H 223, 643–652. https://doi.org/10.1243/09544119JEIM546.

Budday, S., Sommer, G., Birkl, C., Langkammer, C., Haybaeck, J., Kohnert, J., Bauer, M., Paulsen, F., Steinmann, P., Kuhl, E., Holzapfel, G.A., 2017a. Mechanical characterization of human brain tissue. Acta Biomater. 48, 319–340. https://doi.org/10.1016/j.actbio.2016.10.036.

Budday, S., Sommer, G., Holzapfel, G.A., Steinmann, P., Kuhl, E., 2017b. Viscoelastic parameter identification of human brain tissue. J. Mech. Behav. Biomed. Mater. 74, 463–476. https://doi.org/10.1016/j.jmbbm.2017.07.014.

Budday, S., Ovaert, T.C., Holzapfel, G.A., Steinmann, P., Kuhl, E., 2019. Fifty shades of brain: a review on the mechanical testing and modeling of brain tissue. Arch. Comput. Methods Eng. 53, 2284. https://doi.org/10.1007/s11831-019-09352-w.

Butz, K.D., Chan, D.D., Nauman, E.A., Neu, C.P., 2011. Stress distributions and material properties determined in articular cartilage from MRI-based finite strains. J. Biomech. 44, 2667–2672. https://doi.org/10.1016/j.jbiomech.2011.08.005.

Charlebois, M., McKee, M.D., Buschmann, M.D., 2004. Nonlinear tensile properties of bovine articular cartilage and their variation with age and depth. J. Biomech. Eng. 126, 129–137. https://doi.org/10.1115/1.1688771.

COMSOL, The Structural Mechanics Module User's Guide.

Deneweth, J.M., McLean, S.G., Arruda, E.M., 2013. Evaluation of hyperelastic models for the non-linear and non-uniform high strain-rate mechanics of tibial cartilage. J. Biomech. 46, 1604–1610. https://doi.org/10.1016/j.jbiomech.2013.04.014.

Distler, T., McDonald, K., Heid, S., Karakaya, E., Detsch, R., Boccaccini, A.R., 2020. Ionically and enzymatically dual cross-linked oxidized alginate gelatin hydrogels with tunable stiffness and degradation behavior for tissue engineering. ACS Biomater. Sci. Eng. 6, 3899–3914. https://doi.org/10.1021/acsbiomaterials.0c00677.

Distler, T., Kretzschmar, L., Schneidereit, D., Girardo, S., Goswami, R., Friedrich, O., Detsch, R., Guck, J., Boccaccini, A.R., Budday, S., 2021. Mechanical properties of cell- and microgel bead-laden oxidized alginate-gelatin hydrogels. Biomater. Sci. 9, 3051–3068. https://doi.org/10.1039/d0bm02117b.

Dusfour, G., LeFloc'h, S., Cañadas, P., Ambard, D., 2020. Heterogeneous mechanical hyperelastic behavior in the porcine annulus fibrosus explained by fiber orientation: an experimental and numerical approach. J. Mech. Behav. Biomed. Mater. 104, 103672 https://doi.org/10.1016/j.jmbbm.2020.103672.

Freutel, M., Schmidt, H., Dürselen, L., Ignatius, A., Galbusera, F., 2014. Finite element modeling of soft tissues: material models, tissue interaction and challenges. Clin. Biomech. 29, 363–372. https://doi.org/10.1016/j.clinbiomech.2014.01.006.

Freutel, M., Galbusera, F., Ignatius, A., Dürselen, L., 2015. Material properties of individual menisci and their attachments obtained through inverse FE-analysis. J. Biomech. 48, 1343–1349. https://doi.org/10.1016/j.jbiomech.2015.03.014.

García, J.J., Cortés, D.H., 2006. A nonlinear biphasic viscohyperelastic model for articular cartilage. J. Biomech. 39, 2991–2998. https://doi.org/10.1016/j.jbiomech.2005.10.017.

Halonen, K.S., Mononen, M.E., Jurvelin, J.S., Töyräs, J., Salo, J., Korhonen, R.K., 2014. Deformation of articular cartilage during static loading of a knee joint–experimental and finite element analysis. J. Biomech. 47, 2467–2474. https://doi.org/10.1016/j.jbiomech.2014.04.013.

Harjanto, D., Maffei, J.S., Zaman, M.H., 2011. Quantitative analysis of the effect of cancer invasiveness and collagen concentration on 3D matrix remodeling. PLoS One 6, e24891. https://doi.org/10.1371/journal.pone.0024891.

Holzapfel, G.A., 2010. Nonlinear Solid Mechanics: A Continuum Approach for Engineering. Repr, Wiley, Chichester.

Kreller, T., Distler, T., Heid, S., Gerth, S., Detsch, R., Boccaccini, A.R., 2021. Physico-chemical modification of gelatine for the improvement of 3D printability of oxidized

alginate-gelatine hydrogels towards cartilage tissue engineering. Mater. Des. 208, 109877 https://doi.org/10.1016/j.matdes.2021.109877.
Langelier, E., Buschmann, M.D., 2003. Increasing strain and strain rate strengthen transient stiffness but weaken the response to subsequent compression for articular cartilage in unconfined compression. J. Biomech. 36, 853–859. https://doi.org/10.1016/s0021-9290(03)00006-x.
Lee, H., Campbell, W.D., Canning, M.E., Theis, K.M., Ennis, H.Y., Jackson, R.L., Wright, J.C., Hanson, R.R., 2016. Correlation between signalment and the biphasic hyperelastic mechanical properties of equine articular cartilage. Biotribology 7, 31–37. https://doi.org/10.1016/j.biotri.2016.07.001.
Lee, H., Campbell, W.D., Theis, K.M., Canning, M.E., Ennis, H.Y., Jackson, R.L., Hanson, R.R., 2020. Comparison between the hyperelastic behavior of fresh and frozen equine articular cartilage in various joints. J. Biomech. Eng. 142 https://doi.org/10.1115/1.4044031.
Liu, B., Lad, N.K., Collins, A.T., Ganapathy, P.K., Utturkar, G.M., McNulty, A.L., Spritzer, C.E., Moorman, C.T., Sutter, E.G., Garrett, W.E., DeFrate, L.E., 2017. In vivo tibial cartilage strains in regions of cartilage-to-cartilage contact and cartilage-to-meniscus contact in response to walking. Am. J. Sports Med. 45, 2817–2823. https://doi.org/10.1177/0363546517712506.
Matlab, R 2018. Update 2 (9.5.0.1033004. The MathWorks Inc, Natick, Massachusetts.
Ogden, R.W., 1972. Large deformation isotropic elasticity – on the correlation of theory and experiment for incompressible rubberlike solids. Proc. Roy. Soc. Lond. A 326, 565–584. https://doi.org/10.1098/rspa.1972.0026.
Ogden, R.W., Saccomandi, G., Sgura, I., 2004. Fitting hyperelastic models to experimental data. Comput. Mech. 34, 484–502. https://doi.org/10.1007/s00466-004-0593-y.
Oloyede, A., Flachsmann, R., Broom, N.D., 1992. The dramatic influence of loading velocity on the compressive response of articular cartilage. Connect. Tissue Res. 27, 211–224. https://doi.org/10.3109/03008209209006997.
Reuter, T., Ponomarev, I., 2015. Biomechanical parameter determination of scaffold-free cartilage constructs (SFCCs) with the hyperelastic material models Yeoh, Ogden and Demiray. Current Directions in Biomedical Engineering 1, 442–445. https://doi.org/10.1515/cdbme-2015-0106.
Sasson, A., Patchornik, S., Eliasy, R., Robinson, D., Haj-Ali, R., 2012. Hyperelastic mechanical behavior of chitosan hydrogels for nucleus pulposus replacement-experimental testing and constitutive modeling. J. Mech. Behav. Biomed. Mater. 8, 143–153. https://doi.org/10.1016/j.jmbbm.2011.12.008.
Schwarz, S., Kuth, S., Distler, T., Gögele, C., Stölzel, K., Detsch, R., Boccaccini, A.R., Schulze-Tanzil, G., 2020. 3D printing and characterization of human nasoseptal chondrocytes laden dual crosslinked oxidized alginate-gelatin hydrogels for cartilage repair approaches. Mater. Sci. Eng. C Mater. Biol. Appl. 116, 111189 https://doi.org/10.1016/j.msec.2020.111189.
Sheu, M.-T., Huang, J.-C., Yeh, G.-C., Ho, H.-O., 2001. Characterization of collagen gel solutions and collagen matrices for cell culture. Biomaterials 22, 1713–1719. https://doi.org/10.1016/S0142-9612(00)00315-X.
Sophia Fox, A.J., Bedi, A., Rodeo, S.A., 2009. The basic science of articular cartilage: structure, composition, and function. Sport Health 1, 461–468. https://doi.org/10.1177/1941738109350438.
Treloar, L.R.G., 1944. Stress-strain data for vulcanised rubber under various types of deformation. Trans. Faraday Soc. 40, 59. https://doi.org/10.1039/TF9444000059.
Upadhyay, K., Subhash, G., Spearot, D., 2020. Hyperelastic constitutive modeling of hydrogels based on primary deformation modes and validation under 3D stress states. Int. J. Eng. Sci. 154, 103314 https://doi.org/10.1016/j.ijengsci.2020.103314.
van Mow, C., Ratcliffe, A., Robin Poole, A., 1992. Cartilage and Diarthrodial Joints as Paradigms for Hierarchical Materials and Structures.
Weizel, A., Distler, T., Schneidereit, D., Friedrich, O., Bräuer, L., Paulsen, F., Detsch, R., Boccaccini, A.R., Budday, S., Seitz, H., 2020. Complex mechanical behavior of human articular cartilage and hydrogels for cartilage repair. Acta Biomater. 118, 113–128. https://doi.org/10.1016/j.actbio.2020.10.025.
Yeoh, O.H., 1993. Some forms of the strain energy function for rubber. Rubber Chem. Technol. 66, 754–771. https://doi.org/10.5254/1.3538343.
Zahedmanesh, H., Stoddart, M., Lezuo, P., Forkmann, C., Wimmmer, M.A., Alini, M., van Oosterwyck, H., 2014. Deciphering mechanical regulation of chondrogenesis in fibrin-polyurethane composite scaffolds enriched with human mesenchymal stem cells: a dual computational and experimental approach. Tissue Eng. 20, 1197–1212. https://doi.org/10.1089/ten.TEA.2013.0145.

journal of the mechanical behavior of biomedical materials 138 (2023) 105618

Contents lists available at ScienceDirect

Journal of the Mechanical Behavior of Biomedical Materials

journal homepage: www.elsevier.com/locate/jmbbm

Time-dependent hyper-viscoelastic parameter identification of human articular cartilage and substitute materials

A. Weizel [a,*], T. Distler [b], R. Detsch [b], A.R. Boccaccini [b], H. Seitz [a], S. Budday [c,**]

[a] Chair of Microfluidics, Faculty of Mechanical Engineering and Marine Technology, University of Rostock, Rostock, Germany
[b] Institute of Biomaterials, Department of Materials Science and Engineering, Friedrich-Alexander-University Erlangen-Nürnberg, 91058, Erlangen, Germany
[c] Institute of Applied Mechanics, Department of Mechanical Engineering, Friedrich-Alexander-Universität Erlangen-Nürnberg, Erlangen, Germany

ARTICLE INFO

Keywords:
Human articular cartilage
Hydrogels
Tissue engineering
Finite viscoelasticity
Parameter identification

ABSTRACT

Numerical simulations are a valuable tool to understand which processes during mechanical stimulations of hydrogels for cartilage replacement influence the behavior of chondrocytes and contribute to the success or failure of these materials as implants. Such simulations critically rely on the correct prediction of the material response through appropriate material models and corresponding parameters. In this study, we identify hyper-viscoelastic material parameters for numerical simulations in COMSOL Multiphysics® v. 5.6 for human articular cartilage and two replacement materials, the commercially available ChondroFiller^{liquid} and oxidized alginate gelatin (ADA-GEL) hydrogels. We incorporate the realistic experimental boundary conditions into an inverse parameter identification scheme based on data from multiple loading modes simultaneously, including cyclic compression-tension and stress relaxation experiments. We provide individual parameter sets for the unconditioned and conditioned responses and discuss how viscoelastic effects are related to the materials' microstructure. ADA-GEL and ChondroFiller^{liquid} exhibit faster stress relaxation than cartilage with lower relaxation time constants, while cartilage has the largest viscoelastic stress contribution. The elastic response predominates in ADA-GEL and ChondroFiller^{liquid}, while the viscoelastic response predominates in cartilage. These results will help to simulate mechanical stimulations, support the development of suitable materials with distinct mechanical properties in the future and provide parameters and insight into the time-dependent material behavior of human articular cartilage.

1. Introduction

The function of cartilage is to provide frictionless articular motion of the joints and damping during cyclic compression occurring during walking (Martínez-Moreno et al., 2019). These unique mechanical properties of cartilage are determined by its structure and composition. Cartilage consists of an extracellular matrix (ECM) incorporating chondrocytes. The healthy ECM of cartilage consists mainly of water with a proportion of 85%, which decreases linearly to the subchondral zone to 70% (van Mow et al., 1984). In addition, the ECM contains hydrophilic and negatively charged proteoglycans (GAGs) (Martínez-Moreno et al., 2019). It can therefore store high amounts of water. The solid part of the ECM consists mainly of collagen type II (90–95%) and other collagen types such as IX and XI, in addition to GAGs (Martínez-Moreno et al., 2019).

Osteoarthritis (OA) is the most degenerative disease related to joints, with 303,1 million prevalent cases in 2017, which increased in most countries and is expected to rise due to of longer life expectancy and ageing of the global population (Safiri et al., 2020). During the development of OA, dramatic changes occur mainly in the superficial zone of cartilage, such as disorientation and degradation of collagen fibrils. In addition, OA also causes a decrease in proteoglycans and collagen, followed by an increase in fluid within the tissue (Saarakkala et al., 2010). These structural changes lead to a reduction in static and dynamic stiffness and increased permeability (Ebrahimi et al., 2019). Macroscopically, OA leads to a decrease in elastic properties and an increase in viscoelastic properties (Kleemann et al., 2005) (Ebrahimi et al., 2019). The reduced load capacity of osteoarthritic cartilage leads to higher strains than in healthy cartilage for the same loading (Saarakkala et al., 2010).

* Corresponding author.
** Corresponding author.
E-mail addresses: alina.weizel@uni-rostock.de (A. Weizel), silvia.budday@fau.de (S. Budday).

https://doi.org/10.1016/j.jmbbm.2022.105618
Received 22 September 2022; Received in revised form 2 December 2022; Accepted 8 December 2022
Available online 9 December 2022

Among the numerous regenerative medicine approaches to find the perfect replacement material for cartilage to heal OA, is the research and development of new cartilage replacement materials based on hydrogels. These include hydrogels based on collagen type I (mostly of animal origin), but also hydrogels made from alginate, agarose, gelatin, and chitosan (Stampoultzis et al., 2021). Hydrogels are promising materials for cartilage regeneration and consist of a network of hydrophilic macromolecules that allow the hydrogels to store a lot of water (Caccavo et al., 2018). The chemical composition and the mechanical properties of the hydrogels are optimized through research studies to make them attractive for cartilage cells and achieve material properties similar to native cartilage.

A promising approach involving the implantation of hydrogels is matrix-associated chondrocyte implantation (MACI) (Stampoultzis et al., 2021). During this procedure, a hydrogel is enriched with chondrocytes in vitro prior to implantation. Although this method can be of great help for the patients, it does not lead to the development of mechanically identical hyaline cartilage but rather a fibrous tissue with less suitable mechanical properties. One idea to circumvent this issue is to tune the implant properties as close to native cartilage as possible before implantation by means of various stimulation mechanisms.

The most promising stimulation mechanisms are hydrostatic pressure, direct compression, fluid shear (Martínez-Moreno et al., 2019) (Stampoultzis et al., 2021) (Meinert et al., 2017), and electrical stimulation (Brighton et al., 2008) (Krueger et al., 2021). These stimulations positively affect the synthesis of collagen type II and glycosaminoglycans (GAGs) and promote chondrogenesis (Martínez-Moreno et al., 2019). Mechanical stimulation leads to mechanotransduction in chondrocytes (Sarrigiannidis et al., 2021), i.e., a relayed electrochemical signal in which the primary cilium plays a crucial role. This influences cell migration, differentiation and cell survival (Martínez-Moreno et al., 2019).

The mechanical environment sensed by cells is defined by the material properties of the scaffold and the loading during stimulation simultaneously (Babalola and Bonassar, 2009). Individually adapting loading parameters and the scaffold material with altered mechanical properties would fundamentally change the biomechanical environment and thus the cell-material interaction. Both, the elastic and viscoelastic properties of the scaffold influence the mechanotransduction, migration, differentiation and proliferation of cells. Therefore, several studies have elaborated the impact of single (material) properties on chondrocytes or have identified factors that alter single cell responses (Lee et al., 2017) (Zahedmanesh et al., 2014). Lee et al. (2017) have shown that fast mechanical stress relaxation increases the ECM expression. On the other hand, Zahedmanesh et al. (2014) have shown that only a combination of compression and interfacial shear loading induced chondrogenesis to mesenchymal stem cells (MSCs). Also Silver et al. discussed in (Silver et al., 2004) and (Silver and Bradica, 2002) that dynamic and cyclic external forces on cartilage support collagen and aggrecan biosynthesis and reduce inflammatory responses. The reason for this effort in tissue engineering is that cartilage has a reduced healing potential because it is an avascular tissue that receives its nutrients by diffusion from the synovial fluid (Martínez-Moreno et al., 2019).

Finite element simulations are essential to fully understand the stresses and strains acting on scaffolds during stimulations. Different modelling approaches have been applied for cartilage and hydrogels using the finite element method (FEM). In case the hydrogel and the cartilage are assumed to be monophasic, hyperelastic and viscoelastic material laws can be used (Springhetti and Selyutina, 2018) (Richard et al., 2013) (Steinmann et al., 2012). To explicitely model the biphasic nature of cartilage and hydrogels, poroelastic effects can be taken into account. While hyperelasticity is capable of capturing the nonlinearity as pointed out in (Weizel et al., 2022), it cannot describe the time-dependent behavior, i.e., the hysteresis and conditioning as outlined in (Weizel et al., 2020). The time-dependent behavior of cartilage and hydrogels can also be associated with various time scales and physical phenomena. In the case of cartilage, the interaction of proteins like GAGs and collagen induce a viscoelastic material response, whereas the motion of fluid within the ECM leads to a poroelastic behavior. Considering ADA-GEL (alginate di-aldehyde), the non-fibrous polymer network leads to viscoelastic effects and fluid movement within the polymer network to poroelastic effects, both resulting in time-dependent material properties. The polymer network of ChondroFiller^{liquid} consists of fibrous and non-fibrous components and is surrounded by fluid. Here, interactions of the polymer network can also trigger viscoelastic material behavior, and again the fluid movement within the polymer network poroelastic behavior.

To be able to numerically predict the response of hydrogels during stimulation as well as the response of native cartilage by using the FEM, it is key to use appropriate material models and corresponding parameters. In this study, we inversely identify hyper-viscoelastic material parameters in COMSOL Multiphysics® v. 5.6 by incorporating the realistic experimental boundary conditions and using data from multiple loading modes simultaneously. We provide individual parameter sets for the unconditioned and conditioned responses, respectively.

2. Materials and methods

2.1. Experiment

2.1.1. Materials fabrication and composition

In this study, we determine time-dependent material parameters for human articular cartilage (n = 3), ChondroFiller^{liquid} (n = 6) and ADA-GEL (n = 8). Fig. 1 B shows the experimental setup and an exemplary sample of the materials tested in our previous mechanical experiments in (Weizel et al., 2020).

We harvested the human articular cartilage from the knee of a 62 years old body donor. Therefore, we punched discs with a diameter of d = 8 mm from the condyle of the knee. The specimen hight was approximately 2094 ± 320 µm and was defined by the natural thickness of the cartilage tissue. After extraction, we kept the fresh cartilage tissue hydrated using phosphate-buffered saline solution at 4 °C until testing.

We made ADA-GEL hydrogels by mixing 5 ml ADA (alginate di-aldehyde, 7.5% (w/v), Degree of Oxidation ~19%, synthesized by controlled oxidation using 9.375 mmol NaIO4 as described elsewhere (Distler et al., 2020)), and 5 ml gelatin (7.5% (w/v), Type A, from porcine skin, Bloom 300, Sigma Aldrich), precursor, leading to a final concentration of 3.75% (w/v) ADA-GEL by stirring for 10 min at room

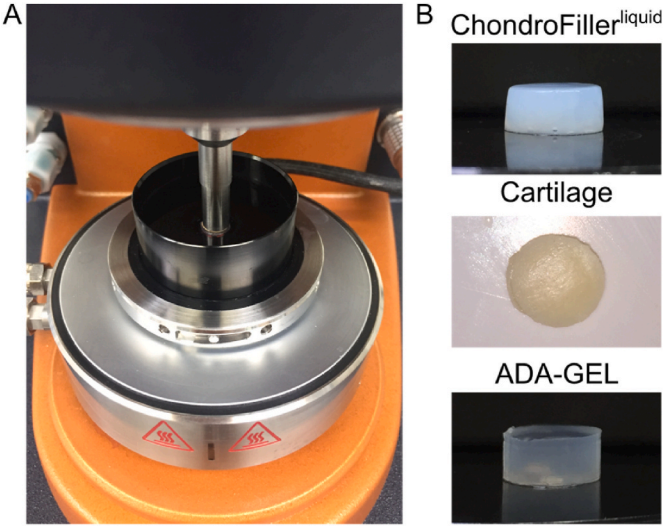

Fig. 1. A) Experimental setup with mounted specimen prior to testing B) Cylindrical specimens of ChondroFiller^{liquid}, cartilage and ADA-GEL with 8 mm diameter.

temperature (22 °C, RT). We put the precursor in a cylindrical silicon mold (diameter = 8 mm, height = 4 mm) and facilitated simultanous ionic cross-linking with 0.1 M $CaCl_2$ and enzymatic cross-linking with 2.5% (w/v) microbial transglutaminase (mTG, Ajinomoto Co.,Inc, ACTIVA® WM, 85–135 U/g, Japan) solution for 24h. For detailed ADA-GEL fabrication, refer to (Distler et al., 2020).

The collagen type I based ChondroFiller^{liquid} (supplied by Meidrix Biomedicals GmbH, Esslingen, Germany) is a dual-chamber syringe system. The collagen type I was obtained by acid extraction from rat tendons. The larger syringe chamber contains 10 mg/ml collagen type I and the smaller a neutralization gel consisting of water, HEPES buffer (Gibco HEPES, 4-(2-hydroxyethyl)-1-piperazineethanesulfonic acid, Thermofisher Scientific, Germany), NaCl and NaOH. We put the precursor in the same 8 mm diameter silicon mold as ADA-GEL for hydrogel formation. The samples were gelled at RT with a final concentration of 8 mg/ml and were stored at 4 °C for 24 h. During the gelation process, fibrillogenesis occurs in which the collagen type I monomers self-assemble into fibrillar and non-fibrillar structures (see Fig. 11).

2.1.2. Experimental setup and testing protocol

We performed all tests with the Discovery HR-3 rheometer from TA Instruments (New Castle, Delaware, USA) shown in Fig. 1 A. First, we glued all samples to the upper specimen holder and then to the lower using sandpaper and cyanoacrylate adhesive, as described in detail in (Weizel et al., 2020). The vertical movement of the upper specimen holder initiated the deformation according to the protocol in Table 1. We kept the specimens in a hydrated environment at 37 °C during the tests. For parameter identification, we developed a combined testing protocol. First, we loaded ChondroFiller^{liquid} and ADA-GEL with cyclic loading with two sets of three cycles of 10% strain and 20% strain, respectively. Afterwards, we performed stress relaxation experiments, first in compression and then in tension at 15% strain. Due to cartilage's higher stiffness, we had to reduce the maximum strains from 10%, 20% and 15%–1%, 2.5% and 5%, respectively. For the hydrogels, we chose stress relaxation holding times short enough not to include additional effects like swelling or degradation. We performed the whole testing protocol in Table 1 on the same sample to avoid inter-specimen variations. In this way, we achieve that the parameters obtained consistently represent the average material behavior under all four loading conditions simultaneously (Weizel et al., 2022).

2.2. Modelling

In a previous study (Weizel et al., 2022), we had investigated the time-independent material response and identified appropriate hyperelastic material models and parameters for cartilage, ADA-GEL and ChondroFiller^{liquid} in COMSOL Multiphysics® v. 5.6. In this study, we extend those efforts to also consider the time-dependent behavior. The model implemented in COMSOL Multiphysics® v. 5.6, which was used in the current work, is based on large strain viscoelasticity, according to G. A. Holzapfel (2010) (COMSOL).

2.2.1. Kinematics of finite viscoelasticity

We describe the deformation during the experiments with the theory of nonlinear continuum mechanics by introducing the deformation map $\boldsymbol{\varphi}$, which maps the position $\boldsymbol{X}$ from the reference or material configuration $B_0 \in \mathbb{R}^3$ in the new position $\boldsymbol{x} = \boldsymbol{\varphi}(\boldsymbol{X}, t)$ describing the deformed, current or spatial configuration B_t. As a primary measure of deformation in nonlinear continuum mechanics, we introduce the deformation gradient $\boldsymbol{F}(\boldsymbol{X}, t) = \nabla_{\boldsymbol{X}} \boldsymbol{\varphi}(\boldsymbol{X}, t)$. For a homogeneous and uniaxial incompressible deformation in compression and tension, the deformation gradient can be written as

$$\boldsymbol{F} = \begin{bmatrix} \lambda_1 & & \\ & \lambda_2 & \\ & & \lambda_3 \end{bmatrix}$$

with $\lambda_1 = \lambda$ and $\lambda_{2,3} = 1/\sqrt{\lambda}$ as the principal stretches and λ as the axial stretch.

A strain measure independent of rigid body motion is the right Cauchy-Green deformation tensor $\boldsymbol{C} = \boldsymbol{F}^{\mathrm{T}} \cdot \boldsymbol{F}$, and its invariants I_1 and I_2 are

$$I_1(\boldsymbol{C}) = trace\,(\boldsymbol{C}) = \lambda_1^2 + \lambda_2^2 + \lambda_3^2 \tag{1}$$

$$I_2(\boldsymbol{C}) = \frac{1}{2}\left[trace(\boldsymbol{C})^2 - trace\left(\boldsymbol{C}^2\right)\right] = \lambda_1^2\lambda_2^2 + \lambda_2^2\lambda_3^2 + \lambda_3^2\lambda_1^2. \tag{2}$$

To account for finite viscoelasticity, the deformation gradient $\boldsymbol{F}$ is multiplicatively decomposed into an elastic $\boldsymbol{F_e}$ and a viscous $\boldsymbol{F_v}$ part

$$\boldsymbol{F} = \boldsymbol{F}_e\,\boldsymbol{F}_v \tag{3}$$

The elastic right Cauchy-Green deformation tensor is defined as

$$\boldsymbol{C}_e = \boldsymbol{F}_e^T\boldsymbol{F}_e \tag{4}$$

and the viscous right Cauchy-Green deformation tensor as

$$\boldsymbol{C}_v = \boldsymbol{F}_v^T\boldsymbol{F}_v \tag{5}$$

2.2.2. Constitutive equations for hyper-viscoelastic material models

The large strain viscoelastic model implemented in COMSOL Multiphysics, is based on dividing the free energy into an isochoric Ψ_{iso}^{∞}, a volumetric Ψ_{vol}^{∞} and a viscoelastic $\sum_{m=1}^{N}\Psi_m$ (with m = number of viscoelastic branches) contribution (see Fig. 2),

$$\Psi_s = \Psi_{iso}^{\infty} + \Psi_{vol}^{\infty} + \sum_{m=1}^{N}\Psi_m \tag{6}$$

In the case of incompressibility, the volumetric free energy Ψ_{vol}^{∞} can be omitted, and the total free energy yields

$$\Psi_s = \Psi_{iso}^{\infty} + \sum_{m=1}^{N}\Psi_m \tag{7}$$

The second Piola-Kirchhoff stress is then defined as

Table 1
Combined testing protocol for hyper-viscoelastic parameter identification (Weizel et al., 2020).

1	3 cycles compression and tension	ADA-GEL and ChondroFiller^{liquid}: nominal strain ε_{nom} = 10% cartilage: nominal strain ε_{nom} = 1%
2	3 cycles compression and tension	ADA-GEL and ChondroFiller^{liquid}: nominal strain ε_{nom} = 20% cartilage: nominal strain ε_{nom} = 2.5%
3	stress relaxation in compression	ADA-GEL and ChondroFiller^{liquid}: nominal strain ε_{nom} = 15%, t_{hold} = 150s cartilage: nominal strain ε_{nom} = 5%, t_{hold} = 1000s
4	stress relaxation in tension	ADA-GEL and ChondroFiller^{liquid}: nominal strain ε_{nom} = 15%, t_{hold} = 150s

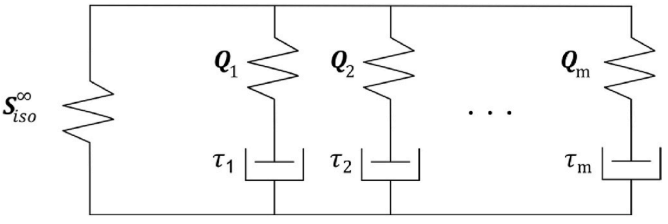

Fig. 2. Schematic rheological model with spring and dashpot elements of large strain (hyper-)viscoelastic model in COMSOL Multiphysics® v. 5.6 with S_{iso}^{∞} as the main hyperelastic branch and Q_m as the viscoelatic sidebranches.

$$\boldsymbol{S} = 2\frac{\partial \Psi_s}{\partial \mathbf{C}} = \boldsymbol{S}_{iso}^{\infty} + \sum_{m=1}^{N} \boldsymbol{Q}_m \tag{8}$$

where the non-equilibrium or viscoelastic second Piola-Kirchhoff stress is

$$\boldsymbol{Q}_m = 2\frac{\partial \Psi_m}{\partial \mathbf{C}} \tag{9}$$

The linear time evolution of the non-equilibrium stress tensors $\boldsymbol{Q}_m$ in each viscoelastic branch is given by

$$\dot{\boldsymbol{Q}}_m + \frac{\boldsymbol{Q}_m}{\tau_m} = \dot{\boldsymbol{S}}_{iso,m} = \beta_m \dot{\boldsymbol{S}}_{iso}^{\infty} \tag{10}$$

The solutions of this evolution equation (10) for a semi-open time interval $t \in (0, T]$ can be derived by

$$\boldsymbol{Q}_m = e^{-T/\tau_m}\, \boldsymbol{Q}_{m,0} + \int_{0^+}^{T} e^{[-(T-t)/\tau_m]}\, \dot{\boldsymbol{S}}_{iso,m}(t)dt \tag{11}$$

where $\boldsymbol{S}_{iso,m}$ is the isochoric second Piola-Kirchhoff stress tensor in the viscoelastic branch m and can be derived from the free energy of the main hyperelastic branch Ψ_{iso}^{∞} and the energy factor β_m

$$\boldsymbol{S}_{iso,m} = 2\frac{\partial \Psi_{iso,m}}{\partial \mathbf{C}} = 2\beta_m \frac{\partial \Psi_{iso}^{\infty}}{\partial \mathbf{C}} = \beta_m \boldsymbol{S}_{iso}^{\infty} \tag{12}$$

A direct relation to a Prony series is thereby given by

$$\beta_m = w_m \frac{G_0}{G_\infty} = \frac{G_m}{G_\infty} \tag{13}$$

where w_m are the weights describing the ratio between long term G_∞ and instantaneous stiffness G_0 in the generalized Maxwell model illustrated in Fig. 2, with the relation

$$\Gamma(t) = G_0 w_\infty + G_0 \sum_{m=1}^{N} w_m \exp\left(-\frac{t}{\tau_m}\right). \tag{14}$$

The weights are restricted by the expression

$$w_\infty + \sum_{m=1}^{N} w_m = 1\,. \tag{15}$$

The first term Ψ_{iso}^{∞} in Equation (7) characterizes the isochoric hyperelastic response in the equilibrium state of the solid. For the hyperelastic contributions, we chose the models which best represent the time-independent material response of the corresponding material according to our previous study in (Weizel et al., 2022).

For ADA-GEL, we use the Mooney-Rivlin 5 term model, which is expressed in terms of the first and second invariants $I_1(\boldsymbol{C})$ and $I_2(\boldsymbol{C})$ with the strain energy function

$$\begin{aligned}\Psi_{MR} = {} & C_{10}\,(I_1 - 3) + C_{01}\,(I_2 - 3) + C_{20}\,(I_1 - 3)^2 \\ & + C_{02}\,(I_2 - 3)^2 + C_{11}\,(I_1 - 3)(I_2 - 3)\end{aligned} \tag{16}$$

and the equilibrium shear modulus

$$\begin{aligned}\mu_{\infty,MR} = {} & 2(C_{10} + C_{01}) + 2C_{11}(I_1 - 3) + 2C_{11}(I_2 - 3) + 4C_{02}(I_2 - 3) \\ & + 4C_{20}(I_1 - 3)\end{aligned} \tag{17}$$

where, C_{10}, C_{01}, C_{11}, C_{02} and C_{20} denote the material constants.

For cartilage and ChondroFiller^{liquid}, we consider the Ogden 2 term model according to (Weizel et al., 2022) with the general strain energy

$$\Psi_{iso,Ogden}^{\infty} = \sum_{p=1}^{N} \frac{\mu_p}{\alpha_p} \left(\lambda_1^{\alpha_p} + \lambda_2^{\alpha_p} + \lambda_3^{\alpha_p} - 3\right) \tag{18}$$

where μ_p are the shear moduli and α_p are the nonlinearity parameters. The equilibrium modulus

$$\mu = \frac{1}{2} \sum_{p=1}^{N} \mu_p\, \alpha_p \tag{19}$$

results in

$$\mu_{\infty,Ogden2t} = \frac{1}{2}(\mu_1\, \alpha_1 + \mu_2\, \alpha_2) \tag{20}$$

2.3. Inverse parameter identification of hyper-viscoelastic parameters

For the parameter identification, we simultaneously use data from unconfined compression, tension, compression relaxation, and tension relaxation experiments (Weizel et al., 2020) to capture the complex time-dependent behavior of human cartilage, ADA-GEL and ChondroFiller^{liquid}. In addition, we use the entire loading history, including all cycles as well as both loading and unloading. We identify two different parameter sets that describe the conditioned and unconditioned material behavior by considering the first and the third loading cycle during the fitting procedure, respectively.

Fig. 3 summarizes the scheme of the inverse parameter identification. Our two dimensional and axisymmetric finite element model in COMSOL Multiphysics® v. 5.6 consists of a triangular mesh. We subject the numerical sample to exactly the same loading sequence (time-strain: *t-ε)* as performed during the experiments by using the experimental displacement and boundary conditions in the simulation (see (Weizel et al., 2022) and (Weizel et al., 2020)). At the upper boundary, we extract the reaction force F_{sim} and pass it to the least square solver lsqnonlin in Matlab to minimize the objective function $F(x)$,

$$\min_x \|F(x)\|_2^2 = \sum_i F^2(x) = \sum_i \left(F_{exp} - F_{sim}\right)_i^2 \tag{21}$$

to determine the material parameters x_{opt}.

To assess the goodness of the fit, we evaluate the coefficient of determination,

$$R^2 = 1 - \frac{SSR}{SST} \tag{22}$$

where SST is the Sum of Squares Total defined as

$$SST = \sum_{i=!}^{n} \left(F_{exp,i} - \overline{F}_{exp,i}\right)^2 \tag{23}$$

with the experimentally measured reaction forces and their mean values

$$\overline{F}_{exp,i} = 1/n \sum_{i=!}^{n} F_{exp,i} \tag{24}$$

$$SSR = \sum_{i=!}^{n} \left(F_{exp,i} - F_{sim,i}\right)^2 \tag{25}$$

is the Sum of the Squares of the Residual with the simulated reaction forces $F_{sim,i}$. The values of the coefficient of determination range between 0 and 1: $0 \leq R^2 \leq 1$, where a value of 1 represents perfect agreement.

3. Results

3.1. Performance of hyper-viscoelastic material model for various loading conditions

Fig. 4 shows the qualitative performance of a hyper-viscoelastic material model based on the Mooney-Rivlin 5 term model and two viscoelastic elements when compared to exemplary experimental data for different loading modes (Weizel et al., 2022). The hyper-viscoelastic model in COMSOL Multiphysics® v. 5.6 well captures the conditioning in both compression and tension (Fig. 4, left). Also the qualitative stress relaxation response in compression and tension of experiment and simulation agree well (Fig. 4, right). However, while the experiments

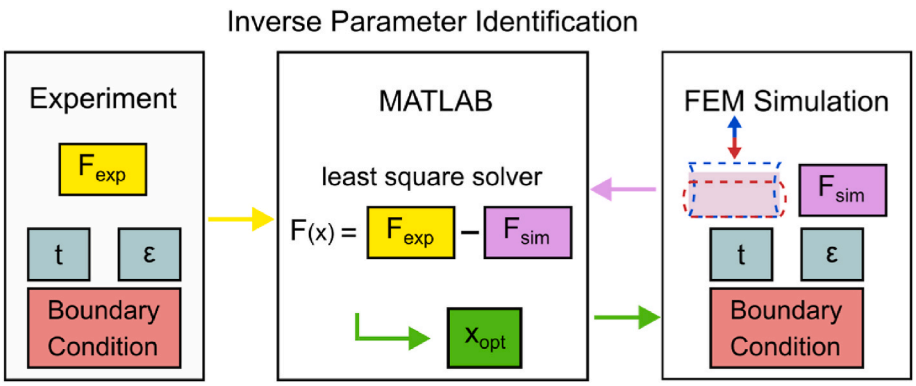

Fig. 3. Scheme of the inverse parameter identification.

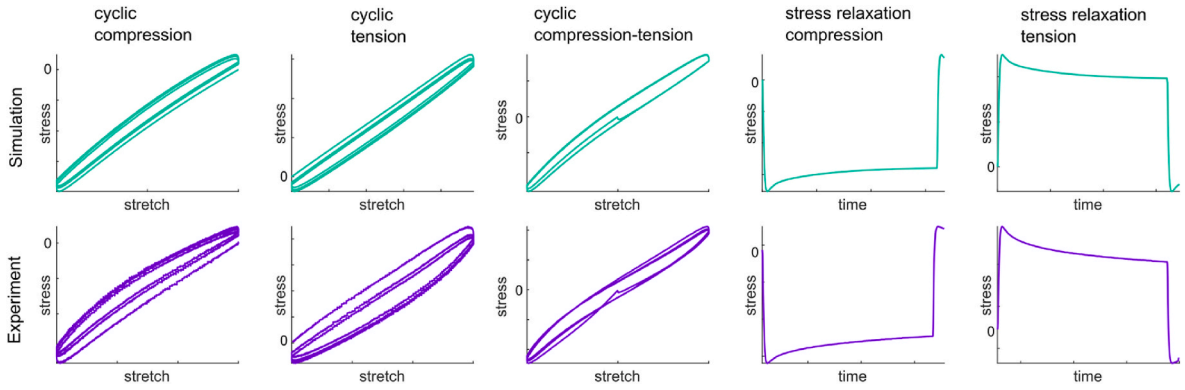

Fig. 4. Exemplary simulated and experimentally measured response during cyclic compression, cyclic tension, cyclic compression-tension, stress relaxation in compression and stress relaxation in tension for the example of ADA-GEL and a hyper-viscoelastic material model based on the Mooney-Rivlin 5 term model for the hyperelasticity and two viscoelastic elements.

show a decrease in the stress after the first cycle in cyclic compression-tension loading, the simulation shows the opposite behavior, especially in compression, where the stress increases (Fig. 4, center).

Fig. 5 summarizes the qualitative hysteresis areas for cyclic loading in tension, compression and compression-tension. For the individual experiments in compression and tension, the qualitative course of the hysteresis areas of the experiment and the simulation agree. However, the first cycle of cyclic compression-tension loading in the simulation (red circle) shows the smallest hysteresis area in contrast to the observations during the experiments, where the hysteresis is largest for the first cycle.

3.2. Time-dependent material behavior of ADA-GEL

Fig. 6 illustrates the results of the inverse parameter identification for ADA-GEL and the unconditioned and conditioned material responses, respectively. The hyper-viscoelastic model combining the Mooney-Rivlin 5 term model with two viscoelastic elements is capable of capturing the pronounced nonlinearity in tension and compression at larger strains of up to 20%. Still, the model slightly underestimates the stresses at the smaller strain level of up to 10% for both the unconditioned and conditioned material responses. Two viscoelastic elements in the model are sufficient to capture time-dependent effects represented by the stress relaxation behavior and the hysteretic cyclic compression-tension response.

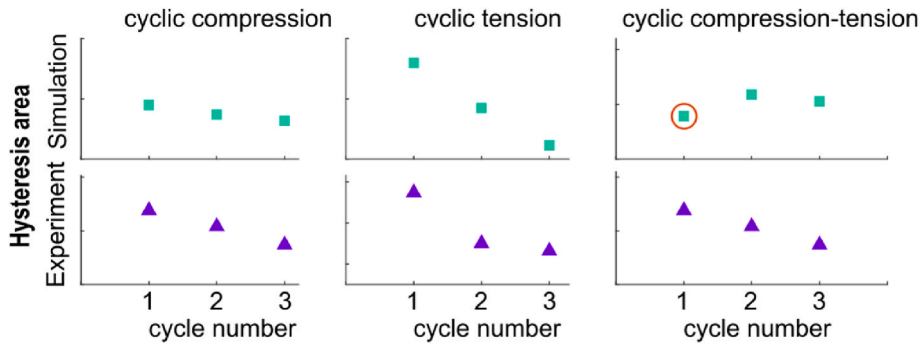

Fig. 5. Qualitative hysteresis areas for simulated and experimentally obtained data during cyclic compression, cyclic tension and cyclic compression-tension loading for example of ADA-GEL and a hyper-viscoelastic material model based on the Mooney-Rivlin 5 term model for the hyperelasticity and two viscoelastic elements. The red cycle denotes the first cycle of cyclic compression-tension loading in the simulation with the smallest hysteresis area in contrast to the experiments.

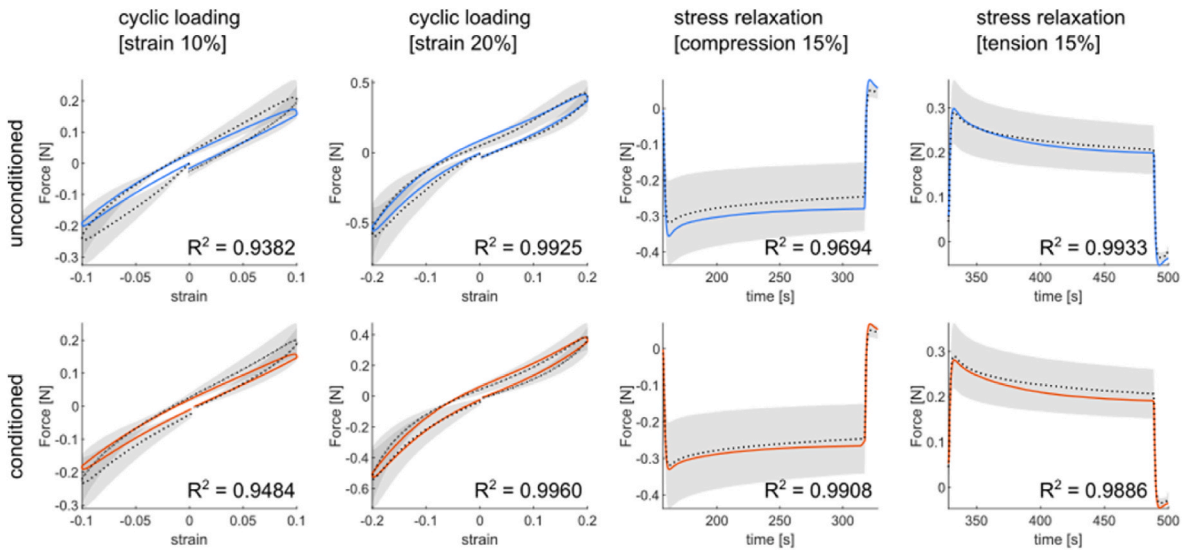

Fig. 6. Performance of hyper-viscoelastic model based on the Mooney-Rivlin 5 term hyperelastic model with two viscoelastic elements to capture the averaged experimental data of ADA-GEL (black dashed line shown with standard deviations in shaded grey) for the unconditioned (blue line, top) and conditioned (red line, bottom) material responses with coefficients of determination R^2.

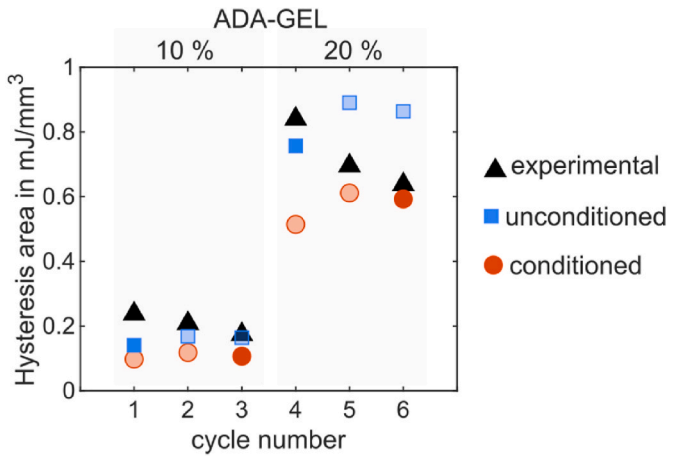

Fig. 7. Hysteresis area corresponding to experimental data (black) and simulated unconditioned (blue) and conditioned (red) material response of ADA-GEL for each cycle at two strain levels (10% and 20%).

Fig. 7 compares the hysteresis area for each loading cycle based on the simulations using the unconditioned (blue) and conditioned (red) parameter sets with the experimental (black) data. In both experiment and simulation, hysteresis areas increase for a higher strain level. The hysteresis areas predicted when using the unconditioned parameter set are higher than for the conditioned parameter set. According to the observations in Section 3.1, the model predicts that the hysteresis area increases from the first to the second cycle before it starts to decrease again, while the experiments show a steady decrease in the hysteresis area with increasing number of cycles at the same strain level. Expectedly, the hysteresis areas of simulation and experiment agree best for the data used for parameter identification (first and fourth cycle for the unconditioned parameters; third and sixth cycle for the conditioned parameters).

Table 2 summarizes the hyper-viscoelastic parameters, the equilibrium shear modulus and the coefficients of determination for the unconditioned and conditioned material responses, respectively. Considering the equilibrium response, represented by the hyperelastic parameters and the shear modulus μ_∞, the unconditioned response yielded a higher shear modulus compared to the conditioned response. The time constants τ_1 and τ_2 for the unconditioned and conditioned material responses are similar but have different contributions to the overall response, represented by β_1 and β_2. After conditioning, β_1 and thus the viscoelastic stress fraction associated with the first time constant decreases. In contrast, β_2 increases after conditioning, so that the contribution of the higher, second time constant to the overall response increases.

3.3. Time-dependent material behavior of cartilage

Fig. 8 illustrates the results of the inverse parameter identification for cartilage and the unconditioned and conditioned material responses, respectively. The hyper-viscoelastic model combining the Ogden 2 term model with two viscoelastic elements is capable of capturing the pronounced nonlinearity of the loading curve at the highest strain level of 5% nominal strain and the complete stress relaxation in compression. Nevertheless, the model slightly underestimates the tensile stresses at the smaller strain level of up to 1% and slightly overestimates the tensile stresses at the medium strain level of up to 2.5% for both the unconditioned and conditioned material responses.

Fig. 9 compares the hysteresis areas for each loading cycle based on the simulations using the unconditioned (blue) and conditioned (red) parameter sets with the experimental (black) data.

Table 2
Hyper-viscoelastic parameters and equilibrium shear modulus μ_∞ for the conditioned and unconditioned material response of ADA-GEL with corresponding coefficients of determination R^2.

ADA-GEL	hyperelastic parameters						viscoelastic parameters				
	c_{10} in kPa	c_{01} in kPa	c_{11} in kPa	c_{02} in kPa	c_{20} in kPa	μ_∞ in kPa	β_1	τ_1 in s	β_2	τ_2 in s	R^2
unconditioned	2.1264	0.5153	−1.6718	−1.2485	5.6873	5.2834	0.1977	4.7482	0.2097	51.6052	0.9886
conditioned	2.1226	0.3942	−1.6573	−1.1933	5.5141	5.0335	0.1318	4.6654	0.2186	51.2747	0.9861

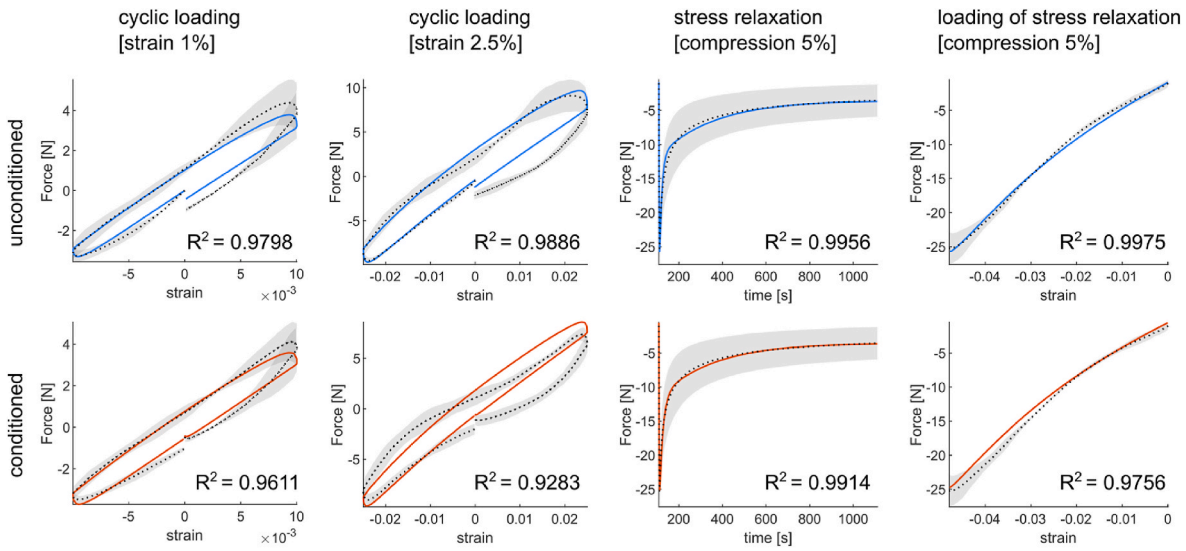

Fig. 8. Performance of hyper-viscoelastic model based on the Ogden 2 term hyperelastic model with two viscoelastic elements to capture the averaged experimental data of cartilage (black dashed line shown with standard deviations in shaded grey) for the unconditioned (blue line, top) and conditioned (red line, bottom) material responses with coefficients of determination R^2.

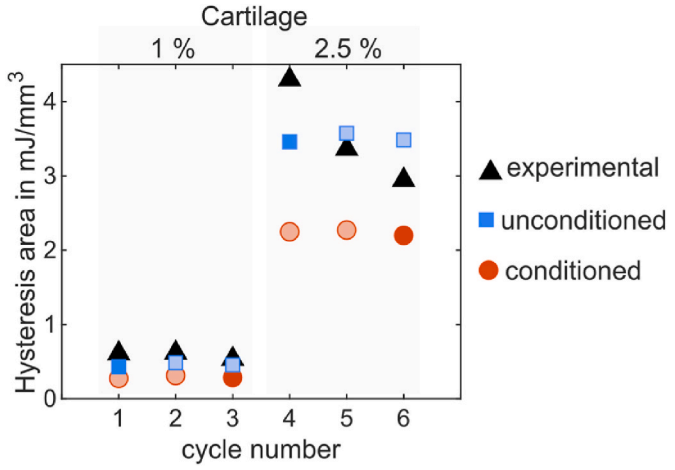

Fig. 9. Hysteresis area corresponding to experimental data (black) and simulated unconditioned (blue) and conditioned (red) material response of cartilage for each cycle at two strain levels (1% and 2.5%).

As for ADA-GEL, in both experiment and simulation, hysteresis areas increase for a higher strain level. The hysteresis areas predicted when using the unconditioned parameter set are higher than for the conditioned parameter set. According to the observations in Section 3.1, the model predicts that the hysteresis area increases from the first to the second cycle before it starts to decrease again, while the experiments show a steady decrease in the hysteresis area with increasing number of cycles at the same strain level. The hysteresis areas of the unconditioned (corresponding to the first and fourth cycles) material response of the simulation agree best with the hysteresis areas of the experiment in all cycles. The hysteresis areas of the conditioned material response in the simulation represent the experimental less accurately.

Table 3 presents the hyper-viscoelastic parameters, the equilibrium shear modulus and the coefficients of determination for the unconditioned and conditioned material responses, respectively. Unlike in our former publication (Weizel et al., 2020), we chose the Ogden 2 term model instead of the Ogden 1 term model for the unconditioned response of cartilage because the Ogden 1 term model performed very poorly for the nonlinear loading curve in the stress relaxation data (see Fig. 8).

Considering the equilibrium response, represented by the hyperelastic parameters and the shear modulus μ_∞, the unconditioned response yielded a higher shear modulus compared to the conditioned response. The time constant τ_1 for the unconditioned response is smaller than for the conditioned response. The contribution of the first time constant τ_1 to the viscoelastic non-equilibrium response, represented by β_1 decreases for the conditioned response, while β_2 and the corresponding time constant τ_2 remain nearly the same.

3.4. Time dependent material behavior of ChondroFiller^{liquid}

A simultaneous fit of all four loading modes, as performed for ADA-GEL and cartilage, shows that the hyper-viscoelastic model cannot well represent the material response of ChondroFiller^{liquid} (see Fig. S 1). Our previous study suggests that after a total deformation of 15% nominal strain, ChondroFiller^{liquid} exhibits an irreversibly altered material response (Weizel et al., 2020). Based on these findings, we iteratively determine the reversible loading limit for ChondroFiller^{liquid} shown in Fig. S 2, which is approximately 15%. Consequently, we limited our parameter fits to smaller strains of 10% and had to omit cyclic and stress relaxation experiments of up to 20% nominal strain.

Fig. 10 illustrates the results of the inverse parameter identification

Table 3
Hyper-viscoelastic parameters and equilibrium shear modulus μ_∞ for the conditioned and unconditioned material response of cartilage with corresponding coefficients of determination R^2.

cartilage	hyperelastic parameters					viscoelastic parameters				
	μ_1 in kPa	α_1 in kPa	μ_2 in kPa	α_2 in kPa	μ_∞ in kPa	β_1	τ_1 in s	β_2	τ_2 in s	R^2
unconditioned	15.2937	2.9410	−9.3880	−15.6655	96.0226	5.2909	10.5890	2.3071	250.4918	0.9824
conditioned	14.7483	2.4451	−9.9874	−15.3257	94.5621	4.8260	15.6480	2.2891	249.6252	0.9824

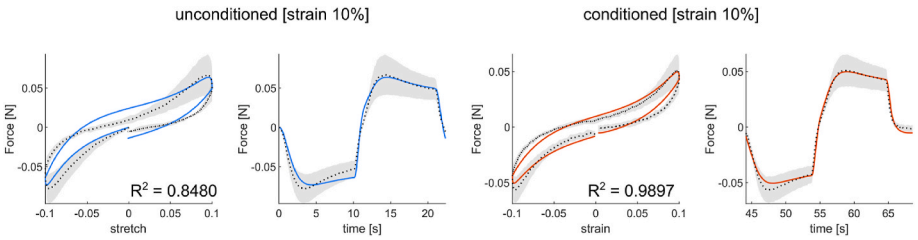

Fig. 10. Performance of hyper-viscoelastic model based on the Mooney-Rivlin 5 term hyperelastic model with two viscoelastic elements to capture the averaged experimental data of ChondroFiller^{liquid} (black dashed line shown with standard deviations in shaded grey) for the unconditioned (blue line) and conditioned (red line) material responses with coefficients of determination R^2.

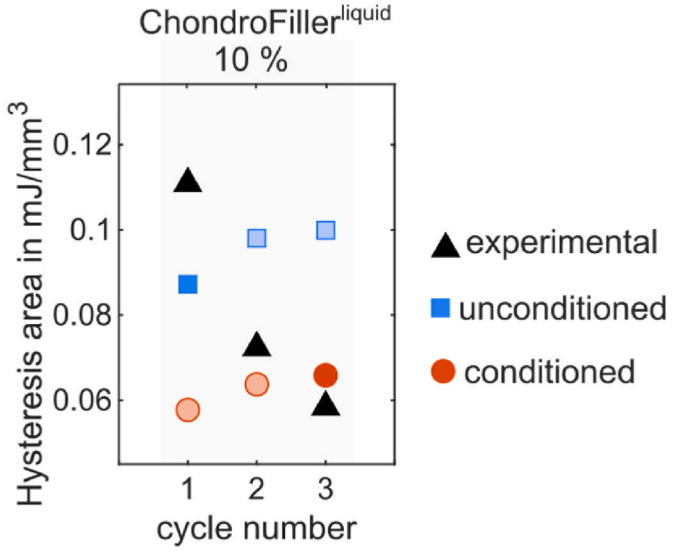

Fig. 11. Hysteresis area corresponding to experimental data (black) and simulated unconditioned (blue) and conditioned (red) material response of ChondroFiller^{liquid} for each cycle at 10%.

for ChondroFiller^{liquid} and the unconditioned and conditioned material responses, respectively. The hyper-viscoelastic model combining the Ogden 2 term model with two viscoelastic elements is capable of capturing the pronounced nonlinearity in tension and compression, and the overall stresses are in the range of the experimental standard deviations.

Fig. 11 compares the hysteresis area for each loading cycle based on the simulations using the unconditioned (blue) and conditioned (red) parameter sets with the experimental (black) data. In the experiment, the hystereses decrease with introducing a new cycle, and in contrast, the hystereses increase in the simulation with subsequent cycles. The hystereses obtained using the unconditioned parameters are higher than for the conditioned parameters. Nevertheless, hystereses of the conditioned (corresponding with the third cycle) material response from the experiment and the simulation show the best agreement.

Table 4 summarizes the hyper-viscoelastic parameters, the equilibrium shear modulus, and the coefficients of determination for the unconditioned and conditioned material responses, respectively. Considering the equilibrium response, represented by the hyperelastic parameters and the shear modulus μ_∞, the unconditioned response yielded a higher shear modulus compared to the conditioned response. The time constant τ_2 for the unconditioned and conditioned material responses are similar, where τ_1 in the unconditioned parameter set is lower than for the conditioned parameter set. The contribution of both time constants τ_1 and τ_2 and the viscoelastic stress fractions, represented by β_1 and β_2, decreases for the conditioned material response compared to the unconditioned material response.

4. Discussion

In this study, we have identified hyper-viscoelastic material model parameters for cartilage, ADA-GEL and ChondroFiller^{liquid}, to describe the conditioned and unconditioned material responses Furthermore, we have assessed the capability of hyper-viscoelastic material models in COMSOL Multiphysics v. 5.6 to qualitatively capture various loading conditions (see Chapter 3.1). In the following, we discuss the performance of the calibrated models, the model parameters, and the origin of viscoelasticity for all three materials.

4.1. Hyper-viscoelastic model performance and constitutive parameters

The calibrated hyper-viscoelastic models capture the unconditioned and conditioned material behavior under cyclic compression-tension loading and stress relaxation in compression and tension at three different strain levels. We used all loading modes simultaneously for parameter identification as well as both loading and unloading curves. For the hydrogels, we introduced three strain levels of 10, 15 and 20% nominal strain, for cartilage 1, 2.5 and 5% nominal strain. From a physiological point of view, sustained loading, resulting from standing or sitting, or repetitive loading, resulting from walking, leads to a reduction of cartilage height and to strains ranging from 2 to 6%. This lies within the tested strain range so that the identified parameters should well capture the corresponding material response (Liu et al., 2017). Depending on the application, we propose to use either the unconditioned or conditioned hyper-viscoelastic parameter set. The parameters based on the unconditioned response are suitable for initial, dynamic or in vitro loading scenarios, while those based on the conditioned response rather represent the material behavior for repetitive loading scenarios that occur during sustained walking, standing, sitting, or in vitro long term mechanical stimulations in devices, such as the one presented by Meinert et al. in (Meinert et al., 2017).

Table 4
Hyper-viscoelastic parameters and equilibrium shear modulus μ_∞ for the conditioned and unconditioned material response of ChondroFiller^{liquid} with corresponding coefficients of determination R^2 .

ChondroFiller^{liquid}	hyperelastic parameters					viscoelastic parameters				
	μ_1 in kPa	α_1 in kPa	μ_2 in kPa	α_2 in kPa	μ_∞ in kPa	β_1	τ_1 in s	β_2	τ_2 in s	R^2
unconditioned	0.0187	22.4476	−0.0247	−18.4281	0.4375	0.9890	3.8227	1.2514	100.5009	0.8480
conditioned	0.0197	22.5983	−0.0200	−16.2780	0.3854	0.6916	6.1978	0.9274	101.1096	0.9107

The equilibrium response of all materials of interest is characterized by an asymmetric behavior in tension and compression, and a pronounced nonlinearity. Based on our previous publication (Weizel et al., 2022), we chose appropriate hyperelastic models best capturing these features for the individual materials. For both, ChondroFiller^{liquid} and cartilage, we chose the Ogden 2 term model. We note that while the Ogden 1 term model performed best for the unconditioned response of cartilage in (Richard et al., 2013), the model is not capable of capturing the high nonlinearity in the loading curve during stress relaxation experiments. For ADA-GEL, we chose the Mooney-Rivlin 5 term model, which represents the hyperelastic material behavior the best according to (Weizel et al., 2022). To capture viscoelastic effects, namely hysteresis, conditioning, and stress relaxation, additional material parameters, the loss factors β_i, are introduced to quantify the viscoelastic stress fractions for the non-equilibrium responses with corresponding time constants τ_i. Our study shows that $i = 2$ viscoelastic elements are necessary to well capture the viscoelastic responses for all three materials.

When comparing the unconditioned and conditioned material parameter sets, we observe similar trends for all three materials. The equilibrium shear modulus μ_∞ and the first viscoelastic loss factor β_1 decreases for the conditioned material response compared to the unconditioned material response. The short time constant τ_1 remains approximately constant for ADA-GEL and increases only slightly for ChondroFiller^{liquid} and cartilage. The second loss factor β_2 increases for ADA-GEL and decreases only marginally for cartilage, while the corresponding longer time constant τ_2 remains approximately constant for all materials. This shows that neglecting the first unconditioned loading cycle reduces the equilibrium shear modulus and the contribution of the first, short-term viscoelastic element to the overall stress. We note that in the case of ChondroFiller^{liquid}, we only used a limited set of data; thus, the calibration of the second time constant and loss factor is less reliable.

Compared to our previous publication focusing merely on the hyperelastic response (neglecting porous and viscous effects) of the three materials (see Table 5), we obtained similar shear moduli for ADA-GEL and ChondroFiller^{liquid}. The equilibrium shear moduli for cartilage, however, lie in the range of 95 kPa and thus differs significantly from the previously determined shear modulus of 454.0671 kPa (Steinmann et al., 2012). Cartilage relaxes the slowest when comparing all materials and does not reach equilibrium after the three cycles of preconditioning, contrary to ADA-GEL and ChondroFiller^{liquid}. This is represented by the differences in the shear moduli of cartilage obtained here and in (Weizel et al., 2022). Physiologically, viscoelastic effects, i.e., higher stiffness at higher strain rates, is functionally important: it protects cartilage during impact loading (Silver et al., 2004).

4.2. Differences in the viscoelasticity of the different materials

The viscoelasticity represented by β varies between the three materials. Cartilage exhibited the highest amount of viscous dissipation or stress relaxation, followed by ChondroFiller^{liquid} and then ADA-GEL. Elastic energy dominates in ChondroFiller^{liquid} and especially in ADA-GEL. In cartilage, the viscous energy dominates the response during compression and tension. Considering the short-term response, ADA-GEL and ChondroFiller^{liquid} relax similarly fast, while the corresponding stress relaxation time constant for cartilage is two to three times higher. Also, cartilage has the highest τ_2 and needs more time to reach equilibrium than the other two materials. The importance of a distinct consideration of how much and how fast the material relaxes in three dimensional hydrogel cell cultures is emphasized in (Hazur et al., 2021) and (Lee et al., 2017): Hazur et al. (2021) showed an enhanced proliferation, migration and elongation of cells due to a higher amount of stress relaxation of ADA-GEL hydrogels; Lee et al. (2017) decreased stress relaxation times of ionically cross-linked alginate by adding polyethylene glycol (PEG) spacers and showed a positive correlation with chondrocyte matrix formation and chondrogenic phenotype (Lee et al., 2017).

Table 5
Overview of shear moduli $\mu_{hyperelastic}$ (marked with *) determined in Weizel et al. (2022) only based on hyperelastic data for the conditioned material responses and equilibrium shear moduli μ_∞ determined in this study for ADA-GEL, cartilage and ChondroFiller^{liquid}.

	conditioned	unconditioned	conditioned
	$\mu_{hyperelastic}$* in kPa	μ_∞ in kPa	μ_∞ in kPa
ADA-GEL	5.8442*	5.2834	5.0335
ChondroFiller^{liquid}	0.3712*	0.4375	0.3854
Cartilage	454.0671*	96.0226	94.5621

4.3. Structural origin of viscoelasticity

The differences in the viscoelasticity of the three materials analyzed in this study can be attributed to differences in their structure and composition. The type of chemical bonding, for instance, can dictate the mechanical behavior of the hydrogels (Charbonier et al., 2021) (Zhang and Khademhosseini, 2017) (Vedadghavami et al., 2017). Covalently crosslinked hydrogels can show mainly elastic material behavior, while hydrogels with hydrophobic interactions show preferably visco-(poro) elastic or even viscoplastic material behavior (Caccavo et al., 2018). Viscoelasticity results, on the one hand, from volume-preserving structural shape changes and "small" movement of water molecules (Caccavo et al., 2018). In addition, poroelastic effects occur that can be attributed to "long-distance" motion of water not preserving the hydrogel volume (Caccavo et al., 2018) as the water is free to leave the hydrogel network upon deformation. As a result, it is crucial to consider the mechanisms of mechanical deformation and the chemical crosslinkings that underly the different materials when interpreting the observed mechanical responses and the corresponding material parameters identified in this study.

Under physiological conditions, human articular **cartilage** experiences multiple loading modes simultanously. During locomotion, the sliding of the joints induces frictional shear forces, which lead to tensile forces in the cartilage tissue (Silver and Bradica, 2002). At the same time, weight-bearing results in compressive forces (Silver and Bradica, 2002). Cartilage can withstand these compressive forces due to the swelling pressure caused by the high negative charge of sulfated GAG (glycosaminoglycan) chains (Silver and Bradica, 2002). The elastic behavior of cartilage is associated with energy storage through the stretching of collagene molecules in the cross-linked fibrils (Silver et al., 2002a). Its physiological function is to store and redirect energy to the adjacent bone during locomotion (Silver and Bradica, 2002), whereas viscous effects have a damping function and are associated with the energy dissipation caused by slippage of adjacent collagen fibrils (Silver et al., 2002a).

As illustrated in Fig. 12, the **ADA-GEL** hydrogel system used in this study is composed of ionic (Ca2+) cross-linking, covalent (enzymatic, ε(γ -glutamyl)lysine) isopeptide bonding (enabled by microbial transglutaminase) and reversible-covalent (Schiff's base) cross-linking (Distler et al., 2020). As Zhao et al. (Holzapfel, 2010) illustrated, covalent cross-linking in alginate hydrogels leads to characteristic poroelastic effects, characterized by the escape of fluid upon deformation. The weight changes due to the fluid release, and the corresponding stress relaxation time depends on the diameter of the sample (Holzapfel, 2010). In ionically cross-linked alginate gels, the relaxation is caused by two superimposed viscoelastic and poroelastic processes depending on the characteristic length, which is also a characteristic of poroelasticity (Distler et al., 2020). This indicates that the mechanisms underlying time-dependent material behavior and stress relaxation in our multi-crosslinked hydrogels are a superposition of viscoelastic and poroelastic effects. We suppose that viscoplastic effects are negligible since covalent cross-linking promotes elastic effects and impairs the

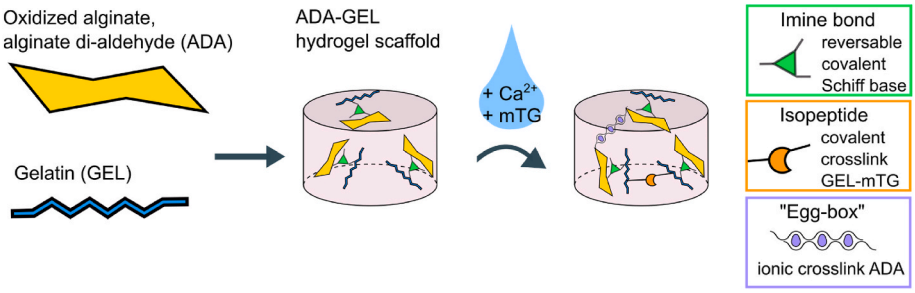

Fig. 12. Simplified schematic illustration of crosslinking mechanisms in ionically and enzymatically crosslinked ADA-GEL hydrogels, adapted from (Distler et al., 2020). Mixing gelatin (GEL) and oxidized alginate (ADA) results in the formation of a hydrogel due to the formation of reversible covalent imine bonds via Schiff base formation. By adding a cross-linking solution containing Ca^{2+} and mTG, ionic crosslinking is formed by divalent cations between guluronic acid blocks of the ADA chain (Mørch et al., 2006), while covalent isopeptide bonds are formed between glutamin and lysin groups of gelatin by the mTG enzymatic crosslinking (Distler et al., 2020).

viscoplastic effects in the herein used ADA-GEL (Holzapfel, 2010) (Caccavo et al., 2018).

ChondroFiller^{liquid} is composed of collagen type I, which in turn consists of collagen fibers. These collagen fibers can form randomly aligned or orientated structures (Sarrigiannidis et al., 2021). The aggregation to fibrillar hydrogels depends on many factors such as gelation temperature, pH, extraction mechanism (acid extraction or pepsin extraction) and collagen concentration (Sarrigiannidis et al., 2021) (Antoine et al., 2014) (Fratzl). As described in (Weizel et al., 2020), a mixture of fibrillar and non-fibrillar phases form ChondroFiller^{liquid}, which may result from the two-syringe mixing mechanism during hydrogel casting and crosslinking (Weizel et al., 2020). As shown in Fig. 13, collagen type I has a hierarchical structure. To form a triple helix molecular structure, glycine, proline and hydroxyproline are translated to form peptide chains which ultimately form a triple helix (Castro et al., 2018) (Salvatore et al., 2021). Triple helix molecules form fibrils that assemble during fibrillogenesis into fibrous macrostructures. Water surrounds and stabilizes the triple helix through hydrogen bonds and moves freely between the inter-fibrillar spaces (Salvatore et al., 2021). Hydrogen bonds are weak in comparison to primary covalent bonds and are assumed to dominate the mechanical deformation mode of collagen type I hydrogels (Fratzl). In this study, in the case of ChondroFiller^{liquid}, we observe a complex, superimposed elastic, viscoelastic, and either viscoplastic or damage behavior, with potential additional poroelatic effects (Nam et al., 2016). Silver et al. suggested that in self-assembling collagen type I hydrogels, the elasticity is more likely caused by direct deformation of the triple helix, and the viscosity occurs due to the sliding of adjacent fibrils and fibril bundles (Silver et al., 2002b) (Fratzl). When exceeding a deformation ~10% nominal strain, our experimental results suggest that ChondroFiller^{liquid} shows a viscoplastic or damage behavior. Hydrogels that feature "weak" bonds in comparison to covalent bonds (such as hydrogen bonds in collagen, or ionic crosslinking bonds in ADA-GEL), show a more viscoelasticity or even viscoplastic response (Nam et al., 2016) (Chaudhuri et al., 2020). However, covalent cross-linking seems to result in a more elastic hydrogel behavior (Holzapfel, 2010) (Nam et al., 2016). Besides viscoelasticity, viscoplasticity is linked to mechanical confinement and thus affects also cell proliferation, spreading and migration (Chaudhuri et al., 2020) (Nam et al., 2016). Advanced viscoplastic models such as the Bergström-Boyce model, the Arruda-Boyce viscoplastic model, or the three-net model have been presented earlier (Bergström, 2015) and can best reflect the complex material behavior of polymers.

A precise distinction between the individual mechanisms during deformation is not possible through our experimental method. Still, a possible poroelastic contribution can be assumed, which is implicitly captured by our hyper-viscoelastic model, which predicts lower stresses during the initial loading segment than in the subsequent second and third cycles, which is consistent with our experimental observations for all three materials. We hypothesize that this effect is caused by the leakage of pore fluid during the initial loading. Previous studies also observed this effect during cyclic shear tests of human brain tissue (Budday et al., 2017).

5. Limitations and future directions

A limitation of our study is that we assume isotropic material behavior for cartilage, although the structure of cartilage is known to be anisotropic. Furthermore, we only considered a single donor in our experimental trials and thus cannot account for variations in material properties between individual donors of different sex and age. Although we collected cartilage samples from macroscopically healthy areas, it is reasonable to assume that the cartilage donor had osteoarthritis. However, we did not histologically examine the cartilage to determine the degree of degeneration.

With our testing approach, it was not possible to accurately differentiate poroelastic material behavior from viscoelastic material behavior. While we could implicitly capture porous effects using a hyper-viscoelastic material approach, an extension to poro-hyper-viscoelasticity could be meaningful for certain applications in the future. Still, we note that it is advisable to use a viscoelastic model instead of a poro-viscoelastic model to save computational cost whenever the application does not require to explicitly model the fluid flow. Finally, ChondroFiller^{liquid} showed good agreement for the reversible hyper-viscoelastic material behavior up to 10% strain. However, irreversible deformation occurred at higher strains, which indicates that a visco-plastic or damage material model will be necessary to fully capture

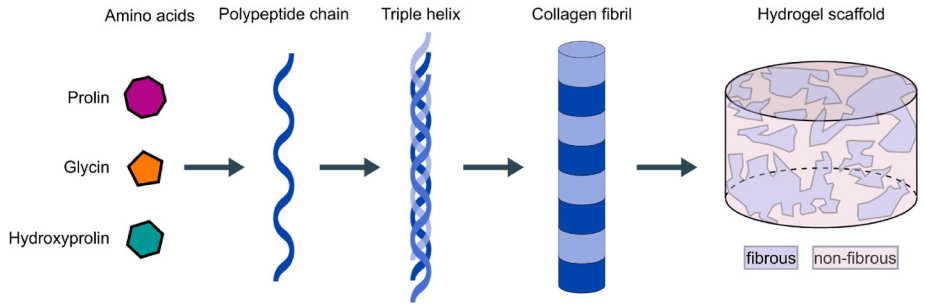

Fig. 13. Schematic illustration of the hierarchical collagen type I structure of a ChondroFiller^{liquid} hydrogel scaffold.

the behavior at higher strains. The consideration of viscoplasticity or damage effects are not the focus of this study but we will consider those in following studies.

Although we have considered compressive and tensile deformation, we lack data obtained from shear tests.

6. Conclusion

We have determined hyper-viscoelastic parameters for numerical simulations in COMSOL Multiphysics® v. 5.6 that capture the conditioned and unconditioned responses of human articular cartilage, ADA-GEL and ChondroFiller^{liquid}. To identify the material parameters, we have used several loading conditions simultaneously, i.e., cycling loading and stress relaxation in tension and compression.

Hyper-viscoelastic laws can well describe the material behavior of ChondroFiller^{liquid} up to a deformation of 10% (nominal strain). At strains greater than 10% (nominal strain), irreversible deformation occurs. ADA-GEL is closer to cartilage in its elastic properties, while ChondroFiller^{liquid} is more similar to cartilage in its viscous properties. Viscoelasticity predominates the response of cartilage, whereas ADA-GEL and ChondroFiller^{liquid} show an opposite trend with a dominance of the elastic material behavior. Both ChondroFiller^{liquid} and ADA-GEL show a faster stress relaxation behavior than cartilage.

Our data can be used for finite element simulations in different situations, e.g., for simulating dynamic processes with the unconditioned parameter set or for repeated physiological loads and in vitro stimulations with the conditioned parameter set. Furthermore, the results of this study serve as a basis to tagetedly develop suitable substitute materials for cartilage that mimic the mechanical material behavior as closely as possible.

CRediT authorship contribution statement

A. Weizel: Writing – review & editing, Writing – original draft, Methodology, Investigation, Conceptualization, Writing – review & editing, Writing – original draft, Visualization, Methodology, Investigation, Formal analysis, Data curation, Conceptualization. **T. Distler:** Investigation. **R. Detsch:** Funding acquisition. **A.R. Boccaccini:** Project administration, Funding acquisition. **H. Seitz:** Project administration, Funding acquisition. **S. Budday:** Writing – review & editing, Writing – original draft, Methodology, Conceptualization.

Declaration of competing interest

The authors declare that they have no known competing financial interests or personal relationships that could have appeared to influence the work reported in this paper.

Data availability

Data will be made available on request.

Acknowledgements

The research was funded by the Deutsche Forschungsgemeinschaft (DFG, German Research Foundation) – SFB 1270/1;2 - 299150580 and the grant BU 3728/1-1. We also acknowledge the kind support by the Emerging Fields Initiative (EFI) by the FAU.

Appendix A. Supplementary data

Supplementary data to this article can be found online at https://doi.org/10.1016/j.jmbbm.2022.105618.

References

Antoine, E.E., Vlachos, P.P., Rylander, M.N., 2014. Review of collagen I hydrogels for bioengineered tissue microenvironments: characterization of mechanics, structure, and transport, Tissue engineering. Part B, Reviews 20, 683–696.
Babalola, O.M., Bonassar, L.J., 2009. Parametric finite element analysis of physical stimuli resulting from mechanical stimulation of tissue engineered cartilage. J. Biomech. Eng. 131, 61014.
Bergström, J., 2015. Mechanics of Solid Polymers: Theory and Computational Modeling. Elsevier, Amsterdam [u.a.
Brighton, C.T., Wang, W., Clark, C.C., 2008. The effect of electrical fields on gene and protein expression in human osteoarthritic cartilage explants, the Journal of bone and joint surgery. American 90, 833–848.
Budday, S., Sommer, G., Haybaeck, J., Steinmann, P., Holzapfel, G., Kuhl, E., 2017. Rheological Characterization of Human Brain Tissue. undefined.
Caccavo, D., Cascone, S., Lamberti, G., Barba, A.A., 2018. Hydrogels: experimental characterization and mathematical modelling of their mechanical and diffusive behaviour. Chem. Soc. Rev. 47, 2357–2373.
Castro, A.P.G., Yao, J., Battisti, T., Lacroix, D., 2018. Poroelastic modeling of highly hydrated collagen hydrogels: experimental results vs. Numerical simulation with custom and commercial finite element solvers. Front. Bioeng. Biotechnol. 6, 142.
Charbonier, F., Indana, D., Chaudhuri, O., 2021. Tuning viscoelasticity in alginate hydrogels for 3D cell culture studies. Current protocols 1, e124.
Chaudhuri, O., Cooper-White, J., Janmey, P.A., Mooney, D.J., Shenoy, V.B., 2020. Effects of extracellular matrix viscoelasticity on cellular behaviour. Nature 584, 535–546.
COMSOL, The Structural Mechanics Module User's Guide.
Distler, T., McDonald, K., Heid, S., Karakaya, E., Detsch, R., Boccaccini, A.R., 2020. Ionically and enzymatically dual cross-linked oxidized alginate gelatin hydrogels with tunable stiffness and degradation behavior for tissue engineering. ACS Biomater. Sci. Eng. 6, 3899–3914.
Ebrahimi, M., Ojanen, S., Mohammadi, A., Finnilä, M.A., Joukainen, A., Kröger, H., Saarakkala, S., et al., 2019. Elastic, viscoelastic and fibril-reinforced poroelastic material properties of healthy and osteoarthritic human tibial cartilage. Ann. Biomed. Eng. 47, 953–966.
Peter Fratzl, Collagen: Structure and Mechanics.
Hazur, J., Endrizzi, N., Schubert, D.W., Boccaccini, A.R., Fabry, B., 2021. Stress relaxation amplitude of hydrogels determines migration, proliferation, and morphology of cells in 3-D culture. Biomater. Sci. 10, 270–280.
Holzapfel, G.A., 2010. Nonlinear Solid Mechanics: A Continuum Approach for Engineering. Wiley, Chichester.
Kleemann, R.U., Krocker, D., Cedraro, A., Tuischer, J., Duda, G.N., 2005. Altered Cartilage Mechanics and Histology in Knee Osteoarthritis: Relation to Clinical Assessment (ICRS Grade).
Krueger, S., Riess, A., Jonitz-Heincke, A., Weizel, A., Seyfarth, A., Seitz, H., Bader, R., 2021. Establishment of a new device for electrical stimulation of non-degenerative cartilage cells in vitro. Int. J. Mol. Sci. 22, 394.
Lee, H.-P., Gu, L., Mooney, D.J., Levenston, M.E., Chaudhuri, O., 2017. Mechanical confinement regulates cartilage matrix formation by chondrocytes. Nat. Mater. 16, 1243–1251.
Liu, B., Lad, N.K., Collins, A.T., Ganapathy, P.K., Utturkar, G.M., McNulty, A.L., Spritzer, C.E., et al., 2017. In vivo tibial cartilage strains in regions of cartilage-to-cartilage contact and cartilage-to-meniscus contact in response to walking. Am. J. Sports Med. 45, 2817–2823.
Martínez-Moreno, D., Jiménez, G., Gálvez-Martín, P., Rus, G., Marchal, J.A., 2019. Cartilage biomechanics: a key factor for osteoarthritis regenerative medicine, Biochimica et biophysica acta. Molecular Basis Dis. 1865, 1067–1075.
Meinert, C., Schrobback, K., Hutmacher, D.W., Klein, T.J., 2017. A novel bioreactor system for biaxial mechanical loading enhances the properties of tissue-engineered human cartilage. Sci. Rep. 7, 16997.
Mørch, Y.A., Donati, I., Strand, B.L., Skjåk-Braek, G., 2006. Effect of Ca2+, Ba2+, and Sr2+ on alginate microbeads. Biomacromolecules 7, 1471–1480.
Nam, S., Lee, J., Brownfield, D.G., Chaudhuri, O., 2016. Viscoplasticity enables mechanical remodeling of matrix by cells. Biophys. J. 111, 2296–2308.
Richard, F., Villars, M., Thibaud, S., 2013. Viscoelastic modeling and quantitative experimental characterization of normal and osteoarthritic human articular cartilage using indentation. J. Mech. Behav. Biomed. Mater. 24, 41–52.
Saarakkala, S., Julkunen, P., Kiviranta, P., Mäkitalo, J., Jurvelin, J.S., Korhonen, R.K., 2010. Depth-wise progression of osteoarthritis in human articular cartilage: investigation of composition, structure and biomechanics. Osteoarthritis Cartilage 18, 73–81.
Safiri, S., Kolahi, A.-A., Smith, E., Hill, C., Bettampadi, D., Mansournia, M.A., Hoy, D., et al., 2020. Global, regional and national burden of osteoarthritis 1990-2017: a systematic analysis of the Global Burden of Disease Study 2017. Ann. Rheum. Dis. 79, 819–828.
Salvatore, L., Gallo, N., Natali, M.L., Terzi, A., Sannino, A., Madaghiele, M., 2021. Mimicking the hierarchical organization of natural collagen: toward the development of ideal scaffolding material for tissue regeneration. Front. Bioeng. Biotechnol. 9, 644595.
Sarrigiannidis, S.O., Rey, J.M., Dobre, O., González-García, C., Dalby, M.J., Salmeron-Sanchez, M., 2021. A tough act to follow: collagen hydrogel modifications to improve mechanical and growth factor loading capabilities. Materials Today Bio 10, 100098.
Silver, F.H., Bradica, G., 2002. Mechanobiology of cartilage: how do internal and external stresses affect mechanochemical transduction and elastic energy storage? Biomech. Model. Mechanobiol. 1, 219–238.

Silver, F.H., Bradica, G., Tria, A., 2002a. Elastic Energy Storage in Human Articular Cartilage: Estimation of the Elastic Modulus for Type II Collagen and Changes Associated with Osteoarthritis.
Silver, F.H., Ebrahimi, A., Snowhill, P.B., 2002b. Viscoelastic properties of self-assembled type I collagen fibers: molecular basis of elastic and viscous behaviors. Connect. Tissue Res. 43, 569–580.
Silver, F.H., Bradica, G., Tria, A., 2004. Do changes in the mechanical properties of articular cartilage promote catabolic destruction of cartilage and osteoarthritis? Matrix Biol. 23, 467–476.
Springhetti, R., Selyutina, N.S., 2018. Viscoelastic modeling of articular cartilage under impact loading. Meccanica 53, 519–530.
Stampoultzis, T., Karami, P., Pioletti, D.P., 2021. Thoughts on cartilage tissue engineering: a 21st century perspective. Current Res. Translat. Med. 69, 103299.
Steinmann, P., Hossain, M., Possart, G., 2012. Hyperelastic models for rubber-like materials: consistent tangent operators and suitability for Treloar's data. Arch. Appl. Mech. 82, 1183–1217.
van Mow, C., Holmes, M.H., Michael Lai, W., 1984. Fluid Transport and Mechanical Properties of Articular Cartilage: A Review.
Vedadghavami, A., Minooei, F., Mohammadi, M.H., Khetani, S., Rezaei Kolahchi, A., Mashayekhan, S., Sanati-Nezhad, A., 2017. Manufacturing of hydrogel biomaterials with controlled mechanical properties for tissue engineering applications. Acta Biomater. 62, 42–63.
Weizel, A., Distler, T., Schneidereit, D., Friedrich, O., Bräuer, L., Paulsen, F., Detsch, R., et al., 2020. Complex mechanical behavior of human articular cartilage and hydrogels for cartilage repair. Acta Biomater. 118, 113–128.
Weizel, A., Distler, T., Detsch, R., Boccaccini, A.R., Bräuer, L., Paulsen, F., Seitz, H., et al., 2022. Hyperelastic parameter identification of human articular cartilage and substitute materials. J. Mech. Behav. Biomed. Mater., 105292
Zahedmanesh, H., Stoddart, M., Lezuo, P., Forkmann, C., Wimmmer, M.A., Alini, M., van Oosterwyck, H., 2014. Deciphering mechanical regulation of chondrogenesis in fibrin-polyurethane composite scaffolds enriched with human mesenchymal stem cells: a dual computational and experimental approach, Tissue engineering. Part. Accel. 20, 1197–1212.
Zhang, Y.S., Khademhosseini, A., 2017. Advances in engineering hydrogels. Science 356.